CHEMO-RESISTANCE IN GASTROINTESTINAL CANCERS

EDITED BY: Xia Li, Dong-Hua Yang and Prathibha Ranganathan
PUBLISHED IN: Frontiers in Oncology

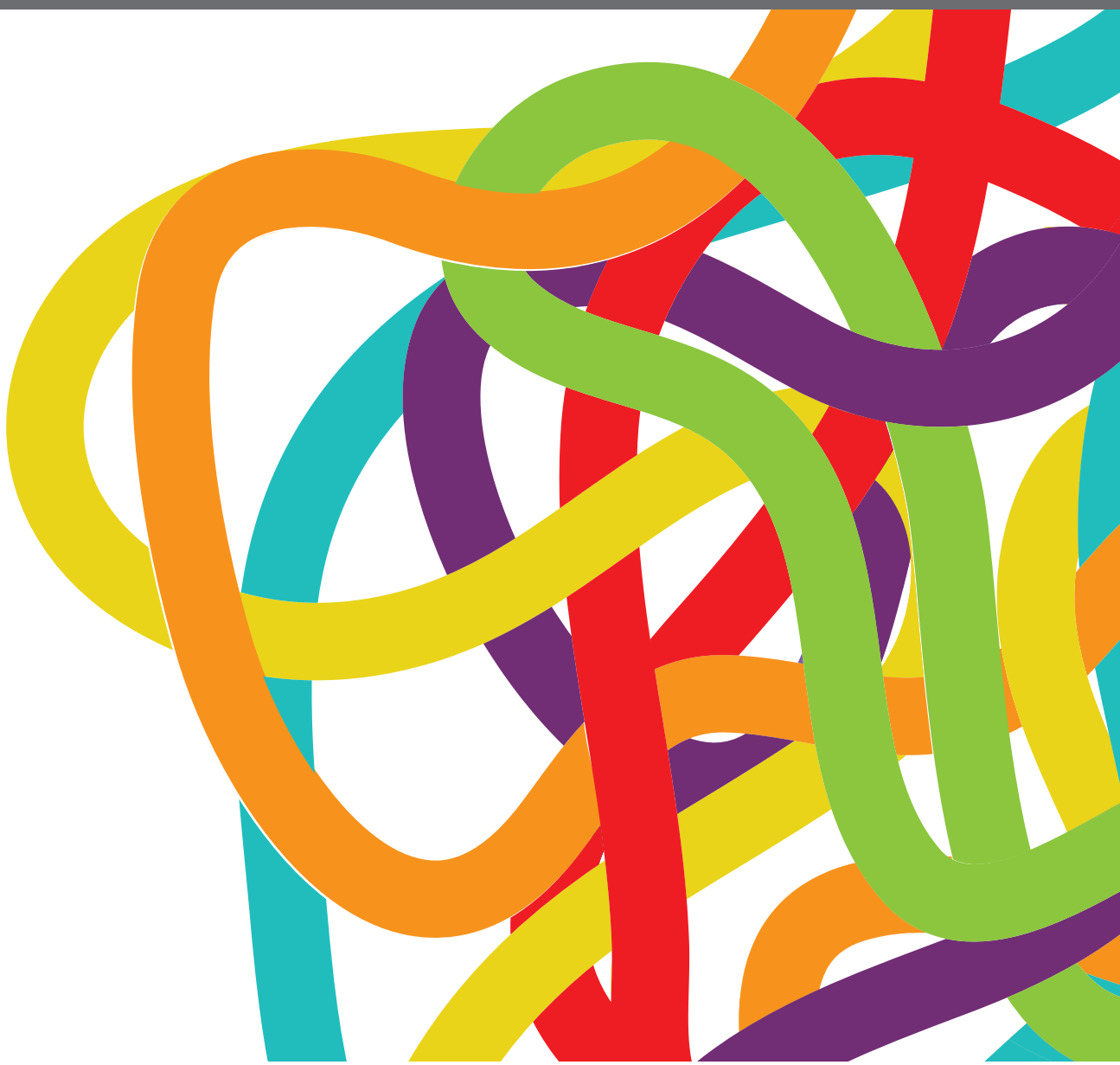

frontiers Research Topics

frontiers

ISSN 1664-8714
ISBN 978-2-88974-776-4
DOI 10.3389/978-2-88974-776-4

About Frontiers

Frontiers is more than just an open-access publisher of scholarly articles: it is a pioneering approach to the world of academia, radically improving the way scholarly research is managed. The grand vision of Frontiers is a world where all people have an equal opportunity to seek, share and generate knowledge. Frontiers provides immediate and permanent online open access to all its publications, but this alone is not enough to realize our grand goals.

Frontiers Journal Series

The Frontiers Journal Series is a multi-tier and interdisciplinary set of open-access, online journals, promising a paradigm shift from the current review, selection and dissemination processes in academic publishing. All Frontiers journals are driven by researchers for researchers; therefore, they constitute a service to the scholarly community. At the same time, the Frontiers Journal Series operates on a revolutionary invention, the tiered publishing system, initially addressing specific communities of scholars, and gradually climbing up to broader public understanding, thus serving the interests of the lay society, too.

Dedication to Quality

Each Frontiers article is a landmark of the highest quality, thanks to genuinely collaborative interactions between authors and review editors, who include some of the world's best academicians. Research must be certified by peers before entering a stream of knowledge that may eventually reach the public - and shape society; therefore, Frontiers only applies the most rigorous and unbiased reviews.
Frontiers revolutionizes research publishing by freely delivering the most outstanding research, evaluated with no bias from both the academic and social point of view. By applying the most advanced information technologies, Frontiers is catapulting scholarly publishing into a new generation.

What are Frontiers Research Topics?

Frontiers Research Topics are very popular trademarks of the Frontiers Journals Series: they are collections of at least ten articles, all centered on a particular subject. With their unique mix of varied contributions from Original Research to Review Articles, Frontiers Research Topics unify the most influential researchers, the latest key findings and historical advances in a hot research area! Find out more on how to host your own Frontiers Research Topic or contribute to one as an author by contacting the Frontiers Editorial Office: frontiersin.org/about/contact

CHEMO-RESISTANCE IN GASTROINTESTINAL CANCERS

Topic Editors:
Xia Li, Shenzhen Institutes of Advanced Technology, Chinese Academy of Sciences (CAS), China
Dong-Hua Yang, St. John's University, United States
Prathibha Ranganathan, Centre for Human Genetics (CHG), India

Citation: Li, X., Yang, D.-H., Ranganathan, P., eds. (2022). Chemo-Resistance in Gastrointestinal Cancers. Lausanne: Frontiers Media SA.
doi: 10.3389/978-2-88974-776-4

Table of Contents

frontiers in Oncology

EDITORIAL
published: 28 January 2022
doi: 10.3389/fonc.2022.821212

Editorial: Chemo-Resistance in Gastrointestinal Cancers

Xia Li[1]*, *Dong-Hua Yang*[2] *and Prathibha Ranganathan*[3]

[1] Research Center for Biomedical Information Technology, Shenzhen Institutes of Advanced Technology, Chinese Academy of Sciences, Shenzhen, China, [2] College of Pharmacy and Health Sciences, St. John's University, Queens, NY, United States, [3] Centre for Human Genetics (CHG), Bengaluru, India

Keywords: gastric cancer, drug-resistance, mechanism, targets, biomarker

Editorial on the Research Topic

Chemo-Resistance in Gastrointestinal Cancers

Gastrointestinal (GI) cancers are a group of diseases originating from different organs of the gastrointestinal tract, with very high ranking of cancer incidence and mortality (1). Chemotherapy is widely used in GI cancer treatment, and is the preferred choice of treatment for patients who cannot undergo surgical resection or in patients with advanced metastases (2). Patients with GI cancer can benefit from chemotherapy including these commonly used chemotherapeutic agents, adriamycin, platinum drugs, 5-fluorouracil, vincristine, and paclitaxel. However, it is often observed that there is poor or no response to chemotherapy, and even in patients who respond well during primary treatment, the long-term results are disappointing. The development of chemo-resistance is a major obstacle in management of GI cancers. Various causes of drug resistance have been identified, which include inactivation of apoptosis signaling pathways, loss of cell cycle checkpoint control, accelerated cell proliferation and autophagy flux, enhanced DNA damage repair capacity, cancer stem cells, as well as epithelial-mesenchymal transition (3–5). Unfortunately, the precise mechanism of adaptive changes during development of chemo-resistance in GI cancers is still unclear. An insight into the mechanisms of chemo-resistance in GI cancers may help to devise better and personalized treatment strategies.

This Research Topic was aimed at bringing together clinical and basic scientists and to address the problem of chemo-resistance from multiple perspectives. True to its aim, this collection has a variety of articles including original research, review of literature and case reports. They cover areas such as signaling pathways, non-coding RNAs, cancer stem cells, and biomarkers to predict tumor outcome.

The Mitogen Activated Protein Kinase (MAPK) pathway is one of the most important signaling pathways involved in normal cellular processes, and plays a key role in the development and progression of cancer (6). Once activated, MAPK exerts an important role in converting extracellular stimuli into a wide range of cellular responses. Increasing evidences support its role in response to chemotherapeutic agents (7, 8). Upon stimulation, ERK1/2 signaling could decrease the sensitivity to sorafenib in hepatocellular carcinoma cells (9). Understanding the main effector genes along with downstream pathways can identify potential therapeutic targets. In this special guest edition, Li B. et al. discovered that phosphorylation of endogenous ERK1/2 could be stimulated by GCDA (Glycochenodeoxycholate) in hepatocellular carcinoma cells. Disruption of the effect of GCDA by blocking phosphorylation and nuclear accumulation of ERK1/2 could be potentially a mode of managing GCDA-related liver cancer and chemo-resistance. In addition, Gao et al. demonstrated that CIDEA expression promoted the chemosensitivity of esophageal cancer cells to cisplatin by activation

OPEN ACCESS

Edited and reviewed by:
Liang Qiao,
Westmead Institute for Medical Research, Australia

Correspondence:
Xia Li
xia.li@siat.ac.cn;
bioinflix@126.com

Specialty section:
This article was submitted to Gastrointestinal Cancers, a section of the journal Frontiers in Oncology

Received: *24 November 2021*
Accepted: *05 January 2022*
Published: *28 January 2022*

Citation:
Li X, Yang D-H and Ranganathan P (2022) Editorial: Chemo-Resistance in Gastrointestinal Cancers. Front. Oncol. 12:821212. doi: 10.3389/fonc.2022.821212

of JNK. This study further suggests a tumor suppressor role for CIDEA as well and opens a possibility of using this as a target for combinatorial therapy. A study by Li Y. et al. reported a case of advanced colorectal cancer who was successfully treated using anti-EGFR drugs (cetuximab) in combination with anti-VEGF agents (fruquintinib) after development of resistance to chemotherapy. The mechanism underlying the success of this combinatorial therapy however needs further investigation.

In GI cancers, multiple deregulated noncoding RNAs (ncRNAs), including miRNAs and lncRNAs, play pivotal roles in the development of chemo-resistance (10, 11). In this regard, Qian et al. found that miR-454-3p was significantly up-regulated in oxaliplatin-resistant colorectal cancer cells and miR-454-3p promoted oxaliplatin resistance by targeting PTEN and activating the AKT signaling pathway. PI3K/AKT/mTOR pathway is also one of the most important signaling pathways involved in chemo-resistance in many human cancers (12). The contribution by Chen et al. demonstrated that HOXA13 overexpression increased 5-fluorouracil resistance in gastric cancer cells, and the expression of HOXA13 was directly suppressed by miR-139-5p. Bai et al. demonstrated the role of lncRNA AC007639.1 in chemo-resistance of hepatocellular carcinoma using a combination of bioinformatics and experimental approaches. These findings highlight targeting ncRNAs may act as a potential therapeutic strategy for reducing resistance to chemotherapy. Given the importance of ncRNAs in cancer, systematic exploration of the crosstalk with other molecular players should aid in a better understanding of their roles during the process of development of drug resistance of GI cancer patients.

A study by Liu et al. demonstrated the role of cancer stem cells as well as epithelial-mesenchymal transition (EMT) responsible for the development of chemo-resistance in esophageal cancer. Cancer stem cells have been reported in different GI cancers and are thought to be responsible for tumor initiation, metastasis, and drug resistance (13). The role of EMT in cancer drug resistance has long been suggested. It is worth noting that tumor microenvironment (TME) is also a factor mediating EMT-driven drug resistance, and the interactions of cancer cells with TME are crucial in EMT and drug resistance (14). Therefore it would be necessary to delineate detailed relationships of cancer cells and TME during chemo-resistance, such as the spatial locations of cancer and immune cells in the tumor tissues and specific ligand-receptor interactions between them.

Identification of biomarkers could improve diagnosis, prognosis, prediction of recurrence and treatment response. Many studies have contributed to the discovery of prognostic biomarkers, but the clinical need lies much more in the predictive biomarkers which would aid in deciding therapeutic approaches to improve patient outcomes. In this context, Sun et al. comprehensively reviewed progresses on the sensitivity prediction of neoadjuvant chemoradiotherapy for GI cancers in the aspects of microRNAs, metabolic enzymes, exosomes, other biomarkers, inflammatory indicators, and imageological assessments. Notably, a recent review has a special focus on the immune markers from TME and discusses their predictive roles on response to cytotoxic chemotherapy in colorectal cancer (15). The emerging move to the discovery and establishment of biomarkers from TME has the potential to develop more robust biomarkers for therapy benefit and resistance of chemotherapy. Alternatively, prediction of drug sensitivity through bioinformatics and computational biology could represent one efficient way to manage large and complex data sets, and provide prior information in the theoretical guidance. Innovative and advanced biomarker prediction approaches, together with large cohorts validation, should be more extensively designed and conducted in the near future.

Altogether, the articles collected in this Research Topic provide a series of insightful sets of data to better understand molecular events involved in the development of chemo-resistance in GI cancers. These findings offer implications in potential therapeutic targets identification, and provide insight on further drug-resistance research. It is our hope that this effort would pave the way for more inter-disciplinary work with the goal of better management of GI cancers.

AUTHOR CONTRIBUTIONS

All authors listed have made a substantial, direct and intellectual contribution to the work, and approved it for publication.

REFERENCES

1. Thrift AP, El-Serag HB. Burden of Gastric Cancer. *Clin Gastroenterol Hepatol* (2020) 18(3):534–42. doi: 10.1016/j.cgh.2019.07.045
2. Wagner AD, Syn NL, Moehler M, Grothe W, Yong WP, Tai BC, et al. Chemotherapy for Advanced Gastric Cancer. *Cochrane Database System Rev* (2017) 8:CD004064. doi: 10.1002/14651858.CD004064.pub4
3. Nies AT, Magdy T, Schwab M, Zanger UM. Role of ABC Transporters in Fluoropyrimidine-Based Chemotherapy Response. *Adv Cancer Res* (2015) 125:217–43. doi: 10.1016/bs.acr.2014.10.007
4. Hammond WA, Swaika A, Mody K. Pharmacologic Resistance in Colorectal Cancer: A Review. *Ther Adv Med Oncol* (2016) 8(1):57–84. doi: 10.1177/1758834015614530
5. Czabotar PE, Lessene G, Strasser A, Adams JM. Control of Apoptosis by the BCL-2 Protein Family: Implications for Physiology and Therapy. *Nat Rev Mol Cell Biol* (2014) 15(1):49–63. doi: 10.1038/nrm3722
6. Khavari TA, Rinn J. Ras/Erk MAPK Signaling in Epidermal Homeostasis and Neoplasia. *Cell Cycle* (2007) 6(23):2928–31. doi: 10.4161/cc.6.23.4998
7. Deacon K, Mistry P, Chernoff J, Blank JL, Patel R. P38 Mitogen-Activated Protein Kinase Mediates Cell Death and P21-Activated Kinase Mediates Cell Survival During Chemotherapeutic Drug-Induced Mitotic Arrest. *Mol Biol Cell* (2003) 14(5):2071–87. doi: 10.1091/mbc.e02-10-0653
8. Lou X, Zhou Q, Yin Y, Zhou C, Shen Y. Inhibition of the Met Receptor Tyrosine Kinase Signaling Enhances the Chemosensitivity of Glioma Cell Lines to CDDP Through Activation of P38 MAPK Pathway. *Mol Cancer Ther* (2009) 8(5):1126–36. doi: 10.1158/1535-7163.MCT-08-0904
9. Zhong J, Yu X, Dong X, Lu H, Zhou W, Li L, et al. Downregulation of Secreted Clusterin Potentiates the Lethality of Sorafenib in Hepatocellular Carcinoma in Association With the Inhibition of ERK1/2 Signals. *Int J Mol Med* (2018) 41 (5):2893–900. doi: 10.3892/ijmm.2018.3463
10. Zhang F, Li Y, Xu W, He L, Tan Y, Xu H. Long non-Coding RNA ZFAS1 Regulates the Malignant Progression of Gastric Cancer *via* the microRNA-200b-3p/Wnt1 Axis. *Biosci Biotechnol Biochem* (2019) 83(7):1289–99. doi: 10.1080/09168451.2019.1606697
11. Xi Z, Si J, Nan J. LncRNA MALAT1 Potentiates Autophagyassociated Cisplatin Resistance by Regulating the Microrna30b/Autophagyrelated Gene

5 Axis in Gastric Cancer. *Int J Oncol* (2019) 54(1):239–48. doi: 10.3892/ijo.2018.4609
12. Fattahi S, Amjadi-Moheb F, Tabaripour R, Ashrafi GH, Akhavan-Niaki H. PI3K/AKT/mTOR Signaling in Gastric Cancer: Epigenetics and Beyond. *Life Sci* (2020) 262:118513. doi: 10.1016/j.lfs.2020.118513
13. Taniguchi H, Moriya C, Igarashi H, Saitoh A, Yamamoto H, Adachi Y, et al. Cancer Stem Cells in Human Gastrointestinal Cancer. *Cancer Sci* (2016) 107 (11):1556–62. doi: 10.1111/cas.13069
14. Erin N, Grahovac J, Brozovic A, Efferth T. Tumor Microenvironment and Epithelial Mesenchymal Transition as Targets to Overcome Tumor Multidrug Resistance. *Drug Resist Updates: Rev Commentaries Antimicrob Anticancer Chemother* (2020) 53:100715. doi: 10.1016/j.drup.2020.100715
15. Wilkinson K, Ng W, Roberts TL, Becker TM, Lim SH, Chua W, et al. Tumour Immune Microenvironment Biomarkers Predicting Cytotoxic Chemotherapy Efficacy in Colorectal Cancer. *J Clin Pathol* (2021) 74(10):625–34. doi: 10.1136/jclinpath-2020-207309

Conflict of Interest: The authors declare that the research was conducted in the absence of any commercial or financial relationships that could be construed as a potential conflict of interest.

frontiers in Oncology

ORIGINAL RESEARCH
published: 03 February 2021
doi: 10.3389/fonc.2020.627845

Down-Regulation of CIDEA Promoted Tumor Growth and Contributed to Cisplatin Resistance by Regulating the JNK-p21/Bad Signaling Pathways in Esophageal Squamous Cell Carcinoma

*Ya-Ping Gao[1], Lei Li[2], Jie Yan[1], Xiao-Xia Hou[3], Yong-Xu Jia[1], Zhi-Wei Chang[1], Xin-Yuan Guan[2] and Yan-Ru Qin[1]**

[1] Department of Clinical Oncology, The First Affiliated Hospital, Zhengzhou University, Zhengzhou, China, [2] Department of Clinical Oncology, The University of Hong Kong, Hong Kong, China, [3] Department of Clinical Oncology, The Third Peoples Hospital of Zhengzhou, Zhengzhou, China

OPEN ACCESS

Edited by:
Xia Li,
Shenzhen Institutes of Advanced Technology (CAS), China

Reviewed by:
Hamid Morjani,
Université de Reims Champagne-Ardenne, France
Kamini Singh,
Memorial Sloan Kettering Cancer Center, United States

***Correspondence:**
Yan-Ru Qin
yanruqin@163.com

Specialty section:
This article was submitted to Gastrointestinal Cancers, a section of the journal Frontiers in Oncology

Received: 10 November 2020
Accepted: 15 December 2020
Published: 03 February 2021

Citation:
Gao Y-P, Li L, Yan J, Hou X-X, Jia Y-X, Chang Z-W, Guan X-Y and Qin Y-R (2021) Down-Regulation of CIDEA Promoted Tumor Growth and Contributed to Cisplatin Resistance by Regulating the JNK-p21/Bad Signaling Pathways in Esophageal Squamous Cell Carcinoma. Front. Oncol. 10:627845. doi: 10.3389/fonc.2020.627845

Esophageal squamous cell carcinoma (ESCC) is one of the most common malignancies with poor prognosis and lack of effective targeted therapies. In this study, we investigated the tumor suppressive role of the cell death inducing DFF like effector A (CIDEA) in ESCC. Firstly, public datasets and ESCC tissue microarray analysis showed that CIDEA was frequently down-regulated at both the mRNA and protein level. This was significantly associated with low differentiation and TNM stage in ESCC, and indicated poor prognosis for ESCC patients. Bisulfite genomic sequencing (BGS) and methylation-specific PCR (MSP) analysis revealed that the down-regulation of CIDEA was associated with hypermethylation of its promoter, which was also correlated with the poor prognosis in ESCC patients. *In vitro* and *in vivo* functional studies demonstrated that CIDEA decreased cell growth, foci formation, DNA replication, and tumorigenesis in nude mice. Further study revealed that, during starvation or cisplatin induced DNA damage, CIDEA facilitated the G1-phase arrest or caspase-dependent mitochondrial apoptosis through the JNK-p21/Bad pathway. Therefore, CIDEA is a novel tumor suppressor gene that plays an important role in the development and progression of ESCC, and may provide a potential therapeutic target for patients with ESCC.

Keywords: esophageal squamous cell carcinoma, cell death inducing DFF like effector A, methylation, cisplatin, apoptosis

INTRODUCTION

Esophageal squamous cell carcinoma (ESCC) is a major subtype of esophageal cancer that ranks sixth in the causes of cancer-related death all worldwide (1). The incidence and mortality of ESCC has an extremely uneven geographical distribution, as more than half of ESCC cases occur in China, particularly in Linzhou, Henan (1, 2). Although great progress has been made in early diagnosis and

treatment, the 5-year survival rate of ESCC patients is still poor (3, 4). Above all, it is essential to investigate the molecular mechanisms involved in ESCC development and progression to facilitate novel diagnostic biomarkers and candidate treatment targets specific to ESCC.

The Cancer Genome Atlas (TCGA, https://www.cancer.gov/tcga) (5, 6), a large-scale genomic dataset, provide an opportunity to better understand the biological systems of cancer. Thus, the mRNA expression and clinical survival data of ESCC in the TCGA data portal was comprehensively analyzed. Among the top 100 genes with differential expression in ESCC, only 17 genes, including cell death inducing DFF like effector A (CIDEA), were associated with prognostic significance.

CIDEA is a member of the cell death inducing DFF like effector (CIDE) family, which was initially identified in 1998 by sequence homology to the N-terminal region of the apoptotic DNA fragmentation factors 45 (DFF45) (7). DFF is a heterodimeric protein composed of DFF45 (45kDa) and DFF40 (40kDa) subunits that plays a main role in the process of DNA fragmentation during apoptosis. The apoptotic role of CIDEA was demonstrated by a study reporting that ectopic-expression of CIDEA induced DNA fragmentation and apoptosis in multiple human cell lines (7). However, the underlying mechanism of CIDE-induced apoptosis is not conclusive. It was considered to be independent of the caspase pathway, since the apoptosis induced by CIDEA could not be blocked by a pan-caspase inhibitor (7). A later study showed that apoptosis induced by CIDEA was dependent on caspase 3 activation and the release of cytochrome c from mitochondria (8, 9). In addition, CIDEA is also reported to be involved in insulin sensitivity and lipid metabolism (10–13). Mice deficient in CIDEA exhibit a lean phenotype, increased metabolic rate and reduction of lipid droplet size in the white adipose tissue. The functions of CIDEA proteins may provide a link between energy metabolism and apoptosis. In glioblastoma, CIDEA is reportedly down-regulated and is a regulator of glioma cells, where ectopic expression of CIDEA triggered apoptosis, actin cytoskeletal disruption, and cell cycle arrest (14). After a decade of study, however, the physiological role and function of CIDE proteins have not been clearly elucidated.

In the present study, we investigated the possible role of CIDEA in the development and progression of ESCC. To determine the role of CIDEA, we evaluated the expression status of CIDEA and methylation of its promoter in primary ESCC tissues and ESCC cell lines. Functional assays with CIDEA overexpressing cell lines were performed to characterize the biological effects of CIDEA in ESCC tumorigenicity. The tumor-suppressive mechanism of CIDEA and its potential as a new prognostic biomarker and therapeutic target in ESCC were also addressed.

MATERIALS AND METHODS

Cell Lines and Clinical Specimens

A total of seven esophageal cancer cell lines were used in this study. Six of them were acquired from the German Resource Center for Biological Material (DSMZ) (Braunschweig, Germany), including KYSE30, KYSE140, KYSE150, KYSE180, KYSE410, and KYSE510. The EC109 cell line was a kind gift from Professor Tsao (The University of Hong Kong). The HEK 293-FT cells were purchased from Thermo Fisher Scientific (Waltham, MA). All cell lines used in this study underwent short tandem repeat (STR) profiling, and tested negative for mycoplasma by PCR. Cells were cultured in DMEM medium with 10% fetal bovine serum (FBS) (Gibco BRL, NY), and incubated at 37°C in a humidified atmosphere with 5% CO_2.

All the primary ESCC tumor and non-tumor tissues, including 78 pairs for RNA extraction and 248 pairs for a tissue microarray (TMA), were collected from Linzhou Cancer Hospital (Henan, China). The patients enrolled in this study received no treatment before surgery. This study was approved by the Institutional Ethics Review Board of the First Associated Hospital (Zhengzhou University) and written informed consent form was obtained from all patients.

ESCC Tissue Array and Immunohistochemistry (IHC)

IHC staining was performed according to the standard streptavidin-biotin-peroxidase complex method (15). Staining intensity was scored as: negative (0), weak (1), moderate (2), and strong (3). The proportion of CIDEA-positive cells was scored as 0% (0), 1–10% (1), 10–50% (2), 50–75% (3), and ≥75% (4). The IHC score was calculated by multiplying staining intensity and the proportion of positive cells. CIDEA level data was subjected to ROC curve analysis and a cutoff value of 5 was determined for CIDEA. Down-regulation of CIDEA was defined as a score ≤5.

Quantitative Real-Time PCR Analysis (qRT-PCR) and Reverse Transcription

PCR Analysis (RT-PCR)

Total RNA was extracted with TRIzol® reagent (Invitrogen). Reverse transcription was performed using the PrimeScript RT reagent Kit with gDNA Eraser (TaKaRa, Japan). The relative mRNA levels were determined by qRT-PCR with SYBR Green SuperMix (Roche, Basel, Switzerland) on a Roche LightCycler480. The comparative Ct method was used to calculate the relative expression of RNAs with β-Actin as an internal control. PCR amplifications were conducted with the GoTaqGreen Master mix kit (Promega Corporation, Madison, WI, USA) on a S1000 Thermal Cycler (Bio-Rad Laboratories, USA). PCR products were examined by 1.5% agarose gel electrophoresis. The primer sequences used for PCR were: CIDEA, forward, 5'-GCCGAAGAGGTCGGGAATAG-3', and reverse, 5'-TATCCACACGTGAACCT GCC-3'; β-Actin, forward, 5' CATGTACGTTGCTATCCAGGC-3', and reverse, 5'-CTCCTTAATGTCACGCACGAT-3'.

DNA Methylation Analysis

Genomic DNA was extracted with a genomic DNA extraction kit (Tiangen, China). Purified DNA samples underwent bisulfite treatment using the EpiTect Bisulfite Kit (Qiagen, Germany). Bisulfite sequencing PCR (BSP) and Methylation-specific PCR (MSP) were performed with specific primers targeting the

sequence between −400 and −250 bp of the CIDEA promoter region, where BSP showed difference in KYSE410, KYSE30 and KYSE150. Primers for methylation detection were designed with MethPrimer. The primers used for BSP were as follows: forward, TGTTTATGA-TATGGTTTTGAGAGTAG; and reverse, TATA TAAATTTTAAACCCAAACCAC. The methylation-specific primers used were as follows: m1: AGCGGGTAGGAAG-TTTAGGC, m2: ATTTTAAACCCAAACCACGAAT. The unmethylation-specific primers used were as follows u1: TAGTGGGTAGGAAGTTTAGGTGT, u2: TAAAT-TTTAAACCCAAACCACAAAT.

Establishment of CIDEA Overexpressing ESCC Cell Lines

The control plasmids and pEZ-Lv105-CIDEA were purchased from GeneCopoeia (Guangzhou, China). Their functions were confirmed by sequencing. Lentivirus-containing CIDEA was packaged in 293FT cells and stably transfected into the KYSE30 and KYSE150 cell lines with the ViraPowerTM Lentiviral Packaging Mix (Invitrogen, Carlsbad, CA), following the manufacturer's instructions.

Cell Proliferation Assay and Foci Formation Assay

Cell proliferation assay was performed with a CCK-8 assay kit (Dojindo, Japan), according to the manufacturer's instructions. Briefly, cells (1×10^3 cells/well) were seeded into 96-well plates and the cell growth rate was monitored for 7 consecutive days. For foci formation assay, cells (1×10^3 cells/well) were seeded into six-well plates and cultured for 2 weeks. Then, cells were fixed with 75% ethanol and stained with 1% crystal violet. Finally, colonies containing with more than 50 cells were counted. Three independent assays were carried out.

Western Blotting Analysis and Antibodies

Western blotting analysis was performed following the standard protocols (BioRad). Total proteins from tissues and cells were extracted with RIPA lysis buffer (Cell Signaling Technology) supplemented with protease inhibitor and phosphatase inhibitor. Antibodies used in this study were CIDEA (NBP1-76950, Novus), GAPDH (AM1020B, Abgent), p21 (#2947, Cell Signaling Technology), CylinD1 (#2926, Cell Signaling Technology), CDK4 (#12790, Cell Signaling Technology), p-JNK (Thr183/Tyr185) (#4668, Cell Signaling Technology), Bad (#9239, Cell Signaling Technology), Caspase9 (#9508, Cell Signaling Technology), and PARP (#9542, Cell Signaling Technology).

EdU (5-Ethynyl-2′-deoxyuridine) Incorporation Assay

EdU incorporation assay was performed with the Cell-Light EdU Apollo567 In Vitro Kit (Ribobio, China) according the manufacturer's instructions. Imaging was performed on an Olympus FV-1000 confocal microscope. Red nuclei EdU cells were examined by randomly counting 10 fields in the middle of the microscope slide and were expressed as a percentage of the total population. Three independent assays were carried out.

In Vivo Xenograft Assay

The control and CIDEA over-expressing cells of KYSE150 cells (5×10^6) were subcutaneously injected into the left and right dorsal flanks of 4-week-old female BALB/C nude mice, which were purchased from the Guangdong Animal Center (Guangzhou, China). Tumor volumes were measured every 4 days using calipers and calculated as volume (mm^3) = L (length)×W (width)^2×0.5. One month later, the tumors were removed, weighed, and fixed in the formaldehyde solution for hematoxylin-eosin (HE) staining and IHC study. Animal experiments were conducted in accordance with the guidelines of the Institutional Animal Care and Use Committee.

Cell Cycle and Cell Apoptosis Analysis

The cell cycle and cell apoptosis analyses were performed with the Cell Cycle Assay KIT (Wanleibio, China) and Annexin V FITC Apoptosis Detection Kit (Dojindo, Japan), respectively, following the manufacturer's instructions. Cells were analyzed by a flow cytometry (CytoFlex, Beckman Coulter). Apoptosis was measured as the proportion of cells with Annexin V+/PI− and Annexin V+/PI+ fluorescence. Three independent assays were carried out.

Mitochondrial Membrane Potential Assay

Mitochondrial membrane potential (MMP) was assessed with the fluorescent probe JC-1 (Biyuntian, China) according to the manufacturer's instructions. The fluorescence was analyzed by a flow cytometry (CytoFlex, Beckman-Coulter). Green (∼525 nm) fluorescence represents JC-1 monomers and red (∼590 nm) fluorescence represented JC-1 aggregates. The change of red to green fluorescence signaled a decrease in MMP.

Statistical Analysis

SPSS software (version 23.0, Chicago, IL) and GraphPad Prism software (version 7.0, La Jolla, CA) were used for statistical analyses. A paired Student's *t* test was performed to analyze the difference in mRNA expression between ESCC and normal tissues. Kaplan-Meier plots and log-rank tests were used for overall survival (OS) analysis and disease-free survival (DFS) analysis. Pearson's chi-square test was used to analyze the correlation between CIDEA expression and clinicopathological parameters in ESCC. Univariate and multivariate Cox proportional hazards regression models were performed to evaluate independent prognostic factors of ESCC. Unpaired *t* test was performed to compare the significant differences between the two groups in foci formation, EdU incorporation and cell apoptosis. Data are shown as mean ± SD. $P < 0.05$ was considered statistically significant.

RESULTS

Down-Regulation of CIDEA was Associated With a Poor Outcome in ESCC Patients

To explore the potential role of CIDEA in ESCC, the alteration of CIDEA was screened in multiple ESCC cohorts including

GSE67269 (16) in GEO, Su's (17) cohort in Oncomine, and TCGA (**Figure 1A**). Next, qRT-PCR was performed in a set of 78 pairs of ESCC and non-tumor tissues to confirm the public biostatistics. The down-regulation of CIDEA was detected in all the 78 ESCC tissues, but only observed in 46/78 (58.9%) of non-tumor tissues (**Figure 1B**). Consistently, the mRNA expression of CIDEA was significantly down-regulated in ESCC tissues.

The protein expression of CIDEA was determined by Western blotting analysis in 10 pairs of ESCC and non-tumor tissues **(Figure 1C)** and *via* IHC in a tissue microarray (TMA) containing 248 pairs of ESCC and non-tumor tissues **(Figure 1D)**. Results showed that the protein level of CIDEA was down-regulated in ESCC. In addition, Kaplan-Meier analysis based on the TMA showed that ESCC patients with low CIDEA levels had significantly shorter overall survival (OS) ($P < 0.0001$) than patients with high CIDEA levels (**Figure 1E**). Kaplan-Meier survival analysis based on the TCGA database also demonstrated the shorter OS time ($P = 0.0043$) **(Figure 1F)** and disease-free survival (DFS) time ($P = 0.016$) **(Figure 1F)** in ESCC patients with low CIDEA expression.

Furthermore, the association of CIDEA down regulation with clinicopathological characteristics was analyzed and summarized. CIDEA down regulation was significantly correlated with poor tumor differentiation, advanced clinical staging, and lymph node metastasis **(Table 1)**. Cox regression analysis using age, sex, differentiation, lymph node metastasis,

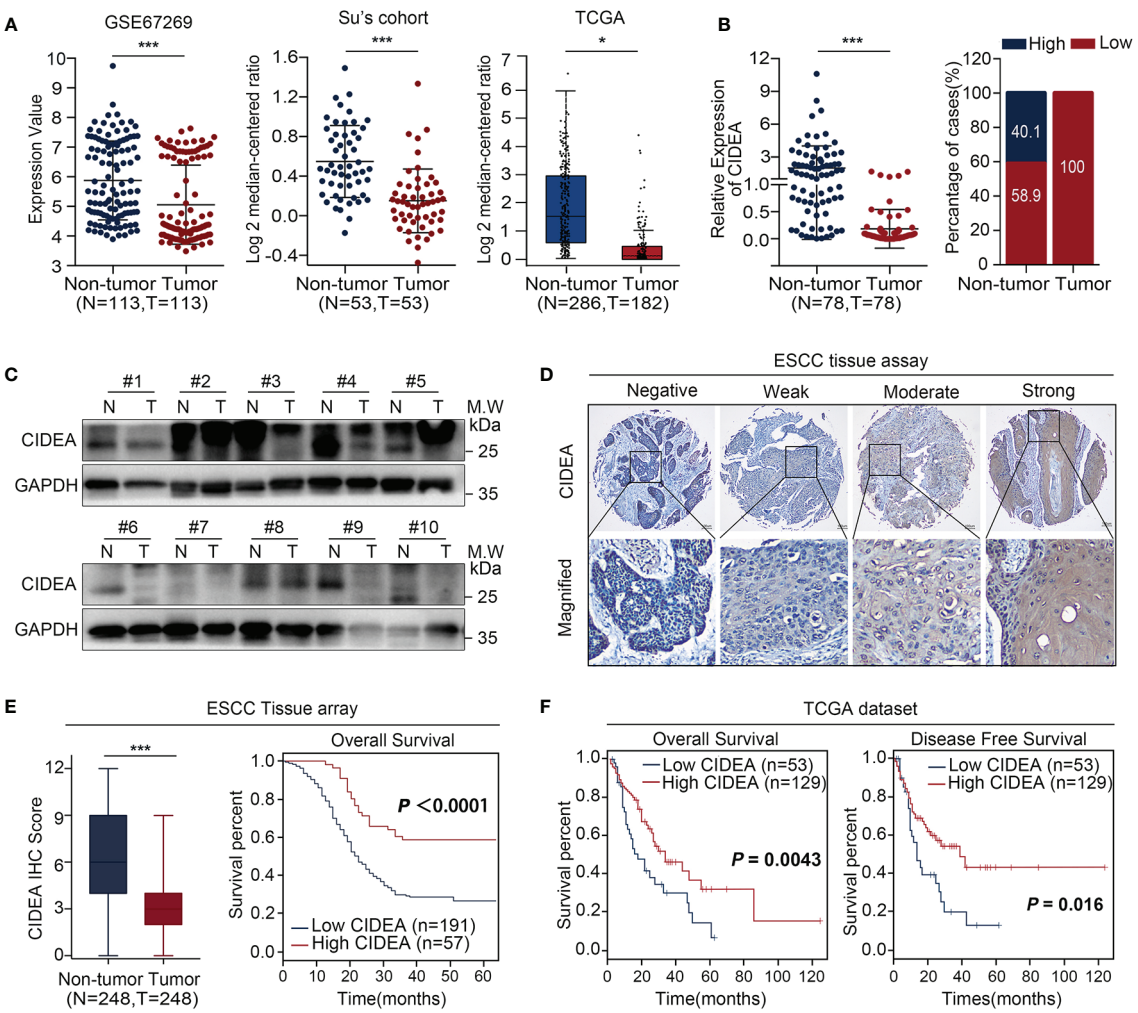

FIGURE 1 | CIDEA expression was downregulated in ESCC, and low expression correlated with poor survival. **(A)** CIDEA expression was compared between ESCC tumor and normal esophageal samples derived from the GEO, Oncomine and TCGA databases. **(B)** The mRNA level of CIDEA was detected by qRT-PCR in 78 pairs of ESCC tissues and adjacent non-tumor tissues with β-actin as the internal reference control. CIDEA expression fractions in 78 ESCC tissues and adjacent non-tumor tissues. **(C)** The protein levels of CIDEA in 10 pairs of ESCC tumors (T) and corresponding normal esophageal (N) tissues were analyzed by Western blotting with GAPDH as the loading control. **(D)** Representative pictures of IHC staining of CIDEA in an ESCC tissue microarray (n = 248). Scale bars, 100 μm. **(E)** CIDEA staining scores in ESCC tumors and the corresponding non-tumor tissues (n = 248). **(E, F)** Kaplan-Meier analysis indicated that the down-regulation of CIDEA was negatively correlated with overall survival (OS) time and disease free survival (DFS) time in ESCC tissue microarray (n = 248) and TCGA dataset (n = 182). Data are presented as the mean ± SD. $^{*}P < 0.05$; $^{**}P < 0.01$; $^{***}P < 0.001$.

TABLE 1 | Associations between CIDEA levels in tumor tissues and clinicopathological characteristics in ESCC patients.

Variable	Total	expression low group, N (%)	*P*-value
Age at diagnosis			0.99
≤60	139	107(76.98)	
>60	109	84(77.06)	
Gender			0.37
Male	139	110 (79.14)	
Female	109	81 (74.31)	
Location			
Upper	53	39 (73.85)	0.268
Middle	169	129 (76.33)	
Lower	26	123(89.46)	
Differentiation			
Well/moderate	180	132(73.33)	**0.025**
Poor	68	59(86.76)	
Lymph node metastasis			**0.0035**
N0	154	107 (69.48)	
N1	94	84 (89.36)	
TNM stage			**0.0028**
Early(I/II)	179	129(72.07)	
Advanced(III/IV)	69	62(89.86)	

Statistical significance (P < 0.05) is shown in bold.

and TNM stage as covariates further demonstrated that CIDEA level is an independent risk factor for OS (HR = 1.480, 95% CI = 1.184–1.851, **Figure 2**). Taken together, the results indicated that the down-regulation of CIDEA expression had a positive effect on the progression of ESCC.

Down-Regulation of CIDEA was Associated With Aberrant Promoter Methylation

To explore whether down-regulation of CIDEA is associated with aberrant DNA methylation in ESCC, the data from TCGA was analyzed. Results showed that the promoter methylation of CIDEA in ESCC (with a median beta-value of 0.257) was much higher than in normal esophageal tissues (with a median beta-value of 0.091) (**Figure 3A**). The beta-value was used as a measure of methylation level, which ranges from 0 (no methylation) to 1 (complete methylation). In addition, there was a significantly negative correlation between the DNA methylation and mRNA expression of CIDEA (Pearson correlation, r =−0.284; $P = 0.001$) (**Figure 3B**).

RT-PCR and Western blotting analysis indicated that silenced or down-regulated mRNA and protein expression level of CIDEA was observed in six of seven ESCC cell lines, except for KYSE410 cells (**Figure 3C**). To confirm whether the methylation of CIDEA is related to its down-regulation, KYSE30 and KYSE150 cells with CIDEA low-expression were treated with 5-Aza-dC, which is a potent inhibitor of DNA methyltransferase. As shown in **Figure 3D**, after 5-Aza-dC treatment, the cellular expression of CIDEA was restored at both the mRNA and protein levels.

A potential CpG island within the upstream region of CIDEA was predicted by the public online tool MethPrimer (http://www.urogene.org/methprimer), which implied an epigenetic mechanism in the regulation of CIDEA expression. The methylation level of 10 CpG sites within the promoter region (−579 to −348) of CIDEA was analyzed in KYSE410, KYSE30, and KYSE150 cells *via* sodium bisulfite sequencing (BGS) and methylation-specific PCR (MSP). BGS analysis showed that KYSE410 cells with up-regulated CIDEA had much lower methylation levels within the region compared with KYSE30 and KYSE150 cells, in which CIDEA is down-regulated (**Figure 3E**). Next, MSP was performed to validate the methylation levels within the region in the seven ESCC cell lines and a cohort of 50 pairs of ESCC and normal tissues. Compared with untreated cells, methylation was significantly reduced in KYSE30 and KYSE150 cells treated with 5-Aza-dC (**Figure 3F**). Moreover, the results showed a higher level of methylation in tumor tissues than nontumor tissues (**Figure 3G**).

In addition, the relationship between DNA methylation of CIDEA and the prognostic value of each CpG site in ESCC was identified *via* MethSurv (https://biit.cs.ut.ee/methsurv/) (18). Results indicated that the methylation of cg12642717 in CIDEA was associated with the highest HR. Overall, six hyper-methylated CpG sites in CIDEA were significantly associated with poor survival, including cg07824824, cg19883905, cg03245632, cg12395205, cg12072560, and cg0570033 (**Figure 3H**).

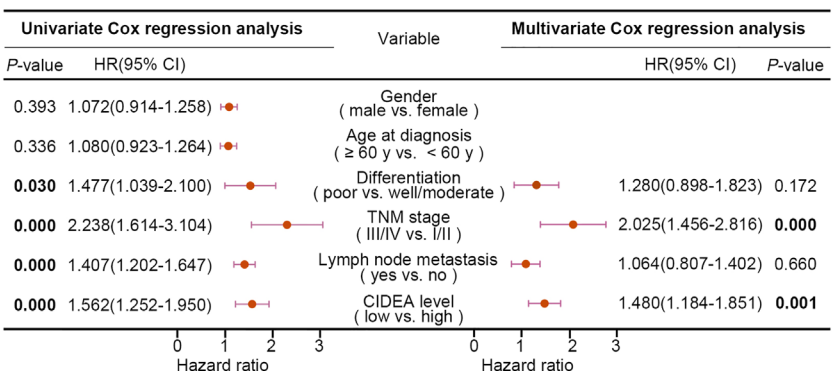

FIGURE 2 | Univariate and multivariate Cox regression analyses of various factors associated with overall survival in patients with ESCC. HR, hazards ratio; CI, confidence interval. Statistical significance ($P < 0.05$) is shown in bold.

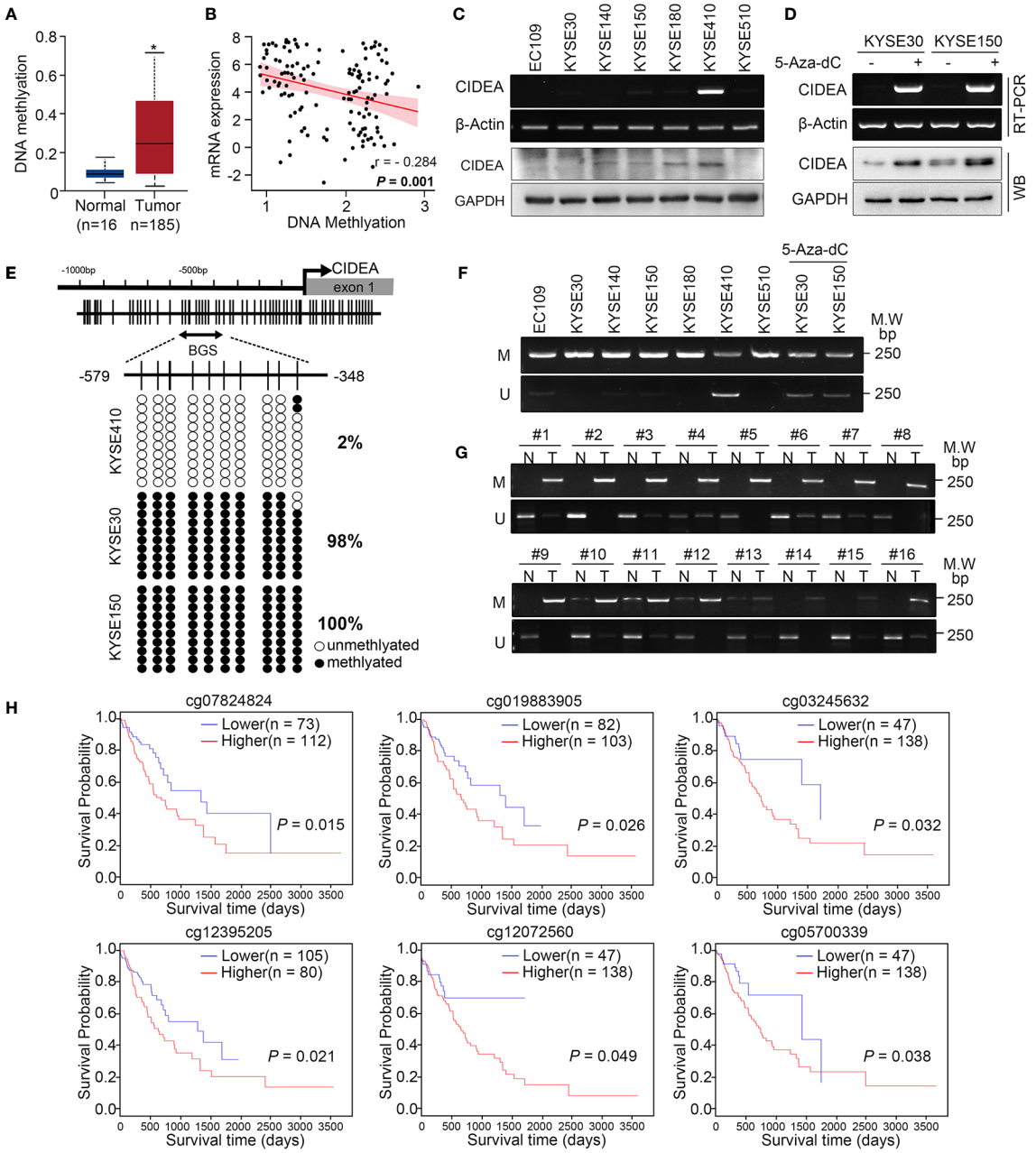

FIGURE 3 | The CIDEA promoter was hyper-methylated and correlated with decreased expression of CIDEA. **(A)** The methylation level of the CIDEA promoter in TCGA ESCC samples. **(B)** Pearson's correlation between DNA methylation and mRNA levels of CIDEA in TCGA ESCC samples. **(C)** The mRNA and protein level of CIDEA in seven ESCC cell lines were detected by RT-PCR and Western blotting with GAPDH or β-actin as loading controls. **(D)** RT-PCR and Western blotting analysis showing restored expression of CIDEA in both KYSE30 and KYSE510 cells treated with 5-AZA-DC (10 μM) for 72 h. +, 5-AZA-DC treated; -, 5-AZA-DC untreated. **(E)** The methylation status of individual CpG sites in the CIDEA promoter (between –579 and –348 bp from the transcription start site) were detected by bisulfite sequencing (BGS) in three ESCC cell lines (KYSE410, KYSE30, and KYSE150). Each row represents an individual cloned allele. The black circles show methylated CpG sites and the white circles show unmethylated CpG sites. **(F, G)** Representative methylation-specific PCR (MSP) analysis of CIDEA in ESCC cell lines and ESCC tissue samples. M, methylated allele; U, unmethylated allele. N, nontumor tissue; T, tumor tissue. **(H)** Kaplan-Meier plot showing the impact of CIDEA methylation sites of CIDEA on OS in ESCC patient as analyzed by the MethSurv webtool. Data are presented as the mean ± SD. *$P < 0.05$; **$P < 0.01$; ***$P < 0.001$.

Collectively, these results suggest that the down-regulation of CIDEA was closely associated with promoter hypermethylation, and the methylation of CIDEA is associated with ESCC patient survival.

CIDEA Suppressed ESCC Tumor Growth

To explore the biological role of CIDEA in ESCC, CIDEA was over-expressed in the two ESCC cell lines KYSE30 and KYSE150 with relatively low expression of CIDEA. Ectopic expression of

CIDEA was determined by RT-PCR and Western blotting (**Figure 4A**). First, *in vitro* functional assays were used to measure the tumorigenicity of CIDEA. The cell growth assay and colony formation assay showed that the cell growth in the CIDEA-overexpressing KYSE30 and KYSE150 cells was significantly lower than in the control cells (**Figures 4B, C**). In addition, the EdU incorporation assay also verified that the proliferative potential decreased in CIDEA-overexpressing cells (**Figure 4D**). Further, the subcutaneous tumor xenograft assay in immunodeficient nude mice showed that the size and weight of xenograft tumors developed from CIDEA-overexpressing cells was significantly lower than in the controls (**Figure 4E**). Furthermore, IHC staining showed that the expression of CIDEA in xenograft tumors induced by CIDEA overexpressing cells was higher, while the expression of the proliferation marker Ki-67 was lower compared to the controls (**Figure 4F**).

Ectopic Expression of CIDEA Promoted G1-Phase Arrest During Serum Starvation

To explore the mechanism of CIDEA inhibition of tumor cell growth, flow cytometry was used to examine cell cycle distribution. There was no significant difference in cell distribution between CIDEA overexpressing cells and control cells under normal conditions. However, after exposure to serum-free medium for 48 h, the population of cells in the G1 phase increased in CIDEA overexpressing KYSE30 and KYSE150 compared with the control cells (**Figures 5A, B**). To further characterize the mechanism by which CIDEA induced G1/S cell cycle arrest, the expression of G1/S checkpoint-related cell cycle regulators was determined by Western blotting. Under the normal conditions and serum starvation, the cellular level of p21 increased, whereas the expression of CDK4 and cyclinD1 were down-regulated in CIDEA overexpressing cells compared with control cells. In addition, during serum starvation, the level

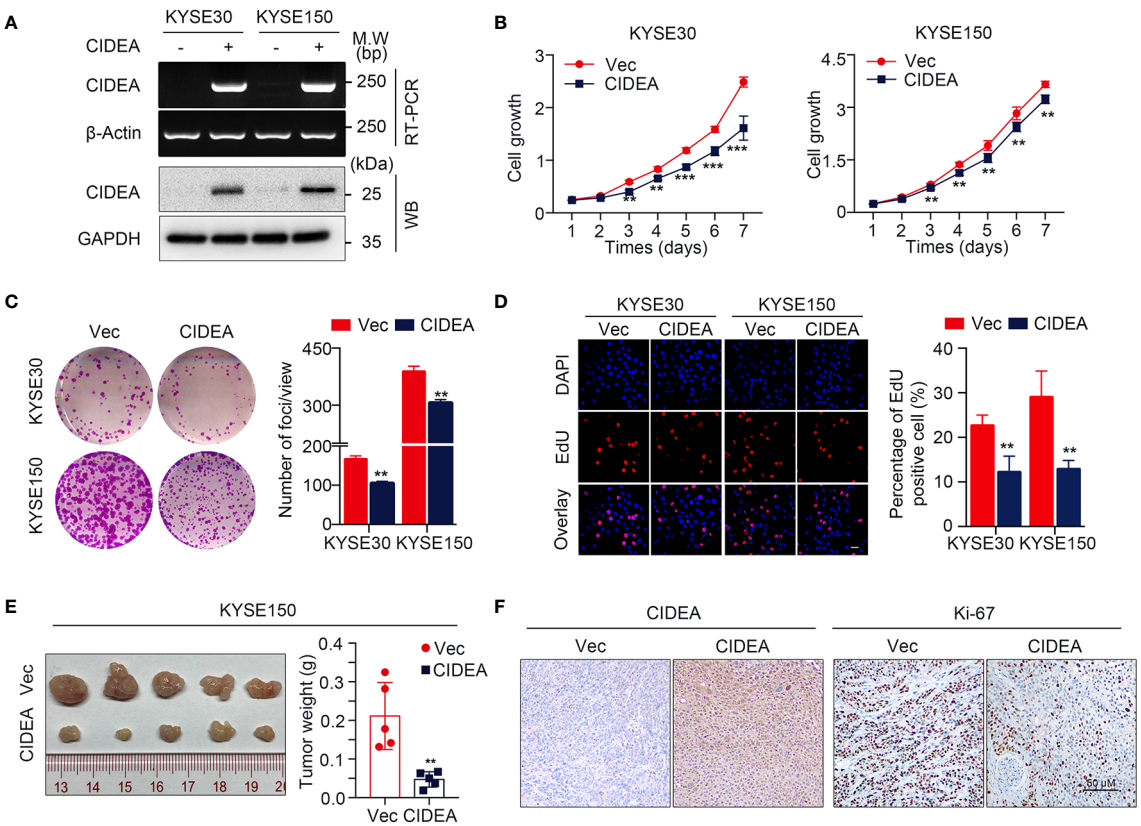

FIGURE 4 | Ectopic expression of CIDEA suppressed ESCC tumor growth. **(A)** CIDEA mRNA and protein levels were detected by RT-PCR and Western blotting in CIDEA-transfected KYSE30 and KYSE150 cells. GAPDH or β-actin was used as the loading control. **(B)** Cell growth rate in CIDEA-transfected and empty vector-transfected KYSE30 and KYSE150 cells was measured by CCK8 proliferation assay for 7 consecutive days. **(C)** Representative images of decreased foci formation in monolayer culture induced by CIDEA overexpression in KYSE30 or KYSE150 cells. **(D)** Representative images (left) and quantitative statistics (right) of EdU incorporation assay showed the decreased replication of DNA in cells induced by CIDEA overexpression. Red, duplicated cells; blue, cell nucleus. Scale bars, 50 μm. **(E)** Images of xenograft tumors derived from KYSE150-transfected cells their vectors in nude mice. Tumor weights were compared between CIDEA over-expressing and control cells. **(F)** Representative IHC images of CIDEA and Ki-67 expression in xenograft tumors derived from CIDEA over-expressing and control cells. Scale bar = 50 μm. Statistical data are represented as mean ± SD. $^{*}P < 0.05$; $^{**}P < 0.01$; $^{***}P < 0.001$.

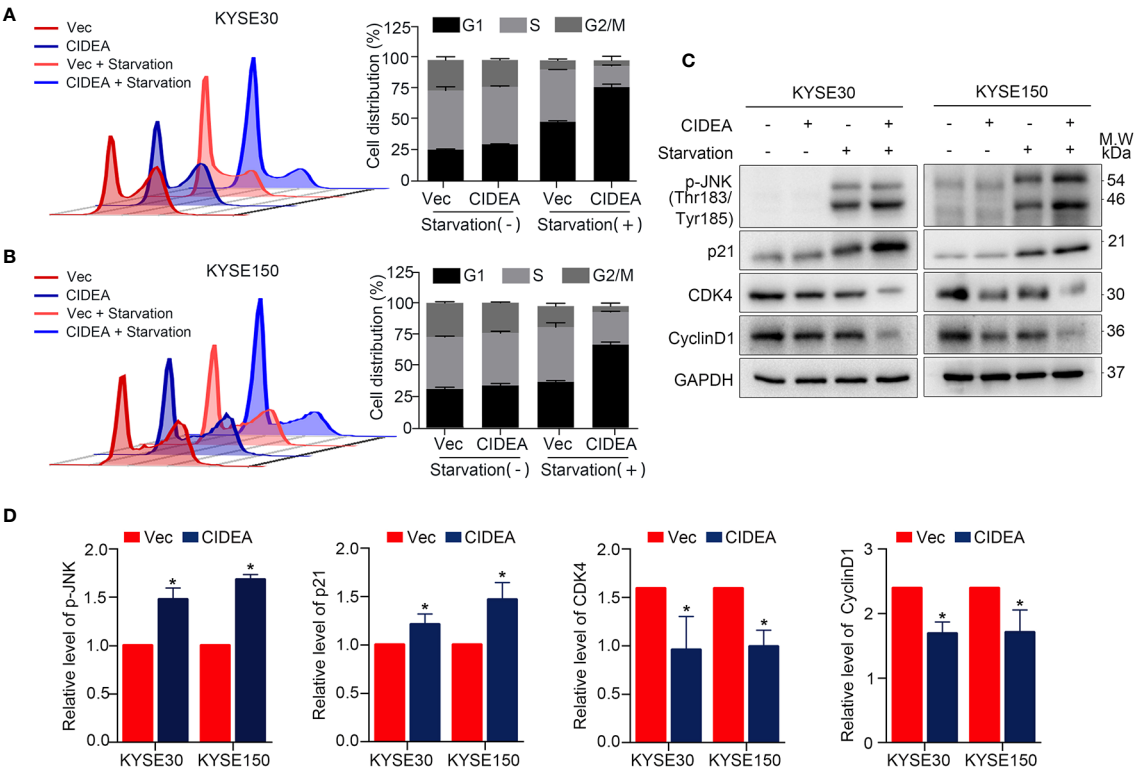

FIGURE 5 | CIDEA blocked G1/S transition in ESCC cells. **(A, B)** Effect of CIDEA overexpression on the cell cycle progression of KYSE30 and KYSE150 cells. **(C)** Expression levels of cell cycle associated molecules were determined by Western blotting in KYSE30 and KYSE150 cells. GAPDH was used as a loading control. **(D)** Quantification of p-JNK, p21, CDK4, and CyclinD1 in KYSE30 and KYSE150 cells treated with serum starvation.

of phosphorylated JNK was greatly increased in CIDEA overexpressing cells compared with control cells (**Figures 5C, D**). Collectively, these data demonstrate that CIDEA inhibits cell growth by promoting cell G1-phase arrest.

Ectopic Expression of CIDEA Promoted Cisplatin-Induced Apoptosis Through the Caspase-Dependent Mitochondrial Pathway

The potential role of CIDEA in apoptosis was explored in CIDEA overexpressing and control cells with or without cisplatin treatment, as cisplatin is a drug that is widely applied in the treatment of ESCC. First, flow cytometric analysis for Annexin V/PI staining was performed. Before cisplatin treatment, the apoptosis rate was found slightly increased in CIDEA overexpressing cells compared to controls. When cells were treated with cisplatin, the apoptosis rate significantly increased in CIDEA overexpressing cells compared with control cells (**Figure 6A**). To evaluate whether the mitochondrial pathway contributed to the cisplatin-induced apoptosis in CIDEA overexpressing cells, changes in MMP were determined *via* JC-1 probe and flow cytometry. A significant decrease in MMP levels and a considerably higher ratio of JC-1 monomers occurred in CIDEA overexpressed cells treated with cisplatin, as shown in **Figure 6B**. Next, cells were subjected to different concentrations of cisplatin for 24 h and the cell viability was determined by CCK-8 assay. As shown in **Figure 6C**, CIDEA reduced the viability of cisplatin treated cells. Finally, the expression levels of apoptosis-associated proteins were examined by Western blotting. Compared with control cells, activated caspase-9 and PARP cleavage were significantly elevated in CIDEA overexpressing cells after cisplatin treatment. Same as the cellular stress caused by starvation, during cisplatin caused DNA damage, the activation of JNK was improved in CIDEA overexpressing cells (**Figures 6D, E**). Together, our results demonstrate that CIDEA, in addition to its function in inhibiting tumor cell growth, can also promote the sensitivity to cisplatin (**Figure 7**), which is an important tumor treatment modality.

DISCUSSION

As one of the most common types of cancer, ESCC is difficult to treat due to its high rate of malignancy, high mortality and relapse rate, and poor therapeutic response. Although great progress has been made in the early diagnosis and treatment of ESCC, the clinical outlook is still not optimistic, and the 5-year survival rate is less than 30% (19). Thus, a better understanding

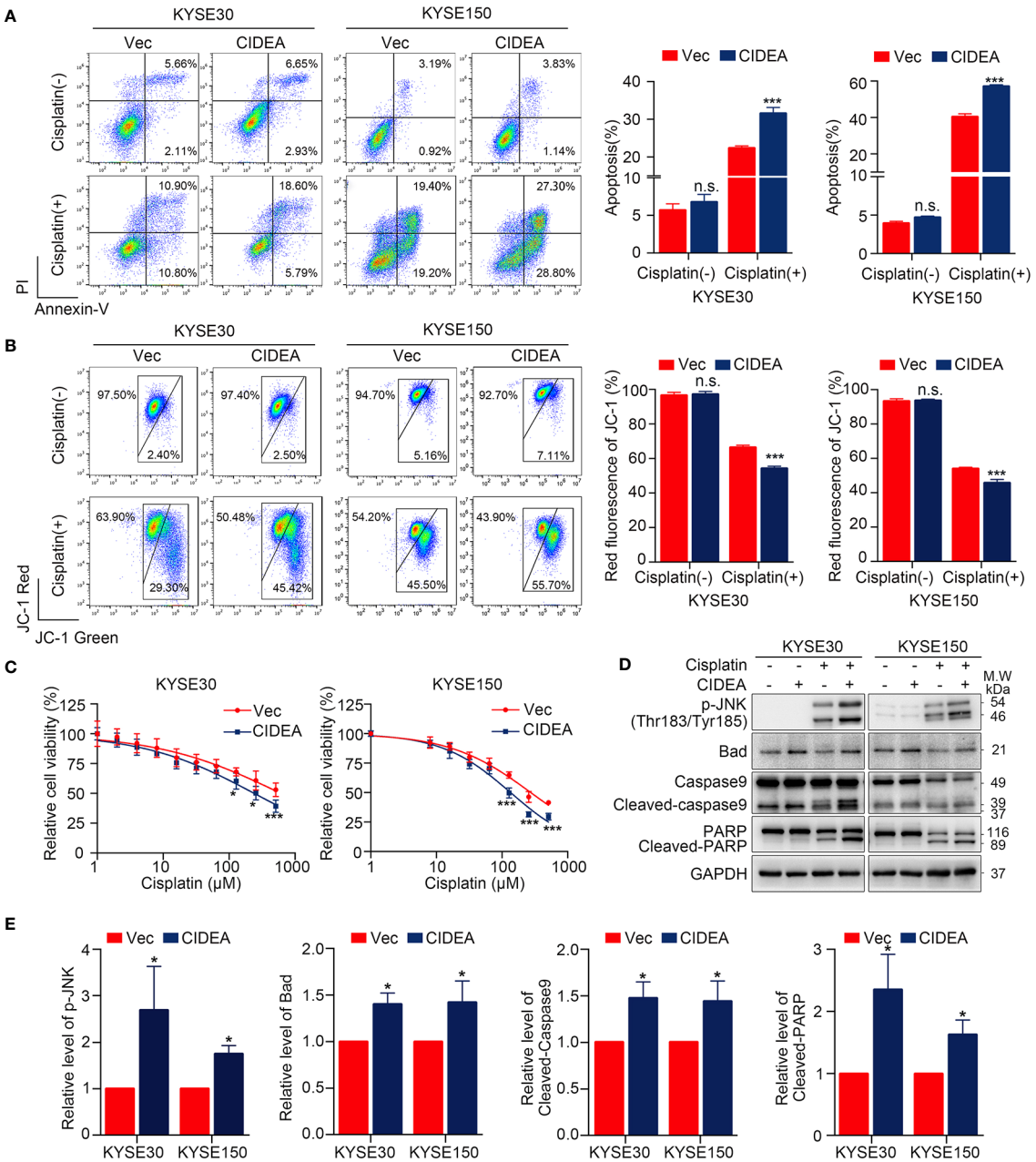

FIGURE 6 | Overexpression of CIDEA promoted apoptosis in ESCC cells. **(A)** Cisplatin treated cells were stained for Annexin V/PI and analyzed FACS. The percentage of Annexin V+ cells is shown. **(B)** Mitochondrial potential was measured by flow cytometry using the JC-1 molecular probe in ESCC cells with or without cisplatin treatment. Enhanced green fluorescence ratio of cells indicated a decrease in mitochondrial potential. **(C)** Cell viability of CIDEA overexpressing cells and control cells treated with different concentrations of cisplatin. **(D)** Caspase-9, PARP, and p-JNK were detected in CIDEA overexpressing cells and control cells with or without cisplatin treatment. **(E)** Quantification of p-JNK, Bad, cleaved-Caspase9, and cleaved-PARP in KYSE30 and KYSE150 cells treated with cisplatin. Statistical data are represented as mean ± SD. $^{*}P < 0.05$; $^{**}P < 0.01$; $^{***}P < 0.001$; n.s., $P > 0.05$.

of esophageal cancer at both the genome and proteome level is of great significance. This would enable clinicians to accurately understand the heterogeneity of patients with esophageal cancer and conduct personalized treatment, not only avoiding unnecessary waste but improving the patient prognosis.

Although CIDEA has been identified and characterized in humans for several decades, but there remains a lack of research focused on the function and clinical significance of CIDEA in ESCC. Here, we explored the anti-oncogenic effect and the potential mechanism of CIDEA in ESCC development and

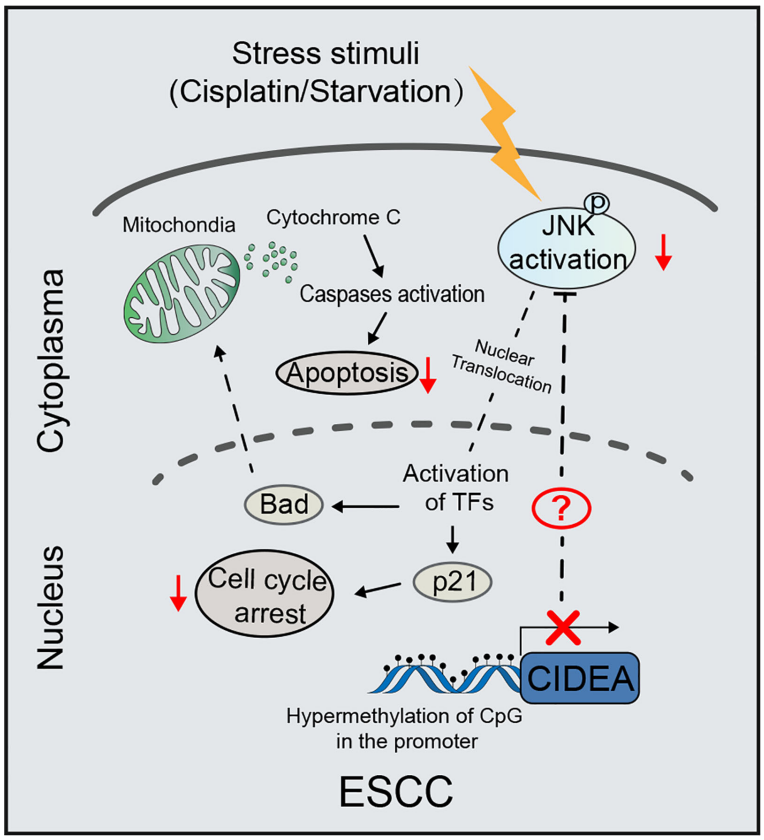

FIGURE 7 | Schematic diagram illustrating the proposed tumor-suppressive mechanism of CIDEA under stress stimuli. In ESCC, the CIDEA is down-regulated due to promoter hypermethylation. When cells are stimulated with cisplatin or starvation, the activation of JNK is inhibited in ESCC with low CIDEA expression. As a result, the cisplatin-induced apoptosis and starvation-induced cell cycle arrest are suppressed. Therefore, we reason that CIDEA promotes the chemosensitivity of esophageal cancer cells to cisplatin and inhibits cell growth *via* the regulation of p-JNK.

progression. Upon the analysis of multiple public databases and our local cohorts, we found that CIDEA is down-regulated in ESCC both at the mRNA and protein levels. Aside from ESCC, public database results also showed that CIDEA was down-regulated in other malignant tumor types such as bladder urothelial carcinoma (BLCA), breast invasive carcinoma (BRCA), glioblastoma multiforme (GBM), head and neck squamous cell carcinoma (HNSC). Additionally, we also found that the down-regulation of CIDEA in ESCC was positively associated with tumor differentiation, TNM stage, lymph node metastasis. Furthermore, survival analysis suggested that CIDEA down-regulation indicated poor prognosis in patients with ESCC, indicating that CIDEA has the potential to serve as a novel prognostic biomarker for ESCC patients.

In cancer, aberrant methylation of CpG islands in DNA promoter regions serves as an important mechanism for the inactivation of tumor suppressor genes (20, 21). An analysis of the 1.5 kb human CIDEA promoter region showed that CpG methylation plays a key role in establishing and maintaining tissue- and cell- specific transcription of the CIDEA gene by regulating Sp1/Sp3 binding (22). This study demonstrated that the promoter hypermethylation is a possible mechanism for inactivation of CIDEA. In addition, hypermethylation of CIDEA was correlated with the poor outcome of ESCC patient. Thus, the identification of changes in CIDEA methylation during the ESCC tumorigenesis is of tremendous importance. This could contribute to early detection and new drug development for ESCC patients (23).

The tumor-suppressive function of CIDEA was demonstrated by both *in vitro* and *in vivo* assays. We showed that ectopic expression of CIDEA effectively suppressed cell proliferation, foci formation, DNA replication, and tumorigenesis in immunodeficient nude mice. Mechanism investigation found that the inhibitory effects of CIDEA on cell proliferation might be due to hindering the transition from G1-phase to S-phase. we found that, during serum starvation, the level of CKD4 and Cyclin D1 significantly decreased and p21 was up-regulated in CIDEA overexpressing cells, which facilitated the G1-phase arrest. Consistent with the previous studies that the JNK pathway can be activated by various stress stimuli like environmental stresses, DNA damage, and inflammatory cytokines (24–26), the level of p-JNK (Thr183/Tyr185) was markedly elevated in CIDEA

overexpressing cells during serum starvation. Besides, the relationship between CIDEA and starvation-related signaling pathways required further experiments to clarify. In summary, we showed that during serum starvation, CIDEA facilitated the phosphorylation and activation of JNK, which in turn led to the activation of nuclear transcription factors. Thus, the transcript level of p21 gene was elevated and cells were arrested in the G1-phase.

Due to the low screening rate and the absence of obvious symptoms in the early stage of ESCC, 80–90% of ESCC cases are diagnosed as advanced ESCC, resulting in a missed opportunity for radical surgery. Platinum-based chemoradiotherapy is the standard treatment for patients with advanced and postoperative recurrent esophageal cancer. However, the chemoresistance is a key factor in the low effectiveness of treatment. Considering the pro-apoptotic role of CIDEA, it is essential to explore whether CIDEA can predict the therapeutic effect of cisplatin in ESCC patient. Our study showed that, the cisplatin-induced apoptosis, which is mainly regulated by the mitochondrial apoptosis pathway, was promoted by CIDEA. This was shown as detectable activation of caspase-9 and an obvious decrease in MMP. In response to cisplatin induced DNA damage, the activation of JNK facilitated by CIDEA promoted the transcription of pro-apoptotic protein (25, 27), including Bad. In addition, the genetic dependency of CIDEA was analyzed in the Cancer Dependency Map (DepMap) (http://depmap.org/portal) (28), which indicated a moderate dependency of CIDEA for esophageal cancer cell survival. Therefore, there should be some other factors to facilitate the tumor suppressor function of CIDEA, which required further experiments to elucidate. Collectively, we provide evidences of an important role for CIDEA in elevating sensitivity of ESCC cells to cisplatin-induced apoptosis, which suggests a potential role for CIDEA in predicting cisplatin response.

In summary, we report that CIDEA was frequently downregulated in ESCC and functions as a tumor-suppressor by regulating ESCC proliferation and apoptosis through the JNK-p21/Bad pathway. Importantly, a better understanding of the role of CIDEA may provide a novel biomarker for predicting the therapeutic effect of cisplatin and survival for patients with ESCC.

DATA AVAILABILITY STATEMENT

The original contributions presented in the study are included in the article/supplementary materials. Further inquiries can be directed to the corresponding author.

ETHICS STATEMENT

The studies involving human participants were reviewed and approved by Institutional Ethics Review Board of the First Associated Hospital (Zhengzhou University). The patients/participants provided their written informed consent to participate in this study. The animal study was reviewed and approved by Institutional Animal Care and Use Committee, Sun Yat-sen University Cancer Center.

AUTHOR CONTRIBUTIONS

Y-PG, LL: acquisition, analysis, and interpretation of data. Y-PG: drafting of the manuscript. JY, X-XH, Y-XJ, X-YG, and Z-WC: technical and material support; Y-RQ: study design and supervision. All authors contributed to the article and approved the submitted version.

FUNDING

This work was supported by the National Natural Science Foundation of China (81772554, 8187111604, 82072604 and 82072738), the Basic and Applied Basic Research Foundation of Guangdong Province (2019A1515110660).

ACKNOWLEDGMENTS

We thank Jia-Rong Zhan from the Sun Yat-sen University for assistance of bioinformatics analysis.

REFERENCES

1. Bray F, Ferlay J, Soerjomataram I, Siegel RL, Torre LA, Jemal A. Global cancer statistics 2018: GLOBOCAN estimates of incidence and mortality worldwide for 36 cancers in 185 countries. *CA Cancer J Clin* (2018) 68(6):394–424. doi: 10.3322/caac.21492
2. Zhang Y. Epidemiology of esophageal cancer. *World J Gastroenterol* (2013) 19 (34):5598–606. doi: 10.3748/wjg.v19.i34.5598
3. Yoshimizu S, Yoshio T, Ishiyama A, Tsuchida T, Horiuchi Y, Omae M, et al. Long-term outcomes of combined endoscopic resection and chemoradiotherapy for esophageal squamous cell carcinoma with submucosal invasion. *Dig Liver Dis* (2018) 50(8):833–8. doi: 10.1016/j.dld.2018.01.138
4. Rustgi AK, El-Serag HB. Esophageal carcinoma. *N Engl J Med* (2014) 371 (26):2499–509. doi: 10.1056/NEJMra1314530
5. Deng M, Brägelmann J, Schultze JL, Perner S. Web-TCGA: an online platform for integrated analysis of molecular cancer data sets. *BMC Bioinf* (2016) 17:72. doi: 10.1186/s12859-016-0917-9
6. Cerami E, Gao J, Dogrusoz U, Gross BE, Sumer SO, Aksoy BA, et al. The cBio cancer genomics portal: an open platform for exploring multidimensional cancer genomics data. *Cancer Discovery* (2012) 2(5):401–4. doi: 10.1158/2159-8290.CD-12-0095
7. Inohara N, Koseki T, Chen S, Wu X, Núñez G. CIDE, a novel family of cell death activators with homology to the 45 kDa subunit of the DNA fragmentation factor. *EMBO J* (1998) 17(9):2526–33. doi: 10.1093/emboj/17.9.2526
8. Erdtmann L, Franck N, Lerat H, Le Seyec J, Gilot D, Cannie I, et al. The hepatitis C virus NS2 protein is an inhibitor of CIDE-B-induced apoptosis. *J Biol Chem* (2003) 278(20):18256–64. doi: 10.1074/jbc.M209732200
9. Liu K, Zhou S, Kim JY, Tillison K, Majors D, Rearick D, et al. Functional analysis of FSP27 protein regions for lipid droplet localization, caspase-dependent apoptosis, and dimerization with CIDEA. *Am J Physiol Endocrinol Metab* (2009) 297(6):E1395–413. doi: 10.1152/ajpendo.00188.2009
10. Zhou Z, Yon Toh S, Chen Z, Guo K, Ng CP, Ponniah S, et al. Cidea-deficient mice have lean phenotype and are resistant to obesity. *Nat Genet* (2003) 35 (1):49–56. doi: 10.1038/ng1225
11. Li JZ, Ye J, Xue B, Qi J, Zhang J, Zhou Z, et al. Cideb regulates diet-induced obesity, liver steatosis, and insulin sensitivity by controlling lipogenesis and fatty acid oxidation. *Diabetes* (2007) 56(10):2523–32. doi: 10.2337/db07-0040

12. Hallberg M, Morganstein DL, Kiskinis E, Shah K, Kralli A, Dilworth SM, et al. A functional interaction between RIP140 and PGC-1alpha regulates the expression of the lipid droplet protein CIDEA. *Mol Cell Biol* (2008) 28 (22):6785–95. doi: 10.1128/MCB.00504-08
13. Li F, Gu Y, Dong W, Li H, Zhang L, Li N, et al. Cell death-inducing DFF45-like effector, a lipid droplet-associated protein, might be involved in the differentiation of human adipocytes. *FEBS J* (2010) 277(20):4173–83. doi: 10.1111/j.1742-4658.2010.07806.x
14. Chatterjee A, Mondal P, Ghosh S, Mehta VS, Sen E. PPARγ regulated CIDEA affects pro-apoptotic responses in glioblastoma. *Cell Death Discovery* (2015) 1:15038. doi: 10.1038/cddiscovery.2015.38
15. Jia Y, Gao Y, Li J, Chang Z, Yan J, Qin Y. Prognostic implications of MYBL2 in resected Chinese gastric adenocarcinoma patients. *Onco Targets Ther* (2019) 12:1129–35. doi: 10.2147/OTT.S188820
16. Yang H, Su H, Hu N, Wang C, Wang L, Giffen C, et al. Integrated analysis of genome-wide miRNAs and targeted gene expression in esophageal squamous cell carcinoma (ESCC) and relation to prognosis. *BMC Cancer* (2020) 20 (1):388. doi: 10.1186/s12885-020-06901-6
17. Su H, Hu N, Yang HH, Wang C, Takikita M, Wang QH, et al. Global gene expression profiling and validation in esophageal squamous cell carcinoma and its association with clinical phenotypes. *Clin Cancer Res* (2011) 17 (9):2955–66. doi: 10.1158/1078-0432.CCR-10-2724
18. Modhukur V, Iljasenko T, Metsalu T, Lokk K, Laisk-Podar T, Vilo J. MethSurv: a web tool to perform multivariable survival analysis using DNA methylation data. *Epigenomics* (2018) 10(3):277–88. doi: 10.2217/epi-2017-0118
19. Lagergren J, Smyth E, Cunningham D, Lagergren P. Oesophageal cancer. *Lancet* (2017) 390(10110):2383–96. doi: 10.1016/S0140-6736(17)31462-9
20. Lakshminarasimhan R, Liang G. The Role of DNA Methylation in Cancer. *Adv Exp Med Biol* (2016) 945:151–72. doi: 10.1007/978-3-319-43624-1_7
21. Jones PA. Functions of DNA methylation: islands, start sites, gene bodies and beyond. *Nat Rev Genet* (2012) 13(7):484–92. doi: 10.1038/nrg3230
22. Li D, Da L, Tang H, Li T, Zhao M. CpG methylation plays a vital role in determining tissue- and cell-specific expression of the human cell-death-inducing DFF45-like effector A gene through the regulation of Sp1/Sp3 binding. *Nucleic Acids Res* (2008) 36(1):330–41. doi: 10.1093/nar/gkm1028
23. Viswakarma N, Yu S, Naik S, Kashireddy P, Matsumoto K, Sarkar J, et al. Transcriptional regulation of Cidea, mitochondrial cell death-inducing DNA fragmentation factor alpha-like effector A, in mouse liver by peroxisome proliferator-activated receptor alpha and gamma. *J Biol Chem* (2007) 282 (25):18613–24. doi: 10.1074/jbc.M701983200
24. Yosef R, Pilpel N, Papismadov N, Gal H, Ovadya Y, Vadai E, et al. p21 maintains senescent cell viability under persistent DNA damage response by restraining JNK and caspase signaling. *EMBO J* (2017) 36(15):2280–95. doi: 10.15252/embj.201695553
25. Dhanasekaran DN, Reddy EP. JNK-signaling: A multiplexing hub in programmed cell death. *Genes Cancer* (2017) 8(9-10):682–94. doi: 10.18632/genesandcancer.155
26. Kumar A, Singh UK, Kini SG, Garg V, Agrawal S, Tomar PK, et al. JNK pathway signaling: a novel and smarter therapeutic targets for various biological diseases. *Future Med Chem* (2015) 7(15):2065–86. doi: 10.4155/fmc.15.132
27. Picco V, Pagès G. Linking JNK Activity to the DNA Damage Response. *Genes Cancer* (2013) 4(9-10):360–8. doi: 10.1177/1947601913486347
28. Tsherniak A, Vazquez F, Montgomery PG, Weir BA, Kryukov G, Cowley GS, et al. Defining a Cancer Dependency Map. *Cell* (2017) 170(3):564–76.e16. doi: 10.1016/j.cell.2017.06.010

Conflict of Interest: The authors declare that the research was conducted in the absence of any commercial or financial relationships that could be construed as a potential conflict of interest.

frontiers in Oncology

REVIEW
published: 16 April 2021
doi: 10.3389/fonc.2021.641304

The Sensitivity Prediction of Neoadjuvant Chemotherapy for Gastric Cancer

Juan Sun[1,2†], *Xianze Wang*[1,2†], *Zimu Zhang*[1,2], *Ziyang Zeng*[1,2], *Siwen Ouyang*[1,2] *and Weiming Kang*[1,3*]

[1] Chinese Academy of Medical Sciences and Peking Union Medical College, Beijing, China, [2] Peking Union Medical College Hospital (CAMS), Beijing, China, [3] Department of General Surgery, Peking Union Medical College Hospital (CAMS), Beijing, China

OPEN ACCESS

Edited by:
Xia Li,
Shenzhen Institutes of Advanced Technology (CAS), China

Reviewed by:
Maria Principia Scavo, National Institute of Gastroenterology S. de Bellis Research Hospital (IRCCS), Italy
Lais Palhares, Federal University of Rio Grande do Norte, Brazil
Yee Ung, Sunnybrook Health Sciences Centre, Canada

***Correspondence:**
Weiming Kang
kangweiming@163.com

†These authors share first authorship

Specialty section:
This article was submitted to Gastrointestinal Cancers, a section of the journal Frontiers in Oncology

Received: 14 December 2020
Accepted: 22 March 2021
Published: 16 April 2021

Citation:
Sun J, Wang X, Zhang Z, Zeng Z, Ouyang S and Kang W (2021) The Sensitivity Prediction of Neoadjuvant Chemotherapy for Gastric Cancer. Front. Oncol. 11:641304. doi: 10.3389/fonc.2021.641304

The overall efficacy of neoadjuvant chemoradiotherapy (NACT) for locally advanced gastric cancer (LAGC) has been recognized. However, the response rate of NACT is limited due to tumor heterogeneity. For patients who are resistant to NACT, not only the operation timing will be postponed, patients will also suffer from the side effects of it. Thus, it is important to develop a comprehensive strategy and screen out patients who may be sensitive to NACT. This article summarizes the related research progress on the sensitivity prediction of NACT for GC in the following aspects: microRNAs, metabolic enzymes, exosomes, other biomarkers; inflammatory indicators, and imageological assessments. The results showed that there were many studies on biomarkers, but no unified conclusion has been drawn. The inflammatory indicators are related to the survival and prognosis of patients under NACT. For imageological assessments such as CT, MRI, and PET, with careful integration and optimization, they will have unique advantages in early screening for patients who are sensitive to NACT.

Keywords: gastric cancer, biomarkers, inflammatory indicators, imageological assessments, neoadjuvant chemotherapy

INTRODUCTION

Gastric cancer (GC) is one of the most common digestive system tumors. According to GLOBOCAN estimates in 2018, the prevalence of GC ranks the fifth among all cancers, with approximately 1.034 million new cases worldwide. Meanwhile, GC-related deaths rank the third, with more than 783,000 patients annually (1). In China, there were 679,000 new cases and 498,000 deaths in 2015, which accounted for 42.6 and 45% of the global total, respectively (2).

Since early-stage GCs are absent of specific symptoms, 80–90% of GC patients are in the advanced stages at their first visits (3, 4), and the proportion of patients with stage II–III GCs in China is as high as 58.0% (5). Surgery is the main treatment for GC, but the long-term survival rate of LAGC patients after surgery is still less than 20–30% (4). Therefore, the NACT which aims at improving the prognosis of LAGC patients came into being. The superiorities of NACT, such as reducing the tumor size, achieving the complete pathological remission (PR), increasing the R0 resection rate, improving the overall survival (OS) and disease-free survival (DFS), have been

verified by numerous large-scale RCTs (6–8). In 2007, NACT was officially adopted by NCCN guidelines, and it has become the standard treatment for LAGC patients since then (5).

However, due to the tumor heterogeneity, the clinical response rate of NACT is barely satisfactory (9). For patients who are resistant to NACT, the operation timing is postponed while the primary tumor may progress during the treatment. More than that, the NACT-induced adverse events which could have been avoided, may deteriorate the general condition of those patients (10, 11). Therefore, mining the reliable indicators that can predict the sensitivity of chemotherapy is in great need, so as to screen out GC patients who are suitable for NACT. In addition, the optimal course of NACT is still uncertain, so monitoring indicators can help to evaluate the efficacy of NACT and select the appropriate surgical timing in real time. All of the above are hot topics which can boost the effect of NACT and help achieve the individualized treatments for GC patients.

In this article, we reviewed six categories of indicators which showed promising effects in predicting and monitoring the sensitivity and efficacy of NACT in GC treatment. Although most of them have not been studied thoroughly and few conclusions have been drawn, it will inspire us to design a well-organized and individual-oriented NACT strategy for GC patients.

miRNA

MicroRNA (miRNA) is a type of non-coding single-stranded small RNA molecule with a length of about 18–25 nucleotides, and more than 900 miRNAs have been identified (12). By binding to the 3 ′UTRs of mRNAs, miRNAs regulate the expression of more than one-third of genes and participate in varies biological processes (13). Recently, studies have shown that the abundance of some miRNAs may help to explain the mechanisms of chemotherapy; thus, the variation of them can be used for chemoresistance monitoring (**Table 1**).

Apoptosis

Drug induced endogenous and exogenous apoptosis in cancer cells is one of the main mechanisms of chemotherapy (14). However, this process can be impaired by miRNAs *via* regulating the expression of certain genes, which participate in apoptosis-related signaling pathways.

BCL-2 is one of the most important anti-apoptotic genes and is also frequently regulated by miRNAs. In 2008, Xia et al. (15) found that miR-15b and miR-16 were down-regulated in GC-resistant cell lines SGC7901/VCR. Meanwhile, over-expression of miR-15b and miR-16 can increase the apoptosis of normal GC cells (SGC7901) by inhibiting the expression of the BCL-2, thereby reducing the resistance to adriamycin (ADR),

TABLE 1 | The potential mechanism of miRNAs for causing chemotherapy resistance in GC.

Mechanism		miRNAs	Target(s)	Expression	Drug
Apoptosis	**BCL-2**	miR-15b, miR-16, miR-200bc/429	BCL-2	↓	DDP,ADR, VCR,VP-16
		miR-497			DDP, ADR, VP-16
		miR-1217, miR-143, miR-136			DDP
		miR-429			5-FU
		miR-181b			5-FU,DDP, ADR,VCR, VP-16
		miR-204			5-FU,OXA
	PI3K/Akt	miR-193-3p, miR-147	PTEN	↑	5-FU
		miR-106a, miR-21-5p			DDP
		miR-4295	LRIGI		
		miR-375	ERBB2	↓	
		miR-126	EGFA		
		miR-19a/b	PTEN	↑	DDP, ADR,5-FU
		miR-316-5p	FOXMI	↓	Docetaxel
	MAPK	miR-206	MAPK	↓	DDP
		miR-135b-5p	MSTI, KLF4	↑	
	NF-κB	miR-145	APRIL	↓	DDP
		miR-20a	CYLD	↑	
	Cell cycle arrest	miR-31	ZH2	↓	5-FU
		miR-223	FBXW7	↑	DDP
Elevated drug efflux		miR-27a	BCL-2, P-gp, LRP	↓	OXA
		miR-508-5p	ABCBI, ZNRDI		5-FU,DDP, VCR,ADR
		miR-361-3p	ABCBI		OXA
		miR-21	P-gp	↑	PTX
		miR-19a/b			ADR
Autophagy		miR-30a	LC3-II	↓	DDP
		miR-181a	ATG5		
		miR-23b-3p	ATGI2		5-FU,DDP, VCR
		miR-148a-3p	AKAPI, RABI2		DDP
Drug targets		miR-34c-5p	MAPT	↓	PTX

ADR, doxorubicin; VCR, vincristine; Vp-16, etoposide; DDP, cisplatin; PTX, paclitaxel; 5-FU, fluorouracil; OXA, oxaliplatin.
Expression level: Upregulation(↑) or down-regulation(↓) of miRNA in drug-resistant GC cell lines compared with that in parental cells.

vincristine (VCR), etoposide (VP-16), and cisplatin (DDP). Later, more mechanisms have been proposed to explain the miRNA-mediated chemotherapy resistance of GC cells on BCL-2, such as miR-200bc/429, miR-1217, miR-143, and so on (16–18). These results partially elaborated the chemoresistance to DDP, 5-FU, *etc*, as well as the multidrug resistance (MDR).

In addition to BCL-2 protein, miRNA can also regulate the apoptosis of GC cells induced by chemotherapy drugs through other pathways. For example, miR-193-3p (19), miR-147 (20), miR-106a (21), miR-21-5p (22), and miR-19a /b (23) are all highly expressed in drug-resistant GC cell lines, and reducing their expression will inhibit the PI3K/Akt cellular signal transduction pathway of by promoting the expression of PTEN, thus promoting the apoptosis of GC cells. Additionally, up-regulating miR-206 (24) expression can weaken the proliferation of drug-resistant GC cells, facilitate cell apoptosis, and decrease DDP resistance *via* targeted inhibition of MAPK3 (mitogen activating protein kinase 3) expression. The down-regulation of miR-135b-5p (25) induced apoptosis, and it inhibited proliferation and DDP resistance of GC cells by inactivating the MAPK signaling pathway and increasing the expression of MST1 (mammalian ste20-like kinase 1). The canonical NF-κB pathway was involved in DDP resistance too. For example, miR-145 (26) regulated the sensitivity of GC cells to DDP by regulating the expression of APRIL (a proliferation-inducing ligand) through NF-κB pathway. MiR-20a (27) directly repressed the expression of CYLD (cylindromatosis), leading to activation of the NF-κB pathway and the downstream targets, livin and survivin (members of the inhibitor of apoptosis protein family, function as anti-apoptotic factors), which potentially induced GC chemoresistance. Moreover, miR-31 (28) and miR-223 (29) lead to apoptosis by blocking the cell cycle in the DNA replication process, thus enhancing the chemotherapy sensitivity of 5-FU and DDP for GC.

Elevated Drug Efflux

Chemotherapy resistance in GC is also associated with drug efflux caused by the overexpression of some membrane transporters, the most important of which is the ATP-binding cassette (ABC) transporter family (30, 31), which is represented by P-glycoprotein (P-gp), which can pump anti-tumor drugs from inside to outside so that tumor cells can escape from the cytotoxic effect of and show resistance to chemotherapy drugs (30).

Some studies have conducted in-depth studies on the relationship between miRNA and GC chemotherapy resistance from the perspective of P-gp pathway. A study published by Zhao (32) in 2011 showed that down-regulation of miR-27a could significantly reduce the expression of P-gp and decrease the transport of ADR, leading to the accumulation of ADR in GC cells, thus enhancing the sensitivity of chemotherapy. Further studies by Zhao (33) in 2015 showed that hypoxia-inducible factor (HIF)-1 radiation influenced the expression of P-gp, LRP, and BCL-2 by regulating miR-27a, resulting in chemotherapy resistance of GC cells. In addition, miR-19a/b (23), miR-508-5p (34), miR-30a (35), miR-21 (36) and miR-361-3p (37) have also been proved to increase the excretion of chemotherapy drugs by regulating the expression of P-gp on the membranes of GC cells, resulting in decreased sensitivity to chemotherapy.

Other Pathways for GC Chemo-Resistance

The mechanism of GC chemotherapy resistance is very complicated. In addition to the abovementioned apoptosis, cell cycle changes, and efflux of chemotherapy drugs, there are other mechanisms involved, such as autophagy and changes in drug targets.

In normal cells, autophagy can play an anticancer role by maintaining gene stability, while in cancer cells, autophagy can provide energy to cancer cells and promote the survival of tumor cells under stressful conditions, such as radiotherapy or chemotherapy (38). MiRNAs can also regulate the autophagy of tumor cells, causing drug resistance to NACT. For example, miR-30a (39), miR-181a (40), and miR-148a-3p (41) were confirmed to have low expression in drug-resistant GC cells, and *in vivo* and *in vitro* experiments showed that they all caused DDP resistance by regulating the autophagy of GC cells. Additionally, miR-23b-3p (42) leads to enhanced autophagy of GC cells through targeted regulation of ATGI2 (autophagy-related gene 12), thereby causing drug resistance to DDP, 5-FU, and VCR.

The changes in the chemotherapy drug targets caused by miRNA in GC have also been investigated. In 2013, Wu (43) reported that mir-34c-5p can regulate the expression of microtubule-associated protein tau (MAPT), which can stabilize the microtubule structure by promoting the accumulation of tubule proteins into microtubules. They found that the decreased expression of miR-34c-5p in paclitaxel-resistant GC tissues was accompanied by the increase of MAPT levels. Upon regulation of miR-34c-5p, the expression of MAPT was significantly reduced, leading to the increased sensitivity of drug-resistant GC cells to paclitaxel (PTX).

MicroRNA plays important roles in cell development, proliferation, differentiation, apoptosis, gene regulation, and disease occurrence, especially in the development of tumors and drug resistance. Changing the expression level of miRNA in tumors is expected to become a new treatment strategy. With the deepening of research, more and more miRNAs will become molecular markers to judge the sensitivity and prognosis of tumor treatment, guide individualized treatment, and improve the tumor therapeutic effect.

METABOLIC ENZYMES RELATED TO FLUOROURACIL RESISTANCE

Regarding NACT for GC, NCCN guidelines have been updated continuously in recent years. Fluorouracil and cisplatin (FP) were classified as a category 1 recommendation in 2013, and fluorouracil and oxaliplatin were classified as a category 2A recommendation in 2017. In 2018, docetaxel, oxaliplatin, leucovorin, and fluorouracil (FLOT) were listed as a category 1 recommendation for NACT of GC (5). Therefore, fluorouracil is always used in NACT for GC, but due to its drug resistance, the single-drug effective rate of 5-FU is only 20%, and the overall

effective rate of the first-line chemotherapy based on 5-FU is less than 40%; thus some patients cannot benefit from NACT (44). Therefore, it has become an urgent problem to explore the indicators related to the sensitivity of 5-FU drugs to chemotherapy. Among them, thymidylate synthase (TS), thymidine phosphorylase (TP) and dihydropyrimidine dehydrogenase (DPD) are the research hotspots.

5-FU is a thynoside synthase inhibitor. When 5-FU penetrates tumor cells, it is converted into fluorouracil deoxynucleotide (Fd UMP), which is covalently combined with reduced tetrahydrofolic acid (CH2FH4) and TS, forming a ternary complex to inhibit the activity of TS and interfere with DNA synthesis of tumor cells (45). TP is the last rate-limiting enzyme for the conversion of 5-FU prodrugs to fluorouracil. After oral administration of the drug into the body, 5-FU is converted into 5-fluoro-2-deoxyuracil nucleotide (Fd Urd) in the liver. On the one hand, the drug is converted into Fd UMP to inhibit TS. On the other hand, the drug is catalyzed into 5-FU by TP (46). DPD is the starting and rate-limiting enzyme of 5-FU catabolism. More than 85% of 5-FU is reduced into inactive metabolites by DPD in liver and other tissues, which are excreted by the kidney; thus, the activity of DPD is closely related to the efficiency of 5-FU (47). Therefore, the relationship between the expression levels of the enzymes TS, TP, and DPD and the chemotherapy sensitivity and prognosis of patients with GC to 5-FU is still a hot topic in the field of NACT.

Initially, in 2000, Salonga (48) found that colon cancer patients with low expression levels of DPD, TS, and TP before chemotherapy were sensitive to 5-FU. Subsequently, in 2002, Tershima (49) reported that the activity of DPD in GC tissues could predict the chemotherapy sensitivity and drug resistance of tumors to 5-FU. In 2004, Wang (50) detected overexpressed TS in the analysis of 5-FU-resistant cancer cell lines by DNA microarray, and Etienne (51) also confirmed that TS was closely related to the chemotherapy sensitivity of 5-FU. In the same year, Ma (52) evaluated four kinds of GC cells and three kinds of colon cancer cells and found that cell lines with low DPD expression level were more sensitive to 5-FU, and DPD mRNA could not even be detected in the most sensitive cell line HCT-8. At the same time, it was found that TS may contribute greatly to the sensitivity of FdUrd, and the higher the TS mRNA levels, the higher the IC50 (50% growth inhibitory concentration) of FdUrd. Then Napieralski (53) found that patients with high DPD expression were insensitive to 5-FU and had poor prognosis, while patients with low DPD expression were just the opposite. Sasako M (54) showed that high TS and DPD gene expression in tumors was associated with enhanced benefit from postoperative adjuvant S-1 treatment in gastric cancer. Later in 2016, a meta-analysis covered 555 patients with GC treated with S-1 showed that there was a significant difference in ORR (objective response rate) between patients with high/+ and low/− expression of DPD (55).

It can be seen from the above studies that the enzymes related to fluorouracil metabolism have always been the focus of NACT, but they are mainly limited to *in vitro* experiments; thus, the systematic *in vivo* experiments on NACT of GC still require further exploration.

EXOSOMES

Exosomes are also one of the star molecules in new biomarkers. They are small lipid bilayer extracellular vesicles loading a variety of cargo, including DNA, mRNA, miRNA, circular RNA, protein, *etc* (56), typically 30–100 nm in size, and can be detected in various biological fluids, such as serum, urine and saliva (57). More and more reports have shown that exosomes play an important role in tumor growth, metastasis, angiogenesis and immune regulation by acting as information communicators (58–60). Moreover, exosomes have recently been found to be involved in the regulation of cancer chemoresistance (61–63), GC is surely included.

In 2020 Sun MY (64) demonstrated that RPS3 (Ribosomal Protein S3) expression levels were significantly elevated in cisplatin-resistant gastric cancer cell line SGC7901 and the exosomal delivery of RPS3 might induce chemoresistance phenotypes from cisplatin-resistant gastric cancer cells to sensitive cancer cells by regulating the PI3K-Akt-cofilin-1 signaling pathway. And Zhang QM (65) indicated that exosomes with si-c-Met can inhibit the invasion and migration of GC cells and promote apoptosis *in vitro* and inhibit tumor growth *in vivo*, reversing the resistance to cisplatin in GC.

In addition to proteins, RNAs in exosomes were also found to be associated with chemosensitivity in GC. Zhang HY (66) showed that cisplatin and paclitaxel promoted exosomal miR-522 secretion from CAFs (cancer-associated fibroblasts), leading to ALOX15 (arachidonate lipoxygenase 15) suppression and decreased lipid-ROS (toxic lipid peroxides) accumulation in GC cells, and ultimately result in decreased chemo-sensitivity. Furthermore, it was reported that exosome miR-155-5p directly inhibits GATA3 (GATA binding protein 3) and TP53INP1 (tumor protein p53-induced nuclear protein 1) to induce paclitaxel resistant GC cells to sensitive ones (67). And Wang SM (68) found that exosomal circPRRX1 (circular paired-related homeobox 1) strengthened doxorubicin resistance of GC cells by modulating miR-3064-5p/PTPN14 (non-receptor tyrosine phosphatase 14) signaling pathway.

Exosomes contain not only proteins but also a significant amount of nucleic acids, including DNA, mRNAs, miRNAs, circular RNAs (circRNAs) and long non-coding RNAs (lncRNAs) (69), as well as cholesterols, diglycerides, phospholipids, glycerophospholipids, sphingomyelins, and ceramides (70). In order to identify more sensitive and specific exosomes to guide individual chemotherapy choices, future studies should further clarify the roles and potential mechanisms of exosomes in cancer with more chemotherapeutic drugs.

OTHER CHEMOTHERAPY-RELATED BIOMARKERS

Biomarkers are the most cutting-edge research direction for the prediction of the chemotherapy sensitivity of GC. In addition to miRNAs and fluorouracil metabolic enzymes, glutathione S-transferase (GST) is also involved. In 2006, Goekkurt (71) analyzed the polymorphism of GST genes in 52 patients

withLAGC who received 5-Fu or DDP in NACT and found that the efficacy in patients with the GSTP-105Val/Val gene subtype (67%) was better than those with at least one 105Ile allele (21%).

In 2017, Li (72) detected the expression of P-glycoprotein (P-gp), glutathione S-transferase-π (GST-π), topoisomerase II (topo II), multidrug resistance gene-associated protein (MRP), lung resistance-related protein (LRP), Ki-67, and p53 in cancer tissues of 93 elderly patients with AGEJ (adenocarcinoma of gastroesophageal junction) before NACT and then analyzed the relationship between the expression of these proteins and the curative effect of NACT. The results showed that only the expressions levels of ki-67 ($p = 0.003$) and p53 ($p = 0.009$) were significantly correlated with the sensitivity to NACT, and the increased expression of ki-67 and the decreased expression of p53 predicted the SOX insensitivity of elderly patients with AGEJ.

In 2019, Hashimoto (73) compared the mismatch repair genes MLH-1 and PD-L1 of 110 GC patients who received different NACTs with 175 patients who did not receive any NACT and found that the NACT response of MLH1-negative patients was significantly lower than that of MLH1-positive patients (16.7 *vs.* 61.2%, $P = 0.005$), while there was no significant difference between patients with high and low PD-L1 expression (55.9 *vs.* 56.6%, $P = 0.95$). Therefore, it is recommended that MLH1-negative patients with GC should be treated with surgery alone, while patients with other types of GC should be treated with a combination of surgery and preoperative or postoperative chemotherapy. The study also showed that poor prognosis of MLH1-positive patients with GC can be improved by NACT. At the same time, PD-L1 expression did not have any predictive characteristics for prognosis or NACT response.

With the characterization of more biomarkers and the improvement of various detection levels, a growing number of markers such as tumor markers (for example, CEA, CA19-9, CA153, CA72-4, AFP) (74), circulating free DNA (cfDNA) (75), and circulating tumor cells (CTC) (76), were used to predict the sensitivity of NACT for GC to provide clinical evidence of individualized diagnoses and treatment plans. However, due to the small sample size, different chemotherapy options, and the presence of so many biomarkers, but very few with specificities, the use of biomarkers to specifically predict the sensitivity of NACT for GC still requires our further efforts and exploration.

INFLAMMATORY MARKERS

Some studies have found that the occurrence and development of tumors are closely related to systemic inflammatory responses (77), and some of the inflammatory markers may be associated with the effectiveness of NACT (78). A 2014 study by Borsig (79) noted that peripheral blood tests can reflect the level of inflammation at the time of tumorigenesis and that inflammatory markers such as C-reactive protein (CRP), white blood cells (WBC), and neutrophil–lymphocyte ratio (NLR) and platelet–lymphocyte ratio (PLR) can all be used as prognostic factors for patients with various malignancies. In LAGC, high NLR is considered to be an effective predictor of survival, and in 2014, Mohamed (80) found that a high level of NLR indicates a worse PFS (progression free survival) and OS (overall survival) in patients with LAGC undergoing NACT. The Glasgow prognostic score (GPS), which is calculated from CRP and serum albumin (ALB), is considered as a comprehensive indicator reflecting the systemic inflammatory response and nutritional status. Studies have shown that in some tumors, GPS is related to the effectiveness of NACT and prognosis. In patients with AGEJ, an increase in GPS score may indicate a decrease in the tolerance and efficacy of NACT and a reduction in survival time.

In the tumor microenvironment, macrophages are known as tumor-associated macrophages (TAMs), which are one of the most abundant immune cells. The degree of TAMs' infiltration in tumor tissues was positively correlated with the adverse prognosis of various tumors, including GC. TAMs promote tumor progression by secreting a variety of inflammatory factors, including growth factors, chemokines, and cytokines (81). Macrophages are divided into M1 and M2 types. M1 macrophages have pro-inflammatory effects, producing various cytokines and chemokines, such as IL-12 (interleukin 12), CXCL9 (C-X-C motif ligand 9), and TNF-α (tumor necrosis factor-α) (82). M2 macrophages produce anti-inflammatory cytokines, such as TGF-β (transforming growth factor-β) and IL-10 (83). In the GC mouse models, macrophages were recruited by chemokines and cytokines derived by epithelia (84–89), and they produced pro-inflammatory cytokines such as TNF-α and stimulated tumor growth (88, 90). Moreover, the depletion of macrophages in these mouse models inhibited the proliferation and tumorigenesis of epithelia (87, 89, 90). Besides, gene expression and a novel associated cytokine panel were also linked to GC metastasis. For example, in 2020 Qeadan (91) found that MK2 (Map kinase-activated protein kinase 2) expression and a panel of associated cytokines secreted by GC cells, including G-CSF (granulocyte colony-stimulating factor), GM-CSF (granulocyte-macrophage colony-stimulating factor), Mip-1β (macrophage inflammatory protein-1β), IFN-α (interferon-α), MCP-1 (monocyte chemotactic protein 1), IL-1β, IL-6, and TNF-α to be linked to GC metastasis. But more future studies are needed to clarify the precise role of macrophages, cytokines, and other inflammatory markers in the NACT of GC.

CT, MRI, PET AND OTHER IMAGING EVALUATION INDICATORS

At present, the evaluation of the efficacy of chemotherapy for GC is still mainly based on the response evaluation criteria in solid tumors (RECIST) and WHO (World Health Organization) standards, which are evaluated by measuring the changes of maximum diameter and area of tumors before and after chemotherapy (92, 93). However, the stomach is a cavity organ, thus changes in its wall thickness, peristalsis, tumor morphology, and measurement angle will make the measurements of lesion size inaccurate (94). Theoretically, the morphological changes are the result of changes in the biological behavior of the lesion. After NACT, the lesions should have already changed functionally before morphological changes occurred, mainly manifesting as

the reduction of tumor local blood perfusion (95). Therefore, if imageological assessments can be used to observe tumor-associated vessels in GC patients, it would be of great clinical significance.

In 2014, Hansen found that after chemotherapy for GC, the tumor volume and surface permeability value (an indicator of tumor local vascular permeability) in CT (computed tomography) perfusion parameters both decreased significantly (96). Moreover, energy spectral CT can accurately reflect the true iodine concentration (97), and iodine concentration can accurately reflect the blood supply and vascular conditions of lesions (98), so the energy spectrum CT is also used to evaluate the vascularization after NACT for GC. In 2005, Tang's study showed that there was a significant difference in iodine concentration in the arteriovenous phase before and after NACT, and the change of iodine concentration was significantly correlated with tumor regression grade (99). Some studies also used iodine uptake (IU) as a functional parameter to assess the sensitivity of chemotherapy in other tumors, but further research is still needed on NACT for GC. There are also other imageological assessments. For instance, in 2016, Lee analyzed 11 LAGC patients after NACT by PET and MRI (magnetic resonance imaging), showing that K (trans) and iAUC (initial area under the curves) values can be used as early predictive markers for chemotherapy response (100). Latter in 2018, the study of Schneider showed that in GC or AGEJ patients, after the first cycle of NACT PET-CT (positron emission tomography–computed tomography)cannot accurately predict the overall pathological response, but it can accurately detect patients who are insensitive to NACT and should be operated upon immediately or treated in combination with other methods (101).

CONCLUSION

NACT is currently an effective treatment for GC, but not all patients are sensitive to it. Therefore, searching for specific indicators to predict the sensitivity of NACT in GC, individualized diagnosis and treatment are still important parts of clinical research content. At present, whether biomarkers, inflammatory markers, or imageological assessments are used, it is still difficult to select patients who are sensitive to NACT. Most of the current research involves single-center macroscopic studies. Therefore, multicenter studies with larger samples in terms of proteomics, transcriptomics, and genomics, are needed to select the indicators for predicting the efficacy and prognosis of NACT to help screen out patients for tailored treatments.

AUTHOR CONTRIBUTIONS

JS and XW were responsible for collecting, sorting out data and writing articles, were co-first authors. ZZh, ZZe and SO were responsible for collecting data. WK was responsible for putting forward ideas and reviewing articles, was corresponding author of this paper. All authors approved it for publication. All authors contributed to the article and approved the submitted version.

FUNDING

CSCO-ROCHE Research Fund No. Y-2019 Roche-015; Beijing Xisike Clinical Oncology Research Foundation Y-HS2019-43; Wu Jieping Medical Foundation No. 320. 6750.19020

REFERENCES

1. Bray F, Ferlay J, Soerjomataram I, Siegel RL, Torre LA, Jemal A. Global cancer statistics 2018: GLOBOCAN estimates of incidence and mortality worldwide for 36 cancers in 185 countries. *CA: Cancer J Clin* (2018) 68 (6):394–424. doi: 10.3322/caac.21492
2. Ferlay J, Soerjomataram I, Dikshit R, Eser S, Mathers C, Rebelo M, et al. Cancer incidence and mortality worldwide: sources, methods and major patterns in GLOBOCAN. *Int J Cancer* (2012) 136(5):E359–86. doi: 10.1002/ijc.29210
3. Roukos DH. Current status and future perspectives in gastric cancer management. *Cancer Treat Rev* (2000) 26(4):243–55. doi: 10.1053/ctrv.2000.0164
4. Ang J, Hu L, Huang PT, Wu JX, Huang LN, Cao CH, et al. Contrast-enhanced ultrasonography assessment of gastric cancer response to neoadjuvant chemotherapy. *World J Gastroenterol* (2012) 18(47):7026–32. doi: 10.3748/wjg.v18.i47.7026
5. Wang XZ, Zeng ZY, Ye X, Sun J, Zhang ZM, Kang WM. Interpretation of the development of neoadjuvant therapy for gastric cancer based on the vicissitudes of the NCCN guidelines. *World J Gastrointest Oncol* (2020) 12 (1):37–53. doi: 10.4251/wjgo.v12.i1.37
6. Cunningham D, Allum WH, Stenning SP, Thompson JN, Van de Velde CJH, Nicolson M, et al. Participants: Perioperative chemotherapy versus surgery alone for resectable gastroesophageal cancer. *New Engl J Med* (2006) 355(1):11–20. doi: 10.1056/NEJMoa055531
7. Schuhmacher C, Gretsche S, Lordick F, Reichardt P, Hohenberger W, Eisenberger CF, et al. Neoadjuvant chemotherapy compared with surgery alone for locally advanced cancer of the stomach and cardia: European Organisation for Research and Treatment of Cancer randomized trial 40954. *J Clin Oncol Off J Am Soc Clin Oncol* (2009) 28(35):5210–8. doi: 10.1200/jco.2009.26.6114
8. Ychou M, Boige V, Pignon J-P, Conroy T, Bouché O, Lebreton G, et al. Perioperative chemotherapy compared with surgery alone for resectable gastroesophageal adenocarcinoma: an FNCLCC and FFCD multicenter phase III trial. *J Clin Oncol Off J Am Soc Clin Oncol* (2010) 29(13):1715–21. doi: 10.1200/jco.2010.33.0597
9. De Vita F, Orditura M, Matano E, Bianco R, Carlomagno C, Infusino S, et al. A phase II study of biweekly oxaliplatin plus infusional 5-fluorouracil and folinic acid (FOLFOX-4) as first-line treatment of advanced gastric cancer patients. *Br J Cancer* (2005) 92(9):1644–9. doi: 10.1038/sj.bjc.6602573
10. Broxterman HJ, Gotink KJ, Verheu HMW. Understanding the causes of multidrug resistance in cancer: a comparison of doxorubicin and sunitinib. *Drug Resist Upd Rev Commentaries Antimicrob Anticancer Chemother* (2009) 12:114–26. doi: 10.1016/j.drup.2009.07.001
11. Hudler P. Challenges of deciphering gastric cancer heterogeneity. *World J Gastroenterol* (2015) 21(37):10510–27. doi: 10.3748/wjg.v21.i37.10510
12. Jewell JL, Flores F, Guan K-L. Micro(RNA) managing by mTORC1. *Mol Cell* (2015) 57(4):575–6. doi: 10.1016/j.molcel.2015.02.006
13. Garofalo M, Croce CM. microRNAs: Master regulators as potential therapeutics in cancer. *Annu Rev Pharmacol Toxicol* (2011) 51:25–43. doi: 10.1146/annurev-pharmtox-010510-100517
14. Mitani Y, Oue N, Matsumura S, Yoshida K, Noguchi T, Ito M, et al. Reg IV is a serum biomarker for gastric cancer patients and predicts response to

5-fluorouracil-based chemotherapy. *Oncogene* (2007) 26(30):4383–93. doi: 10.1038/sj.onc.1210215
15. Xia L, Zhang D, Du R, Pan Y, Zhao L, Sun S, et al. miR-15b and miR-16 modulate multidrug resistance by targeting BCL2 in human gastric cancer cells. *Int J Cancer* (2008) 123(2):372–9. doi: 10.1002/ijc.23501
16. Zhu W, Xu H, Zhu D, Zhi H, Wang T, Wang J, et al. miR-200bc/429 cluster modulates multidrug resistance of human cancer cell lines by targeting BCL2 and XIAP. *Cancer Chemother Pharmacol* (2012) 69(3):723–31. doi: 10.1007/s00280-011-1752-3
17. Yang M, Shan X, Zhou X, Qiu T, Zhu W, Ding Y, et al. miR-1271 regulates cisplatin resistance of human gastric cancer cell lines by targeting IGF1R, IRS1, mTOR, and BCL2. *Anti-Cancer Agents Medicinal Chem* (2014) 14 (6):884–91. doi: 10.2174/1871520614666140528161318
18. Zhao X, Hu GF, Shi YF, Xu W. Research Progress in microRNA-Based Therapy for Gastric Cancer. *Onco Targets Ther* (2019) 12:11393–411. doi: 10.2147/OTT.S221354
19. Jian B, Li Z, Xiao D, He G, Bai L, Yang Q. Downregulation of microRNA-193-3p inhibits tumor proliferation migration and chemoresistance in human gastric cancer by regulating PTEN gene. *Tumour Biol* (2016) 37 (7). doi: 10.1007/s13277-015-4727-x
20. Shen J, Niu W, Zhang H, Jun M, Zhang H. Downregulation of MicroRNA-147 Inhibits Cell Proliferation and Increases the Chemosensitivity of Gastric Cancer Cells to 5-Fluorouracil by Directly Targeting PTEN. *Oncol Res* (2018) 26(6):901–11. doi: 10.3727/096504017x15061902533715
21. Fang Y, Shen H, Li H, Cao Y, Qin R, Long L, et al. miR-106a confers cisplatin resistance by regulating PTEN/Akt pathway in gastric cancer cells. *Acta Biochim Biophys Sin* (2013) 45(11):963–72. doi: 10.1093/abbs/gmt106
22. Zheng P, Chen L, Yuan X, Luo Q, Liu Y, Xie G, et al. Exosomal transfer of tumor-associated macrophage-derived miR-21 confers cisplatin resistance in gastric cancer cells. *J Exp Clin Cancer Res CR* (2017) 36(1):53. doi: 10.1186/s13046-017-0528-y
23. Wang F, Li T, Zhang B, Li H, Wu Q, Yang L, et al. MicroRNA-19a/b regulates multidrug resistance in human gastric cancer cells by targeting PTEN. *Biochem Biophys Res Commun* (2013) 434(3):688–94. doi: 10.1016/j.bbrc.2013.04.010
24. Chen Z, Gao Y-J, Hou R-Z, Ding D-Y, Song D-F, Wang D-Y, et al. MicroRNA-206 facilitates gastric cancer cell apoptosis and suppresses cisplatin resistance by targeting MAPK2 signaling pathway. *Eur Rev Med Pharmacol Sci* (2019) 23(1):171–80. doi: 10.26355/eurrev_201901_16761
25. Zhou J, Chen Q. Poor expression of microRNA-135b results in the inhibition of cisplatin resistance and proliferation and induces the apoptosis of gastric cancer cells through MST1-mediated MAPK signaling pathway. *FASEB J Off Publ Fed Am Soc Exp Biol* (2019) 33(3):3420–36. doi: 10.1096/fj.201800618RRR
26. Zhi X, Tao J, Xiang G, Cao H, Liu Z, Yang K, et al. APRIL induces cisplatin resistance in gastric cancer cells via activation of the NF-κB pathway. *Cell Physiol Biochem* (2015) 35(2):571–85. doi: 10.1159/000369720
27. Zhu M, Zhou X, Du Y, Huang Z, Zhu J, Xu J, et al. miR-20a induces cisplatin resistance of a human gastric cancer cell line via targeting CYLD. *Mol Med Rep* (2016) 14(2):1742–50. doi: 10.3892/mmr.2016.5413
28. Sun K, Shen X, Yang D, Gan M, Liu G, Zhang Y, et al. MicroRNA-31 triggers G/M cell cycle arrest, enhances the chemosensitivity and inhibits migration and invasion of human gastric cancer cells by downregulating the expression of zeste homolog 2 (ZH2). *Arch Biochem Biophys* (2019) 663:269–75. doi: 10.1016/j.abb.2019.01.023
29. Zhou X, Jin W, Jia H, Yan J, Zhang G. MiR-223 promotes the cisplatin resistance of human gastric cancer cells via regulating cell cycle by targeting FBXW7. *J Exp Clin Cancer Res* (2015) 34:28. doi: 10.1186/s13046-015-0145-6
30. Holohan C, Van Schaeybroeck S, Longley DB, Johnston Cancer drug resistance PG. an evolving paradigm. *Nat Rev Cancer* (2013) 113(10):714–26. doi: 10.1038/nrc3599
31. Giovannetti E, Erozenci A, Smit J, Danesi R, Peters GJ. Molecular mechanisms underlying the role of microRNAs (miRNAs) in anticancer drug resistance and implications for clinical practice. *Crit Rev Oncol/Hematol* (2012) 81(2):103–22. doi: 10.1016/j.critrevonc.2011.03.010
32. Zhao X, Yang L, Hu J. Down-regulation of miR-27a might inhibit proliferation and drug resistance of gastric cancer cells. *J Exp Clin Cancer Res* (2011) 30:55. doi: 10.1186/1756-9966-30-55
33. Zhao Q, Li Y, Tan B, Fan L, Yang P, Tian Y. HIF-1α Induces Multidrug Resistance in Gastric Cancer Cells by Inducing MiR-27a. *PloS One* (2015) 10 (8):e0132746. doi: 10.1371/journal.pone.0132746
34. Shang Y, Zhang Z, Liu Z, Feng B, Ren G, Li K, et al. miR-508-5p regulates multidrug resistance of gastric cancer by targeting ABCB1 and ZNRD1. *Oncogene* (2013) 33(25):3267–76. doi: 10.1038/onc.2013.297
35. Li C, Zou J, Zheng G, Chu J. MiR-30a Decreases Multidrug Resistance (MDR) of Gastric Cancer Cells. *Med Sci Monitor* (2016) 22:4509–15. doi: 10.12659/MSM.898415
36. Giovannetti E, Funel N, Peters GJ, Del Chiaro M, Erozenci LA, Vasile E, et al. MicroRNA-21 in pancreatic cancer: correlation with clinical outcome and pharmacologic aspects underlying its role in the modulation of gemcitabine activity. *Cancer Res* (2010) 70(11):4528–38. doi: 10.1158/0008-5472.can-09-4467
37. Wu X, Zheng Y, Han B, Dong X. Long noncoding RNA BLACAT1 modulates ABCB1 to promote oxaliplatin resistance of gastric cancer via sponging miR-361. *Biomed Pharmacother = Biomed Pharmacother* (2018) 99:832–8. doi: 10.1016/j.biopha.2018.01.130
38. Liu X, Zhao P, Wang X, Wang L, Zhu Y, Gao W. Triptolide Induces Glioma Cell Autophagy and Apoptosis via Upregulating the ROS/JNK and Downregulating the Akt/mTOR Signaling Pathways. *Front Oncol* (2019) 9:387. doi: 10.3389/fonc.2019.00387
39. Du X, Liu B, Luan X, Cui Q, Li L. miR-30 decreases multidrug resistance in human gastric cancer cells by modulating cell autophagy. *Exp Ther Med* (2017) 15(1):599–605. doi: 10.3892/etm.2017.5354
40. Zhao J, Nie Y, Wang H, Lin Y. MiR-181a suppresses autophagy and sensitizes gastric cancer cells to cisplatin. *Gene* (2016) 576:828–33. doi: 10.1016/j.gene.2015.11.013
41. Li B, Wang W, Li Z, Chen Z, Zhi X, Xu J, et al. MicroRNA-148a-3p enhances cisplatin cytotoxicity in gastric cancer through mitochondrial fission induction and cyto-protective autophagy suppression. *Cancer Lett* (2017) 410:212–27. doi: 10.1016/j.canlet.2017.09.035
42. An Y, Zhang Z, Shang Y, Jiang X, Dong J, Yu P, et al. miR-23b-3p regulates the chemoresistance of gastric cancer cells by targeting ATG12 and HMGB2. *Cell Death Dis* (2015) 6:e1766. doi: 10.1038/cddis.2015.123
43. Wu H, Huang M, Lu M, Zhu W, Shu Y, Cao P, et al. Regulation of microtubule-associated protein tau (MAPT) by miR-34c-5p determines the chemosensitivity of gastric cancer to paclitaxel. *Cancer Chemother Pharmacol* (2013) 71(5):1159–71. doi: 10.1007/s00280-013-2108-y
44. Okano H, Kawahara H, Toriya M, Nakao K, Shibata S, Imai T. Function of RNA-binding protein Musashi-1 in stem cells. *Exp Cell Res* (2005) 306 (2):349–56. doi: 10.1016/j.yexcr.2005.02.021
45. Li Q, Pan D, Zhang J, Yang F. Identification of the thymidylate synthase within the genome of white spot syndrome virus. *J Gen Virol* (2004) 85:2035–44. doi: 10.1099/vir.0.80048-0
46. Yao L, Itoh S, Furuta I. Thymidine phosphorylase expression in oral squamous cell carcinoma. *Oral Oncol* (2002) 38(6):584–90. doi: 10.1016/s1368-8375(01)00113-0
47. Diasio RB. Oral DPD-inhibitory fluoropyrimidine drugs. *Oncol (Williston Park NY)* (2000) 14:19–23. doi: 10.1215/15228517-2-4-239
48. Salonga D, Danenberg KD, Johnson M, Metzger R, Groshen S, Tsao-Wei DD, et al. Colorectal tumors responding to 5-fluorouracil have low gene expression levels of dihydropyrimidine dehydrogenase, thymidylate synthase, and thymidine phosphorylase. *Clin Cancer Res* (2000) 6 (4):1322–7. doi: 10.1093/carcin/21.4.849
49. Terashima M, Irinoda T, Fujiwara H, Nakaya T, Takagane A, Abe K, et al. Roles of thymidylate synthase and dihydropyrimidine dehydrogenase in tumor progression and sensitivity to 5-fluorouracil in human gastric cancer. *Anticancer Res* (2002) 22:761–8. doi: 10.1097/00001813-200203000-00015
50. Wang W, Cassidy J, O'Brien V, Ryan KM, Collie-Duguid E. Mechanistic and predictive profiling of 5-Fluorouracil resistance in human cancer cells. *Cancer Res* (2004) 64(22):8167–76. doi: 10.1158/0008-5472.can-04-0970
51. Etienne M-C, Ilc K, Formento J-L, Laurent-Puig P, Formento P, Cheradame S, et al. Thymidylate synthase and methylenetetrahydrofolate reductase gene polymorphisms: relationships with 5-fluorouracil sensitivity. *Br J Cancer* (2004) 90(2):526–34. doi: 10.1038/sj.bjc.6601523
52. Ma T, Zhu Z-G, Ji Y-B, Zhang Y, Yu Y-Y, Liu B-Y, et al. Correlation of thymidylate synthase, thymidine phosphorylase and dihydropyrimidine dehydrogenase with sensitivity of gastrointestinal cancer cells to

5-fluorouracil and 5-fluoro-2'-deoxyuridine. *World J Gastroenterol* (2004) 10(2):172–6. doi: 10.3748/wjg.v10.i2.172
53. Napieralski R, Ott K, Kremer M, Specht K, Vogelsang H, Becker K, et al. Combined GADD45A and thymidine phosphorylase expression levels predict response and survival of neoadjuvant-treated gastric cancer patients. *Clin Cancer Res* (2005) 11(8):3025–31. doi: 10.1158/1078-0432.ccr-04-1605
54. Sasako M, Terashima M, Ichikawa W, Ochiai A, Kitada K, Kurahashi I, et al. Impact of the expression of thymidylate synthase and dihydropyrimidine dehydrogenase genes on survival in stage II/III gastric cancer. *Gastric Cancer* (2015) 18(3):538–48. doi: 10.1007/s10120-014-0413-8
55. Wang D, Yu X, Wang X. High/positive expression of 5-fluorouracil metabolic enzymes predicts better response to S-1 in patients with gastric cancer: a meta-analysis. *Int J Biol Markers* (2016) 31(2):e101–9. doi: 10.5301/jbm.5000202
56. Colombo M, Raposo G, Théry C. Biogenesis, secretion, and intercellular interactions of exosomes and other extracellular vesicles. *Annu Rev Cell Dev Biol* (2014) 30:255–89. doi: 10.1146/annurev-cellbio-101512-122326
57. Hou J, Jiang W, Zhu L, Zhong S, Zhang H, Li J, et al. Circular RNAs and exosomes in cancer: a mysterious connection. *Clin Trans Oncol* (2018) 20 (9):1109–16. doi: 10.1007/s12094-018-1839-y
58. Meehan K, Vella L. The contribution of tumour-derived exosomes to the hallmarks of cancer. *Crit Rev Clin Lab Sci* (2016) 53(2):121–31. doi: 10.3109/10408363.2015.1092496
59. Ruivo C, Adem B, Silva M, Melo S. The Biology of Cancer Exosomes: Insights and New Perspectives. *Cancer Res* (2017) 77(23):6480–8. doi: 10.1158/0008-5472.can-17-0994
60. Brinton L, Sloane H, Kester M, Kelly K. Formation and role of exosomes in cancer. *Cell Mol Life Sci* (2015) 72(4):659–71. doi: 10.1007/s00018-014-1764-3
61. Sharma A. Chemoresistance in cancer cells: exosomes as potential regulators of therapeutic tumor heterogeneity. *Nanomed (London England)* (2017) 12 (17):2137–48. doi: 10.2217/nnm-2017-0184
62. Butera G, Pacchiana R, Donadelli M. Autocrine mechanisms of cancer chemoresistance. *Semin Cell Dev Biol* (2018) 78:3–12. doi: 10.1016/j.semcdb.2017.07.019
63. Sousa D, Lima R, Vasconcelos M. Intercellular Transfer of Cancer Drug Resistance Traits by Extracellular Vesicles. *Trends Mol Med* (2015) 21 (10):595–608. doi: 10.1016/j.molmed.2015.08.002
64. Sun M, Xu B, Wu Q, Cai S, Chen W, Li D, et al. Cisplatin-Resistant Gastric Cancer Cells Promote the Chemoresistance of Cisplatin-Sensitive Cells via Exosomal RPS3 Mediated PI3K-Akt-cofilin-1 Signaling Axis. *Res Square* (2020) 9:618899. doi: 10.21203/rs.3.rs-44042/v1
65. Zhang Q, Zhang H, Ning T, Liu D, Deng T, Liu R, et al. Exosome-Delivered c-Met siRNA Could Reverse Chemoresistance to Cisplatin in Gastric Cancer. *Int J Nanomed* (2020) 15:2323–35. doi: 10.2147/ijn.s231214
66. Zhang H, Deng T, Liu R, Ning T, Ba Y. CAF secreted miR-522 suppresses ferroptosis and promotes acquired chemo-resistance in gastric cancer. *Mol Cancer* (2020) 19(1). doi: 10.1186/s12943-020-01168-8
67. Wang M, Qiu R, Yu S, Xu X, Li G, Gu R, et al. Paclitaxel-resistant gastric cancer MGC-803 cells promote epithelial-to-mesenchymal transition and chemoresistance in paclitaxel-sensitive cells via exosomal delivery of miR-155-5p. *Int J Oncol* (2018) 54:326–38. doi: 10.3892/ijo.2018.4601
68. Wang S, Ping M, Song B, Guo Y, Li Y, Jia J. Exosomal CircPRRX1 Enhances Doxorubicin Resistance in Gastric Cancer by Regulating MiR-3064-5p/PTPN14 Signaling. *Yonsei Med J* (2020) 61(9). doi: 10.3349/ymj.2020.61.9.750
69. Li W, Li C, Zhou T, Liu X, Liu X, Li X, et al. Role of exosomal proteins in cancer diagnosis. *Mol Cancer* (2017) 16(1):145. doi: 10.1186/s12943-017-0706-8
70. Subra C, Laulagnier K, Perret B, Record M. Exosome lipidomics unravels lipid sorting at the level of multivesicular bodies. *Biochimie* (2007) 89 (2):205–12. doi: 10.1016/j.biochi.2006.10.014
71. Goekkurt E, Hoehn S, Wolschke C, Wittmer C, Stueber C, Hossfeld DK, et al. Polymorphisms of glutathione S-transferases (GST) and thymidylate synthase (TS)–novel predictors for response and survival in gastric cancer patients. *Br J Cancer* (2005) 94(2):281–6. doi: 10.1038/sj.bjc.6602891
72. Li S, Li B, Wang J, Zhang D, Liu Z, Zhang Z, et al. Identification of Sensitivity Predictors of Neoadjuvant Chemotherapy for the Treatment of Adenocarcinoma of Gastroesophageal Junction. *Oncol Res* (2017) 25 (1):93–7. doi: 10.3727/096504016x14719078133564
73. Hashimoto T, Kurokawa Y, Takahashi T, Miyazaki Y, Tanaka K, Makino T, et al. Predictive value of MLH1 and PD-L1 expression for prognosis and response to preoperative chemotherapy in gastric cancer. *Gastric Cancer* (2019) 22(4):785–92. doi: 10.1007/s10120-018-00918-4
74. Pan Y. Clinical Significance of Serum Tumor Markers in Patients With Gastric Cancer. *China Continuing Med Educ* (2017) 009(011):111–3.
75. Fang WL, Lan YT, Huang KH, Liu CA, Hung YP, Lin CH, et al. Clinical significance of circulating plasma DNA in gastric cancer. *Int J Cancer* (2016) 138(12):2974–83. doi: 10.1002/ijc.30018
76. Kongwang H, Yiwen W, Ming L, Longlong L, Qingfa W, Hao L. Application of circulating tumor cell detection in decision making of neoadjuvant chemotherapy for gastric cancer. *Tumor* (2018) 38(12):1130–36. doi: 10.3781/j.issn.1000-7431.2018.33.478
77. Elinav E, Nowarski R, Thaiss CA, Hu B, Jin C, Flavell RA. Inflammation-induced cancer: crosstalk between tumours, immune cells and microorganisms. *Nat Rev Cancer* (2013) 13(11):759–71. doi: 10.1038/nrc3611
78. Roxburgh CS, McMillan DC. Role of systemic inflammatory response in predicting survival in patients with primary operable cancer. *Future Oncol (London England)* (2010) 6(1):149–63. doi: 10.2217/fon.09.136
79. Borsig L, Wolf MJ, Roblek M, Lorentzen A, Heikenwalder M. Inflammatory chemokines and metastasis–tracing the accessory. *Oncogene* (2013) 33 (25):3217–24. doi: 10.1038/onc.2013.272
80. el Aziz LMA. Blood neutrophil-lymphocyte ratio predicts survival in locally advanced cancer stomach treated with neoadjuvant chemotherapy FOLFOX 4. *Med Oncol (Northwood London England)* (2014) 31(12):311. doi: 10.1007/s12032-014-0311-2
81. Oya Y, Hayakawa Y, Koike K. Tumor microenvironment in gastric cancers. *Cancer Sci* (2020) 111(8):2696–707. doi: 10.1111/cas.14521
82. Biswas S, Mantovani A. Macrophage plasticity and interaction with lymphocyte subsets: cancer as a paradigm. *Nat Immunol* (2010) 11 (10):889–96. doi: 10.1038/ni.1937
83. Oishi S, Takano R, Tamura S, Tani S, Iwaizumi M, Hamaya Y, et al. M2 polarization of murine peritoneal macrophages induces regulatory cytokine production and suppresses T-cell proliferation. *Immunology* (2016) 149 (3):320–8. doi: 10.1111/imm.12647
84. Okumura T, Ericksen R, Takaishi S, Wang S, Dubeykovskiy Z, Shibata W, et al. K-ras mutation targeted to gastric tissue progenitor cells results in chronic inflammation, an altered microenvironment, and progression to intraepithelial neoplasia. *Cancer Res* (2010) 70(21):8435–45. doi: 10.1158/0008-5472.can-10-1506
85. Katoh M. Epithelial-mesenchymal transition in gastric cancer (Review). *Int J Oncol* (2005) 27(6):1677–83. doi: 10.1007/s00268-009-0184-2
86. Oshima H, Oshima M, Inaba K, Taketo M. Hyperplastic gastric tumors induced by activated macrophages in COX-2/mPGES-1 transgenic mice. *EMBO J* (2004) 23(7):1669–78. doi: 10.1038/sj.emboj.7600170
87. Kaparakis M, Walduck A, Price J, Pedersen J, van Rooijen N, Pearse M, et al. Macrophages are mediators of gastritis in acute Helicobacter pylori infection in C57BL/6 mice. *Infect Immun* (2008) 76(5):2235–9. doi: 10.1128/iai.01481-07
88. Oshima H, Hioki K, Popivanova B, Oguma K, Van Rooijen N, Ishikawa T, et al. Prostaglandin E_2 signaling and bacterial infection recruit tumor-promoting macrophages to mouse gastric tumors. *Gastroenterology* (2011) 140(2):596–607.e7. doi: 10.1053/j.gastro.2010.11.007
89. Petersen C, Weis V, Nam K, Sousa J, Fingleton B, Goldenring J. Macrophages promote progression of spasmolytic polypeptide-expressing metaplasia after acute loss of parietal cells. *Gastroenterology* (2014) 146 (7):1727–38.e8. doi: 10.1053/j.gastro.2014.02.007
90. Oguma K, Oshima H, Aoki M, Uchio R, Naka K, Nakamura S, et al. Activated macrophages promote Wnt signalling through tumour necrosis factor-alpha in gastric tumour cells. *EMBO J* (2008) 27(12):1671–81. doi: 10.1038/emboj.2008.105
91. Qeadan F, Bansal P, Hanson J, Beswick E. The MK2 pathway is linked to G-CSF, cytokine production and metastasis in gastric cancer: a novel intercorrelation analysis approach. *J Trans Med* (2020) 18(1):137. doi: 10.1186/s12967-020-02294-z

92. Miller AB, Hoogstraten B, Staquet M. A. Winkler: Reporting results of cancer treatment. *Cancer* (1981) 47(1):207–14. doi: 10.1002/1097-0142(19810101)47:1<207::aid-cncr2820470134>3.0.co;2-6
93. Watanabe H, Okada M, Yashushi K, Satoucho M, Sato Y, Yamabe Y, et al. New response evaluation criteria in solid tumours-revised RECIST guideline (version 1.1). *Gan to kagaku ryoho Cancer Chemother* (2009) 36(13):2495–501. doi: 10.1016/S1359-6349(09)70018-7
94. Ott K, Fink U, Becker K, Stahl A, Dittler H-J, Busch R, et al. Prediction of response to preoperative chemotherapy in gastric carcinoma by metabolic imaging: results of a prospective trial. *J Clin Oncol* (2003) 21(24):4604–10. doi: 10.1200/jco.2003.06.574
95. Crabb SJ, Patsios D, Sauerbrei E, Ellis PM, Arnold A, Goss G, et al. Tumor cavitation: impact on objective response evaluation in trials of angiogenesis inhibitors in non-small-cell lung cancer. *J Clin Oncol* (2009) 27(3):404–10. doi: 10.1200/jco.2008.16.2545
96. Hansen ML, Fallentin E, Lauridsen C, Law I, Federspiel B, Bæksgaard L, et al. Computed tomography (CT) perfusion as an early predictive marker for treatment response to neoadjuvant chemotherapy in gastroesophageal junction cancer and gastric cancer–a prospective study. *PloS One* (2014) 9(5):e97605. doi: 10.1371/journal.pone.0097605
97. Zhang D, Li X, Liu B. Objective characterization of GE discovery CT750 HD scanner: gemstone spectral imaging mode. *Med Phys* (2011) 38(3):1178–88. doi: 10.1118/1.3551999
98. De Cecco CN, Darnell A, Rengo M, Muscogiuri G, Bellini D, Ayuso C, et al. oncologic applications. *Am J Roentgenol* (2012) 199:S98–S105. doi: 10.2214/ajr.12.9207
99. Tang L, Li Z-Y, Li Z-W, Zhang X-P, Li Y-L, Li X-T, et al. Evaluating the response of gastric carcinomas to neoadjuvant chemotherapy using iodine concentration on spectral CT: a comparison with pathological regression. *Clin Radiol* (2015) 70(11):1198–204. doi: 10.1016/j.crad.2015.06.083
100. Lee DH, Kim SH, Im S-A, Oh D-Y, Kim T-Y, Han JK. Multiparametric fully-integrated 18-FDG PET/MRI of advanced gastric cancer for prediction of chemotherapy response: a preliminary study. *Eur Radiol* (2015) 26(8):2771–8. doi: 10.1007/s00330-015-4105-5
101. Schneider PM, Eshmuminov D, Rordorf T, Vetter D, Veit-Haibach P, Weber A, et al. FDG-PET-CT identifies histopathological non-responders after neoadjuvant chemotherapy in locally advanced gastric and cardia cancer: cohort study. *BMC Cancer* (2018) 18(1):548. doi: 10.1186/s12885-018-4477-4

Conflict of Interest: The authors declare that the research was conducted in the absence of any commercial or financial relationships that could be construed as a potential conflict of interest.

frontiers in Oncology

ORIGINAL RESEARCH
published: 04 May 2021
doi: 10.3389/fonc.2021.638537

MiR-454-3p Promotes Oxaliplatin Resistance by Targeting PTEN in Colorectal Cancer

Xiao-Lan Qian†, Fang Zhou†, Song Xu, Jian Jiang, Zhi-Peng Chen, Shao-Kai Wang, Yun Zuo and Chen Ni**

Department of Oncology, Zhangjiagang First People's Hospital, The Affiliated Zhangjiagang Hospital of Soochow University, Zhangjiagang, China

Colorectal cancer is one of the most common malignancies worldwide. Oxaliplatin is the first-line chemotherapeutic agent for the treatment of advanced colorectal cancer. However, acquired resistance to oxaliplatin limits its therapeutic efficacy, and the underlying mechanism remains largely unclear. In this study, we compared the expression of a panel of microRNAs (miRNAs) between oxaliplatin-sensitive and -resistant HCT-116 colorectal cancer cells. We found that miR-454-3p was significantly up-regulated in oxaliplatin-resistant cells and was the most differently expressed miRNA. Interestingly, we observed that inhibition of miR-454-3p resensitized resistant cells to oxaliplatin and enhanced oxaliplatin-induced cellular apoptosis. Moreover, we determined that miR-454-3p promoted oxaliplatin resistance through targeting PTEN and activating the AKT signaling pathway. *In vivo* study revealed that overexpression of miR-454-3p decreased the sensitivity of HCT-116 xenograft tumors to oxaliplatin treatment in a mouse model. Clinically, overexpression of miR-454-3p was associated with decreased responsiveness to oxaliplatin-based chemotherapy, as well as a short progression-free survival. Taken together, our study indicated that the expression of miR-454-3p could be used to predict oxaliplatin sensitivity, and targeting miR-454-3p could overcome oxaliplatin resistance in colorectal cancer.

Keywords: colorectal cancer, oxaliplatin resistance, miR-454-3P, PTEN, AKT signaling pathway

OPEN ACCESS

Edited by:
Dong-Hua Yang,
St. John's University, United States

Reviewed by:
Jinrong Zhu,
Guangdong Pharmaceutical University, China
Min Sun,
Hubei University of Medicine, China

****Correspondence:***
Yun Zuo
zuoyun1@163.com
Chen Ni
nichen1129@126.com

†These authors have contributed equally to this work

Specialty section:
This article was submitted to Gastrointestinal Cancers, a section of the journal Frontiers in Oncology

Received: *07 December 2020*
Accepted: *15 February 2021*
Published: *04 May 2021*

Citation:
Qian X-L, Zhou F, Xu S, Jiang J, Chen Z-P, Wang S-K, Zuo Y and Ni C (2021) MiR-454-3p Promotes Oxaliplatin Resistance by Targeting PTEN in Colorectal Cancer. Front. Oncol. 11:638537. doi: 10.3389/fonc.2021.638537

INTRODUCTION

Colorectal cancer is the third most commonly diagnosed cancer and the second leading cause of cancer death, accounting for ∼10% of all cancer cases and deaths worldwide (1). Although surgery is considered the only curative treatment for colorectal cancer, chemotherapy remains the most widely used monotherapy or adjuvant therapy for the majority of patients (2, 3). Oxaliplatin, a platinum-based derivative, is the first-line chemotherapeutic agent for the treatment of advanced colorectal cancer (4, 5). However, drug resistance often occurs after a short period of use of oxaliplatin, which leads to therapeutic failure and poor prognoses. Drug resistance limits the efficacy of oxaliplatin and remains a major obstacle to the effective treatment of colorectal cancer (6, 7). Therefore, it is urgent to investigate the underlying molecular mechanism for the development of novel therapeutic strategy to overcome oxaliplatin resistance in colorectal cancer.

MicroRNAs (miRNAs) are a class of small non-coding RNAs consisting of 17–25 nucleotides. MiRNAs regulate gene expression by directly binding to the 3′-untranslated region (UTR)

of target messenger RNAs (mRNAs), triggering these mRNAs to degrade or inhibiting their translation (8). In recent years, increasing studies have confirmed the critical roles of aberrantly expressed miRNAs in chemotherapeutic drug resistance, including oxaliplatin (9–12). However, the molecular mechanism underlying the resistance of colorectal cancer to oxaliplatin modulated by miRNAs was not clearly understood.

In the present study, we identified that miR-454-3p was significantly up-regulated in oxaliplatin-resistant colorectal cancer cells, as compared to that in oxaliplatin-sensitive cells. Inhibition of miR-454-3p increased the antiproliferative activity of oxaliplatin and enhanced cellular apoptosis in oxaliplatin-resistant cells both *in vitro* and *in vivo*. Furthermore, we showed that miR-454-3p promoted oxaliplatin resistance by directly targeting PTEN, thereby down-regulating its expression and activating the AKT signaling pathway. More importantly, we demonstrated that high levels of miR-454-3p expression were negatively correlated with the clinical response to oxaliplatin-based chemotherapy, as well as progression-free survival (PFS). These findings will enhance our understanding of the molecular mechanism underlying the chemoresistance of colorectal cancer and support that miR-454-3p may possess the potential of predicting oxaliplatin sensitivity in colorectal cancer.

MATERIALS AND METHODS

Cell Culture and Reagents

The human colorectal cancer cell line HCT-116 was obtained from the Cell Bank of the Chinese Academy of Sciences (Shanghai, China). Cells were cultured in RPMI-1640 medium (Thermo Scientific, Rockford, IL, USA) supplemented with 10% fetal bovine serum (Thermo Scientific) and 1% penicillin–streptomycin (Thermo Scientific) at 37°C in a humidified incubator with 5% CO_2. Oxaliplatin-resistant colorectal cancer cell line HCT-116/OxR was established in our laboratory through dosage escalation of oxaliplatin beginning from 100 nM. Thereafter, the concentrations of oxaliplatin were elevated in gradient until the cells could stably proliferate in 10 μM of oxaliplatin. HCT-116/OxR cells were cultured in the medium containing 5 μM of oxaliplatin. Oxaliplatin and LY294002 were purchased from Sigma (St. Louis, MO, USA), dissolved in phosphate-buffered saline (PBS) or dimethyl sulfoxide (DMSO), and stored at 4°C or −20°C, respectively.

Cell Transfection

The miR-454-3p mimic (5′-UAGUGCAAUAUUGCUUAUAGGGU-3′), negative control mimic (miR-NC, sequence: 5′-UCACAACCUCCUAGAAAGAGUAGA-3), miR-454-3p inhibitor (anti–miR-454-3p inhibitor, sequence: 5′-ACCCUAUAAGCAAUAUUGCACUA-3′), negative control inhibitor (anti–miR-NC, sequence: 5′-CAGUACUUUUGUGUAGUACAA-3′), and small interfering RNA (siRNA) for PTEN, as well as corresponding negative control (siNC) were obtained from GenePharma (Shanghai, China). For PTEN overexpression, PTEN cDNA sequence was cloned into pcDNA 3.1 vector plasmid. All transfection experiments were performed using Lipofectamine 2000 (Invitrogen, Carlsbad, CA, USA) according to manufacturer's protocol. For stable miR-454-3p overexpression cells, lentiviral plasmids encoding miR-454-3p and negative control (miR-NC) were transfected into 293T packaging cells to generate lentiviruses. HCT-116 cells were infected by the lentiviruses for 24 h and were then selected with 2 μg/mL puromycin for at least 3 days.

Real-Time Polymerase Chain Reaction

Total RNA was extracted from cells using miRNeasy mini kit (Qiagen, Hilden, Germany) and was reversely transcribed to complementary DNA using TaqMan miRNA reverse transcription kit (Applied Biosystems, Foster City, CA, USA) according to the manufacturer's instructions. Quantitative real-time polymerase chain reaction (qRT-PCR) was performed using TaqMan miRNA Assays (Applied Biosystems). *U6* was used as an endogenous control, and the expression of miR-454-3p was quantified using the $2^{-\Delta\Delta Ct}$ method. The real-time PCR primers of miR-454-3p were used as follows: forward: 5′-GCGCGTAGTGCAATATTGCTTA-3, reverse: 5′-AGTGCAGGGTCCGAGGTATT-3, *U6* forward: 5′-TGCGGTGGGTGTCATCAAA-3′, and reverse: 5′-AACGCTTCACGAATTTGCGT-3′.

Cell Viability Assay

After transfection of miR-454-3p mimics, inhibitor, or corresponding controls, cells were seeded in 96-well plates at a density of 4×10^3 cells per well and incubated at 37°C overnight. The cells were then treated with indicated concentrations of oxaliplatin or PBS (negative control) for 48 h. Then, 20 μL medium containing MTT (5 mg/mL; Sigma) was added to each well, and the cells were incubated for another 4 h at 37°C. The MTT containing medium was discharged, and 150 μL DMSO was added to each well to dissolve the new formed formazan. Light absorbance at 570 nm was measured on a microplate reader (Synergy H4, BioTek). The results were represented as mean ± SD from three independent experiments.

Cell Apoptosis

After transfection, cells were treated with indicated concentrations of oxaliplatin or LY294002 for 48 h. For cellular apoptosis qualification, the cells were harvested and stained with annexin V–fluorescein isothiocyanate (FITC) and propidium iodide (PI) for 15 min in the dark. Then, the stained cells were analyzed by flow cytometry to qualify cell apoptosis based on the percentage of annexin V–positive cells. For caspase-3 activity determination, caspase-3 colorimetric assay kits (Beyotime, Shanghai, China) were used according to the manufacturer's protocol. Briefly, cells were washed with cold PBS, resuspended in lysis buffer, and incubated on ice for 15 min. A total of 50 μL cell suspension, 40 μL reaction buffer, and 10 μL Ac-DEVD-pNA were mixed and then incubated at 37°C for 2 h. Light absorbance was measured at 405 nm. The Bradford protein quantitative analysis was used as the reference to normalize expression in each experimental group. The results were represented as mean ± SD from three independent experiments. Representative images from three independent experiments were shown.

Western Blot

Cells were collected and lysed with RIPA lysis buffer. The concentrations of total protein were determined by BCA protein assay kit (Beyotime). Equal amounts of protein samples were subjected to sodium dodecyl sulfate–polyacrylamide gel electrophoresis for separation and were then transferred onto polyvinylidene difluoride membranes (Millipore, Billerica, MA, USA). The membranes were blocked with 1% skim milk for 1 h at room temperature, followed by incubation with primary antibodies at 4°C overnight. After incubation with corresponding secondary antibodies at room temperature for 1 h, the protein bands were detected with chemiluminescence (Millipore) according to manufacturer's instructions. β-Actin was used as an endogenous loading control. Representative data from at least three independent experiments were shown. Antibodies to PTEN, AKT, Bcl-2, Bax, and β-actin were purchased from Proteintech (Rosemont, IL, USA), Antibodies to p-AKT and cleaved caspase-3 were purchased from Cell Signaling Technology (Beverly, MA, USA). Representative images from three independent experiments were shown.

Colony Formation Assay

After transfection, cells were seeded in a six-well plate at a density of 1×10^3 cells per well and incubated at 37°C overnight. The cells were then treated with indicated concentrations of oxaliplatin or PBS (negative control) for 48 h, respectively. Then, fresh medium was replaced to allow cell growth for at least 2 weeks. After staining with gentian violet, colonies formed by more than 50 cells were counted. The results were represented as mean ± SD from three independent experiments.

Luciferase Reporter Assay

The wild-type and mutant 3′-UTRs of PTEN were cloned into a PGL-3 control vector (Promega, Madison, WI, USA). Cells were seeded in 24-well plates and were cotransfected with firefly luciferase reporter vector containing wild-type or mutant 3′-UTRs of PTEN, along with miR-454-3p mimics or miR-NC in combination with pRL-SV40 Renilla luciferase vector using Lipofectamine 2000 (Invitrogen). After incubation at 37°C for 48 h, cells were harvested and analyzed for luciferase activity using dual-luciferase reporter assay system (Promega) according to the manufacturer's protocol. The signal of Renilla luciferase was used as an internal control to normalize the transfection efficacy. The results were represented as mean ± SD from three independent experiments.

In vivo Tumor Xenograft Experiments

All animal experimental protocols were approved by the Medical Ethics Committee of Zhangjiagang First People's Hospital. Male BALB/c nude mice (6 weeks old, weight 18 ± 2 g) were purchased from Shanghai SLAC Laboratory Animal Co., Ltd., and were housed in a specific pathogen-free environment. The mice were randomly divided into two groups ($n = 6$) and subcutaneously injected with HC-116 cells (5×10^6 in 200 μL PBS) stably transfected with miR-454-3p overexpression/negative control vector. The tumor volume was measured using a digital caliper and calculated as $L \times S^2 \times 0.52$ (L represents the longest tumor diameter, and S represents the shortest tumor diameter). The tumor volume and mouse body weight were recorded every 2 days. After the tumors reached a mean volume of 100 mm^3 (8 days after tumor inoculation), the animals began receiving oxaliplatin (5 mg/kg, intraperitoneally) every 4 days. At the end of experiment, the mice were sacrificed by cervical dislocation, and the tumors were harvested and weighed.

Patients and Tumor Tissues

The study fusing human tissues was approved by the Medical Ethics Committee of Zhangjiagang First People's Hospital. A total of 45 human colorectal cancer samples were obtained from the Zhangjiagang First People's Hospital with the informed consent of each patient. All the patients were diagnosed with colorectal cancer based on pathological evidence and received at least six cycles of oxaliplatin-based chemotherapy. They were classified according to the Response Evaluation Criteria in Solid Tumors criteria. Clinicopathological information of the patients is presented in **Table 1**. All tissue samples for RNA extraction were snap-frozen and stored in liquid nitrogen. Levels of miR-454-3p expression in all tissues were normalized to the lowest level of expression. Subsequently, the median miR-454-3p expression in the colorectal cancer tissues was used as the cutoff value to divide the patients into two groups with high or low expression of miR-454-3p.

TABLE 1 | Associations between miR-454-3p levels and clinicopathological characteristics.

Variables	Expression of miR-454-3p		*P*-value[a]
	High	Low	
Age (years)			
<60	10	11	0.720
≥60	13	11	
Gender			
Male	11	10	0.855
Female	12	9	
Tumor location			
Colon	13	12	0.261
Rectum	10	11	
Tumor size (cm)			
<4	12	14	0.705
≥4	11	8	
TNM stage			
I/II	8	9	0.457
III/IV	15	13	
Distant metastasis			
No	17	18	0.691
Yes	6	4	
Oxaliplatin response			
Response	8	17	0.017[b]
Non-response	15	5	

[a] *P-value was estimated by χ^2 test.*
[b] *Statistically significant.*

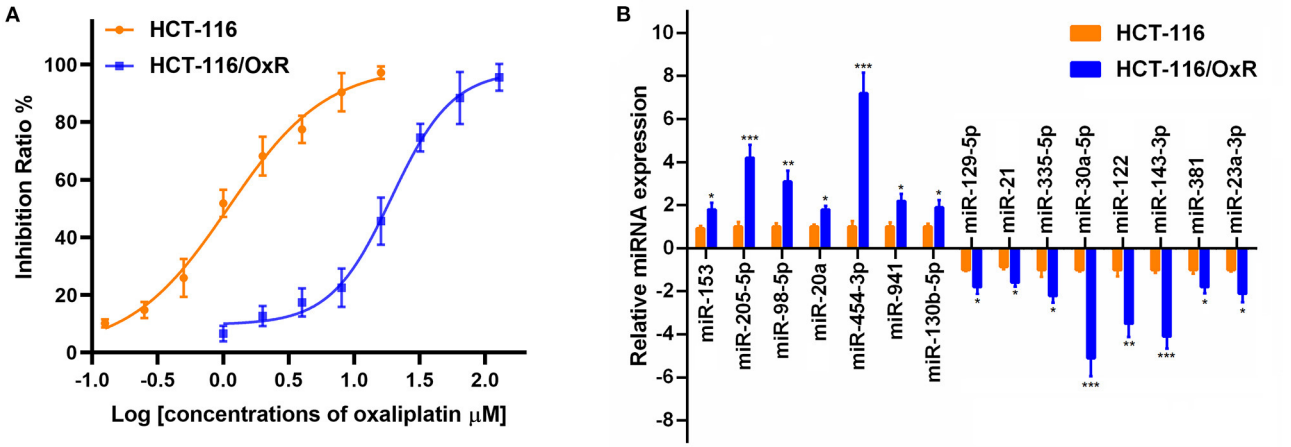

FIGURE 1 | The expression of miRNAs in oxaliplatin-sensitive and -resistant HCT-116 colorectal cancer cells. **(A)** Effects of oxaliplatin on cell viability analyzed using MTT assay in HCT-116 and HCT-116/OxR cells. **(B)** Quantitative RT-PCR analysis on the expression of a panel of miRNAs between HCT-116 and HCT-116/OxR cells. *U6* small nuclear RNA was used as an internal control. Results were presented as mean ± SD from three independent experiments. $^{*}P < 0.05$, $^{**}P < 0.01$, $^{***}P < 0.001$.

RESULTS

The Expression of miR-454-3p Was Up-Regulated in Oxaliplatin-Resistant Colorectal Cancer Cells

To investigate the molecular mechanism underlying the oxaliplatin resistance in colorectal cancer cells, oxaliplatin-resistant HCT-116 cells (HCT-116/OxR) were established by culturing the HCT-116 cells with dosage escalation of oxaliplatin over 6 months. The effects of oxaliplatin on cell viability were analyzed using an MTT assay in HCT-116 and HCT-116/OxR cells. As shown in **Figure 1A**, HCT-116/OxR cells exhibited significant resistance to oxaliplatin, with an IC_{50} value ∼20-fold larger than those of sensitive parental HCT-116 cells. To screen critical miRNAs associated with oxaliplatin resistance in colorectal cancer, we used quantitative RT-PCR assay to detect the expression of a panel of miRNAs composed of the most altered miRNAs in an miRNA microarray analysis (data not shown). As presented in **Figure 1B**, we found that seven miRNAs were up-regulated by more than 2-fold, whereas eight miRNAs were down-regulated by more than 2-fold in oxaliplatin-resistant cells, compared to oxaliplatin-sensitive cells. Specifically, the up-regulated miRNAs included miR-153, miR-205-5p, miR-98-5p, miR-20a, miR-454-3p, miR-941, and miR-130b-5p, whereas the down-regulated miRNAs included miR-129-5p, miR-21, miR-335-5p, miR-30a-5p, miR-122, miR-143-3p, miR-381, and miR-23a-3p. In particular, miR-454-3p was the most differentially expressed miRNA detected, with ∼7-fold higher expression in HCT-116/OxR cells, compared with their parental cells. Therefore, miR-454-3p was selected for further studies.

MiR-454-3p Induced Oxaliplatin Resistance in HCT-116 Colorectal Cancer Cells

To verify the influence of miR-454-3p on cellular sensitivity to oxaliplatin, we transfected miR-454-3p mimics or negative control miRNA (miR-NC) into HCT-116 cells (**Figure 2A**), whereas miR-454-3p inhibitor (anti–miR-454-3p) or inhibitor negative control (anti–miR-NC) was transfected into HCT-116/OxR cells (**Figure 2B**). Cell viability assay showed that overexpression of miR-454-3p significantly induced oxaliplatin resistance in HCT-116 cells, with the IC_{50} value increased from 1.14 ± 0.13 to 5.97 ± 1.14 μM (**Figure 2C**). In contrast, inhibition of miR-454-3p significantly sensitized HCT-116/OxR cells to oxaliplatin, with the IC_{50} value decreased from 21.22 ± 3.32 to 8.48 ± 1.37 μM (**Figure 2D**). In addition, a colony formation assay revealed that overexpression of miR-454-3p attenuated the oxaliplatin-mediated reduction of colonies in HCT-116 cells (**Figures 2E,F**), whereas the inhibition of miR-454-3p enhanced the inhibitory effects of oxaliplatin on colony formation in HCT-116/OxR cells (**Figures 2E,G**). Collectively, these results confirmed the positive correlation between the expression of miR-454-3p and oxaliplatin resistance in colorectal cancer cells.

PTEN Was Identified as the Direct Target of miR-454-3p

Based on the findings mentioned above, we further explored the molecular mechanisms underlying the effects of miR-454-3p on oxaliplatin sensitivity. Four online bioinformatics software programs (TargetScan, miRDB, miRCode, and doRiNA) were used to predict the target of miR-454-3p. A total of 12 common targeted mRNAs were found. Among these 12 targets, PTEN attracted our attention because it is a tumor suppressor, and its aberrant expression contributes to drug resistance and poor prognosis in several human cancers. Therefore, PTEN was chosen for further verification. The predicted correlation between the 3′-UTR of *PTEN* and miR-454-3p is shown in **Figure 3A**. To further confirm whether *PTEN* was the direct target of miR-454-3p, we used luciferase reporter assay to analyze the binding ability of miR-454-3p to wild-type or mutant 3′-UTR of PTEN. As shown in **Figure 3B**, overexpression

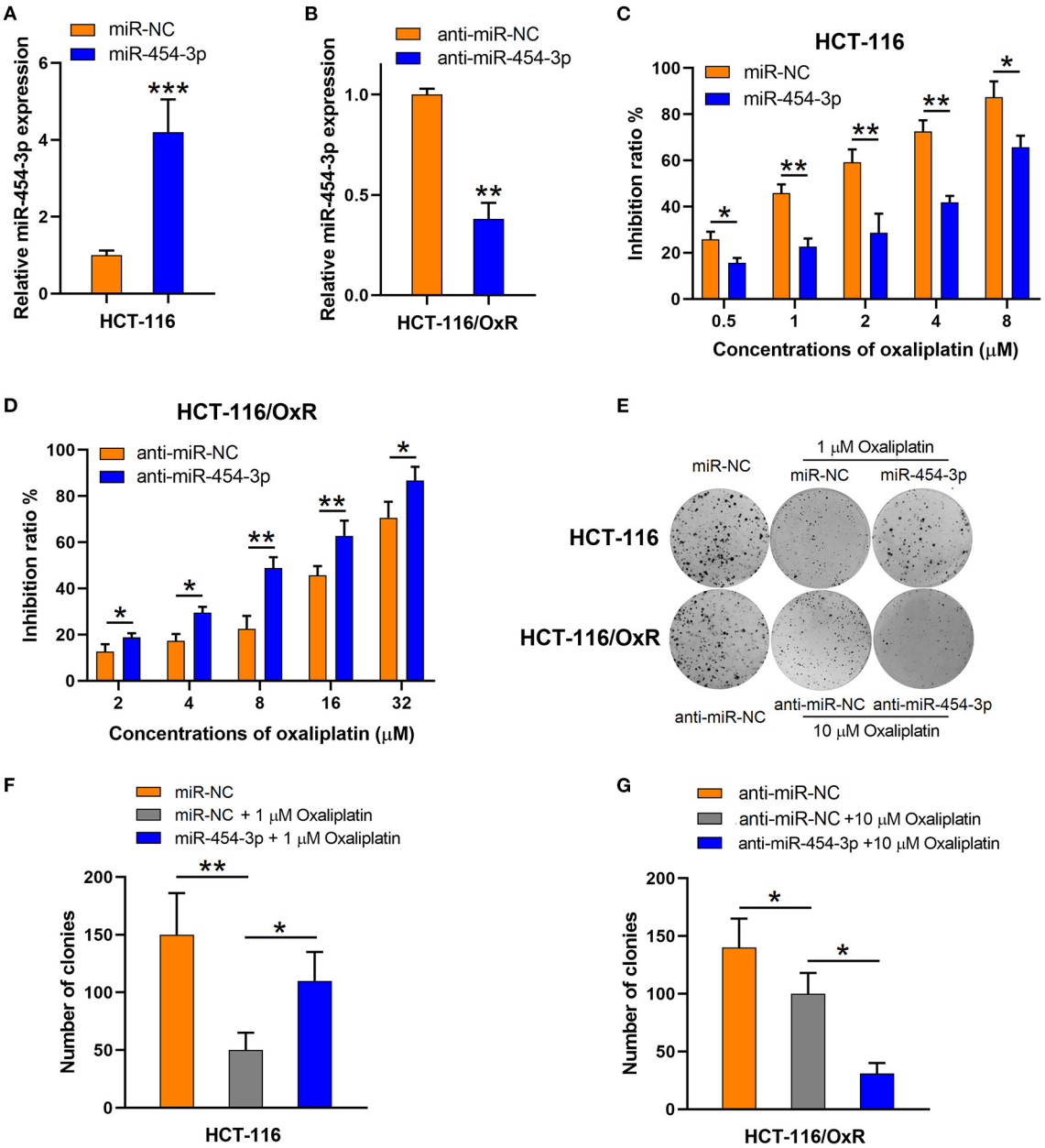

FIGURE 2 | Altering miR-454-3p expression modulates cell sensitivity to oxaliplatin *in vitro*. **(A,B)** Quantitative RT-PCR analysis on relative miR-454-3p expression after miR-454-3p was overexpressed in HCT-116 cells **(A)** or knockdown in HCT-116/OxR cells **(B)**. **(C,D)** Inhibitory effects of oxaliplatin on cell viability determined by MTT assay. **(C)** HCT-116 cells transfected with miR-NC or miR-454-3p, and **(D)** HCT-116/OxR transfected with anti–miR-454-3p or anti–miR-NC. **(E–G)** Inhibitory effects of oxaliplatin on colony formation. **(E,F)** HCT-116 cells transfected with miR-NC or miR-454-3p, and **(E,G)** HCT-116/OxR transfected with anti–miR-454-3p or anti–miR-NC. Results were presented as mean ± SD from three independent experiments. $^{*}P < 0.05$, $^{**}P < 0.01$, $^{***}P < 0.001$.

of miR-454-3p significantly reduced the reporter activity of wild-type *PTEN* 3′-UTR, but the reporter activity of mutant *PTEN* 3′-UTR was not affected in HCT-116 cells, compared to that of miR-NC. Furthermore, a Western blot assay showed that overexpression of miR-454-3p mimics significantly down-regulated the expression of PTEN in HCT-116 cells, whereas the inhibition of miR-454-3p significantly up-regulated the expression of PTEN in HCT-116/OxR cells (**Figure 3C**). These results indicate that *PTEN* is the direct target of miR-454-3p.

MiR-454-3p Inhibited Oxaliplatin-Induced Apoptosis by Down-Regulating PTEN Expression

As the inhibition of apoptosis is considered as the main cause of cellular resistance to oxaliplatin (13, 14), we next sought to determine the effect of miR-454-3p on oxaliplatin-induced apoptosis in colorectal cancer cells. HCT-116 cells overexpressed miR-454-3p or miR-NC, and HCT-116/OxR cells

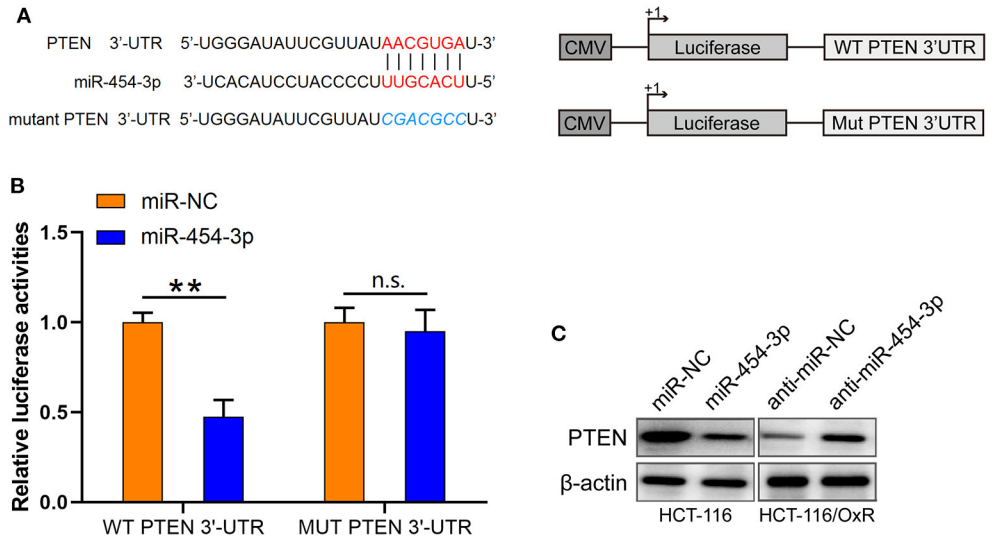

FIGURE 3 | PTEN is a target of miR-454-3p. **(A)** Predicted miR-454-3p binding site in the 3′-UTR of PTEN. **(B)** Luciferase reporter assay confirmed that miR-454-3p bound to 3′-UTR of PTEN. **(C)** Western blotting assay showed the protein level of PTEN after overexpression or knockdown of miR-454-3p. $^{**}P < 0.01$.

transfected with anti–miR-454-3p inhibitor or anti–miR-NC were treated with 2.5 or 20 μM of oxaliplatin, followed by double-staining with annexin V–FITC and PI. Quantitative examination of cellular apoptosis by flow cytometry assay showed that overexpression of miR-454-3p inhibited oxaliplatin-induced cellular apoptosis, which was reversed by additional transfection of PTEN cDNA in HCT116 cells (**Figures 4A,B**). In contrast, inhibition of miR-454-3p increased the oxaliplatin-induced cellular apoptosis, which was reversed by further knockdown of PTEN in HCT-116/OxR cells (**Figures 4A,C**). Furthermore, we showed that overexpression of miR-454-3p significantly decreased caspase-3 activity, whereas the inhibition of miR-454-3p increased caspase-3 activity in HCT-116 or HCT-116/OxR cells, following treatment with oxaliplatin (**Figures 4D,E**). Moreover, overexpressing or silencing PTEN by the transfection of PTEN cDNA or siRNA partially reversed the effect of miR-454-3p on oxaliplatin-induced caspase-3 activity in HCT-116 or HCT-116/OxR cells (**Figures 4D,E**). Collectively, these results suggest that miR-454-3p limited oxaliplatin-induced apoptosis by down-regulating PTEN expression.

MiR-454-3p Suppressed Apoptosis and Induced Oxaliplatin Resistance *via* Activation of AKT Pathway

Since PTEN is a well-known suppressor of the PI3K/AKT/mTOR signaling pathway (15, 16), we next determined the effect of miR-454-3p on PI3K/AKT/mTOR pathway. As shown in **Figure 5A**, overexpression of miR-454-3p increased the phosphorylation of AKT and mTOR in HCT-116 cells, whereas its inhibition decreased the phosphorylation of AKT and mTOR in HCT-116/OxR cells. The expression of total AKT and mTOR was not affected by miR-454-3p. Furthermore, the PI3K inhibitor LY294002 was used to block the PI3K/AKT pathway activated by miR-454-3p. The result revealed that LY294002 reversed miR-454-3p–induced oxaliplatin resistance in HCT-116 cells (**Figure 5B**). Moreover, LY294002 resensitized HCT-116/OxR cells to oxaliplatin treatment (**Figure 5C**). In addition, LY294002 treatment also rescued the effect of miR-454-3p on oxaliplatin-induced caspase-3 activity in HCT-116 or HCT-116/OxR cells (**Figures 5D,E**). Apoptotic-related proteins Bcl-2, Bax, and cleaved caspase-3 were evaluated by Western blotting. As shown in **Figure 5F**, oxaliplatin treatment dramatically up-regulated the ratio of Bax/Bcl-2 expression and induced the cleavage of caspase-3, which were reversed by the overexpression of miR-454-3p. However, LY294002 treatment reduced the effects of miR-454-3p on the decrease of the Bax/Bcl-2 expression ratio and on the inhibition of cleavage of caspase-3. These results demonstrated that miR-454-3p suppresses oxaliplatin-induced apoptosis and leads to resistance to oxaliplatin *via* activating PTEN/AKT/mTOR pathway.

MiR-454-3p Promoted Oxaliplatin Resistance in HCT-116 Colorectal Cancer Cells *in vivo*

To further investigate the effect of miR-454-3p on oxaliplatin resistance *in vivo*, colorectal cancer xenograft models were established by subcutaneously injecting mice with HCT-116 cells that were stably overexpressed miR-454-3p or negative control miRNA (miR-NC). After the tumor value reached 100 mm^3 (8 days after tumor inoculation), the mice began receiving oxaliplatin by intraperitoneal injection every 4 days. As shown in **Figures 6A,B**, the miR-NC–transfected tumors grew slower than the miR-454-3p–overexpressed tumors, indicating that miR-454-3p reduced the sensitivity of colorectal cancer cells to oxaliplatin treatment *in vivo*. Quantitative RT-PCR analysis confirmed the expression of miR-454-3p in HCT-116 cells from

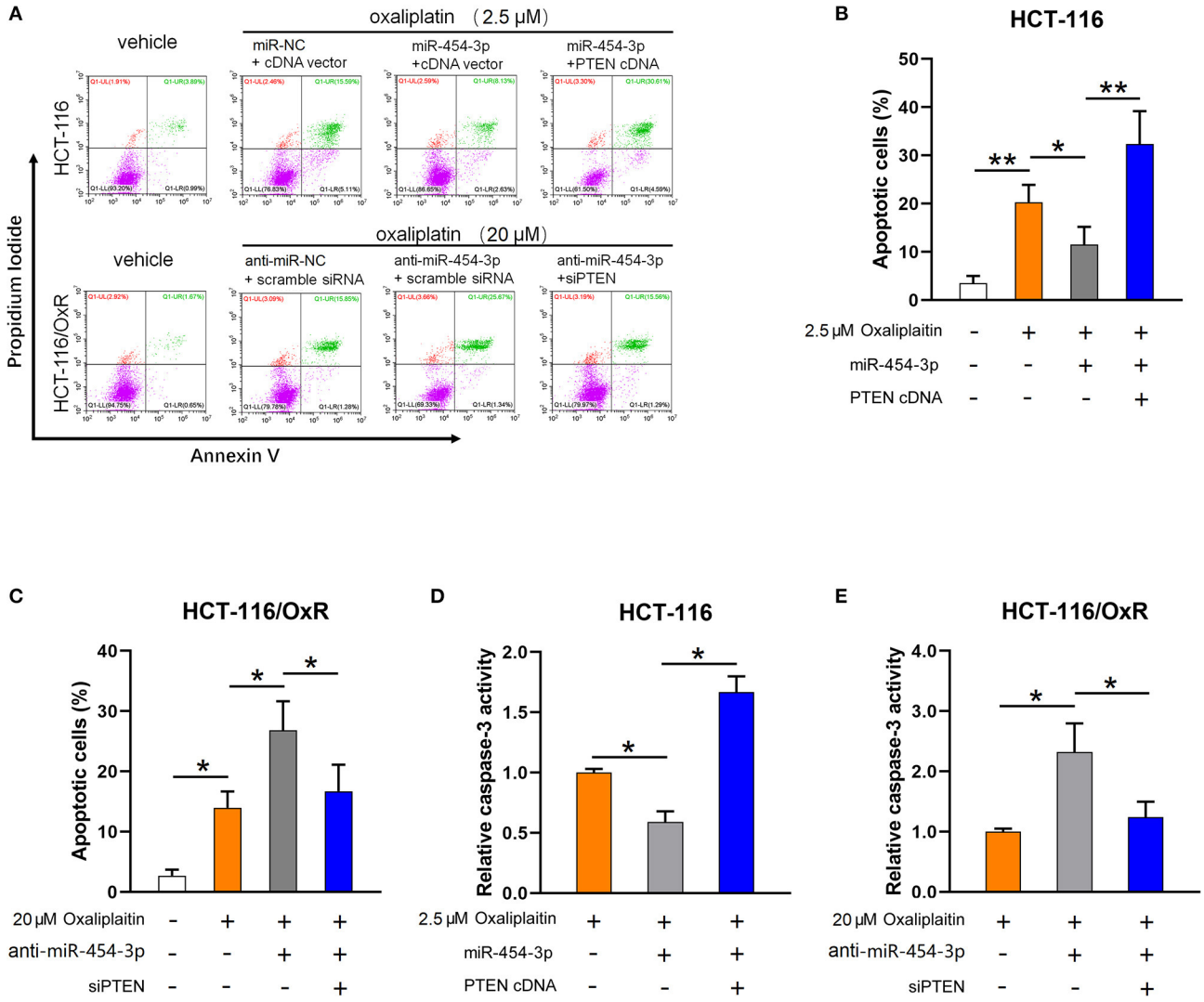

FIGURE 4 | MiR-454-3p attenuates oxaliplatin-induced cell apoptosis through down-regulation of PTEN. **(A–C)** Cell apoptosis qualified by flow cytometry after annexin V–FITC and PI double staining in indicated cells treated with different concentrations of oxaliplatin. **(D,E)** Analysis of caspase-3 activity in indicated cells treated with different concentrations of oxaliplatin. Results were presented as mean ± SD from three independent experiments. $^{*}P < 0.05$, $^{**}P < 0.01$.

representative tumor tissues (**Figure 6C**). These *in vitro* and *in vivo* results revealed that miR-454-3p inhibited oxaliplatin induced-apoptosis and promoted oxaliplatin resistance in colorectal cancer by repressing PTEN expression, thereby enhancing PI3K/AKT signaling pathway (**Figure 6D**).

MiR-454-3p Expression Negatively Correlates With PFS in Colorectal Cancer Patients Who Received Oxaliplatin-Based Chemotherapy

To study the relationship between miR-454-3p and oxaliplatin resistance in colorectal cancer, we selected 45 patients who had received oxaliplatin-based chemotherapy and stratified these individuals into **two** groups of high and low miR-454-3p expression, according to the expression of miR-454-3p in their tumor tissues by quantitative RT-PCR (**Table 1**). Kaplan–Meier analysis showed that colorectal cancer patients with high miR-454-3p expression exhibited shorter PFS than those with low miR-454-3p expression (**Figure 7A**). Moreover, miR-454-3p expression was significantly more up-regulated in patients with non-response to chemotherapy than in those who showed a response (**Figure 7B**). The receiver operating characteristic curve was conducted to assess the predictive value of miR-454-3p expression for response to oxaliplatin. As shown in **Figure 7C**, the area under the curve (AUC) value was 0.723, yielding sensitivity of 71.0% and specificity of 73.2% at the cutoff value of 3.1 (**Figure 7C**). These data suggest the important role of miR-454-3p in promoting oxaliplatin resistance in colorectal cancer.

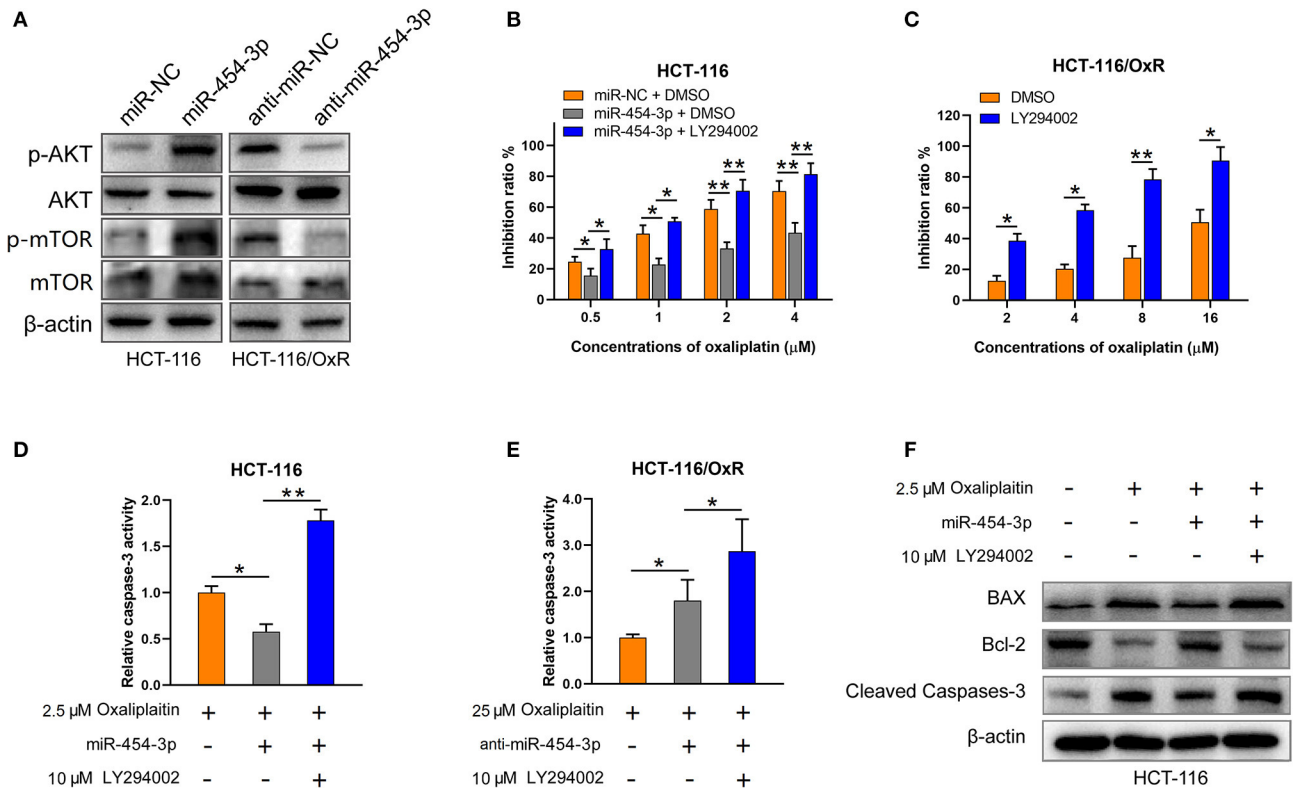

FIGURE 5 | MiR-454-3p suppressed apoptosis and induced oxaliplatin resistance *via* activation of AKT pathway. **(A)** Western blotting on the expression of p-AKT, p-mTOR, total AKT, and total mTOR. β-Actin was used as an endogenous reference. **(B,C)** Cell viability determined by MTT assay in indicated cells treated with oxaliplatin and/or AKT signaling inhibitor LY294002. **(D,E)** Caspase-3 activity in indicated cells treated with different concentrations of oxaliplatin and/or LY294002. **(F)** Western blotting on the expression of apoptosis-related proteins, including Bax, Bcl-2, and cleaved caspase-3. Results were presented as mean ± SD from three independent experiments. $^{*}P < 0.05$, $^{**}P < 0.01$.

DISCUSSION

Oxaliplatin resistance has been recognized as one of the major obstacles preventing the effective therapy in colorectal cancer; however, the underlying molecular mechanism remains largely unclear. A growing number of studies have indicated that aberrant miRNA expression modulates genes related to chemosensitivity or chemoresistance in various human malignancies, including colorectal cancer (17–21). A previous study showed that natural killer cells inhibit oxaliplatin-resistant colorectal cancer by repressing WBSCR22 *via* up-regulating miR-146b-5p (22). In another study, exosome-mediated miR-128-3p delivery was demonstrated to inhibit oxaliplatin-induced epithelial–mesenchymal transition (EMT) and enhanced oxaliplatin response through negative regulation of Bmi1 and MRP5 in colorectal cancer cells (23). In the present study, we compared the expression of a panel of miRNAs between oxaliplatin-sensitive and -resistant HCT-116 colorectal cancer cells by quantitative RT-PCR. Fifteen miRNAs were identified to have more than 2-fold difference in expression between oxaliplatin-sensitive and -resistant cells, including several miRNAs that have been previously reported to be associated with oxaliplatin sensitivity in colorectal and other cancer cells. For instance, it has been reported that miR-153 (24) and miR-20a (25) enhanced oxaliplatin resistance by inhibiting FOXO3a and BNIP2 in colorectal cancer, whereas miR-122 (26, 27) sensitizes hepatocellular carcinoma to oxaliplatin by inhibiting the Wnt/β-catenin pathway.

In this study, we observed that miR-454-3p was the most differently expressed miRNA and significantly up-regulated in oxaliplatin-resistant cells. Furthermore, we showed that the inhibition of miR-454-3p resensitized oxaliplatin-resistant cells to oxaliplatin by enhancing its inhibitory effect on cell viability and colony formation, suggesting the essential role of miR-454-3p in regulating oxaliplatin resistance. Several studies have partially described the mechanisms of miR-454-3p in the promotion or suppression of cancer progression. It has been reported that miR-454-3p promotes breast cancer metastasis through targeting nuclear precursor mRNA domain-containing 1A (RPRD1A), a known tumor suppressor, thereby activating Wnt/β-catenin signaling pathway (28). In cervical cancer, miR-454-3p was found to promote cell proliferation and inhibit apoptosis by targeting tripartite motif-containing 3 (TRIM3) (29). Conversely, miR-454-3p was also observed to act as a tumor suppressor in bladder cancer (30) and non–small cell lung cancer (31) by targeting the EMT inducer ZEB2

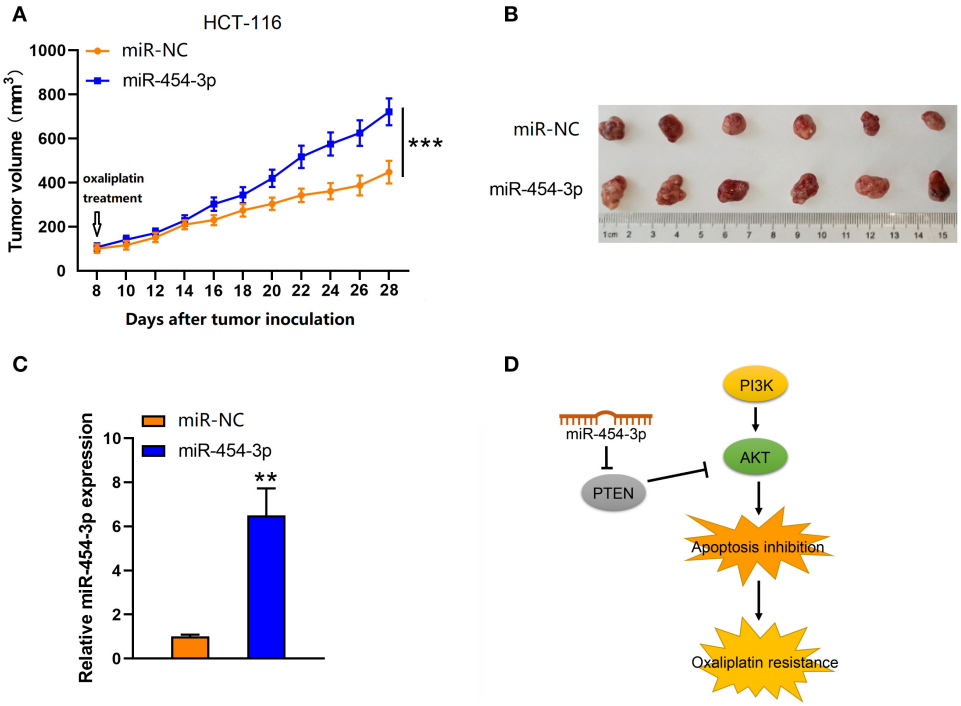

FIGURE 6 | Up-regulation of miR-454-3p reduced the sensitivity of colorectal cancer cells to oxaliplatin *in vivo*. **(A)** Tumor xenografts with HCT-116 cells stably transfected with miR-454-3p or negative control. The mice received oxaliplatin every 4 days starting from the 8th day after tumor inoculation. **(B)** Representative images of dissected tumors in each group. **(C)** Quantitative RT-PCR analysis of the expression of miR-454-3p in representative tumor tissues. **(D)** A proposed mechanism of miR-454-3p mediated oxaliplatin resistance. $^{**}P < 0.01$, $^{***}P < 0.001$.

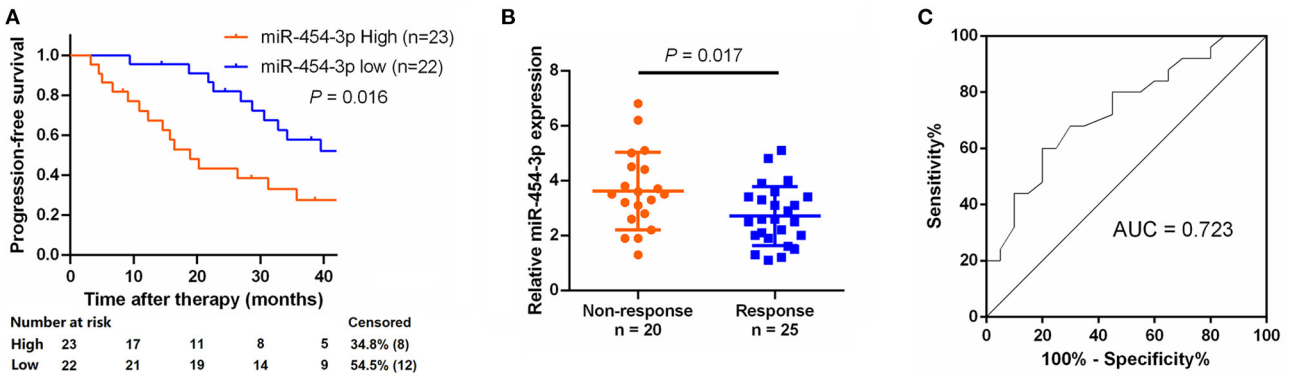

FIGURE 7 | Expression of miR-454-3p correlates with PFS in oxaliplatin treated colorectal cancer patients. **(A)** Colorectal cancer patients who received oxaliplatin-based chemotherapy were separated into groups based on low or high miR-454-3p expression. Kaplan–Meier survival curves were used to compare the PFS between the two groups. **(B)** Expression of miR-454-3p in patients who responded to oxaliplatin ($n = 25$) and who did not respond ($n = 20$) to oxaliplatin was compared using the two-tailed Student *t* test. *U6* small nuclear RNA was used as an internal control. **(C)** ROC curve for patients responding vs. non-responding to oxaliplatin treatment. The AUC value was 0.723, yielding sensitivity of 71.0% and specificity of 73.2% at the cutoff value of 3.1.

or constituent Ca^{2+}-binding protein calbindin 1 (CALB1), respectively. However, the association between miR-454-3p and oxaliplatin resistance is unknown. Therefore, we chose miR-454-3p to further assess its function and directly target the relevant genes in oxaliplatin resistance.

Using a bioinformatics method, together with experimental approaches, we identified *PTEN* as the direct target of miR-454-3p, which was further confirmed by luciferase reporter assay and Western blot analysis. PTEN is a well-characterized tumor suppressor that acts by negatively regulating the PI3K/AKT signaling pathway. Increasing evidence has demonstrated that down-regulation or deficiency of PTEN, resulting in hyperactivation of the PI3K/AKT signaling pathway, is closely associated with resistance to platinum-based

chemotherapy, including oxaliplatin (32–34). Our study showed that overexpression of miR-454-3p down-regulated PTEN expression, but promoted phosphorylation of AKT and mTOR, leading to a reduction in oxaliplatin sensitivity. In contrast, inhibition of miR-454-3p up-regulated PTEN expression, but attenuated the phosphorylation of AKT and mTOR, resulting in resensitization to oxaliplatin. Notably, previous studies reported that miR-454-3p inhibited AKT signaling pathway by targeting insulinlike growth factor 2 mRNA-binding protein 1 (IGF2BP1) in esophageal cancer (ESCA) (35) and targeting c-met in nasopharyngeal carcinoma (36), resulting in the suppression of cell growth and enhancement of cisplatin sensitivity. These inconsistent results may indicate that the role of miR-454-3p in modulating tumor progression and chemotherapeutic sensitivity was dependent on the types of human malignancies.

Several studies have indicated that, once phosphorylated by PI3K, activated AKT has direct effects on the regulators of the apoptotic pathway, including Bcl-2 family members, as such activation of PI3K/AKT signaling could up-regulate Bcl-2 expression and enhance its activity, leading to increased cell survival and reduced chemotherapy-induced apoptosis (37–39). Apoptosis is a major form of cell death, which is tightly regulated by the interaction between antiapoptotic and proapoptotic proteins, particularly the Bcl-2 family (40). The ratio between antiapoptotic and proapoptotic Bcl-2 family proteins has been recognized as an effective indicator to judge whether a cell will progress to apoptosis (41). In the current study, we demonstrated that the overexpression of PTEN or the use of the specific AKT signaling inhibitor LY294002 could overcome miR-454-3p–mediated oxaliplatin resistance and further enhance oxaliplatin-induced cellular apoptosis by decreasing the expression ratio of antiapoptotic factor Bcl-2 to proapoptotic factor Bax.

It has also been suggested that miR-454-3p may be used as a prognostic biomarker in different types of cancers. Ren et al. (28) reported that miR-454-3p could be an independent prognostic factor in breast cancer, and patients with higher miR-454-3p expression experienced poorer overall survival and shorter PFS times. Meanwhile, Li et al. (42) found that overexpression of miR-454-3p was significantly correlated with poor prognosis in hepatocellular carcinoma patients. In contrast, Shao et al. (43) observed that overexpression of miR-454-3p in exosomes in plasma and low miR-454-3p expression in tumor tissue were associated with poor prognosis, indicating the functions of miR-454-3p as a tumor suppressor in glioma. Our present study indicated that overexpression of miR-454-3p suggested short PFS in colorectal cancer patients who received oxaliplatin-based chemotherapy, supporting the potential application of miR-454-3p to predict the prognosis of oxaliplatin-based chemotherapy. After being further validated, the measurement of miR-454-3p in colorectal tumor tissues would be used for the prediction of oxaliplatin treatment response and for the selections of chemotherapeutic regimen. In addition, silencing miR-454-3p by chemical compounds could be a novel therapeutic strategy to sensitize colorectal tumor cells to oxaliplatin treatment.

Although several miRNAs were previously reported to be involved in oxaliplatin resistance in colorectal cancer cells through multiple molecular pathway (9–12), including PTEN-AKT signaling pathway (32–34), to our knowledge, there is no investigation implicating miR-454-3p in chemoresistance of colorectal cancer. Our current study identified miR-454-3p as a critical factor of oxaliplatin resistance in colorectal cancer cells by comparing its expression between oxaliplatin-sensitive and -resistant colorectal cancer cells. In particular, we proved that miR-454-3p directly binds to 3′-UTR of *PTEN* and reduces its expression by analyzing the binding ability of miR-454-3p to wild-type or mutant *PTEN* 3′-UTR.

In conclusion, our study provides evidence that miR-454-3p promoted oxaliplatin resistance in colorectal cancer cells by targeting PTEN expression, which negatively regulated PI3K/AKT signaling pathway. Inhibition of miR-454-3p or restoration of PTEN expression resensitized colorectal cancer cells to oxaliplatin through attenuating PI3K/AKT signaling pathway. Clinically, overexpression of miR-454-3p was associated with a decreased responsiveness to oxaliplatin-based chemotherapy, as well as a short PFS. These data indicated that miR-454-3p possesses the potential of predicting oxaliplatin sensitivity and could be a novel therapeutic target to overcome oxaliplatin resistance in colorectal cancer.

DATA AVAILABILITY STATEMENT

The original contributions presented in the study are included in the article/supplementary material, further inquiries can be directed to the corresponding author/s.

ETHICS STATEMENT

The studies involving human participants were reviewed and approved by Medical Ethics Committee of Zhangjiagang First People's Hospital. The patients/participants provided their written informed consent to participate in this study. The animal study was reviewed and approved by Medical Ethics Committee of Zhangjiagang First People's Hospital.

AUTHOR CONTRIBUTIONS

X-LQ, YZ, and CN designed the projects and wrote the manuscript. X-LQ, FZ, SX, JJ, Z-PC, and S-KW performed the experiments and analyzed the results. All authors read and agreed the final manuscript.

FUNDING

This study was supported by Suzhou Development Plan of Science-technology (Program of Basic and Clinical Medicine No. SYSD2018008), and by Zhangjiagang Science-technology supporting plan (ZKS1814, 2018).

ACKNOWLEDGMENTS

We thank LetPub (www.letpub.com) for its linguistic assistance during the preparation of this manuscript.

REFERENCES

1. Bray F, Ferlay J, Soerjomataram I, Siegel RL, Torre LA, Jemal A. Global cancer statistics 2018: GLOBOCAN estimates of incidence and mortality worldwide for 36 cancers in 185 countries. *CA Cancer J Clin.* (2018) 68:394–424. doi: 10.3322/caac.21492
2. Polastro L, El Hachem G, Hendlisz A. Pseudoadjuvant chemotherapy in resectable metastatic colorectal cancer. *Curr Opin Oncol.* (2018) 30:269–75. doi: 10.1097/CCO.0000000000000455
3. Chan GHJ, Chee CE. Making sense of adjuvant chemotherapy in colorectal cancer. *J Gastrointest Oncol.* (2019) 10:1183–92. doi: 10.21037/jgo.2019.06.03
4. Sanz-Garcia E, Grasselli J, Argiles G, Elez ME, Tabernero J. Current and advancing treatments for metastatic colorectal cancer. *Expert Opin Biol Ther.* (2016) 16:93–110. doi: 10.1517/14712598.2016.1108405
5. Kelland L. The resurgence of platinum-based cancer chemotherapy. *Nat Rev Cancer.* (2007) 7:573–84. doi: 10.1038/nrc2167
6. Yu X, Li Z, Yu J, Chan MT, Wu WK. MicroRNAs predict and modulate responses to chemotherapy in colorectal cancer. *Cell Prolif.* (2015) 48:503–10. doi: 10.1111/cpr.12202
7. Moradi-Marjaneh R, Khazaei M, Seifi S, Hassanian SM, Ferns GA, Avan A. Pharmacogenetics of anticancer drug sensitivity and toxicity in colorectal cancer. *Curr Pharm Des.* (2018) 24:2710–8. doi: 10.2174/1381612824666180727144535
8. Bartel DP. MicroRNAs: target recognition and regulatory functions. *Cell.* (2009) 136:215–33. doi: 10.1016/j.cell.2009.01.002
9. Moradi Marjaneh R, Khazaei M, Ferns GA, Avan A, Aghaee-Bakhtiari SH. MicroRNAs as potential therapeutic targets to predict responses to oxaliplatin in colorectal cancer: From basic evidence to therapeutic implication. *IUBMB Life.* (2019) 71:1428–41. doi: 10.1002/iub.2108
10. Ghanbarian M, Afgar A, Yadegarazari R, Najafi R, Teimoori-Toolabi L. Through oxaliplatin resistance induction in colorectal cancer cells, increasing ABCB1 level accompanies decreasing level of miR-302c-5p, miR-3664-5p and miR-129-5p. *Biomed Pharmacother.* (2018) 108:1070–80. doi: 10.1016/j.biopha.2018.09.112
11. Zhou H, Lin C, Zhang Y, Zhang X, Zhang C, Zhang P, et al. miR-506 enhances the sensitivity of human colorectal cancer cells to oxaliplatin by suppressing MDR1/P-gp expression. *Cell Prolif.* (2017) 50:e12341. doi: 10.1111/cpr.12341
12. Tan S, Shi H, Ba M, Lin S, Tang H, Zeng X, et al. miR-409-3p sensitizes colon cancer cells to oxaliplatin by inhibiting Beclin-1-mediated autophagy. *Int J Mol Med.* (2016) 37:1030–8. doi: 10.3892/ijmm.2016.2492
13. Chen X, Wu Y, Dong H, Zhang CY, Zhang Y. Platinum-based agents for individualized cancer treatment. *Curr Mol Med.* (2013) 13:1603–12. doi: 10.2174/15665240136661311125515
14. Fujie Y, Yamamoto H, Ngan CY, Takagi A, Hayashi T, Suzuki R, et al. Oxaliplatin, a potent inhibitor of survivin, enhances paclitaxel-induced apoptosis and mitotic catastrophe in colon cancer cells. *Jpn J Clin Oncol.* (2005) 35:453–63. doi: 10.1093/jjco/hyi130
15. Luongo F, Colonna F, Calapà F, Vitale S, Fiori ME, De Maria R. PTEN tumor-suppressor: the dam of stemness in cancer. *Cancers.* (2019) 11:1076. doi: 10.3390/cancers11081076
16. Carnero A, Blanco-Aparicio C, Renner O, Link W, Leal JF. The PTEN/PI3K/AKT signalling pathway in cancer, therapeutic implications. *Curr Cancer Drug Targets.* (2008) 8:187–98. doi: 10.2174/156800908784293659
17. Gabra MM, Salmena L. microRNAs and acute myeloid leukemia chemoresistance: a mechanistic overview. *Front Oncol.* (2017) 7:255. doi: 10.3389/fonc.2017.00255
18. Ding B, Lou W, Xu L, Fan W. Non-coding RNA in drug resistance of hepatocellular carcinoma. *Biosci Rep.* (2018) 38:BSR20180915. doi: 10.1042/BSR20180915
19. Kulkarni B, Kirave P, Gondaliya P, Jash K, Jain A, Tekade RK, et al. Exosomal miRNA in chemoresistance, immune evasion, metastasis and progression of cancer. *Drug Discov Today.* (2019) 24:2058–67. doi: 10.1016/j.drudis.2019.06.010
20. Madurantakam Royam M, Ramesh R, Shanker R, Sabarimurugan S, Kumarasamy C, Ramesh N, et al. miRNA predictors of pancreatic cancer chemotherapeutic response: a systematic review and meta-analysis. *Cancers.* (2019) 11:900. doi: 10.3390/cancers11070900
21. Wei L, Wang X, Lv L, Zheng Y, Zhang N, Yang M. The emerging role of noncoding RNAs in colorectal cancer chemoresistance. *Cell Oncol (Dordr).* (2019) 42:757–68. doi: 10.1007/s13402-019-00466-8
22. Zhao H, Su W, Kang Q, Xing Z, Lin X, Wu Z. Natural killer cells inhibit oxaliplatin-resistant colorectal cancer by repressing WBSCR22 *via* upregulating microRNA-146b-5p. *Am J Cancer Res.* (2018) 8:824–34.
23. Liu T, Zhang X, Du L, Wang Y, Liu X, Tian H, et al. Exosome-transmitted miR-128-3p increase chemosensitivity of oxaliplatin-resistant colorectal cancer. *Mol Cancer.* (2019) 18:43. doi: 10.1186/s12943-019-0981-7
24. Zhang L, Pickard K, Jenei V, Bullock MD, Bruce A, Mitter R, et al. miR-153 supports colorectal cancer progression *via* pleiotropic effects that enhance invasion and chemotherapeutic resistance. *Cancer Res.* (2013) 73:6435–47. doi: 10.1158/0008-5472.CAN-12-3308
25. Chai H, Liu M, Tian R, Li X, Tang H. miR-20a targets BNIP2 and contributes chemotherapeutic resistance in colorectal adenocarcinoma SW480 and SW620 cell lines. *Acta Biochim Biophys Sin.* (2011) 43:217–25. doi: 10.1093/abbs/gmq125
26. Cao F, Yin LX. miR-122 enhances sensitivity of hepatocellular carcinoma to oxaliplatin *via* inhibiting MDR1 by targeting Wnt/β-catenin pathway. *Exp Mol Pathol.* (2019) 106:34–43. doi: 10.1016/j.yexmp.2018.10.009
27. Hua Y, Zhu Y, Zhang J, Zhu Z, Ning Z, Chen H, et al. miR-122 targets X-linked inhibitor of apoptosis protein to sensitize oxaliplatin-resistant colorectal cancer cells to oxaliplatin-mediated cytotoxicity. *Cell Physiol Biochem.* (2018) 51:2148–59. doi: 10.1159/000495832
28. Ren L, Chen H, Song J, Chen X, Lin C, Zhang X, et al. MiR-454-3p-mediated Wnt/β-catenin signaling antagonists suppression promotes breast cancer metastasis. *Theranostics.* (2019) 9:449–65. doi: 10.7150/thno.29055
29. Song Y, Guo Q, Gao S, Hua K. miR-454-3p promotes proliferation and induces apoptosis in human cervical cancer cells by targeting TRIM3. *Biochem Biophys Res Commun.* (2019) 516:872–9. doi: 10.1016/j.bbrc.2019.06.126
30. Wang S, Zhang G, Zheng W, Xue Q, Wei D, Zheng Y, et al. MiR-454-3p and miR-374b-5p suppress migration and invasion of bladder cancer cells through targetting ZEB2. *Biosci Rep.* (2018) 38:BSR20181436. doi: 10.1042/BSR20181436
31. Jin C, Lin T, Shan L. Downregulation of calbindin 1 by miR-454-3p suppresses cell proliferation in nonsmall cell lung cancer *in vitro*. *Cancer Biother Radiopharm.* (2019) 34:119–27. doi: 10.1089/cbr.2018.2598
32. Roy S, Yu Y, Padhye SB, Sarkar FH, Majumdar AP. Difluorinated-curcumin (CDF) restores PTEN expression in colon cancer cells by down-regulating miR-21. *PLoS ONE.* (2013) 8:e68543. doi: 10.1371/journal.pone.0068543
33. Liang Y, Zhu D, Zhu L, Hou Y, Hou L, Huang X, et al. Dichloroacetate overcomes oxaliplatin chemoresistance in colorectal cancer through the miR-543/PTEN/Akt/mTOR pathway. *J Cancer.* (2019) 10:6037–47. doi: 10.7150/jca.34650
34. Zhang Y, Liu X, Zhang J, Xu Y, Shao J, Hu Y, et al. Inhibition of miR-19a partially reversed the resistance of colorectal cancer to oxaliplatin *via* PTEN/PI3K/AKT pathway. *Aging.* (2020) 12:5640–50. doi: 10.18632/aging.102929
35. Yan A, Wang C, Zheng L, Zhou J, Zhang Y. MicroRNA-454-3p inhibits cell proliferation and invasion in esophageal cancer by targeting insulin-like growth factor 2 mRNA-binding protein 1. *Oncol Lett.* (2020) 20:359. doi: 10.3892/ol.2020.12223
36. Lin F, Lin X, Xu L, Zhu S. Long noncoding RNA HOXA11-AS modulates the resistance of nasopharyngeal carcinoma cells to cisplatin *via* miR-454-3p/c-Met. *Mol Cells.* (2020) 43:856–69. doi: 10.14348/molcells.2020.0133
37. Zheng Q, Wang B, Gao J, Xin N, Wang W, Song X, et al. CD155 knockdown promotes apoptosis *via* AKT/Bcl-2/Bax in colon cancer cells. *J Cell Mol Med.* (2018) 22:131–40. doi: 10.1111/jcmm.13301
38. Li N, Zhang Z, Jiang G, Sun H, Yu D. Nobiletin sensitizes colorectal cancer cells to oxaliplatin by PI3K/Akt/MTOR pathway. *Front Biosci.* (2019) 24:303–12. doi: 10.2741/4719
39. Rahmani M, Nkwocha J, Hawkins E, Pei X, Parker RE, Kmieciak M, et al. Cotargeting BCL-2 and PI3K induces BAX-dependent mitochondrial apoptosis in AML cells. *Cancer Res.* (2018) 78:3075–86. doi: 10.1158/0008-5472.CAN-17-3024
40. Estaquier J, Vallette F, Vayssiere JL, Mignotte B. The mitochondrial pathways of apoptosis. *Adv Exp Med Biol.* (2012) 942:157–83. doi: 10.1007/978-94-007-2869-1_7

41. Korsmeyer SJ, Shutter JR, Veis DJ, Merry DE, Oltvai ZN. Bcl-2/Bax: a rheostat that regulates an anti-oxidant pathway and cell death. *Semin Cancer Biol.* (1993) 4:327–32.
42. Li Y, Jiao Y, Fu Z, Luo Z, Su J, Li Y. High miR-454-3p expression predicts poor prognosis in hepatocellular carcinoma. *Cancer Manag Res.* (2019) 11:2795–802. doi: 10.2147/CMAR.S196655
43. Shao N, Xue L, Wang R, Luo K, Zhi F, Lan Q. miR-454-3p is an exosomal biomarker and functions as a tumor suppressor in glioma. *Mol Cancer Ther.* (2019) 18:459–69. doi: 10.1158/1535-7163.MCT-18-0725

Conflict of Interest: The authors declare that the research was conducted in the absence of any commercial or financial relationships that could be construed as a potential conflict of interest.

frontiers in Oncology

ORIGINAL RESEARCH
published: 07 May 2021
doi: 10.3389/fonc.2021.671382

Siteng Fang Reverses Multidrug Resistance in Gastric Cancer: A Network Pharmacology and Molecular Docking Study

Lingjian Guo[1†], *Haixia Shi*[2] *and Limin Zhu*[1*†]

[1] LongHua Hospital Shanghai University of Traditional Chinese Medicine, Shanghai, China, [2] Shanghai Ninth People's Hospital Affiliated to School of Medicine, Shanghai Jiao Tong University, Shanghai, China

Siteng Fang (STF) has been shown to inhibit migration, invasion, and adhesion as well as promote apoptosis in gastric cancer (GC) cells. However, whether it can reverse the multidrug resistance (MDR) of GC to chemotherapy drugs is unknown. Thus, we aimed to elucidate the mechanism of STF in reversing the MDR of GC. The chemical composition of STF and genes related to GC were obtained from the TCMNPAS(TCM Network Pharmacology Analysis System, TCMNPAS) Database, and the targets of the active ingredients were predicted using the Swiss Target Prediction Database. The obtained data were mapped to obtain the key active ingredients and core targets of STF in treating GC. The active component-target network and protein interaction network were constructed by Cytoscape and String database, and the key genes and core active ingredients were obtained. The biological functions and related signal pathways corresponding to the key targets were analyzed and then verified *via* molecular docking. A total of 14 core active ingredients of STF were screened, as well as 20 corresponding targets, which were mainly enriched in cancer pathway, proteoglycan synthesis, PI3K-AKT signaling pathway, and focal adhesion. Molecular docking showed that the core active ingredients related to MDR, namely quercetin and diosgenin, could bind well to the target. In summary, STF may reverse the MDR of GC and exert synergistic effect with chemotherapeutic drugs. It mediates MDR mainly through the action of quercetin and diosgenin on the PI3K/AKT signaling pathway. These findings are the first to demonstrate the molecular mechanism of STF in reversing MDR in GC, thus providing a direction for follow-up basic research.

Keywords: Siteng Fang, gastric cancer, network pharmacology, molecular docking, multidrug resistance

OPEN ACCESS

Edited by:
Dong-Hua Yang,
St. John's University,
United States

Reviewed by:
Qin Xu,
Shanghai Jiao Tong University,
China
Li Gao,
Shanxi University, China

***Correspondence:**
Limin Zhu
zhulimin2000@126.com

[†]*These authors have contributed equally to this work and share first authorship*

Specialty section:
This article was submitted to Gastrointestinal Cancers, a section of the journal Frontiers in Oncology

Received: *23 February 2021*
Accepted: *06 April 2021*
Published: *07 May 2021*

Citation:
Guo L, Shi H and Zhu L (2021) Siteng Fang Reverses Multidrug Resistance in Gastric Cancer: A Network Pharmacology and Molecular Docking Study. Front. Oncol. 11:671382. doi: 10.3389/fonc.2021.671382

INTRODUCTION

Gastric cancer (GC) is one of five cancers with the highest incidence in China (1). According to the National Cancer Center, the incidence and mortality of GC ranked second among malignant tumors in China in 2015, and showed an increasing trend each year (2). Moreover, the early diagnosis rate of GC in China is low; patients with GC are often diagnosed with advanced disease.

Thus, GC is a serious threat to the quality of life and health of the Chinese population. Chemotherapy is one of the important approaches to GC treatment. However, multidrug resistance (MDR) has become a common phenomenon, and it is a main reason for chemotherapy failure, making it difficult to improve the survival rate of patients with advanced GC (3). Therefore, overcoming the MDR of GC to chemotherapy and improving the efficacy of anticancer drugs are key issues in the global medical community.

Traditional Chinese medicine (TCM) has been used for the treatment of GC, and clinical studies have shown that TCM can improve the effect of western medicine, reduce the size and clinical stage of tumor, reverse MDR to chemotherapy drugs, relieve adverse reactions to chemotherapy, and improve the quality of life of patients (4). Weichang'an decoction was developed based on the clinical experience of Professor Qiu Jiaxin, a famous TCM doctor in Shanghai, China. It has been used in clinical setting as a hospital preparation for more than 30 years, and its efficacy has been confirmed by experimental studies. Weichang'an decoction can inhibit the metastasis and invasion of GC cells, induce apoptosis, regulate immunity, and regulate the expression of multiple genes (5); Siteng Fang (STF), which is composed of Radix Actinidiae Chinensis, wild grape, *Sargentodoxa* vine, and Chinaroot Greenbrier Rhizome Catbriar, is a small prescription of Weichang'an decoction. Its main efficacies are clearing away heat as well as detoxifying and eliminating pathogenic factors. Clinical research has demonstrated that STF improves the clinical efficacy of chemotherapy drugs and the quality of life of patients with GC (6–8). In addition, STF could inhibit the migration, invasion, and adhesion of GC cells and promote apoptosis (9). We have also previously observed a capacity of STF to reverse MDR (currently not reported). However the underlying molecular mechanism of MDR reversal remains unclear. Therefore, in this study, we aimed to clarify the molecular mechanism of STF in the treatment of GC. For this purpose, we used a combinatorial approach of network pharmacology and molecular docking technology. The findings of our study are the first to report the molecular mechanism of STF in reversing the MDR of GC, and thus will provide a direction for follow-up basic research.

MATERIALS AND METHODS

Screening of Active Ingredients

The network pharmacology analysis system of TCM was developed by Yang Ming, the director of Longhua Hospital Affiliated to Shanghai University of traditional Chinese Medicine (TCM Network Pharmacology Analysis System, TCMNPAS, National Computer Software Registration No. 2019SR1127090) (10). The Chinese names of Radix *Actinidiae chinensis* (mihoutaogen), wild grape (yeputaogen), *Sargentodoxa* vine (daxueteng), and Chinaroot Greenbier Rhizome Catbriar (baqia) were input into the retrieval module of chemical constituents. The Traditional Chinese Medicine Systems Pharmacology Database and Analysis Platform (TCMSP) Version 2.3, Traditional Chinese Medicine Integrated Database (TCMID) Version 2.0, and the Herbal Ingredients' Targets (HIT) Database were screened simultaneously, with TCMNPAS linked to the databases, to determine the chemical composition of STF (11–13). The active STF ingredients were screened based on oral bioavailability (OB) ≥ 30% and drug-likeness (DL) ≥ 0.18 (14) pharmacokinetic characteristics.

Prediction of Drug Targets

To obtain the potential targets of the active ingredients of STF, the SMILES strings obtained from the TCMNPAS Database, were imported into the Swiss Target Prediction Database. Targets with 0 probability were deleted (15).

Collection of GC Related Targets

Disease ID was obtained by inputting the disease keyword "gastric cancer" to the disease gene retrieval module of TCMNPAS. The background automatically connected to GeneCard Database to obtain disease gene and then downloaded and saved the results as GC related targets (16).

Screening of Drug-Disease Key Targets

The targets of the active components of STF and GC-related targets were introduced into venny2.1.0 (https://bioinfogp.cnb.csic.es/tools/venny/index.html), and the intersection was regarded as the target protein of STF in treating GC. Cytoscape 3.7.0 (17) was used to analyze network topology parameters, and the active component-target-disease network diagram was constructed for visualization. Next, to obtain the protein interaction network diagram, the above-mentioned cross-proteins were input in String Database (https://string-db.org), the species was set as "Homo sapiens", and the minimum interaction score was set as 0.4. Finally, the protein interaction data were imported into Cytoscape 3.7.0 to analyze the network topology parameters. The proteins above the median of "Degree" were selected as the key targets, and the corresponding chemical components were the core active components.

Enrichment Analysis of Key Targets

The target obtained from section *Screening of Drug-Disease Key Targets* was transferred into DAVID6.8 (https://david.ncifcrf.Gov) for Gene Ontology (GO) functional enrichment analysis and Kyoto Gene and Genome Encyclopedia (KEGG) pathway enrichment analysis. The species was set as "Homo sapiens", and the result was set as $P<0.05$. GO functional enrichment analysis describes the possible molecular functions of target products, the biological processes involved, and the cellular environment. KEGG pathway enrichment analysis indicates the most significant biological process by classifying the known genome annotation information. Therefore, these methods can predict the potential active components involved in the action mechanism of STF in treating GC.

Molecular Docking Analysis

The protein IDs of the key targets were obtained from the utility module of TCMNPAS and converted into Protein Data Bank (PDB) IDs (every molecular model in the PDB has a unique

accession or identification code). The 3D structure of the key proteins in PDB format were downloaded from the PDB Database (https://www.rcsb.org/). Subsequently, the SMILES strings of the active ingredient numbers, PDB IDs of the key targets, and 3D structure in PDB format obtained from 2.1 were inputted to the molecular docking module of TCMNPAS. The PSOVina algorithm was optimized based on the autodock Vina molecular docking algorithm and used PSOVina for docking (18–21). The energy range was set to 3, the accuracy was 8, and the output was 9 prediction results. The method of protein docking pocket parameters was FromLigand. Finally, the conformation and docking results of the compounds were downloaded and saved. The compound and target protein formats were converted into PDB format by Open Babel (22) and then imported into PyMOL 3.8 (https://pymol.org) to obtain 3D images of molecular docking. When the binding energy is less than -5 kJ/mol, the ligand is regarded to bind well to the receptor.

RESULTS

Active Ingredients

In total, 112 components of STF were obtained from the TCMNPAS Database. After screening and removal of duplicate components according to the set Absorption, Distribution, Metabolism, and Excretion (ADME) parameters, 21 active components were obtained (**Table 1**).

Drug Targets

According to the prediction of Swiss Target Prediction Database, targets with 0 probability were removed; thus, six active components without target information were deleted. Finally, 709 potential targets of STF were obtained.

Gastric Cancer-Related Targets

A total of 515 differentially expressed targets related to GC were identified. APC, CASP10, IRF1, MUTYH, erbB2, FGFR2, PIK3CA, KLF6, KRAS, and CTNNB1 were identified as the proteins with the highest scores.

Drug-Disease Key Targets

From the intersection of the proteins obtained in sections *Drug Targets* and *Gastric Cancer-Related Targets*, 43 proteins involved in the mechanism of STF in treating GC were obtained (**Figure 1A**). The active component-target-disease network diagram was obtained by using Cytoscape 3.7.0. The blue round node represents the potential target of STF in treating GC, the purple rectangle node represents the active component of STF, and the red diamond node represents the targets of GC (**Figure 1B**). The protein interaction was predicted by using the String Database and visualized by Cytoscape 3.7.0. The darker the node, the closer the protein interaction. The top five proteins were AKT1, ESR1, HRAS, EGFR, and STAT3 (**Figure 1C**). According to analysis of network topology parameters, the proteins with more than median Degree of node were selected as key targets. The network contained a total of 20 target proteins (**Table 2**) and 14 core active components (**Table 3**).

Enrichment Analysis of Key Targets

A total of 41 selected key targets were analyzed for GO functional and KEGG pathway enrichment analyses and screened at $P<0.05$. A total of 52 GO biological processes, 9 cell components, 13 molecular functions (**Figure 2A**), and 86 KEGG pathways (**Figure 2B**) were enriched. The enriched molecular functions were ATP binding, protein serine/threonine kinase activity, and metalloendopeptidase activity. The biological processes were mainly involved in the negative regulation of apoptosis, positive regulation of RNA polymerase II

TABLE 1 | Active components list of Siteng Fang.

Number	Compound name	OB (%)	DL
1	beta-sitosterol	36.91	0.75
2	sitosterol	36.91	0.75
3	meso-1,4-Bis-(4-hydroxy-3-methoxyphenyl)-2,3-dimethylbutane	31.32	0.26
4	2-(4-hydroxyphenyl)ethyl (E)-3-(4-hydroxyphenyl)prop-2-enoate	93.36	0.21
5	(-)-catechin	49.68	0.24
6	saringosterol	43.48	0.62
7	methylprotodioscin_	35.12	0.86
8	pseudoprotodioscin_	37.93	0.87
9	Kaempferid	73.41	0.27
10	isoengelitin	34.65	0.7
11	Engelitin	36.27	0.7
12	(2R,3S)-2-(3,5-dihydroxyphenyl)chroman-3,5,7-triol	58.25	0.24
13	astilbin	36.46	0.74
14	taxifolin	57.84	0.27
15	maackoline	56.33	0.92
16	cis-Dihydroquercetin	66.44	0.27
17	diosgenin	80.88	0.81
18	aloe-emodin	83.38	0.24
19	(+)-catechin	54.83	0.24
20	ent-Epicatechin	48.96	0.24
21	quercetin	46.43	0.28

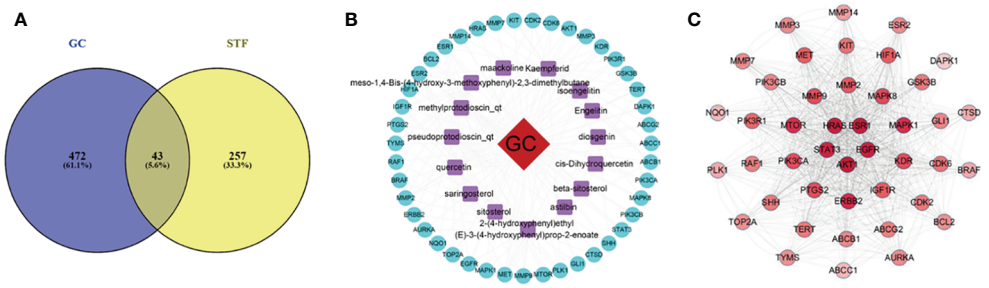

FIGURE 1 | STF-GC gene mapping Venny map **(A)**; Active ingredients-target-disease network **(B)**; PPI network **(C)**.

TABLE 2 | Key targets of STF decoction in the treatment of GC.

Number	Protein Name	Degree
1	AKT1	38
2	ESR1	37
3	HRAS	35
4	EGFR	34
5	STAT3	32
6	ERBB2	30
7	MTOR	29
8	MAPK1	29
9	MAPK8	25
10	PI3KCA	24
11	MMP9	24
12	PTGS2	24
13	KDR	24
14	MMP2	22
15	IGF1R	21
16	HIF1A	21
17	MET	21
18	PIK3R1	19
19	KIT	17
20	CDK6	17

TABLE 3 | Core components of STF in the treatment of GC.

Number	Active Components	Degree
1	Kaempferid	21
2	quercetin	20
3	2-(4-hydroxyphenyl)ethyl (E)-3-(4-hydroxyphenyl)prop-2-enoate	18
4	meso-1,4-Bis-(4-hydroxy-3-methoxyphenyl)-2,3-dimethylbutane	11
5	isoengelitin	6
6	methylprotodioscin_qt	5
7	astilbin	5
8	Engelitin	4
9	diosgenin	4
10	sitosterol	3
11	saringosterol	3
12	beta-sitosterol	2
13	pseudoprotodioscin_qt	2
14	maackoline	2

promoter transcription, and phosphorylation of peptide serine. The cell components were the cell membrane, nucleus, and extracellular matrix. The KEGG pathways were the pathway in cancer, proteoglycan synthesis, PI3K/AKT signaling pathway, focal adhesion, and FOXO signaling pathway.

Molecular Docking Analysis

Two of the screened active components, quercetin and diosgenin, were potentially associated with MDR, as discussed below, and the PI3K/AKT pathway was screened as one of the top 10 KEGG pathways related to MDR. These active

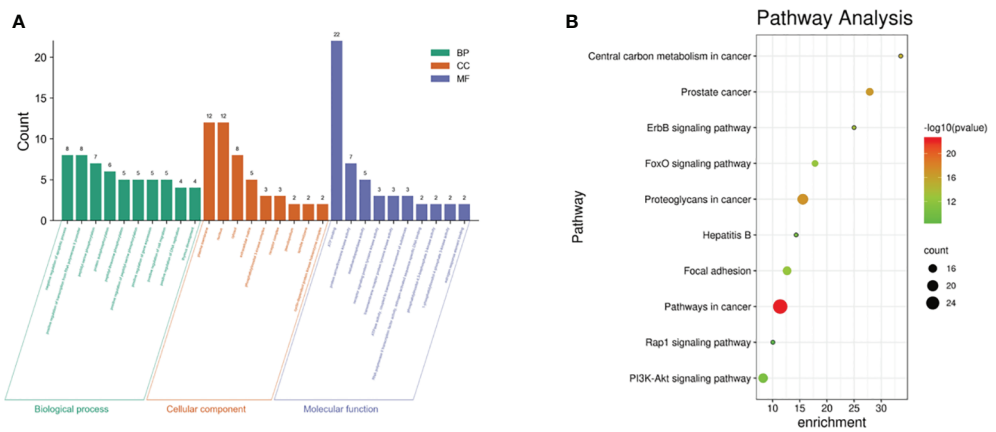

FIGURE 2 | Top 10 GO enrichment classification histogram **(A)**; KEGG enrichment bubble diagram **(B)**.

components were subjected to molecular docking to the receptor proteins of the PI3K/AKT pathway. The results showed that the binding energies of quercetin and diosgenin with the target receptor protein were less than -5 kJ/mol, indicating that they could bind well to the target receptor (**Table 4**). The molecular docking diagram is shown in **Figure 3**. The results confirmed that quercetin and diosgenin could interact with PI3K and AKT. Quercetin and PI3K formed a hydrogen bond through ASP1017. Quercetin and AKT formed three hydrogen bonds through VAL182, TYR306, and ARG308. Diosgenin and PI3K formed a hydrogen bond through ASP1017. Diosgenin and AKT formed a hydrogen bond through GLY775. Quercetin and AKT formed the highest number of hydrogen bonds, and all the binding sites of quercetin and diosgenin with PI3K were on the ASP1017 residue, indicating that quercetin and diosgenin were the two core active components of STF and that the effect of STF in treating GC and reversing MDR might be mediated by the PI3K/AKT signaling pathway.

DISCUSSION

The aim of this study was to elucidate the molecular mechanism of STF in treating GC. A total of 14 core active components of STF were screened out, including kaempferol, quercetin, isoengelitin, methylprotodioscin, and diosgenin. The key signaling pathways included the PI3K/AKT signaling pathway, FOXO signal pathway, and ERBB signaling pathway. Basic studies have confirmed that quercetin, diosgenin, and the PI3K/AKT signaling pathway can regulate MDR to chemotherapeutic drugs. Quercetin is one of the active components of Radix *Actinidiae Chinensis*, and studies had shown that in addition to anti-inflammatory, antioxidant, apoptosis-inducing, and antiangiogenesis effects, quercetin has chemosensitizing effect to enhance the sensitivity of drug-resistant cells to drugs. The effects of quercetin on GC cells have been studied by Sylwia Borska et al. (23) using EPG85-257P cells and daunorubicin-resistant EPG85-257RDB cells. The results showed that quercetin inhibited the growth of the sensitive EPG85-257P cells and had a synergistic effect with daunorubicin. In the drug-resistant EPG85-257RDB cells, quercetin acted as a chemosensitizer, and the drug resistance mechanism of these cells might be related to a decrease in p-glycoprotein (p-gp) expression, obstruction of drug transport, and downregulation of ABCB1 gene expression. The study suggested that quercetin may be effective in reversing the classical drug resistance of GC cells. Zhaolin Chen et al. (24) confirmed that quercetin can increase the accumulation of rhodamine 123 and adriamycin, increase the sensitivity of BEL/5-FU cells to chemotherapeutic drugs, and downregulate the expression of ABCB1, ABCC1, and ABCC2, and that its effect was dependent on FZD7 through the Wnt/β-catenin pathway; quercetin can, at least partially, reverse chemotherapy resistance by inhibiting FZD7. Thus, this compound can be developed into an effective natural sensitizer to reverse the drug resistance of human liver cancer. Diosgenin is one of the active components of Chinaroot Greenbier Rhizome Catbriar, which has pharmacological effects, including anti-inflammatory,

TABLE 4 | The binding energy of key molecules and core targets.

Core active component	Binding energy (KJ/mol)	
	PI3K	AKT
quercetin	-9.0	-8.1
diosgenin	-6.9	-7.9

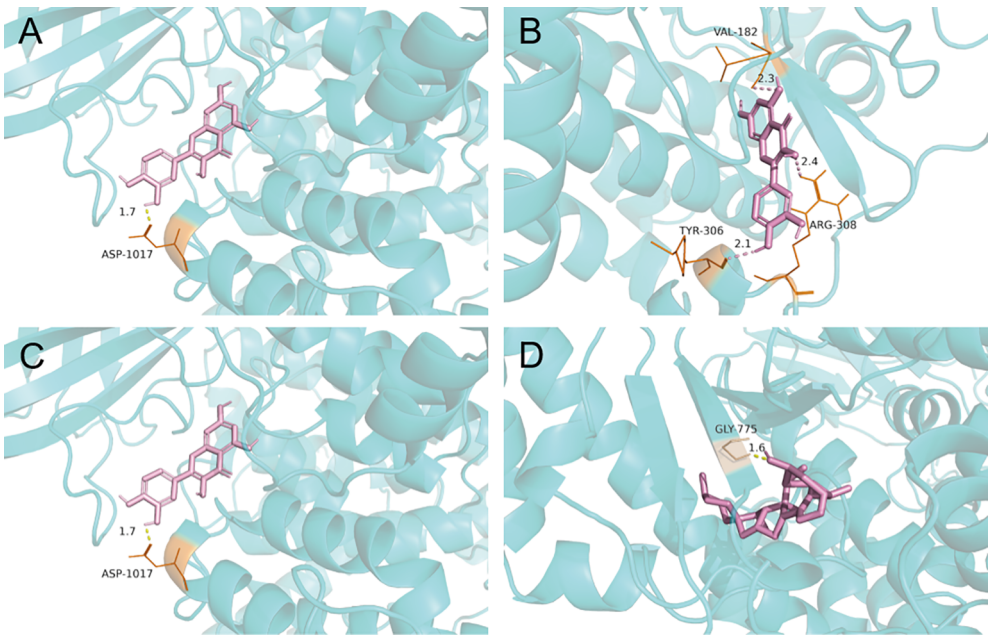

FIGURE 3 | Molecular docking pattern map of quercetin-PI3K **(A)**; Molecular docking pattern map of quercetin-AKT **(B)**; Molecular docking pattern map of diosgenin-PI3K **(C)**; Molecular docking pattern map of diosgenin-AKT **(D)**.

anticancer, antiviral, and hypotensive effects. Bu Tong Sun et al. (25) screened candidate MDR inhibitors among more than 300 natural compounds and revealed that diosgenin exerted inhibitory effect on MDR1 promoter activity. Experiments showed that diosgenin decreased the MDR of HepG2/adriamycin cells, significantly inhibited the expression of P-gp, and increased the accumulation of adriamycin in HepG2/adriamycin cells, indicating that diosgenin is an effective MDR reversal agent and a potential adjuvant drug for tumor chemotherapy. Another study suggested that diosgenin can reverse MDR to adriamycin by inhibiting the nuclear factor kappa B (NF-κB) signaling pathway and downregulating MDR1 expression (26). The PI3K/AKT signaling pathway is the main driving force of various cell functions. Excessive activation of this pathway plays a key role in cancer progression; it can promote tumorigenesis by regulating nutrient metabolism, cell proliferation, cell migration, and angiogenesis. Moreover, abnormal activation of PI3K/AKT is key to the regulation of MDR, mainly through the expression of death-related protein, ABC transporter, and glycogen synthase kinase-3β (GSK-3β), as well as synergistic effect with NF-κB and mammalian target rapamycin (mTOR). Some studies have suggested that P-gp and BCRP can be downregulated by PI3K110α and -110β to restore the drug sensitivity of drug-resistant human epidermoid carcinoma and non-small cell lung cancer, and that ABC family proteins and AKT may play an independent role in enhancing MDR (27–29).

In addition, preliminary research on the mechanism of STF in treating GC showed that STF can inhibit the growth of GC MGC-803 cells by regulating the Smac/Survivin signaling pathway *in vitro*, reduce the adhesion and invasion ability of SGC-7901 cells, inhibit cell migration, and induce apoptosis. Moreover, it can inhibit the growth of SGC-7901 GC cell xenograft tumor in nude mice *in vivo*; this effect may be related to the promotion of apoptosis, upregulation of the expression of apoptosis-related proteins caspase-8 and caspase-9, promotion of PARP editing, and downregulation of Livin protein expression (30–34). STF was also shown to inhibit the invasion, migration, and adhesion of GC cells and promote apoptosis, as confirmed by previous research. Furthermore, at the molecular level, molecular docking analysis showed that quercetin and diosgenin bound well with the active sites of PI3K and AKT, the key targets of the PI3K/AKT pathway, which verified the accuracy of this study to some extent.

In conclusion, this study preliminarily explored the potential molecular mechanism of STF in reversing the MDR of GC to chemotherapy through network pharmacology and molecular docking technology. The present study revealed quercetin and diosgenin as the core active components of STF as well as the PI3K/AKT signaling pathway as an important pathway involved in the effect STF in reversing the MDR of GC. Taken together, our results suggested that STF has the effect of reversing the MDR of GC and that it can play a synergistic effect with chemotherapy drugs. STF mainly reversed MDR through the action of quercetin and diosgenin on the PI3K/AKT signaling pathway. These findings provide a direction for future studies to further explore the mechanism of STF in treating GC. However,

these conclusions were made based on theoretical simulations and thus still need to be verified by experiments. The authors' team will conduct experiments as a follow-up to the present work.

DATA AVAILABILITY STATEMENT

All data generated or analyzed during this study are included in this article.

AUTHOR CONTRIBUTIONS

LG conceptualized and designed the study. LG acquired, analyzed and interpreted the data. LG and HS drafted/revised the work for intellectual content and context. LZ gave the final approval and overall responsibility for the published work. All authors contributed to the article and approved the submitted version.

FUNDING

The research was funded by Shanghai Science and Technology Commission Development Foundation, award number is 16ZR1437500; Shanghai Health and Family Planning Commission of Medical Science and Technology Innovation Project, award number is ZYKC201701009.

ACKNOWLEDGMENTS

The authors would like to thank the participating centers and members. This research did not receive any specific grant from funding agencies in the public, commercial, or not-for-profit sectors.

REFERENCES

1. Chen H, Zheng R, Wang L, Lv Z, Du L, Wei W, et al. Progress in Cancer Epidemiology Research in China in 2019. *Chin J Dis Con* (2020) 24:373–9. doi: 10.16462/j.cnki.zhjbkz.2020.04.001
2. Sun K, Zheng R, Zhang S, Zeng H, Zou X, Chen R, et al. Report of Cancer Incidence and Mortality in Different Areas of China, 2015. *Chin Onc* (2019) 28:1–11. doi: cnki:sun:zhlu.0.2019-01-001
3. Huang WJ, Ruan S, Wen F, Lu X, Gu S, Chen X, et al. Multidrug Resistance of Gastric Cancer: The Mechanisms and Chinese Medicine Reversal Agents. *Cancer Manag Res* (2020) 12:12385–94. doi: 10.2147/CMAR.S274599
4. Liu H. Research Progress on Chinese Materia Medica for Reversing Tumor Multidrug Resistance. *Chin Herb Med* (2015) 46:1096–102. doi: cnki:sun:zcyo.0.2015-07-028
5. Chen W, Bin C, Zhu Y, Zhao A. Research Progress of Professor Qiu's Weichangan in Gastric Cancer. *World Trad Chin Med* (2017) 12:2864–8. doi: cnki:sun:sjza.0.2017-11-074
6. Ma J. Influence of Chemotherapy Combined With Traditional Chinese Medicine Siteng Recipe on the Curative Effect and Survival Quality in Patients With Gastric Cancer After Operation. *Chin Med Mod Dis Edu CN* (2020) 18:129–31. doi: cnki:sun:zzyy.0.2020-15-055
7. Chen Q. Analysis of the Effect of Chemotherapy Combined With Traditional Chinese Medicine Siteng Fang on the Quality of Life of Postoperative Gastric Cancer Patients. *Cardiovasc D Elec J Int Trad Chin West Med* (2020) 8 (02):177–8. doi: 10.16282/j.cnki.cn11-9336/r.2020.02.142
8. Mao ZJ, Shen KP, Zhu LM, Yao Q, Zheng J. Effect of Chemotherapy Combined With Traditional Chinese Medicine Si Teng Fang on the Quality of Life of Patients After Gastric Cancer Surgery. *J Colorectal Anal Surg* (2016) 22(S2):156–7. doi: cnki:sun:dcgm.0.2016-S2-108
9. Zhu L, Shen K, Zhou H, Pan C, Yao Q. Effect of Wei Chang An and Si Teng Fang on Stem Cells CD133~+ of Human Colon Cancer Strains. *J Shanghai Jiaotong Univ (Med E)* (2016) 36:161–165+171. doi: cnki:sun:shey.0.2016-02-006
10. Yang M, Chen JL, Xu LW, Ji G. Navigating Traditional Chinese Medicine Network Pharmacology and Computational Tools. *Evid Based Complement Alternat Med* (2013) 2013:731969. doi: 10.1155/2013/731969
11. Hao Y, Li Y, Kang H, Zhang D, Lin T, Tang K, et al. HIT: Linking Herbal Active Ingredients to Targets. *Nucleic Acids Res* (2011) 39:D1055–9. doi: 10.1093/nar/gkq1165
12. Ru J, Li P, Wang J, Zhou W, Li B, Huang C, et al. TCMSP: A Database of Systems Pharmacology for Drug Discovery From Herbal Medicines. *J Cheminform* (2014) 6:13. doi: 10.1186/1758-2946-6-13
13. Huang L, Xie D, Yu Y, Liu H, Shi Y, Shi T, et al. TCMID 2.0: A Comprehensive Resource for TCM. *Nucleic Acids Res* (2018) 46:D1117–20. doi: 10.1093/nar/gkx1028
14. Yang M, Chen J, Shi X, Xu L, Xi Z, You L, et al. Development of in Silico Models for Predicting P-Glycoprotein Inhibitors Based on a Two-Step Approach for Feature Selection and Its Application to Chinese Herbal Medicine Screening. *Mol Pharm* (2015) 12:3691–713. doi: 10.1021/acs.molpharmaceut.5b00465
15. Gfeller D, Michielin O, Zoete V. Shaping the Interaction Landscape of Bioactive Molecules. *Bioinformatics* (2013) 29:3073–9. doi: 10.1093/bioinformatics/btt540
16. Rappaport N, Twik M, Plaschkes I, Nudel R, Stein T, Levitt J, et al. MalaCards: An Amalgamated Human Disease Compendium With Diverse Clinical and Genetic Annotation and Structured Search. *Nucleic Acids Res* (2017) 45: D877–87. doi: 10.1093/nar/gkw1012
17. Shannon P, Markiel A, Ozier O, Baliga N, Wang J, Ramage D, et al. Cytoscape: A Software Environment for Integrated Models of Biomolecular Interaction Networks. *Genome Res* (2003) 13:2498–504. doi: 10.1101/gr.1239303
18. Trott O, Olson AJ. AutoDock Vina: Improving the Speed and Accuracy of Docking With a New Scoring Function, Efficient Optimization, and Multithreading. *J Comput Chem* (2010) 31:455–61. doi: 10.1002/jcc.21334
19. Ng MC, Fong S, Siu SW. PSOVina: The Hybrid Particle Swarm Optimization Algorithm for Protein-Ligand Docking. *J Bioinform Comput Biol* (2015) 13:1541007. doi: 10.1142/S0219720015410073
20. Tai HK, Jusoh SA, Siu S. Chaos-Embedded Particle Swarm Optimization Approach for Protein-Ligand Docking and Virtual Screening. *J Cheminform* (2018) 10:62. doi: 10.1186/s13321-018-0320-9
21. Burley SK, Berman HM, Bhikadiya C, Bi C, Chen L, Costanzo LD, et al. RCSB Protein Data Bank: Biological Macromolecular Structures Enabling Research and Education in Fundamental Biology, Biomedicine, Biotechnology and Energy. *Nucleic Acids Res* (2019) 47:D464–74. doi: 10.1093/nar/gky1004
22. O'Boyle NM, Banck M, James CA, Morley C, Vandermeersch T, Hutchison GR, et al. Open Babel: An Open Chemical Toolbox. *J Cheminform* (2011) 3:33. doi: 10.1186/1758-2946-3-33
23. Borska S, Chmielewska M, Wysocka T, Zalesinska MD, Zabel M, Dziegiel P, et al. In Vitro Effect of Quercetin on Human Gastric Carcinoma: Targeting Cancer Cells Death and MDR. *Food Chem Toxicol* (2012) 50:3375–83. doi: 10.1016/j.fct.2012.06.035
24. Chen Z, Huang C, Ma T, Jiang L, Tang L, Shi T, et al. Reversal Effect of Quercetin on Multidrug Resistance Via FZD7/β-Catenin Pathway in Hepatocellular Carcinoma Cells. *Phytomedicine* (2018) 43:37–45. doi: 10.1016/j.phymed.2018.03.040

25. Sun BT, Zheng LH, Bao YL, Yu CL, Wu Y, Meng XY, et al. Reversal Effect of Dioscin on Multidrug Resistance in Human Hepatoma HepG2/adriamycin Cells. *Eur J Pharmacol* (2011) 654:129–34. doi: 10.1016/j.ejphar.2010.12.018
26. Wang L, Meng Q, Wang C, Liu Q, Peng J, Huo X, et al. Dioscin Restores the Activity of the Anticancer Agent Adriamycin in Multidrug-Resistant Human Leukemia K562/adriamycin Cells by Down-Regulating MDR1 Via a Mechanism Involving NF-κB Signaling Inhibition. *J Nat Prod* (2013) 76:909–14. doi: 10.1021/np400071c
27. Faes S, Dormond O. PI3K and AKT: Unfaithful Partners in Cancer. *Int J Mol Sci* (2015) 16:21138–52. doi: 10.3390/ijms160921138
28. Liu R, Chen Y, Liu G, Li C, Song Y, Cao Z, et al. PI3K/AKT Pathway as a Key Link Modulates the Multidrug Resistance of Cancers. *Cell Death Dis* (2020) 11:797. doi: 10.1038/s41419-020-02998-6
29. Zhang L, Li Y, Wang Q, Chen Z, Li X, Wu Z, et al. The PI3K Subunits, P110α and P110β are Potential Targets for Overcoming P-gp and BCRP-mediated MDR in Cancer. *Mol Cancer* (2020) 19:10. doi: 10.1186/s12943-019-1112-1
30. Shen K, Liu W, Hu B, Pan C. Impacts of Si Teng Formula on Anoikis Resistance of Human Gastric Cancer SGC-7901 Cell. *Shijie Huaren Xiaohua Zazhi* (2010) 5:1025–8. doi: cnki:sun:xxhb.0.2010-34-004
31. Shen K, Liu W, Hu B, Pan C. Treatment With Sitengfang Decreases Cell Adhesion, Invasion and Migration in Human Gastric Carcinoma Cell Line SGC-7901. *World J Int Med* (2010) 18:3616–20. doi: 10.11569/wcjd.v18.i34.3616
32. He P, Shen K, Hu B, Liang Y. Effects of Siteng Fang on Tumor Growth and Apoptosis in Subcutaneously Transplanted Human Gastric Carcinoma in Nude Mice. *CN J Trad Chin Med Phar* (2013) 28:3632–5. doi: cnki:sun:bxyy.0.2013-12-050
33. He P, Shen K, Hu B, Lu Y. Effects of Siteng Formula on Expression of Caspase-3, Cleaved PARP and Livin in SGC-7901 Gastric Carcinoma. *Chin A TCM* (2014) 32:247–9. doi: 10.13193/j.issn.1673-7717.2014.02.006
34. Wang JW, He P, Hu B, Shen K. Effect and Mechanism of Si Teng Prescription on Growth of MGC-803 Gastric Cancer. *A Chin Med* (2020) 35:2207–11. doi: 10.16368/j.issn.1674-8999.2020.10.492

Conflict of Interest: The authors declare that the research was conducted in the absence of any commercial or financial relationships that could be construed as a potential conflict of interest.

The reviewer QX declared a shared affiliation, with no collaboration, with one of the authors HS to the handling editor at the time of the review.

frontiers in Oncology

ORIGINAL RESEARCH
published: 07 May 2021
doi: 10.3389/fonc.2021.644956

A New Oxaliplatin Resistance-Related Gene Signature With Strong Predicting Ability in Colon Cancer Identified by Comprehensive Profiling

*Qiu Lin, Li Luo and Hua Wang**

Department of Colorectal Surgery, Affiliated Hospital of Integrated Traditional Chinese and Western Medicine, Nanjing University of Chinese Medicine, Nanjing, China

Numerous colon cancer cases are resistant to chemotherapy based on oxaliplatin and suffer from relapse. A number of survival- and prognosis-related biomarkers have been identified based on database mining for patients who develop drug resistance, but the single individual gene biomarker cannot attain high specificity and sensitivity in prognosis prediction. This work was conducted aiming to establish a new gene signature using oxaliplatin resistance-related genes to predict the prognosis for colon cancer. To this end, we downloaded gene expression profile data of cell lines that are resistant and not resistant to oxaliplatin from the Gene Expression Omnibus (GEO) database. Altogether, 495 oxaliplatin resistance-related genes were searched by weighted gene co-expression network analysis (WGCNA) and differential expression analysis. As suggested by functional analysis, the above genes were mostly enriched into cell adhesion and immune processes. Besides, a signature was built based on four oxaliplatin resistance-related genes selected from the training set to predict the overall survival (OS) by stepwise regression and least absolute shrinkage and selection operator (LASSO) Cox analysis. Relative to the low risk score group, the high risk score group had dismal OS ($P < 0.0001$). Moreover, the area under the curve (AUC) value regarding the 5-year OS was 0.72, indicating that the risk score was accurate in the prediction of OS for colon cancer patients (AUC >0.7). Additionally, multivariate Cox regression suggested that the signature constructed based on four oxaliplatin resistance-related genes predicted the prognosis for colon cancer cases [hazard ratio (HR), 2.77; 95% CI, 2.03–3.78; $P < 0.001$]. Finally, external test sets were utilized to further validate the stability and accuracy of oxaliplatin resistance-related gene signature for prognosis of colon cancer patients. To sum up, this study establishes a signature based on four oxaliplatin resistance-related genes for predicting the survival of colon cancer patients, which sheds more light on the mechanisms of oxaliplatin resistance and helps identify colon cancer cases with a dismal prognostic outcome.

Keywords: oxaliplatin resistance, colon cancer, prognostic signature, LASSO, weighted gene co-expression network analyses

OPEN ACCESS

Edited by:
Xia Li,
Shenzhen Institutes of Advanced Technology (CAS), China

Reviewed by:
Kamini Singh,
Memorial Sloan Kettering Cancer Center, United States
Hamid Morjani,
Université de Reims Champagne-Ardenne, France

****Correspondence:***
Hua Wang
825647112@qq.com

Specialty section:
This article was submitted to Gastrointestinal Cancers, a section of the journal Frontiers in Oncology

Received: *22 December 2020*
Accepted: *12 February 2021*
Published: *07 May 2021*

Citation:
Lin Q, Luo L and Wang H (2021) A New Oxaliplatin Resistance-Related Gene Signature With Strong Predicting Ability in Colon Cancer Identified by Comprehensive Profiling. Front. Oncol. 11:644956. doi: 10.3389/fonc.2021.644956

INTRODUCTION

Colon cancer is a frequently occurring gastrointestinal tract (GIT) cancer. As estimated by the International Agency for Research on Cancer (IARC, https://www.iarc.fr/), its morbidity and mortality rates in 2018 are 14.4 and 7.2%, separately, in the world. At present, colon cancer is mainly treated with surgery combined with chemotherapy (1, 2). Great progresses have been made in the early discovery and treatment of colon cancer; as a result, its morbidity and mortality rates decrease by 30–50% among the relapsed or metastatic cases in 5 years of treatment (3). Oxaliplatin is a kind of third-generation platinum-based anticancer drug and a diaminocyclohexane (DACH) platinum, which is now adopted for treating diverse cancers (4, 5). Certain cases can gain benefits from the oxaliplatin-based chemotherapy, yet others show no treatment response because they develop resistance to oxaliplatin (6–9). When used alone, only 20–24% of patients respond to oxaliplatin in the first-line treatment, and around 10% of refractory cases or those who fail in fluorouracil-based treatment respond to it in the second-line treatment (10). Therefore, it is urgently needed to manage oxaliplatin resistance, a cause of the poor survival of patients with advanced colon cancer. Consequently, it is of great significance to establish a signature based on oxaliplatin resistance- and prognosis-related genes for understanding the heterogeneities among colon cancers at the molecular level and improving treatment for these cases.

In recent years, researchers have carried out unsupervised cluster analysis on the transcriptomic data obtained from four colon cancer consensus molecular subtypes (CMSs). Among them, CMS1 stands for microsatellite unstable tumors (MSI) with great immune cell infiltration degree; CMS2 displays the activation patterns of the MYC and WNT pathways; tumors in CMS3 are featured by KRAS mutations as well as metabolic disorder; while CMS4 represents the mesenchymal subtype with epithelial–mesenchymal transition (EMT) and great stromal cell infiltration degree (11). Typically, the above CMS classification system facilitates to predict the patient prognosis, and cancers in CMS4 are linked to the poorest overall survival (OS) and relapse-free survival (RFS) (12). But this classification method cannot be used to estimate drug response in patients due to its oversimplification, so it is not quite helpful in individual treatment (13). Moreover, some biomarkers are utilized for predicting the prognosis of colon cancer patients. For instance, carbohydrate antigen 19-9 (CA19-9) has been identified as a predominant characteristic to diagnose colon cancer in clinical practice (14). CA19-9 is useful for the identification of outcomes of patients with stages I–III colorectal cancer 2 years after their operations (15). Unluckily, the CA19-9 level is neither discovered as the independent prognostic factor or the therapeutic target for improving patient OS nor used to predict patients' susceptibility to therapeutic drugs. Bioinformatic analysis has rapidly emerged as an important approach to assist the investigators in developing novel ideas regarding tumor research (16). More and more studies have recognized that mRNA expression signatures play an important role in predicting patient OS or relapse (17–19), yet no combined analysis is available to examine the relationship of the levels of oxaliplatin resistance-related genes with OS among colon cancer patients.

The present work downloaded the expression profile data of colon cancer cell lines resistant or sensitive to oxaliplatin from the Gene Expression Omnibus (GEO) database (20) and found oxaliplatin resistance-related genes by means of weighted gene co-expression network analysis (WGCNA) along with differential expression analysis. Besides, the mRNA expression pattern data of colon cancer patients in the training and test sets along with their clinical characteristics were analyzed to establish an mRNA-based model as the novel indicator for predicting patient prognosis. As a result, our constructed signature that integrated sufficient transcript data is helpful to risk stratification, which offered an approach to more accurately assess individual treatment for colon cancer cases. The above findings shed more light on the malignancy and treatment for individuals with colon cancer.

MATERIALS AND METHODS

Data Extraction and Study Design

The expression profile data in oxaliplatin-resistant or non-resistant colon cancer cell lines were obtained from GSE77932 and GSE124808 datasets. The feature extraction software 10.7.3.1 (Agilent) was used for feature extraction, and the default parameters were used to analyze the scanned images, so as to obtain the processed signal intensity after background subtraction and spatial trend variation. The scanned data were imported by GeneSpring GX and normalized to 75%. Subsequently, the two datasets were merged and batch processed using the combat function of R package sva (**Figure 1A**), so as to obtain the gene expression matrix. Moreover, to construct the prognosis prediction model, we downloaded three datasets (including gene expression profiles, prognosis information, and other clinical features), namely, GSE17536, GSE17538 (21), and GSE39582 (22), with the first dataset as the training set and the latter two as the validation sets. All data used in this study were openly accessible, so there was no need to obtain approval from the ethics committee.

Differentially Expressed Gene Analysis

We identified differentially expressed genes (DEGs) from colon cancer cells resistant (DLD1-derived oxaliplatin-resistant clones: DLD/OHP1, DLD/OHP4, and DLD/OHP5; HCT116-derived oxaliplatin-resistant clones: HCT/OHP1, HCT/OHP3, and HCT/OHP5) and sensitive (DLD1 and HCT116) to oxaliplatin by adopting limma package (23) in line with the selection thresholds of false discovery rate (FDR) <0.05, $|\log2$ fold change (FC)$| > 1$, and $P < 0.05$. DEGs that satisfied the above thresholds were screened in subsequent analysis. In addition, the limma and pheatmap packages were utilized to draw the volcano plot and heatmap separately.

Identification of Oxaliplatin Resistance-Related Genes by Weighted Gene Co-expression Network Analysis

We constructed a co-expression network that targeted oxaliplatin resistance using the WGCNA package (24). Firstly, we carried out cluster analysis on the samples by hierarchical clustering. A weight co-expression network was constructed using the

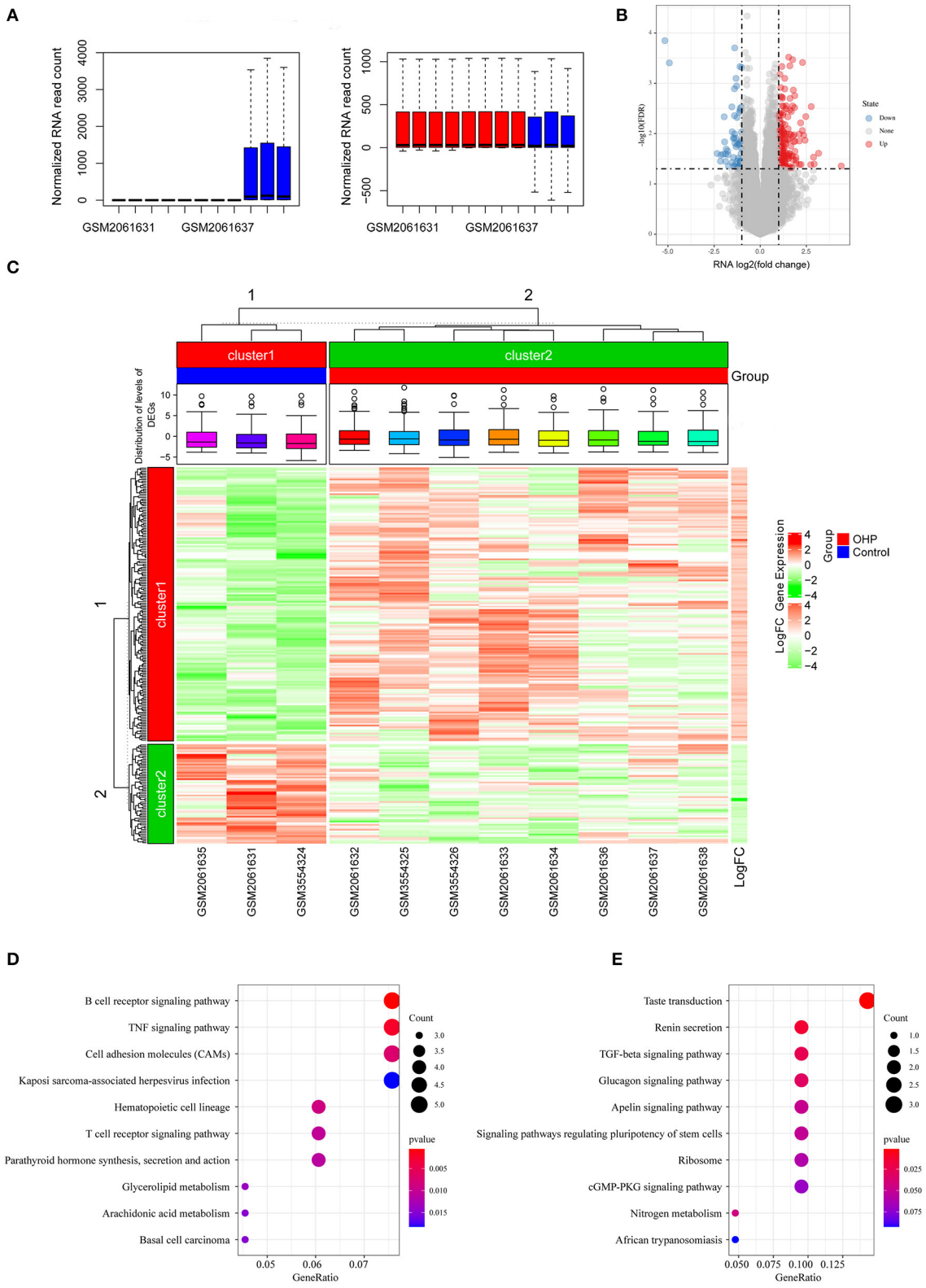

FIGURE 1 | Differentially expressed genes (DEGs) between oxaliplatin-resistant and -sensitive colon cancer cells. **(A)** Boxplot of the distribution of the sample expression profile before and after the removal of the batch effect. **(B)** Volcanogram of DEGs. **(C)** Heatmap of DEGs. **(D)** Kyoto Encyclopedia of Genes and Genomes (KEGG) enrichment analysis of upregulated DEGs. **(E)** KEGG enrichment analysis of downregulated DEGs.

WGCNA of R package, and the soft threshold was set at eight to select the co-expression modules. Later, we confirmed that our established co-expression network was consistent with a scale-free network. In other words, the node/k connectivity [log(k)] logarithm showed a negative correlation with the node [log(P(k)] occurrence probability logarithm, with the coefficient of correlation being >0.8. To guarantee the scale-free network, the β value was set at eight. Later, we transformed the expression matrix to the close matrix and transformed it to the topological matrix to carry out gene clustering based on TOM by adopting the average linkage hierarchical cluster method according to the standards of mixed dynamic shear tree. Besides, over 30 genes were screened for each gene network module. Gene modules were determined by the dynamic shear methods, then the value of each module eigengene was determined successively, modules were subjected to cluster analysis, and the close modules were combined for forming a new module. Thereafter, we also determined the relationships between the gene modules identified and oxaliplatin resistance to mine the substantially associated gene modules for subsequent analysis.

Pathway Enrichment Analysis

Kyoto Encyclopedia of Genes and Genomes (KEGG) analysis was conducted using the clusterProfiler package (25) for exploring and determining the possible biological functions of all critical genes. The significance levels were FDR <0.05 and $P < 0.05$. We employed the R software to draw the bubble plot for result visualization.

Establishment of the Protein–Protein Interaction Network and Topological Analysis

We utilized the Search Tool for the Retrieval of Interacting Genes (STRING) online approach (26) to construct the protein–protein interaction (PPI) network of critical genes. As observed from the graph, all nodes within the network were greatly connected to each other. Then, the topological characters of nodes in the network were further analyzed, and the Degree, Betweenness centrality, Closeness centrality, and Eigenvector centrality values were calculated. In this study, genes in the PPI network that had all parameters greater than or equal to the medians of all nodes were considered to exert core roles in the network (in other words, the key oxaliplatin resistance-related prognostic genes), which were used to construct the subsequent prognosis model of colon cancer.

Establishment of a Risk Assessment Model

The survival and glmnet packages were utilized to select the most appropriate genes that might be used to construct a model by least absolute shrinkage and selection operator (LASSO) Cox regression analysis. Typically, LASSO regression can be used to select variables to fit the high-dimensional generalized linear model. In this study, LASSO regression was conducted to construct a penalty function, which facilitated to obtain the improved model with a reduced number of variables and might avoid overfitting. We employed the glmnet package for determining the penalty parameter lambda through cross-validation; besides, we discovered the best lambda value associated with the lowest error mean of cross-validation. Thereafter, we selected the optimal gene group (lambda = 0.0508) for subsequent model construction. Furthermore, based on the expression profiles of feature genes, we utilized the stepAIC method in MASS package for stepwise multivariate regression analysis. Starting from the most complicated model, we deleted one variable each time in succession to reduce the Akaike Information Criteria (AIC) value (a smaller value indicated the better model, suggesting that the model utilized less parameters to obtain enough degree of fitting). Later, gene sets with the most appropriate AIC value were selected to construct the colon cancer risk prediction model. Then, risk scores were calculated after linearly combining the results of each coefficient determined by LASSO Cox regression multiplied according to the respective gene level and categorized the patients into the high-risk or low-risk groups. Besides, multivariate Cox regression was conducted to analyze whether the risk model was able to independently predict prognosis.

Gene Set Enrichment Analysis

To observe the relationships between risk score and signal pathways, we selected the corresponding gene expression profiles in training set samples for single-sample gene set enrichment analysis (GSEA) using the GSVA function of R package (27) and calculated the scores of each sample in different signal pathways (in other words, we obtained the ssGSEA score of each sample in the corresponding pathway). Furthermore, we determined the correlations of these scores with risk score and selected FDR <0.5 as the criterion to judge pathways significantly related to the risk score.

Statistical Analysis

The R software was employed for statistical analysis. In this study, data were expressed as medians. Log-rank test and Kaplan–Meier method were used to analyze the difference in OS between high and low risk score groups. In addition, the Cox proportional hazard regression model was used for univariate as well as multivariate analysis. The merge script in Perl language was utilized for data set merging. A difference of $P < 0.05$ indicated statistical significance.

RESULTS

Differentially Expressed Genes Between Oxaliplatin-Resistant and -Sensitive Colon Cancer Cells and Pathway Enrichment

In this study, we downloaded the GSE77932 and GSE124808 gene sets from the GEO database to obtain gene expression profiles. As observed from the volcano plot (**Figure 1B**, **Supplementary Table 1**), there was differential mRNA expression in oxaliplatin-resistant colon cancer cells compared with the oxaliplatin-sensitive cells. Relative to the sensitive group, we obtained altogether 229 DEGs in resistant groups, among which 168 were upregulated while 61 were downregulated ($P < 0.05$). We also drew the heatmap to display the significant DEGs (**Figure 1C**). Thereafter, KEGG pathway enrichment was

conducted on DEGs by using clusterProfiler package, which revealed that the upregulated genes were mainly enriched into the B cell receptor signaling pathway and tumor necrosis factor (TNF) signaling pathway, whereas the downregulated genes were mainly enriched into the transforming growth factor (TGF)-beta signaling pathway, Ribosome and cGMP-PKG signaling pathway (**Figures 1D,E**).

Selection of Oxaliplatin Resistance-Related Gene Modules Through Weighted Gene Co-expression Network Analysis

Apart from screening DEGs between oxaliplatin-resistant and -sensitive colon cancer cells, we also established the gene co-expression network to identify gene modules with biological

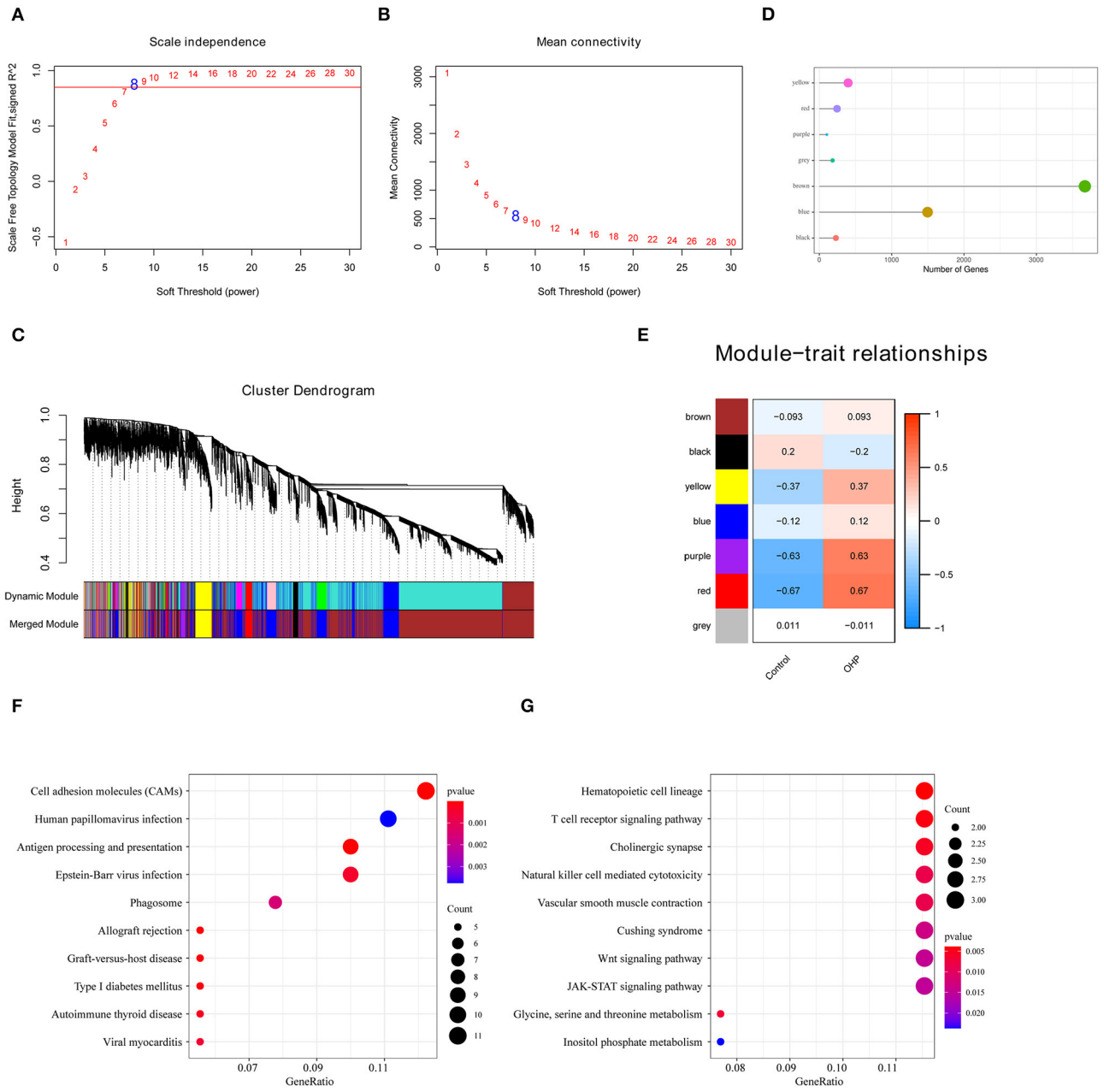

FIGURE 2 | Oxaliplatin resistance-related gene modules mined through weighted gene co-expression network analysis (WGCNA). **(A,B)** Analysis of network topology for various soft-thresholding powers. **(A)** Analysis of the scale-free fit index for various soft-thresholding powers (β). **(B)** Analysis of the mean connectivity for various soft-thresholding powers. **(C)** Gene dendrogram and module colors. **(D)** The number of genes in each module. **(E)** Correlation between each module and oxaliplatin resistance events. **(F)** The Kyoto Encyclopedia of Genes and Genomes (KEGG) enrichment analysis of the genes in the red module. **(G)** The KEGG enrichment analysis of the genes in the purple module.

significance through WGCNA and to better discover the significant oxaliplatin resistance-related genes in the context of colon cancer. We acquired altogether seven modules in later analysis (**Figures 2A–D**). Subsequently, we analyzed the correlations of these gene modules with the oxaliplatin resistance events and discovered that the red and purple modules were most significantly correlated with resistance (**Figure 2E**). Later, those genes in the red and purple modules were subjected to KEGG pathway enrichment by using the clusterProfiler package. As a result, genes in the red module were mainly enriched into Autoimmune thyroid disease, Phagosome, and Cell adhesion molecules (CAMs) pathways; whereas genes in the purple module were mainly enriched into the JAK-STAT, Wnt, and T cell receptor signal pathways (**Figures 2F,G**), demonstrating that the resistance of colon cancer to oxaliplatin might be related to immunity and cell migration.

Identification of Key Oxaliplatin Resistance-Related Genes for Predicting the Prognosis of Colon Cancer

First of all, we had integrated 394 genes in the oxaliplatin resistant-related gene modules (red and purple), with 229 DEGs in between oxaliplatin-sensitive and -resistant colon cancer cell lines. Finally, we acquired 495 genes after removing duplication. Secondly, using univariate survival analysis, we determined the relationships between the expression of these 495 genes and prognosis based on the prognosis data (training set, GSE17536).

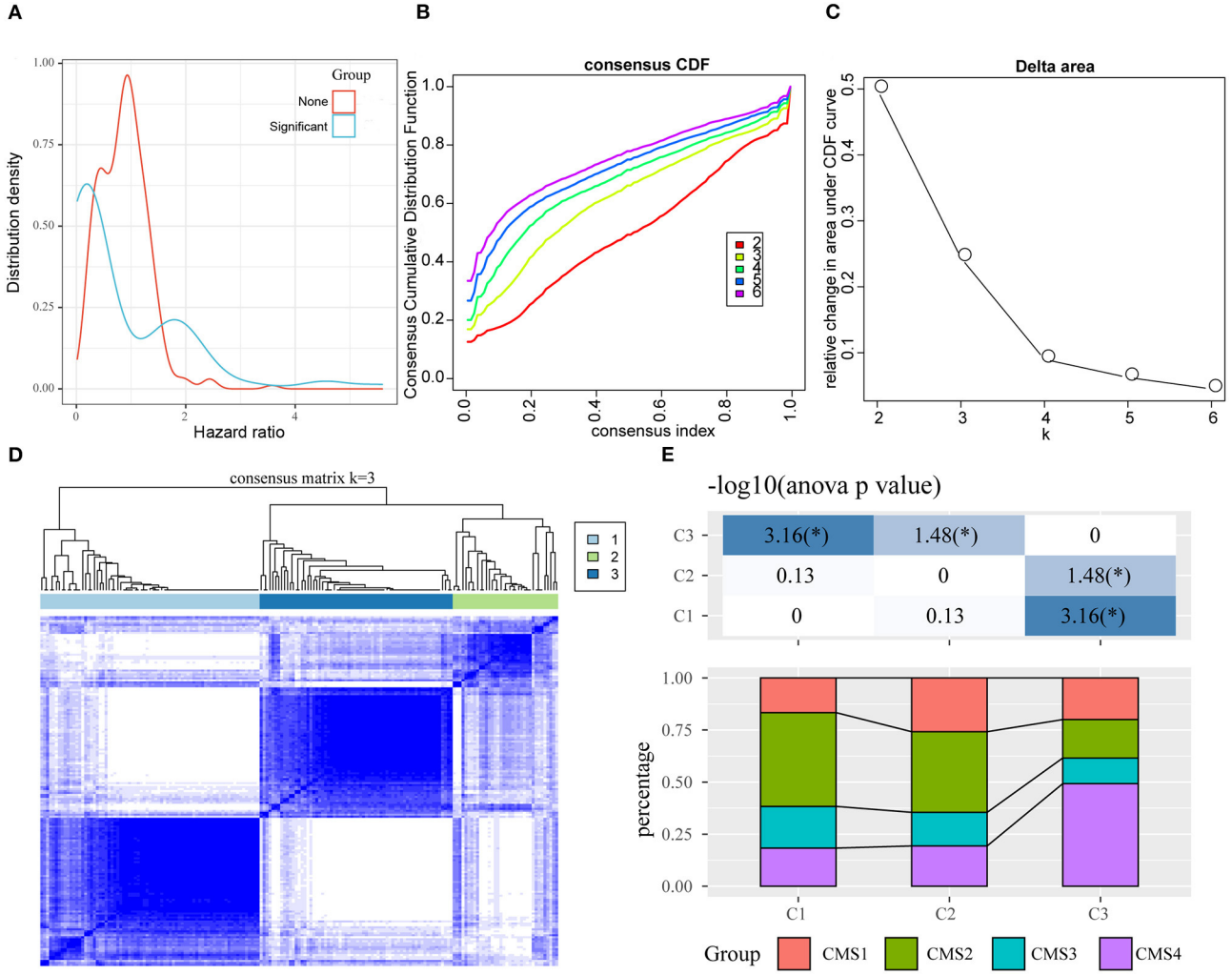

FIGURE 3 | Identification of oxaliplatin resistance-associated subtypes of colon cancer in the training set. **(A)** The hazard ratio (HR) distribution of genes related to oxaliplatin resistance, wherein "Sig" represents the HR distribution of genes significantly related to prognosis and "None" represents the HR distribution of genes not significantly related to prognosis. **(B)** The cumulative distribution function (CDF) curves of consensus scores based on different subtype numbers (k = 2∼6) and the corresponding color are represented, which could help us determine the choice of k when the CDF reaches the maximum (aiming to reach the maximal consistency and cluster confidence). **(C)** The comparison of the relative changes of the area under the CDF curve between k and k−1, which can help users determine the relative increase in consensus and the value of k with significant increase. **(D)** The consensus score matrix of colon cancer samples when k = 3 (1 = C1, 2 = C2, 3 = C3). **(E)** The distribution of samples from the three subtypes in the CMS subgroups.

By adopting the threshold of $P < 0.05$, we obtained 79 genes that showed distinct OS (**Figure 3A**, **Supplementary Table 2**). Furthermore, we used these genes for sample consistent clustering using the R package ConsensusClusterPlus (V1.48.0; parameters: reps = 100, pItem = 0.8, pFeature = 1, and distance = "spearman"). D2 and Euclidean distance (ED) were used as the clustering algorithm and distance metric, respectively. At k = 2–6, the samples were clustered into three clusters (C1, C2, C3; **Figures 3B–D**). We compared the relationships between C1–3 samples and the previous published CMS classification samples. As shown in **Figure 3E**, we discovered that samples in the C3 subtype were mainly enriched into the CMS4 subtype, while those in the C1 subtype were significantly enriched in the CMS2 subtype. In CMS classification, CMS4 had the poorest prognosis, while CMS2 had the best prognosis. This revealed that the expression profiles of these 79 prognosis-based oxaliplatin resistance-related genes were able to classify patient prognosis to some extent.

Thirdly, to further screen the key prognosis genes, we mapped these 79 genes to the STRING database to obtain the protein interaction networks of these genes. As shown in **Figure 4A**, 51 of these 79 genes showed interactions. Subsequently, we analyzed the topological properties of the nodes in the network and calculated degree, Closeness centrality, Betweenness centrality, and Eigenvector centrality (**Supplementary Table 3**). We discovered that the degree of nodes in the network was mainly 1–4 (**Figure 4B**), the closeness centrality was 0.005–0.008 (**Figure 4C**), the betweenness centrality was 0–100 (**Figure 4D**), and the Eigenvector centrality was 0–0.25 (**Figure 4E**). In addition, we also found that there were fewer nodes with higher levels of topological parameters and more nodes with lower ones in the network, which showed a power-law distribution and was in line with the characteristics of biological network. Finally, 15 genes (**Figure 5A**) whose values of all the above four parameters were greater than or equal to the median of all nodes were selected as the key prognostic markers related to the resistance of colon cancer to oxaliplatin, which were used for further analysis and prognosis model construction.

Establishment of the Oxaliplatin Resistance-Related Risk Assessment Model

To investigate the effect of those screened genes in predicting the prognosis of colon cancer, we incorporated 15 key genes into LASSO and stepwise regression for identifying the potent markers. Thereafter, we established a prognosis signature based on four genes [CD22, CASP1, CISH, and activated leukocyte cell adhesion molecule (ALCAM)] to evaluate the prognosis for colon cancer patients (**Figures 5B–D**). Besides, the risk score of every colon cancer case from the training set was determined based on the four gene coefficients.

$$\text{Risk score} = -2.889^{*}CD22 - 0.323^{*}CASP1 - 2.23^{*}CISH + 0.816^{*}ALCAM.$$

After determining the risk scores of all samples in the training set, we divided all samples into high- or low-risk group in line with the median risk score (cutoff = 0). **Figure 6** displays the classification accuracy of our constructed prognosis model for training set samples. It was illustrated from **Figure 6A** that 89 and 88 cases were divided as the low- and high-risk groups, respectively, and the difference in prognosis was statistically significant between both groups ($P < 0.0001$, HR = 2.41, 95% CI = 1.84–3.15). **Figure 6B** displays the receiver operating characteristic (ROC) curves. As observed, the AUC values at 1, 3, and 5 years, respectively, were 0.76, 0.73, and 0.72. Besides, **Figure 6C** revealed that the dead samples had evidently reduced survival time as the risk score increased, and more dead samples were observed in the high-risk group. Moreover, high ALCAM expression was recognized as a risk factor on the basis of changes in the levels of those four prognostic genes as risk score elevated. In comparison, high CD22, CISH, and CASP1 expression was associated with a decreased risk, and they served as the protective factors.

Validation of the Robustness of Our Four-Oxaliplatin Resistance-Related Gene-Based Prognosis Signature

To examine the robustness of our constructed four-gene model, we used the same model and threshold as those in the training set for verification in the test set. **Figure 7** displays the classification accuracy in the first test set (GSE17538). As observed from **Figure 7A**, 115 and 117 cases were divided as low- and high-risk groups, respectively, and there was a significant difference in prognosis between them ($P < 0.0001$, HR = 1.95, 95% CI = 1.59–2.40). **Figure 7B** exhibits the ROC curves, with the AUC values at 1, 3, and 5 years, respectively, being 0.68, 0.68, and 0.71. **Figure 7C** shows similar findings to those obtained from the training set. In other words, dead samples had markedly shorter survival time as the risk score increased, and more dead samples were observed in the high-risk group. In addition, high ALCAM expression was a risk factor, while high CD22, CISH, and CASP1 levels were the protective factors.

Moreover, we also downloaded the GSE39582 dataset (the second test set) from the GEO database as an external dataset and determined the risk scores for all samples by our model. We also used the threshold in the training set for classifying samples into high- or low-risk group. According to **Figure 8A**, the prognosis in the low-risk group was superior to that in the high-risk group. Upon ROC analysis, comparable AUC values at 1–5 years to those of the first test set (GSE17538) and training set were obtained (**Figure 8B**). Furthermore, the associations of those four gene expression levels with risk score were the same as those obtained from the other two datasets (**Figure 8C**). In conclusion, our prognosis model constructed based on four oxaliplatin resistance-related genes performed well in predicting the prognosis for colon cancer.

Clinical Independence of Our Constructed Signature Based on Four Oxaliplatin Resistance-Related Genes

To identify whether our constructed model based on four oxaliplatin resistance-related genes was independent in clinical

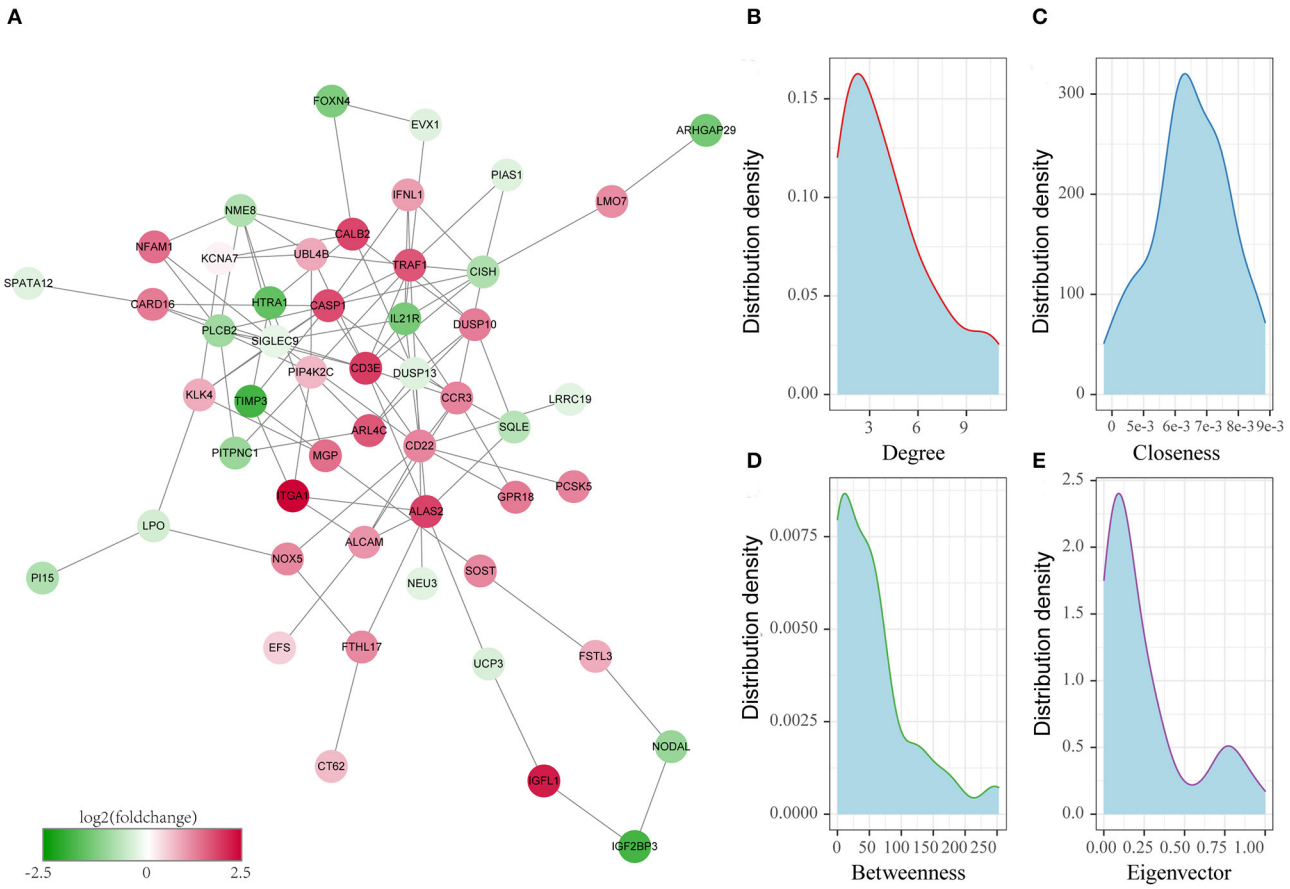

FIGURE 4 | Identification of the key oxaliplatin resistance-related genes for predicting the prognosis of colon cancer. **(A)** Protein–protein interaction (PPI) network of prognostic genes related to oxaliplatin resistance. **(B)** Degree distribution of genes in the network. **(C)** Closeness centrality distribution of genes in the network. **(D)** Betweenness centrality distribution of genes in the network. **(E)** Eigenvector centrality distribution of genes in the network.

practice, we employed univariate as well as multivariate Cox regression analysis on clinical data and risk score from the training set and calculated the corresponding HRs, 95% CIs, and *P*-values. **Figure 9** displays the grouping data of the four-gene signature. Univariate analysis was conducted on training set samples, which suggested that a high risk score, tumor stage III/IV, and Grade 3 showed marked correlations with dismal prognosis, but multivariate analysis discovered that only a high risk score (HR = 2.77, 95% CI = 2.03–3.78, $P = 1.3e^{-10}$) as well as tumor stage IV (HR = 10.11, 95% CI = 3.29–31.03, $P = 5.4e^{-5}$) displayed clinical independence. As a result, the prognosis signature constructed based on the four oxaliplatin resistance-related genes might serve as an independent prognostic indicator to predict patient prognosis clinically for colon cancer patients.

Differences in Pathways Enriched Between High- and Low-Risk Groups Detected by Gene Set Enrichment Analysis

In this study, we used GSEA to examine pathways that were significantly enriched into both groups in the training set and obtained altogether five significantly enriched pathways (**Figure 10**), which included pathways tightly related to tumor occurrence, immunity, and metastasis, such as primary immunodeficiency, adherens junction, as well as pathways in cancer. Such result further verified that the resistance and poor prognosis of colon cancer were related to cancer cell migration and the immunosuppression status in the microenvironment.

DISCUSSION

Colon cancer is one of the most common cancers and remains one of the leading causes of cancer death worldwide (28). Colon cancer represents a complicated disorder that has numerous risk factors, including lifestyle, dietary habit, and genetics (29). Typically, colon cancer is usually featured by its intra-cancer heterogeneity; as a result, each patient is different with regard to the clinical presentations as well as treatment response (30). Therefore, it is necessary to tailor the treatment for colon cancer on the basis of risk and genetic factors of an individual. At present, the oxaliplatin-based chemotherapy is adopted in combination with radical surgery as the standard treatment for cases with colon cancer. Patients respond well

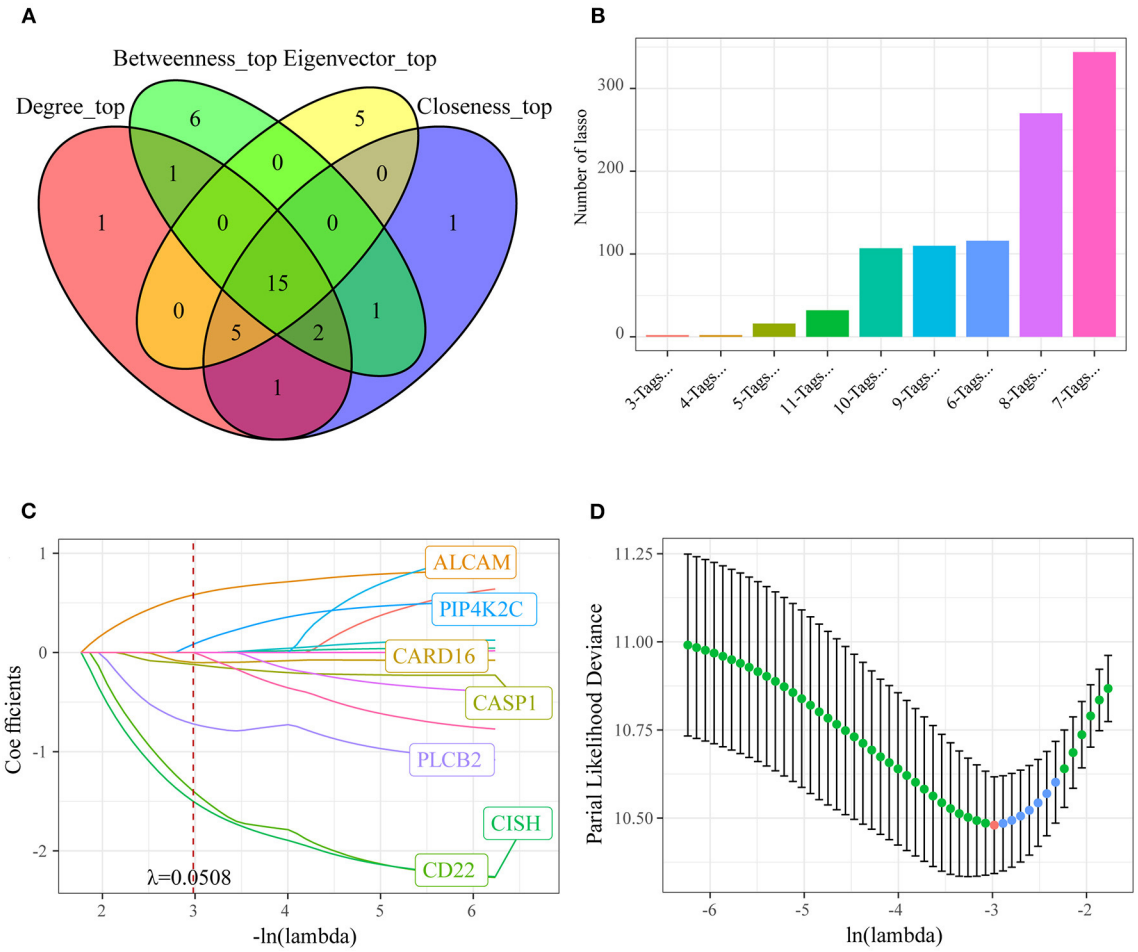

FIGURE 5 | Identifying the prognosis signature related to oxaliplatin resistance for colon cancer by least absolute shrinkage and selection operator (LASSO). **(A)** Fifteen genes whose values of all the above four parameters were greater than or equal to the median of all nodes were selected as the key prognostic markers related to the resistance of colon cancer to oxaliplatin. **(B)** Frequency of different gene combinations in a thousand times of LASSO regressions. **(C)** The changing trajectory of each independent variable. The horizontal axis represents the log value of the independent variable lambda, and the vertical axis represents the coefficient of the independent variable. When lambda = 0.0508, the coefficients were not 0 in seven genes. **(D)** Confidence intervals for each lambda. We chose the lambda with the smallest average standard deviation as the optimal model, that is, lambda = 0.0508.

to the first treatment, but many of them may experience resistance to oxaliplatin and subsequently develop recurrence, resulting in a dismal prognostic outcome (31, 32). Currently, the Tumor, Lymph node, Metastasis (TNM) classification system is widely utilized as the standard to predict relapse among colon cancer cases (33). However, it cannot achieve satisfactory performance in predicting prognosis and managing colon cancer. As a result, many researchers are devoted to developing novel strategies to improve the predicting accuracy of oxaliplatin resistance and patient prognosis and contribute to decision-making for individuals based on molecular biomarkers and clinicopathological features (34, 35).

Some single genes have been suggested as potent approaches to assess colon cancer prognosis. For instance, certain works emphasize on the significance of Wnt5a and Immature Colon Carcinoma Transcript-1 (ICT1) in prognosis prediction (36, 37). Similarly, one article focuses on the significance of the prediction model constructed based on five transcriptional factors in predicting prognosis. This model is constructed using the Cox PH model based on analysis of The Cancer Genome Atlas (TCGA)-derived colon cancer patients by the random forest algorithm (38). Some encouraging results have been discovered, but there is no biomarker available clinically to predict the prognosis for colon cancer. In addition, these prognostic genes and multi-gene signatures have not been identified as prediction factors of a response to chemotherapy in colon cancer. Furthermore, the joint action of several oxaliplatin resistance-related genes on colon cancer prognosis has not been investigated in a large-scale genomic study so far. As a result, it is of great importance to construct a novel model to predict the outcome of oxaliplatin-resistant colon cancer, which may also facilitate the prognosis prediction for colon cancer cases and decision of treatment strategy.

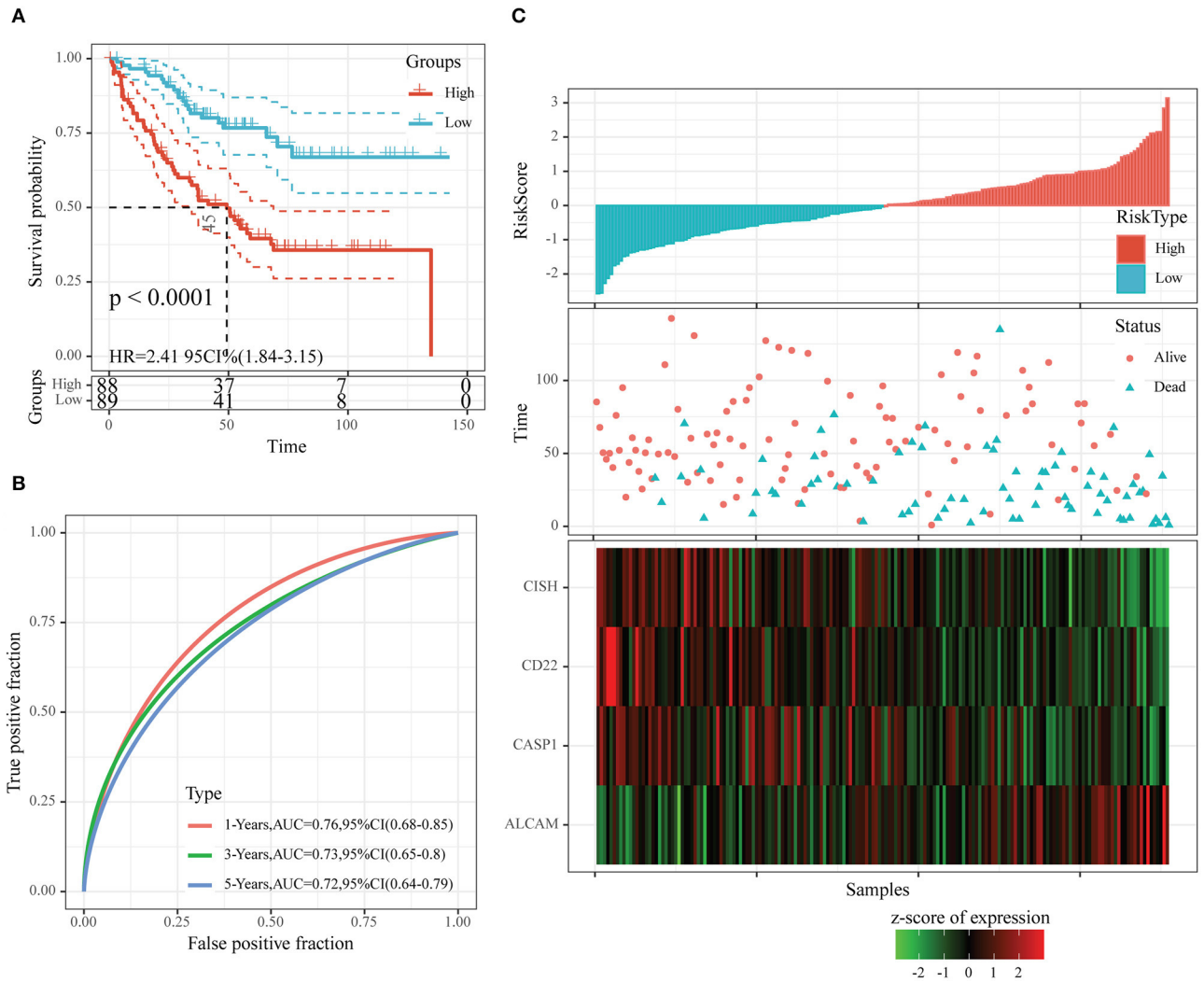

FIGURE 6 | The classification effect of the four-oxaliplatin resistance-related gene-based prognosis signature in the training set. **(A)** Analyzed the prognostic difference after predicted classification according to the four-gene signature in the training set. **(B)** Receiver operating characteristic (ROC) curves of the four-gene signature in colon cancer samples in the training set. **(C)** The relationship of risk score, survival time, and survival status with the expression levels of the four genes in the training set.

Consequently, this study aimed to establish a model based on oxaliplatin resistance-related genes to estimate the OS of colon cancer cases. In this work, we constructed a candidate risk model based on oxaliplatin resistance-related genes to estimate the survival of colon cancer cases based on results of the WGCNA, differential expression analysis, and Cox proportional regression analysis. The risk scores calculated based on the expression levels and coefficients of four mRNAs (ALCAM, CD22, CASP1, and CISH) might be used to precisely and independently predict the prognosis of colon cancer. First of all, altogether, 229 DEGs were identified between colon cancer cells that were resistant and sensitive to oxaliplatin. Secondly, 394 genes were screened from the oxaliplatin resistance-related gene modules on the basis of WGCNA. To explore the biological functions of these screened genes, we carried out KEGG pathway enrichment, which suggested that the above genes were mostly enriched into numerous drug resistance-related pathways, including cell adhesion, JAK-STAT, immune-related pathways, TGF-beta, and Wnt. Thirdly, univariate analysis and PPI network topological analysis were performed to determine the significant oxaliplatin resistance-related genes that might be used to predict the prognosis for colon cancer. Afterward, we established a model to predict the prognosis of colon cancer using four oxaliplatin resistance-related genes (ALCAM, CD22, CASP1, and CISH) on the basis of stepwise regression and LASSO Cox regression. Typically, CD22, CISH, and CASP1 were identified to be the independent protective factors, whereas ALCAM as the risk factor. It was surprising that according to ROC curve and survival analyses, the prognosis model-produced risk score might be utilized to be an accurate OS indicator

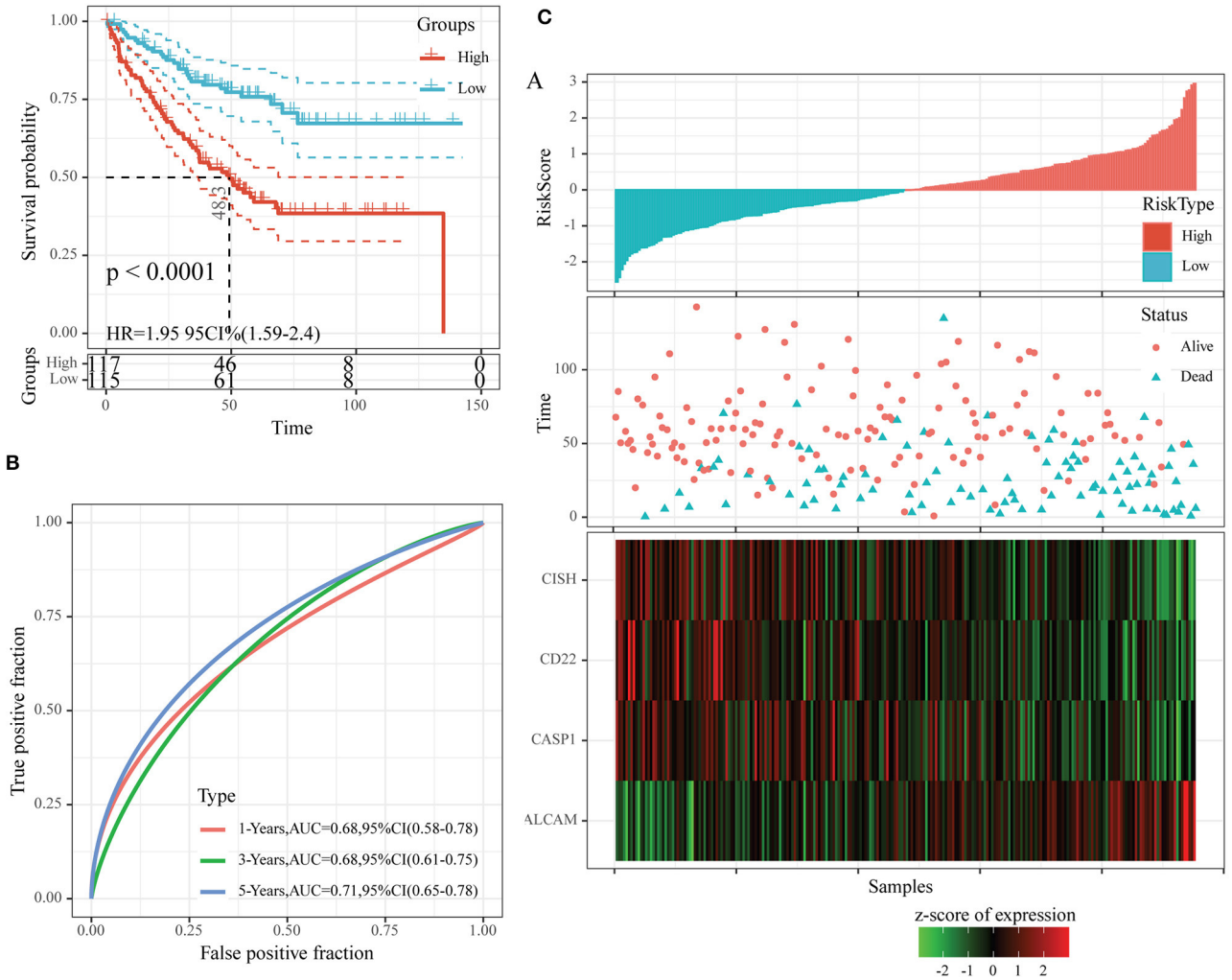

FIGURE 7 | The classification effect of the four-oxaliplatin resistance-related gene-based prognosis signature in the first test set (GSE17538). **(A)** Analyzed the prognostic difference after predicted classification according to the four-gene signature in the first test set (GSE17538). **(B)** Receiver operating characteristic (ROC) curves of the four-gene signature in colon cancer samples in the first test set (GSE17538). **(C)** The relationship of risk score, survival time, and survival status with the expression levels of the four genes in the first test set (GSE17538).

for colon cancer. Besides, we compared our new risk score with the traditional clinicopathological factors, which verified that the prognosis effect was independent. At last, we adopted GSEA to analyze those pathways markedly enriched in the high- or low-risk group and detected five pathways showing significant differential enrichment between the two groups, including pathways that were tightly related to tumor occurrence, metastasis, and immunity, such as primary immunodeficiency, adherens junction, as well as pathways in cancer. The above preliminary results shed new light on the development of markers based on oxaliplatin resistance genes to predict the prognosis of colon cancer. Our proposed risk score may offer a novel direction to evaluate the prognosis for colon cancer, and it is distinct from the conventional evaluation system. It can help to further stratify patients, thus contributing to designing individual treatment and improving patient survival.

Of the screened four genes (ALCAM, CD22, CASP1, and CISH), CD22 is a sialic acid-binding immunoglobulin-like lectin (Siglec) that is highly expressed on B cell lymphomas and is a validated target for antibody and nanoparticle-based therapeutics on non-Hodgkin lymphoma (39, 40). Besides, it is reported in some studies that CD22 exerts an important part in lung cancer (41). ALCAM, a 100- to 105-KDa transmembrane immunoglobulin, has been treated as a tumor-specific prognostic marker and demonstrated to take part in activation of T cells, hematopoiesis, angiogenesis, inflammation, and multiple types

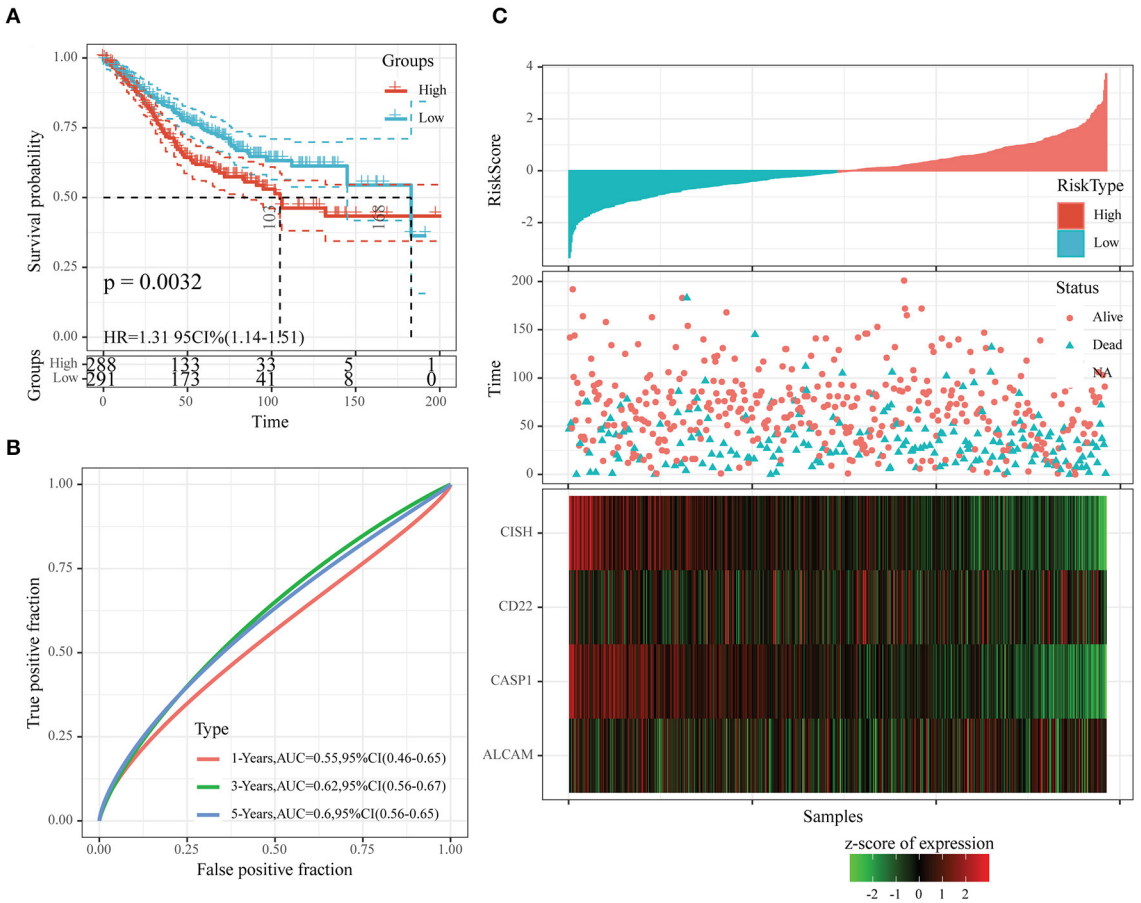

FIGURE 8 | The classification effect of the four-oxaliplatin resistance-related gene-based prognosis signature in the second test set (GSE39582). **(A)** Analyzed the prognostic difference after predicted classification according to the four-gene signature in the second test set (GSE39582). **(B)** Receiver operating characteristic (ROC) curves of the four-gene signature in colon cancer samples in the second test set (GSE39582). **(C)** The relationship of risk score, survival time, and survival status with the expression levels of the four genes in the second test set (GSE39582).

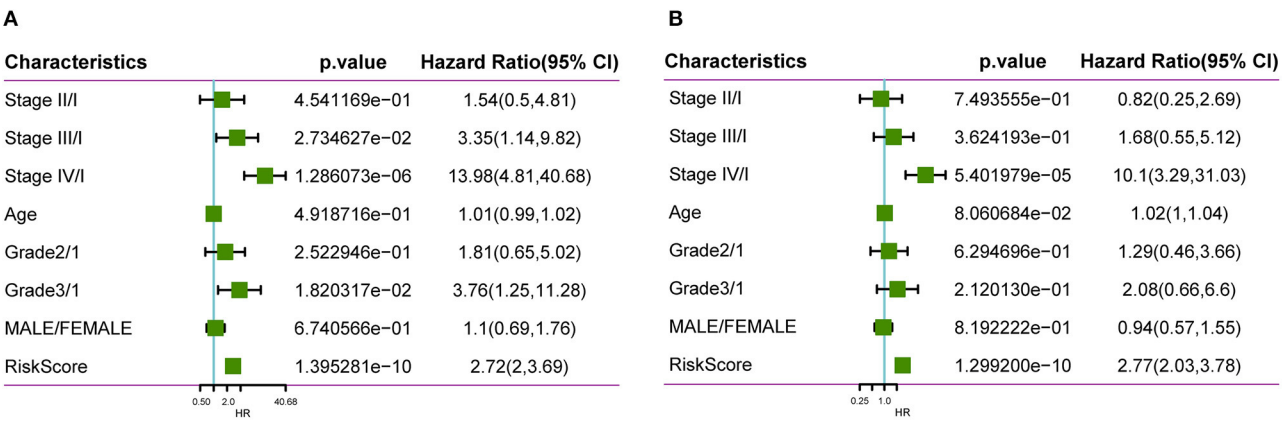

FIGURE 9 | Clinical independence of our constructed signature based on four oxaliplatin resistance-related genes. Univariate **(A)** as well as multivariate **(B)** Cox regression analysis on clinical data and risk score from the training set was employed to calculate the corresponding HRs, 95% CIs, and *P*-values.

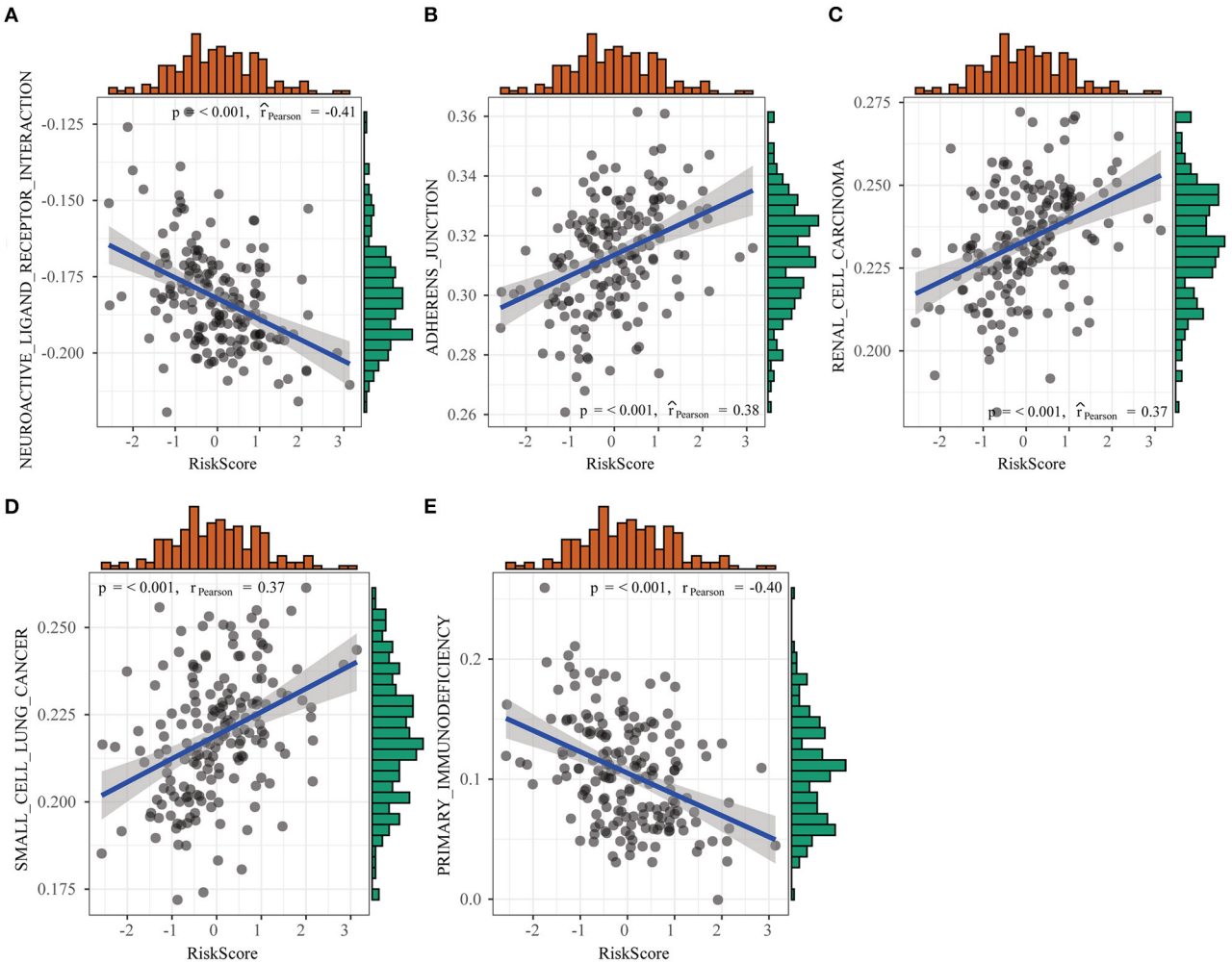

FIGURE 10 | Differences in pathways enriched between high- and low-risk groups detected by gene set enrichment analysis (GSEA).

of tumor propagation and invasiveness (including breast cancer, colorectal cancer, and esophageal cancer) (42–44). CASP1 is the component of the inflammasome that can induce pyroptosis and inhibit angiogenesis and migration of tumor cells (such as lung cancer, breast cancer, and endometrial cancer) (45–47). However, there are few studies on the role of CASP1 in colon cancer. Palmer et al. (48) indicated that CISH, a member of the suppressor of cytokine signaling (SOCS) family, could be induced by TCR stimulation in $CD8^+$ T cells and reduce their functional avidity against tumors.

Certain limitations should be noted in the present work. Firstly, more large-scale studies and more experimental methods should be conducted due to the small sample size in this work. Secondly, the present work focused on analyzing the mRNA expression profiles, but it did not consider the associations among lncRNAs, miRNAs, proteins, and other factors; in this regard, more comprehensive studies are needed. Thirdly, there is little research on the role of CD22, CASP1, and CISH in colon cancer, even though it plays an important role. Therefore, more investigations are needed.

To sum up, this study identifies four oxaliplatin resistance-related genes among the colon cancer patients, which are used to construct a signature to predict patient prognosis. According to our results, our constructed four-gene signature can serve as an independent factor to predict the prognosis for colon cancer patients resistant to oxaliplatin. The above results can be used as candidate biomarkers to predict the prognosis for oxaliplatin-resistant colon cancer and shed more light on the theoretical guidance and decision-making for colon cancer clinically.

DATA AVAILABILITY STATEMENT

The original contributions presented in the study are included in the article/**Supplementary Material**, further inquiries can be directed to the corresponding author/s.

AUTHOR CONTRIBUTIONS

HW and QL conceived and designed the experiments. QL performed the experiments and wrote the paper. LL and HW analyzed the data. All authors have read and approved the final manuscript.

ACKNOWLEDGMENTS

The authors thank members of their laboratory and their collaborators for their research work.

SUPPLEMENTARY MATERIAL

The Supplementary Material for this article can be found online at: https://www.frontiersin.org/articles/10.3389/fonc.2021.644956/full#supplementary-material

Supplementary Table 1 | DEGs between oxaliplatin-resistant and -sensitive colon cancer cells.

Supplementary Table 2 | Seventy nine significantly different oxaliplatin resistance-related genes regarding prognosis were discovered.

Supplementary Table 3 | The topological properties of the nodes in the PPI network.

REFERENCES

1. Taghizadeh H, Prager GW. Personalized adjuvant treatment of colon cancer. *Visc Med.* (2020) 36:397–406. doi: 10.1159/000508175
2. Benson AB, Venook AP, Al-Hawary MM, Cederquist L, Chen YJ, Ciombor KK, et al. NCCN guidelines insights: colon cancer, version 2.2018. *J Natl Compr Canc Netw.* (2018) 16:359–69. doi: 10.6004/jnccn.2018.0021
3. Nakamura Y, Hokuto D, Koyama F, Matsuo Y, Nomi T, Yoshikawa T, et al. The prognosis and recurrence pattern of right- and left- sided colon cancer in Stage II, Stage III, and liver metastasis after curative resection. *Ann Coloproctol.* (2020). doi: 10.3393/ac.2020.09.14. [Epub ahead of print].
4. Mandala M, Ferretti G, Barni S. Oxaliplatin in colon cancer. *N Engl J Med.* (2004) 351:1691–2. doi: 10.1056/NEJM200410143511623
5. Barton MK. Oxaliplatin in the adjuvant treatment of colon cancer. *CA Cancer J Clin.* (2012) 62:3–4. doi: 10.3322/caac.21131
6. Yu T, An Q, Cao XL, Yang H, Cui J, Li ZJ, et al. GOLPH3 inhibition reverses oxaliplatin resistance of colon cancer cells via suppression of PI3K/AKT/mTOR pathway. *Life Sci.* (2020) 260:118294. doi: 10.1016/j.lfs.2020.118294
7. Han Y, Qu YQ, Mok SWF, Chen J, Xia CL, He HQ, et al. A novel drug resistance mechanism: genetic loss of Xeroderma Pigmentosum Complementation Group C (XPC) enhances glycolysis-mediated drug resistance in DLD-1 colon cancer cells. *Front Pharmacol.* (2019) 10:912. doi: 10.3389/fphar.2019.00912
8. Pirpour Tazehkand A, Akbarzadeh M, Velaie K, Sadeghi MR, Samadi N. The role of Her2-Nrf2 axis in induction of oxaliplatin resistance in colon cancer cells. *Biomed Pharmacother.* (2018) 103:755–66. doi: 10.1016/j.biopha.2018.04.105
9. Kozovska Z, Gabrisova V, Kucerova L. Colon cancer: cancer stem cells markers, drug resistance and treatment. *Biomed Pharmacother.* (2014) 68:911–6. doi: 10.1016/j.biopha.2014.10.019
10. Culy CR, Clemett D, Wiseman LR. Oxaliplatin. A review of its pharmacological properties and clinical efficacy in metastatic colorectal cancer and its potential in other malignancies. *Drugs.* (2000) 60:895–924. doi: 10.2165/00003495-200060040-00005
11. Guinney J, Dienstmann R, Wang X, de Reynies A, Schlicker A, Soneson C, et al. The consensus molecular subtypes of colorectal cancer. *Nat Med.* (2015) 21:1350–6. doi: 10.1038/nm.3967
12. Thanki K, Nicholls ME, Gajjar A, Senagore AJ, Qiu S, Szabo C, et al. Consensus molecular subtypes of colorectal cancer and their clinical implications. *Int Biol Biomed J.* (2017) 3:105–11.
13. Sveen A, Cremolini C, Dienstmann R. Predictive modeling in colorectal cancer: time to move beyond consensus molecular subtypes. *Ann Oncol.* (2019) 30:1682–5. doi: 10.1093/annonc/mdz412
14. Luo H, Shen K, Li B, Li R, Wang Z, Xie Z. Clinical significance and diagnostic value of serum NSE, CEA, CA19-9, CA125 and CA242 levels in colorectal cancer. *Oncol Lett.* (2020) 20:742–50. doi: 10.3892/ol.2020.11633
15. Wu T, Mo Y, Wu C. Prognostic values of CEA, CA19-9, and CA72-4 in patients with stages I-III colorectal cancer. *Int J Clin Exp Pathol.* (2020) 13:1608–14.
16. Yang W, Ma J, Zhou W, Li Z, Zhou X, Cao B, et al. Identification of hub genes and outcome in colon cancer based on bioinformatics analysis. *Cancer Manag Res.* (2019) 11:323–38. doi: 10.2147/CMAR.S173240
17. Yang H, Liu H, Lin HC, Gan D, Jin W, Cui C, et al. Association of a novel seven-gene expression signature with the disease prognosis in colon cancer patients. *Aging.* (2019) 11:8710–27. doi: 10.18632/aging.102365
18. Li X, Wen D, Li X, Yao C, Chong W, Chen H. Identification of an immune signature predicting prognosis risk and lymphocyte infiltration in colon cancer. *Front Immunol.* (2020) 11:1678. doi: 10.3389/fimmu.2020.01678
19. Ren J, Feng J, Song W, Wang C, Ge Y, Fu T. Development and validation of a metabolic gene signature for predicting overall survival in patients with colon cancer. *Clin Exp Med.* (2020) 20:535–44. doi: 10.1007/s10238-020-00652-1
20. Clough E, Barrett T. The gene expression omnibus database. *Methods Mol Biol.* (2016) 1418:93–110. doi: 10.1007/978-1-4939-3578-9_5
21. Smith JJ, Deane NG, Wu F, Merchant NB, Zhang B, Jiang A, et al. Experimentally derived metastasis gene expression profile predicts recurrence and death in patients with colon cancer. *Gastroenterology.* (2010) 138:958–68. doi: 10.1053/j.gastro.2009.11.005
22. Marisa L, de Reynies A, Duval A, Selves J, Gaub MP, Vescovo L, et al. Gene expression classification of colon cancer into molecular subtypes: characterization, validation, prognostic value. *PLoS Med.* (2013) 10:e1001453. doi: 10.1371/journal.pmed.1001453
23. Ritchie ME, Phipson B, Wu D, Hu Y, Law CW, Shi W, et al. limma powers differential expression analyses for RNA-sequencing and microarray studies. *Nucleic Acids Res.* (2015) 43:e47. doi: 10.1093/nar/gkv007
24. Langfelder P, Horvath S. WGCNA: an R package for weighted correlation network analysis. *BMC Bioinformatics.* (2008) 9:559. doi: 10.1186/1471-2105-9-559
25. Yu G, Wang LG, Han Y, He QY. clusterProfiler: an R package for comparing biological themes among gene clusters. *OMICS.* (2012) 16:284–7. doi: 10.1089/omi.2011.0118
26. Szklarczyk D, Gable AL, Lyon D, Junge A, Wyder S, Huerta-Cepas J, et al. STRING v11: protein-protein association networks with increased coverage, supporting functional discovery in genome-wide experimental datasets. *Nucleic Acids Res.* (2019) 47:D607–13. doi: 10.1093/nar/gky1131
27. Hanzelmann S, Castelo R, Guinney J. GSVA: gene set variation analysis for microarray and RNA-seq data. *BMC Bioinformatics.* (2013) 14:7. doi: 10.1186/1471-2105-14-7
28. Siegel RL, Miller KD, Goding Sauer A, Fedewa SA, Butterly LF, Anderson JC, et al. Colorectal cancer statistics, 2020. *CA Cancer J Clin.* (2020) 70:145–64. doi: 10.3322/caac.21601
29. Yang Z, Chen Y, Wu D, Min Z, Quan Y. Analysis of risk factors for colon cancer progression. *Onco Targets Ther.* (2019) 12:3991–4000. doi: 10.2147/OTT.S207390
30. Merlano MC, Granetto C, Fea E, Ricci V, Garrone O. Heterogeneity of colon cancer: from bench to bedside. *ESMO Open.* (2017) 2:e000218. doi: 10.1136/esmoopen-2017-000218
31. Therachiyil L, Haroon J, Sahir F, Siveen KS, Uddin S, Kulinski M, et al. Dysregulated phosphorylation of p53, autophagy and stemness attributes the mutant p53 harboring colon cancer cells impaired sensitivity to oxaliplatin. *Front Oncol.* (2020) 10:1744. doi: 10.3389/fonc.2020.01744

32. Huang D, Xue J, Li S, Yang D. Oxaliplatin and infliximab synergize to induce regression of colon cancer. *Oncol Lett.* (2018) 15:1517–22. doi: 10.3892/ol.2017.7468
33. Henson DE, Hueman MT, Chen D, Patel JA, Wang H, Schwartz AM. The anatomy of the TNM for colon cancer. *J Gastrointest Oncol.* (2017) 8:12–9. doi: 10.21037/jgo.2016.11.10
34. Liu Q, Luo D, Cai S, Li Q, Li X. P-TNM staging system for colon cancer: combination of P-stage and AJCC TNM staging system for improving prognostic prediction and clinical management. *Cancer Manag Res.* (2018) 10:2303–14. doi: 10.2147/CMAR.S165188
35. Ogawa S, Itabashi M, Bamba Y, Yamamoto M, Sugihara K. Superior prognosis stratification for stage III colon cancer using log odds of positive lymph nodes (LODDS) compared to TNM stage classification: the Japanese study group for postoperative follow-up of colorectal cancer. *Oncotarget.* (2020) 11:3144–52. doi: 10.18632/oncotarget.27692
36. Lund CM, Dyhl-Polk A, Nielsen DL, Riis LB. Wnt5a expression and prognosis in stage II-III colon cancer. *Transl Oncol.* (2020) 14:100892. doi: 10.1016/j.tranon.2020.100892
37. Lao X, Feng Q, He G, Ji M, Zhu D, Xu P, et al. Immature Colon Carcinoma Transcript-1 (ICT1) expression correlates with unfavorable prognosis and survival in patients with colorectal cancer. *Ann Surg Oncol.* (2016) 23:3924–33. doi: 10.1245/s10434-016-5305-1
38. Liu J, Dong C, Jiang G, Lu X, Liu Y, Wu H. Transcription factor expression as a predictor of colon cancer prognosis: a machine learning practice. *BMC Med Genomics.* (2020) 13:135. doi: 10.1186/s12920-020-00775-0
39. Chen WC, Sigal DS, Saven A, Paulson JC. Targeting B lymphoma with nanoparticles bearing glycan ligands of CD22. *Leuk Lymphoma.* (2012) 53:208–10. doi: 10.3109/10428194.2011.604755
40. Anti-CD20 and CD22 therapy is effective in non-Hodgkin lymphoma. *Cancer Discov.* (2013) 3:OF9. doi: 10.1158/2159-8290.CD-RW2013-014
41. Tuscano JM, Kato J, Pearson D, Xiong C, Newell L, Ma Y, et al. CD22 antigen is broadly expressed on lung cancer cells and is a target for antibody-based therapy. *Cancer Res.* (2012) 72:5556–65. doi: 10.1158/0008-5472.CAN-12-0173
42. Darvishi B, Boroumandieh S, Majidzadeh AK, Salehi M, Jafari F, Farahmand L. The role of activated leukocyte cell adhesion molecule (ALCAM) in cancer progression, invasion, metastasis and recurrence: a novel cancer stem cell marker and tumor-specific prognostic marker. *Exp Mol Pathol.* (2020) 115:104443. doi: 10.1016/j.yexmp.2020.104443
43. Jeong YJ, Oh HK, Park SH, Bong JG. Prognostic significance of Activated Leukocyte Cell Adhesion Molecule (ALCAM) in association with promoter methylation of the ALCAM gene in breast cancer. *Molecules.* (2018) 23:131. doi: 10.3390/molecules23010131
44. Bartolome RA, Pintado-Berninches L, Jaen M, de Los Rios V, Imbaud JI, Casal JI. SOSTDC1 promotes invasion and liver metastasis in colorectal cancer via interaction with ALCAM/CD166. *Oncogene.* (2020) 39:6085–98. doi: 10.1038/s41388-020-01419-4
45. Lasithiotaki I, Tsitoura E, Samara KD, Trachalaki A, Charalambous I, Tzanakis N, et al. NLRP3/Caspase-1 inflammasome activation is decreased in alveolar macrophages in patients with lung cancer. *PLoS ONE.* (2018) 13:e0205242. doi: 10.1371/journal.pone.0205242
46. Jin H, Kim HJ. NLRC4, ASC and caspase-1 are inflammasome components that are mediated by P2Y2R activation in breast cancer cells. *Int J Mol Sci.* (2020) 21:3337. doi: 10.3390/ijms21093337
47. Yang Y, Liu PY, Bao W, Chen SJ, Wu FS, Zhu PY. Hydrogen inhibits endometrial cancer growth via a ROS/NLRP3/caspase-1/GSDMD-mediated pyroptotic pathway. *BMC Cancer.* (2020) 20:28. doi: 10.1186/s12885-019-6491-6
48. Palmer DC, Guittard GC, Franco Z, Crompton JG, Eil RL, Patel SJ, et al. Cish actively silences TCR signaling in CD8+ T cells to maintain tumor tolerance. *J Exp Med.* (2015) 212:2095–113. doi: 10.1084/jem.20150304

Conflict of Interest: The authors declare that the research was conducted in the absence of any commercial or financial relationships that could be construed as a potential conflict of interest.

frontiers in Oncology

ORIGINAL RESEARCH
published: 18 May 2021
doi: 10.3389/fonc.2021.637971

Development of an Aerobic Glycolysis Index for Predicting the Sorafenib Sensitivity and Prognosis of Hepatocellular Carcinoma

Yu Pan[1,2,3,4,5,6†], *Geng-yuan Hu*[5,6,7†], *Shi Jiang*[1,2,3,4,5,6], *Shun-jie Xia*[1,2,3,4,5,6], *Hendi Maher*[1,2,3,4,5,6], *Zhong-jie Lin*[1,2,3,4,5,6], *Qi-jiang Mao*[1,2,3,4,5,6], *Jie Zhao*[1,2,3,4,5], *Liu-xin Cai*[1,2,3,4,5], *Ying-hua Xu*[8*], *Jun-jie Xu*[1,2,3,4,5*] *and Xiu-jun Cai*[1,2,3,4,5*]

[1] *Department of General Surgery, Sir Run-Run Shaw Hospital, Zhejiang University, Hangzhou, China,* [2] *Key Laboratory of Laparoscopic Technology of Zhejiang Province, Hangzhou, China,* [3] *Zhejiang Minimal Invasive Diagnosis and Treatment Technology Research Center of Severe Hepatobiliary Disease, Hangzhou, China,* [4] *Zhejiang Research and Development Engineering Laboratory of Minimally Invasive Technology and Equipment, Hangzhou, China,* [5] *Zhejiang University Cancer Center, Hangzhou, China,* [6] *School of Medicine, Zhejiang University, Hangzhou, China,* [7] *Department of Gastrointestinal Surgery, Shaoxing People's Hospital, Shaoxing Hospital of Zhejiang University, Shaoxing, China,* [8] *Department of Oncology, Sir Run-Run Shaw Hospital, Zhejiang University, Hangzhou, China*

Hepatocellular carcinoma (HCC) is a deadly tumor with high heterogeneity. Aerobic glycolysis is a common indicator of tumor growth and plays a key role in tumorigenesis. Heterogeneity in distinct metabolic pathways can be used to stratify HCC into clinically relevant subgroups, but these have not yet been well-established. In this study, we constructed a model called aerobic glycolysis index (AGI) as a marker of aerobic glycolysis using genomic data of hepatocellular carcinoma from The Cancer Genome Atlas (TCGA) project. Our results showed that this parameter inferred enhanced aerobic glycolysis activity in tumor tissues. Furthermore, high AGI is associated with poor tumor differentiation and advanced stages and could predict poor prognosis including reduced overall survival and disease-free survival. More importantly, the AGI could accurately predict tumor sensitivity to Sorafenib therapy. Therefore, the AGI may be a promising biomarker that can accurately stratify patients and improve their treatment efficacy.

Keywords: hepatocellar carcinoma, aerobic glycolysis, Sorafenib, biomarker, prognosis

OPEN ACCESS

Edited by:
Prathibha Ranganathan, Centre for Human Genetics (CHG), India

Reviewed by:
Manoj Kumar Kashyap, Amity University Gurgaon, India
Priyanka Samji, Sri Ramachandra University, India

***Correspondence:**
Xiu-jun Cai
srrsh_cxj@zju.edu.cn
Jun-jie Xu
walter235@zju.edu.cn
Ying-hua Xu
connich@zju.edu.cn

These authors have contributed equally to this work

Specialty section:
This article was submitted to Gastrointestinal Cancers, a section of the journal Frontiers in Oncology

Received: *04 December 2020*
Accepted: *15 February 2021*
Published: *18 May 2021*

Citation:
Pan Y, Hu G-y, Jiang S, Xia S-j, Maher H, Lin Z-j, Mao Q-j, Zhao J, Cai L-x, Xu Y-h, Xu J-j and Cai X-j (2021) Development of an Aerobic Glycolysis Index for Predicting the Sorafenib Sensitivity and Prognosis of Hepatocellular Carcinoma. Front. Oncol. 11:637971. doi: 10.3389/fonc.2021.637971

INTRODUCTION

Globally, hepatocellular carcinoma (HCC) is the sixth most commonly diagnosed cancer and the fourth leading cause of cancer-related deaths (1). Despite advances in the treatment of HCC, its prognosis remains unsatisfactory, with a 5-year overall survival (OS) rate of 25–55% (2–4). Local recurrence, distal metastasis, and resistance to conventional therapy are the leading causes of HCC progression into late-stage cancer with limited treatment options. Genetic mutations, chromosomal instability, epigenetic changes, and molecular signaling pathway dysregulation are reported causes of hepatocellular carcinogenesis (5). Therefore, advances in the field of molecular oncology are urgently required to improve the prognosis of HCC.

Sorafenib is an oral multitargeted drug that inhibits the activity of several tyrosine kinases (6). Thus, Sorafenib can effectively suppress angiogenesis and cancer proliferation and induce tumor cell apoptosis. Since it was first approved by the US Food and Drug Administration in 2007 as the first-line treatment for advanced HCC, Sorafenib has shown favored clinical benefits. In the Sorafenib Hepatocellular Carcinoma Assessment Randomized Protocol (SHARP) trial, patients who received Sorafenib therapy showed significantly higher median OS compared with the control group (10.7 vs. 7.9 months, respectively) and a 31% reduction in the risk of death (7). In the Asia-Pacific trial, Sorafenib provided a clinical benefit, extending the median survival benefit by 2 months (8). Currently, Sorafenib is still applied as the first-line therapy for advanced HCC patients; even several other tyrosine kinases inhibitors have been evaluated by comparing them to Sorafenib, which did not demonstrate an improvement of prognosis (9–11). However, a large number of patients with HCC show poor response to Sorafenib due to the heterogeneity of the disease and the complex tumor-associated molecular signaling, which lacks generally accepted predictive biomarkers. Furthermore, primary and acquired resistance to Sorafenib are commonly reported and limit the clinical advantages of the drug (12–15).

The Warburg phenotype is a common hallmark of cancer cells, characterized by enhanced glycolysis, even under physiological oxygen conditions (16, 17). By shifting glucose metabolism from oxidative respiration to aerobic glycolysis, tumor cells display enhanced glucose metabolism for producing efficient energy and various metabolic intermediates, which are indispensable for the synthesis of macromolecules and new organelles. Several oncogenes, including Ras, Myc, and HIF1, were reported to drive metabolic adaptations toward aerobic glycolysis (18, 19). Enhanced aerobic glycolysis has been demonstrated to exhibit consistent prognostic patterns and is associated with Sorafenib resistance (20). Increased expression of aerobic glycolysis-related genes, including solute carrier family 2 member 1 (SLC2A1), solute carrier family 2 member 2 (SLC2A2), glucose-6-phosphate dehydrogenase (G6PD), glypican 1 (GPC1), procollagen-lysine, 2-oxoglutarate 5-dioxygenase 2 (PLOD2), and lactate dehydrogenase A (LDHA), has been reported to be associated with aggressive HCC (21–29). Accelerated glucose uptake and lactate synthesis were observed as responses to Sorafenib treatment (30–32). New therapeutic approaches have been reported to attenuate Sorafenib resistance by inhibiting key glycolytic enzymes including 6-phosphofructo-2-kinase/fructose-2,6-biphosphatase 3 (PFKFB3), hexokinase 2 (HK2), and pyruvate kinase M1/2 (PKM2) (33–36). Tumor metabolic heterogeneity is reported to be relevant to tumor subtypes and prognosis (37), but whether heterogeneity in distinct metabolic pathways can be used to stratify HCC into clinically relevant subgroups has not been well-established.

Aerobic glycolysis is a complex biological process involving numerous genes. Thus, constructing a gene signature based on multiple glycolysis-related genes is supposed to be more suitable to represent the aerobic glycolysis pathway than single gene. The development of genomic techniques has unveiled extensive biological information that can be used to explore the underlying mechanisms of tumorigenesis and progression. In this study, we constructed a model named aerobic glycolysis index (AGI) to evaluate the signal of aerobic glycolysis, by utilizing genomic data of hepatocellular carcinoma from The Cancer Genome Atlas (TCGA) project. The AGI was calculated based on the expression of 14 glycolysis-related genes (SLC2A1, SLC2A2, G6PD, LDHA, GPC1, HMMR, PLOD2, GOT2, STC2, CENPA, RARS1, HOMER1, SRD5A3, and TKTL1). The abbreviations list and their expansions for these glycolytic genes are summarized in **Supplementary Table 1**. Then, we assessed whether the AGI was a predictive marker for the prognosis of HCC and sensitivity to Sorafenib. Finally, we used *in vitro* experiments to confirm that AGI was associated with Sorafenib resistance. Significantly, we established a methodology to quantify aerobic glycolysis signaling. The AGI was found to be a robust prognostic biomarker of HCC and a predictive factor of the response to Sorafenib.

MATERIALS AND METHODS

Specimen Collection and RNA Sequencing

In total, 102 pairs of formalin-fixed paraffin-embedded HCC and corresponding normal tissue specimens from the Sir Run Shaw Hospital (SRRSH) were collected. This research was approved by the Institutional Review Board of the SRRSH of Zhejiang University. The patients provided informed consent for the use of their specimens. For RNA sequencing, TRIzol (Invitrogen, USA) was used to extract total RNA. After checking the RNA purity, integrity, and concentration, RNA sequencing was performed on an Illumina platform.

Data Acquisition and Processing

Fragments per kilobase of transcript per million mapped reads (FPKM) RNA-seq data and the clinical characteristics of TCGA samples were downloaded from the UCSC Cancer Browser database. Gene mutation data and copy number information of the TCGA samples were acquired from the cBioPortal database. RNA-seq and clinical data of the LIRI-JP cohort were downloaded from the HCCDB database. The GSE14520, GSE25097, GSE36376, GSE64041, GSE76427, GSE109211, and GSE73571 expression profile was obtained from the Gene Expression Omnibus (GEO) database. The proteomics data of TCGA samples were downloaded from the TCPA database. Drug sensitivity data of HCC cell lines were obtained from the Genomics of Drug Sensitivity in Cancer (GDSC) database and Cancer Cell Line Encyclopedia (CCLE) database. The patient characteristics of TCGA, LIRI-JP, GSE14520, and SRRSH datasets are summarized in **Supplementary Table 2**.

Development of the AGI

Univariate Cox regression was applied to detect the aerobic glycolysis genes related to prognosis. The least absolute shrinkage and selection operator (LASSO) Cox regression model was performed to determine the coefficients for model construction with an optimal log λ (38). The AGI was established with the following formula: Risk score = expression of Gene 1 $\times$ β1 + expression of Gene 2 $\times$ β2+…expression of Gene n $\times$ βn (β

was the weighted coefficient of each gene). For gene expression measured by quantitative real-time PCR (qPCR), the AGI was calculated as the method described by Zheng et al. (39). Total RNAs from cells were extracted using TRIzol (Invitrogen, USA) according to the manufacturer's instructions. Complementary DNA (cDNA) was synthesized using Hifair® II 1st Strand cDNA Synthesis SuperMix for qPCR (Yeasen, Shanghai, China). qPCR was performed using Hieff UNICON® qPCR SYBR Green Master Mix (Yeasen, Shanghai, China). Measurement was carried out by Roche LightCycler 480. Analysis was carried out using the $^{\Delta\Delta}$Ct method. All assays were performed in triplicates, and results were plotted as the mean ± SD. Primer sequences are listed in **Supplementary Table 3**.

Gene Set Enrichment Analysis and Gene Set Variation Analysis

Datasets were divided into two groups according to tissue types or AGI scores. Annotated gene sets were downloaded from the MSigDB database. Gene Set Enrichment Analysis (GSEA) was performed using the R package "GSEAbase." Annotated drug sets were downloaded from the DSigDB database. Gene Set Variation Analysis (GSVA) was performed using the R package "GSVA."

Cell Culture of Liver Cancer Cell Lines

Liver cancer cell lines (SK-Hep-1, Huh7, HepG2, HCCLM3) were purchased from the American Tissue Culture Collection (Manassas, VA, USA) and cultured in accordance with the recommended guidelines. Sorafenib-resistant HCC cell lines were cultured with Sorafenib as previously reported (40, 41).

Cell Viability Test

Cells were seeded in 96-well plates in replicates of three. After incubation with Sorafenib for 48 h, cell viability analysis was performed using the Cell Counting Kit-8 (CCK-8) (Yeasen, Shanghai, China).

Apoptosis Assay

Cells were seeded in six-well plates and mock treated or treated with drugs [Sorafenib, 2-deoxy-D-glucose (2-DG), or a combination of Sorafenib and 2-DG] for 48 h before apoptosis assays. Cell apoptosis was determined using the PI/annexin V-FITC Apoptosis Kit (MULTI SCIENCES, Hangzhou, China).

Transwell Assay

Cells (1×10^5) in serum-free medium were seeded into the upper chambers of Transwell (Corning, Corning, NY, USA), and medium with 10% fetal bovine serum (FBS) was seeded into the lower chambers for 24 h in a humidified incubator at 37°C in 5% CO_2. The cells remaining in the upper chamber were carefully removed using a cotton swab, and cells that migrated to the lower membrane surface were fixed in 4% paraformaldehyde and stained with crystal violet. The experiments were repeated three times.

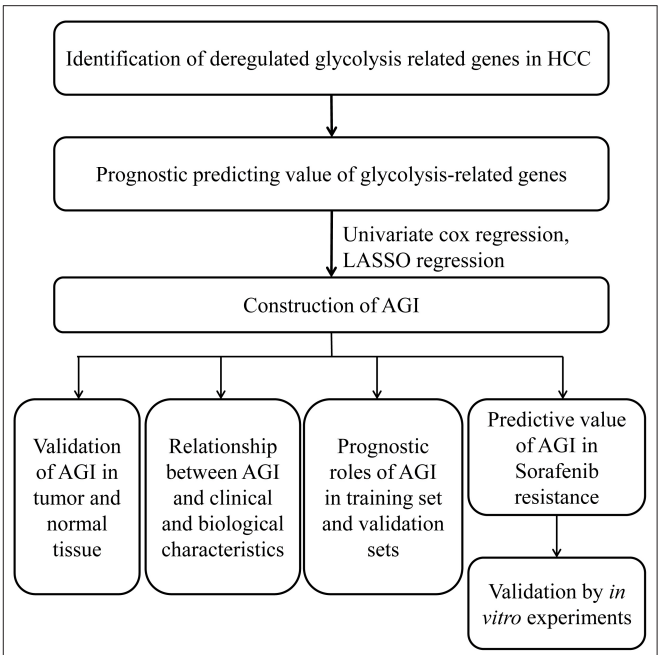

FIGURE 1 | Flowchart presenting the establishment and validation of the gene signature.

Glucose Consumption and Lactic Acid Assays

Cells were seeded into six-well plates at a density of 1×10^6 cells and cultured overnight. Glucose consumption and lactic acid production were detected using glucose assay kit (Solarbio® BC2500) and LA assay kit (Solarbio® BC2230) according to the instruction of the manufacturers, respectively. The experiments were repeated three times.

Statistical Analysis

The univariate Cox regression, LASSO Cox regression model, and multivariate Cox regression model were performed. The OS and disease-free survival (DFS) were compared using the Kaplan–Meier method with the log-rank test. Non-parametric tests or Student's *t*-tests were used to determine the significance of the differences between the subgroups and clinicopathological characteristics. Spearman's correlation test was used to assess the relationship between the AGI and biological pathways and clinicopathological parameters. Statistical analyses were performed using R software (Version 3.6.0). A $P < 0.05$ was considered statistically significant, and all *P*-values were two-tailed.

RESULTS

Establishment of the AGI

This study was conducted according to the flow chart shown in **Figure 1**. Initially, several key genes of glycolysis were observed to be commonly upregulated in tumor tissues compared with

normal tissues in a series of datasets, including TCGA, LIRI-JP, GSE14520, GSE25097, GSE36376, GSE64041, and GSE76427 (**Figure 2A**). The GSEA results revealed that the glycolysis signaling pathway was significantly enriched in HCC tumor tissues compared with normal tissues (**Figure 2B**). These results suggested that the glycolysis signaling pathway may contribute to malignant tumor phenotypes. Because aerobic glycolysis is a complex biological process involving hundreds of genes, using a gene signature comprising multiple genes can predict the tumor characteristics and prognosis more accurately than a single gene. The univariate Cox regression analysis was conducted to determine the prognostically relevant genes related to the aerobic glycolysis, and 80 relevant genes were identified (**Figure 2C**). To further simplify the gene signature of aerobic glycolysis, LASSO regression was performed based on these prognostically relevant genes. Finally, 14 genes were selected to establish the AGI according to the partial likelihood deviance method with an optimal log λ (**Supplementary Figures 1, 2**). Additionally, as shown in **Figure 2D**, the correlations between the AGI and selected aerobic glycolysis-related genes were statistically significant. Furthermore, the correlations between the AGI and several important genes coding the rate-limiting enzymes of glucose metabolism were examined. The results demonstrated that the AGI correlated closely to these genes (HK2, $r = 0.43$, $P < 2.2e^{-16}$; PFKP, $r = 0.39$, $P = 1.4e^{-14}$; PFKFB3, $r = 0.27$, $P = 2e^{-7}$; PKM2, $r = 0.66$, $P < 2e^{-16}$), as shown in **Supplementary Figure 3**.

After the establishment of the AGI, we first tested the capacity of AGI as an acceptable indicator of aerobic glycolysis. The AGI could distinguish HCC tumor tissues from normal tissue samples in the TCGA dataset that significantly higher AGI was observed in tumor samples, indicating enhanced aerobic glycolysis activity in these tumor samples ($P = 8.1e^{-13}$, **Figure 2E**). To further validate the power of the AGI, we examined this index in three other HCC datasets. As shown in **Figure 2E**, a significantly higher AGI was observed in HCC tumor samples compared with normal tissue samples in all of three datasets (GSE64041, $P = 8.1e^{-10}$; GSE14520, $P < 2e^{-16}$; LIRI-JP, $P < 2e^{-16}$). Furthermore, RNA sequencing data from our center (SRRSH) were applied and confirmed the reliability of AGI in distinguishing HCC tumor tissues from normal tissue samples ($P < 2e^{-16}$) (**Figure 2F**). Then, the receiver operating characteristic (ROC) curve and area under the curve (AUC) scores were further evaluated to quantify the accuracy of the AGI to classify tumor and normal tissues. High prediction accuracies were achieved in all datasets, ruling out the possibility of over fitting (TCGA, AUC = 0.916; GSE64041, AUC = 0.825; GSE14520, AUC = 0.945; LIRI-JP, AUC = 0.846, SRRSH set, AUC = 0.902, **Figure 2G**).

Association of the AGI With Genomic and Proteomic Alterations

Using the optimal cutoff value based on prognostic effects, the patients in the TCGA cohort were stratified into high and low AGI groups. The distribution of gene expression in the high and low AGI groups is represented in **Figure 3A**. In particular, we compared the genes encoding key proteins and enzymes of aerobic glycolysis, and most of them were highly expressed in the high AGI group, supporting the close correlation between aerobic glycolysis and the AGI (**Figure 3B**).

Previous reports demonstrated that aerobic glycolysis genes could be regulated by transcription factors such as p53, c-Myc, and HIF-1α. In our study, the high AGI group showed an increased proportion of TP53 mutations and a decreased proportion of CTNNB1 mutations (**Figure 3C**), which were the most common mutations in HCC. Accordingly, patients with a TP53 mutation showed a higher AGI than patients with wild-type TP53. Conversely, patients with a CTNNB1 mutation showed a lower AGI than patients with wild-type CTNNB1 (**Figure 3D**). Next, we investigated the distribution of copy number variations between the high and low AGI groups. The high AGI group showed an increased amplification frequency of Myc, AGO2, EXT1, RAD21, EIF3E, RSPO2, RECQL4, RUNX1T1, NBN, PAG1, and HEY1 (**Figure 3E**). These outcomes may provide novel ideas for investigating the mechanism of tumor aerobic glycolysis and copy number variation.

GSEA of the transcripts in the two groups revealed that gene sets considered to be markers of high malignancy were enriched in the high AGI group, including those E2F targets, Myc targets, epithelial–mesenchymal transition (EMT) regulators, and G2M checkpoints (**Figure 3F** and **Supplementary Table 4**). Conversely, gene sets related to oxidative phosphorylation, peroxisomes, xenobiotic metabolism, and other metabolic processes were enriched in the low AGI group (**Figure 3G** and **Supplementary Table 4**). As the EMT pathway enriched in the high AGI group, we were interested in the relationship between the AGI and tumor invasion capability. The AGI in four liver cancer cell lines (SK-hep-1, Huh7, HepG2, and HCCLM3) was calculated. The result demonstrated that cell lines with high AGI (SK-hep-1, Huh7, and HCCLM3) had increased glucose intake and lactic acid level as compared with the cell line with low AGI (HepG2). More importantly, the Transwell assay revealed that cell lines with high AGI exhibited the greater invasion capability (**Supplementary Figure 4**). Previous studies also have reported a close relationship between aerobic glycolysis and angiogenesis (42–44). In the present study, we compared the expression of several genes involved in angiogenesis between the high and low AGI groups. The results demonstrated that the high AGI group had increased expression of vascular endothelial growth factor A (VEGFA) and VEGFB as compared with the low AGI group (**Supplementary Figure 5**).

Further analysis of proteomic data revealed that the AGI was strongly correlated with the expression of cell-cycle-related proteins, including pChk1, pChk2, and CyclinB1, and other tumor hallmark proteins, such as eIF4G, pPI3K, Src, Smad1, and Smad3 (**Figure 3H**). Furthermore, the AGI was negatively correlated with the expression of Rb, phosphatase and tensin homolog (PTEN), cleaved poly(ADP-ribose) polymerase (PARP) (**Figure 3I**). Collectively, the analysis of gene mutations, copy number variations, classical signaling pathway gene sets, and proteomic data suggests that the AGI is associated with cell proliferation, tumor progression, and the inhibition of apoptosis in HCC.

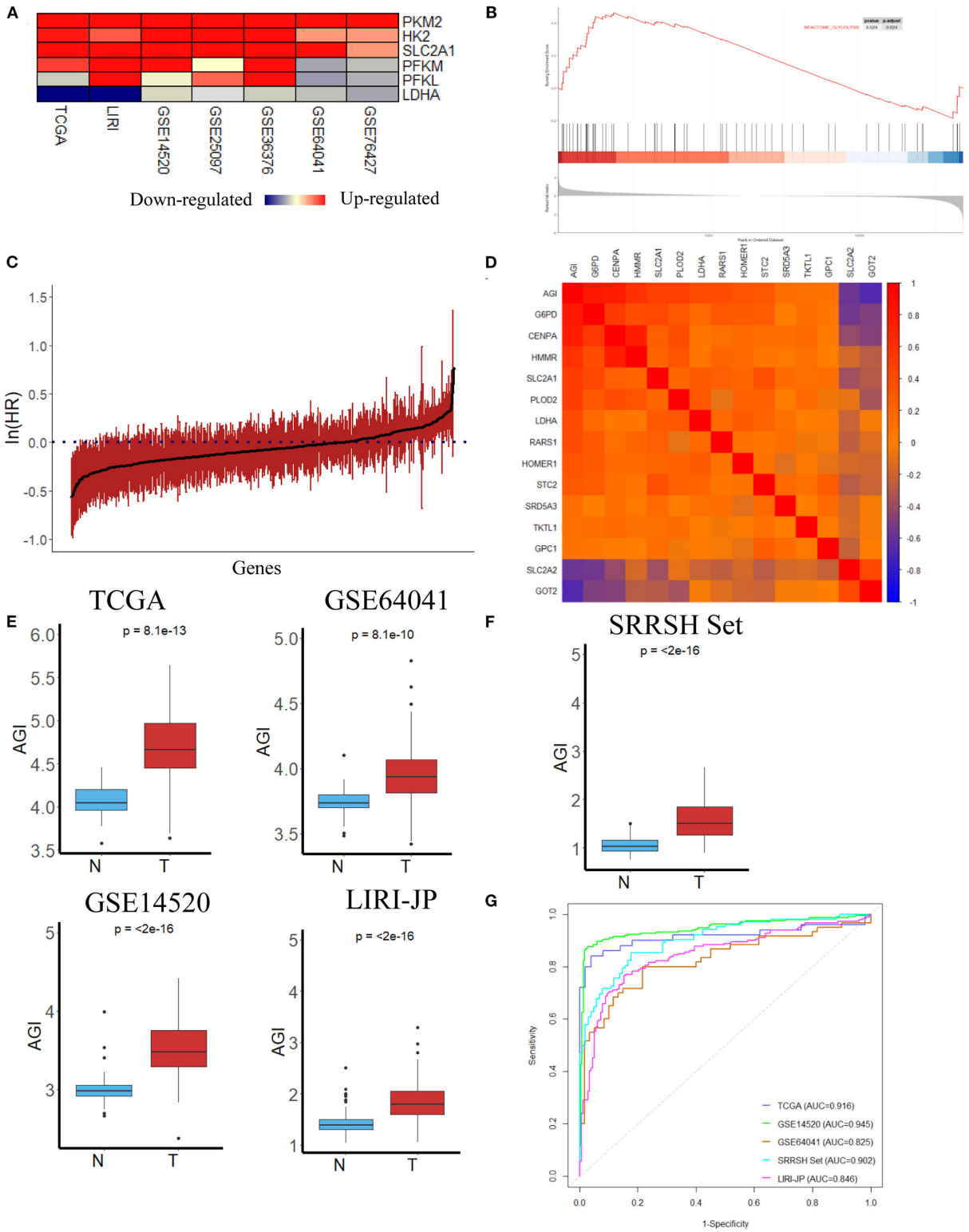

FIGURE 2 | Construction of the aerobic glycolysis index (AGI) model and validation of the AGI in tumor and normal tissues. **(A)** Heatmap of glycolysis-related gene expression in different datasets. **(B)** Gene Set Enrichment Analysis (GSEA) of the glycolysis pathway in GSE14520. **(C)** Bar plot showing the hazard ratio of glycolysis-related genes in The Cancer Genome Atlas (TCGA) cohort using the univariate Cox regression. The bars represent the 95% CI. **(D)** Correlation between the AGI and the selected signature genes in the TCGA cohort. **(E)** Boxplots showing AGI differences in normal and tumor tissues in the TCGA, GSE64041, GSE14520 and LIRI JP datasets. **(F)** Boxplots showing AGI differences in normal and tumor tissues in the SRRSH set. **(G)** Receiver operating characteristic (ROC) curves for tissue type prediction using the AGI as the predictor.

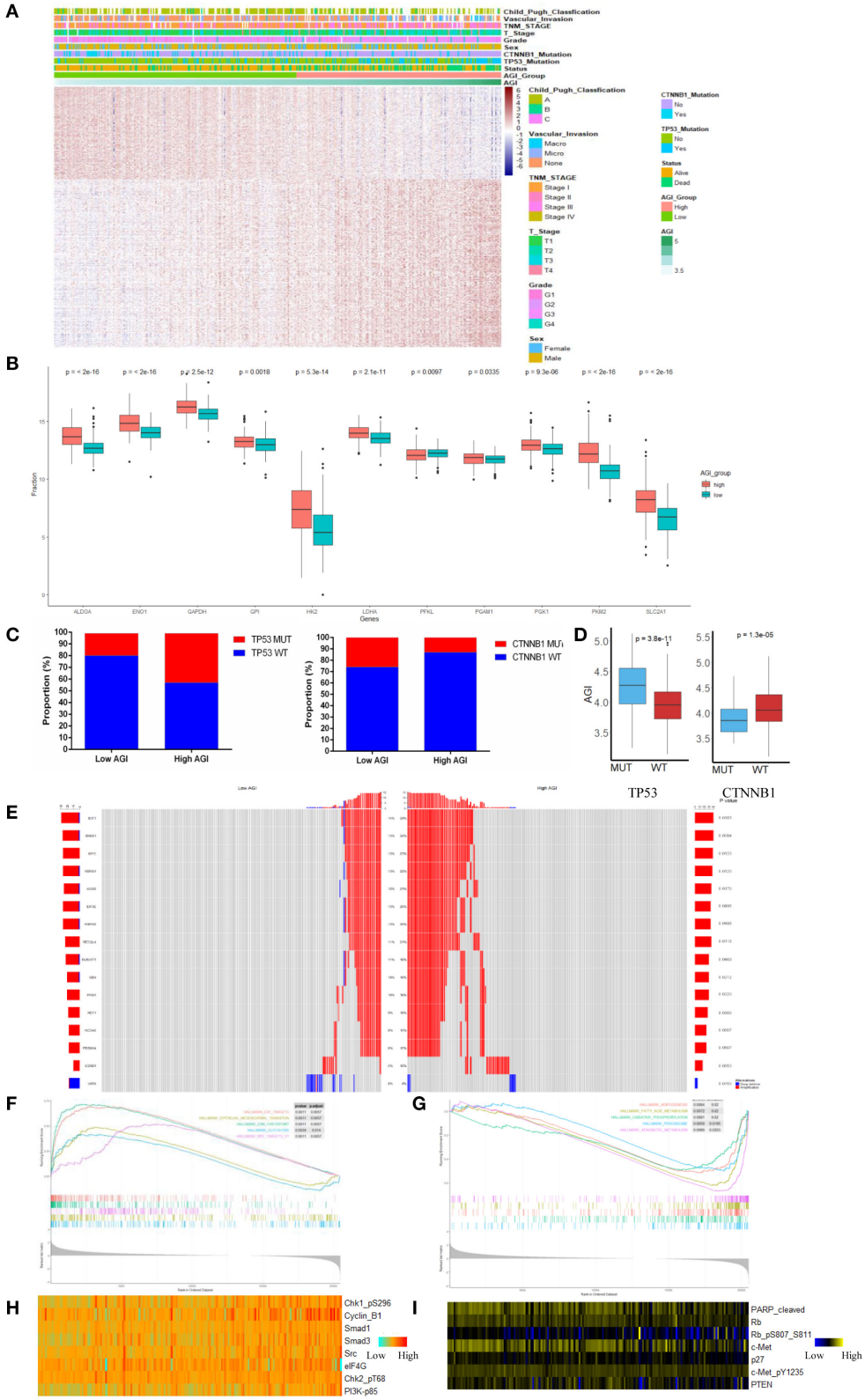

FIGURE 3 | The landscape of biological processes and characteristics of the aerobic glycolysis index (AGI) subgroups. **(A)** Heatmap of common differentially expressed genes based on the expression data in the high and low AGI groups. **(B)** Box plots showing the expression of the selected glycolysis-related genes in The

(Continued)

FIGURE 3 | Cancer Genome Atlas (TCGA) cohort. **(C)** Proportion of TP53 and CTNNB1 mutations in the high and low AGI groups. **(D)** Box plots showing the AGI in patients with TP53 mutations and wild-type TP53 (left) and CTNNB1 mutations and wild-type CTNNB1 (right). **(E)** The oncoPrint of copy number variations was constructed in the high and low AGI subgroups. **(F)** Activated gene sets enriched in the high AGI subgroup. **(G)** Suppressed gene sets enriched in the high AGI group. **(H,I)** Proteins positively **(H)** and negatively **(I)** correlated with the AGI ($P < 0.05$ for all proteins) based on reverse-phase protein arrays analysis of 181 samples from the TCGA using Spearman's rank correlation.

Correlation Between the AGI and Clinical Characteristics

Our data showed that the AGI was closely associated with TP53, Myc, cell cycle, and EMT pathways, and therefore, we next examined whether the AGI is associated with tumor progression and metastasis. We first analyzed the relationship between the AGI and clinical characteristics of HCC patients. A significantly increased AGI was observed in patients with higher tumor grades (**Figure 4A**), advanced T stages, and tumor–node–metastasis (TNM) stages (**Figures 4B,C**) and vascular invasion (**Figure 4D**). Here, we defined early tumor recurrence as a tumor recurring within 2 years after primary treatment and late recurrence as cancer recurring after 2 years. The AGI was significantly higher in patients with early recurrence than in those with late recurrence (**Figure 4E**).

Patients with a higher AGI were associated with a worse prognosis in terms of OS [hazard ratio (HR), 3.43; $P < 0.001$; **Figure 4F**] and DFS (HR, 2.07; $P < 0.001$; **Figure 4G**). The univariate Cox regression analysis revealed that the AGI (HR, 4.132), T stage (HR, 1.675), and TNM stage (HR, 1.661) were risk factors of a worse HCC prognosis (**Figure 4H**), and the multivariate Cox regression analysis showed that the AGI was an independent risk factor of poor prognosis (HR, 4.865; **Figure 4I**). The ROC curve showed that the AGI could accurately predict the 1-year (AUC, 0.787), 3-year (AUC, 0.751), and 5-year OS (AUC, 0.714) of HCC (**Figure 4J**), which was superior to conventional clinical parameters such as the tumor grade, status of vascular invasion, and TNM stage (**Figure 4K**).

Prognostic Value Validation of the AGI

A significantly increased AGI was observed in patients with higher TNM stages in three independent datasets (**Figures 5A–C**). The prognostic value of the AGI in HCC was validated in three independent datasets, including GSE14520 from GEO, LIRC from ICGC, and the SRRSH set from our center. By dividing the datasets into two groups according to the AGI, the distribution of the gene expression profiles and status of patients were consistent with the AGI (**Figures 5D–F**). Similar to the TCGA dataset, the high AGI group showed worse OS (GSE14520: HR, 2.13; **Figure 5G**; LIRC: HR, 2.85; **Figure 5H**; SRRSH set: HR, 2.53; **Figure 5I**) and DFS (GSE14520: HR, 1.67; **Figure 5K**; SRRSH set: HR, 1.77; **Figure 5L**) compared with the low AGI group. The ROC curve demonstrated that the AUCs of the AGI in predicting the 5-year OS of GSE14520, LIRC, and SRRSH sets were 0.676, 0.630, and 0.621, respectively (**Figure 5J**), indicating a robust prognostic value of the AGI.

AGI Predicts Sensitivity to Sorafenib in Both HCC Cell Lines and Patients

Sorafenib is the first-line therapy for advanced HCC. The increased expression of aerobic glycolysis-related genes has been demonstrated to promote Sorafenib resistance (45). Our results showed the AGI was closely related to advanced tumor stages and poor tumor differentiation. Moreover, a high AGI was strongly correlated with EMT, Myc, and cell cycle pathways (**Figure 3B**), which had been reported to be associated with impaired Sorafenib sensitivity and a worse prognosis (45). We were interested in the relationship between the AGI and Sorafenib sensitivity and wondered if the AGI could be a potential biomarker to predict drug sensitivity. Thus, the GSVA was performed, and the results revealed that the low AGI group appeared to be more sensitive to Sorafenib (**Figure 6A**). Then, we verified the relationship between Sorafenib sensitivity and the AGI *in vitro* using the data from the GDSC database, which showed that HCC cell lines with a lower AGI were more sensitive to Sorafenib (**Figure 6B**). Furthermore, a positive correlation between the AGI and the natural logarithm of the IC_{50} was observed ($r = 0.61$, $P = 0.02$, **Figure 6C**). Similarly, using HCC cell line data from the CCLE database, cell lines with a higher AGI showed decreased Sorafenib sensitivity (**Figure 6D**), and a positive correlation between the AGI and the natural logarithm of the EC_{50} of Sorafenib was observed (**Figure 6E**). Although not statistically significant due to a limited sample size, the trends suggested a potential relationship between the AGI and Sorafenib sensitivity *in vitro*. We next calculated the AGI in patients who received Sorafenib therapy using the transcription data from GSE109211 (the STORM trial). The patients who did not respond to Sorafenib showed a higher AGI (**Figure 6F**) and upregulated expression of AGI-related genes (**Figure 6G**). The ROC curve of the AGI in predicting the sensitivity to Sorafenib retrieved an AUC of 0.879 (**Figure 6H**), indicating that the AGI is a reliable biomarker in selecting suitable patients for Sorafenib treatment.

Increased AGI in Sorafenib-Resistant HCC Cell Lines

To further study the relationship between the AGI and Sorafenib resistance, the expression of AGI-related genes was evaluated in different cell lines (SK-hep-1 and Huh-7) at 0, 24, 48, and 72 h after Sorafenib treatment using qPCR. The levels of AGI-related genes substantially elevated following the treatment with Sorafenib, resulting in an increased AGI (**Figure 7A**). These results suggested that the AGI and underlying metabolic remodeling may be closely related to Sorafenib treatment. In previous studies, we reported several HCC cell lines treated with Sorafenib for long term, which could be considered

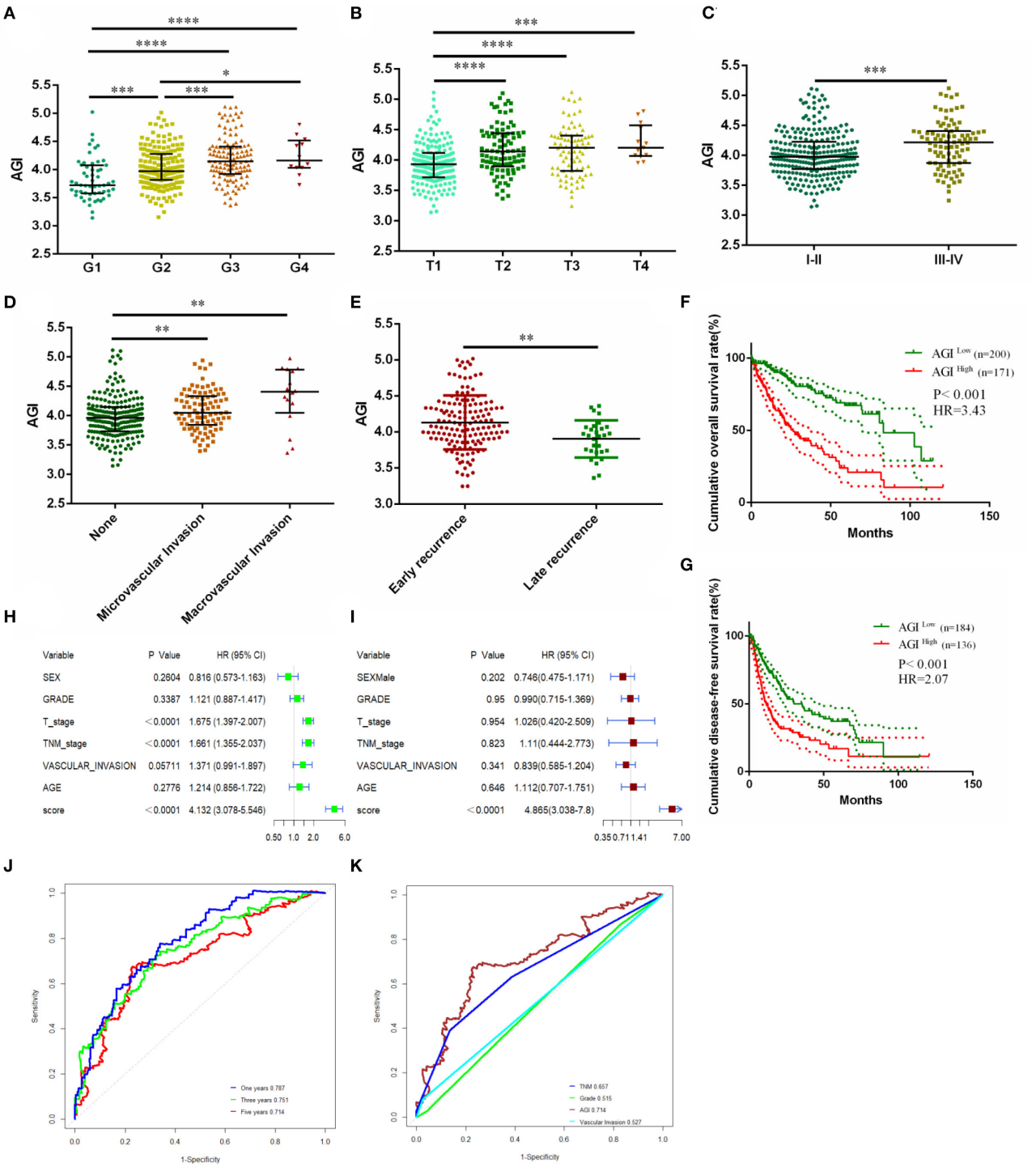

FIGURE 4 | Clinicopathological significance and prognosis prediction value of the AGI. **(A)** Tumor differentiation grade. **(B)** T stage. **(C)** Tumor–node–metastasis (TNM) stage. **(D)** Vascular invasion status. **(E)** Recurrence status. **(F)** Kaplan–Meier plot analysis of overall survival (OS) in the high and low AGI groups. **(G)** Kaplan–Meier plot analysis of disease-free survival (DFS) in the high and low AGI groups. **(H,I)** Forest plot showing the prognostic value of the AGI and clinical characteristics using univariate **(H)** and multivariate **(I)** analysis. **(J)** Time-dependent receiver operating characteristic (ROC) analysis comparing the AGI in predicting the 1-, 3-, and 5-year OS. **(K)** Time-dependent ROC analysis comparing the AGI and clinical characteristics in 5-year OS. $^{*}P < 0.05$, $^{**}P < 0.01$, $^{***}P < 0.001$, $^{****}P < 0.0001$.

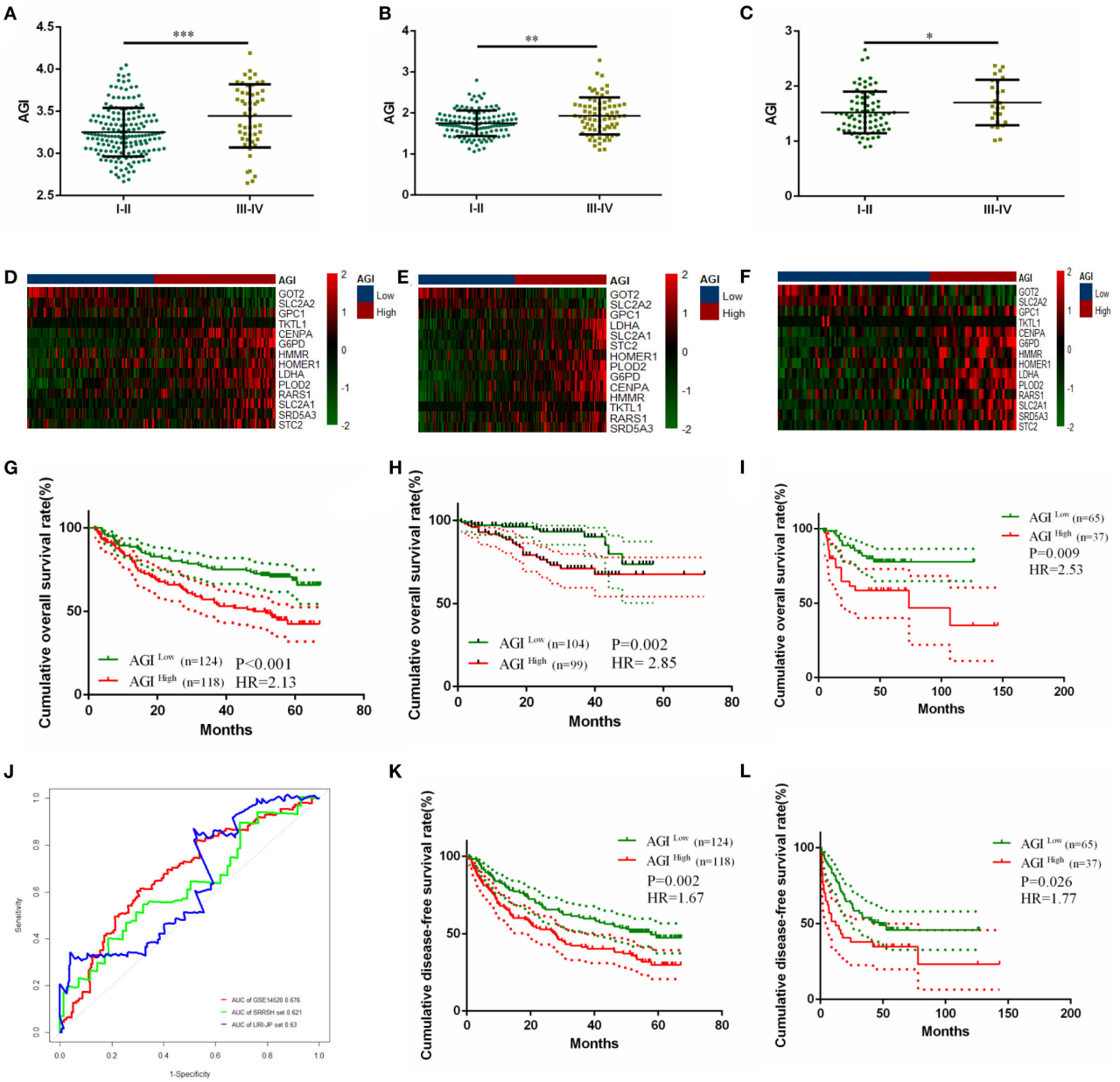

FIGURE 5 | Validating the prognostically predictive value of the aerobic glycolysis index (AGI) in validation datasets. **(A–C)** Value of the AGI in different tumor stages in GSE14520 **(A)**, LIRI-JP **(B)**, and SRRSH set **(C)**. **(D–F)** The heatmap and distribution of the 14 AGI-related gene expression profiles in GSE14520 **(D)**, LIRI-JP **(E)**, and SRRSH set **(F)**. **(G–I)** Kaplan–Meier plot analysis of overall survival (OS) in the high and low AGI subgroups in GSE14520 **(G)**, LIRI-JP **(H)**, and SRRSH set **(I)**. **(J)** Time-dependent ROC analysis comparing the predictive value of the AGI for 5-year OS in the three datasets. **(K,L)** Kaplan–Meier plot analysis of disease-free survival (DFS) in the high and low AGI subgroups in GSE14520 **(K)** and SRRSH set **(L)**. $^{*}P < 0.05$, $^{**}P < 0.01$, $^{***}P < 0.001$.

as models of Sorafenib-resistant (SR) cell lines (40, 41, 46, 47). The RNA-sequencing data revealed a high AGI in SR cell lines (SK-hep-1 and Huh7) (**Figure 7B**). Transcript data from GSE73571 also demonstrated an elevated AGI during the acquisition of Sorafenib resistance (**Figure 7C**). Thus, we proposed the following hypothesis. On the one hand, tumor cells adapted to Sorafenib therapy by shifting to aerobic glycolysis. On the other hand, cells predominantly using aerobic glycolysis were also selected by Sorafenib. Both of these processes resulted in cells with enhanced aerobic glycolysis activity. Because the AGI is applied as a marker of aerobic glycolysis signaling activity, we speculate that the inhibition of aerobic glycolysis may enhance the sensitivity of Sorafenib. A combination of Sorafenib and 2-deoxy-D-glucose (2-DG),

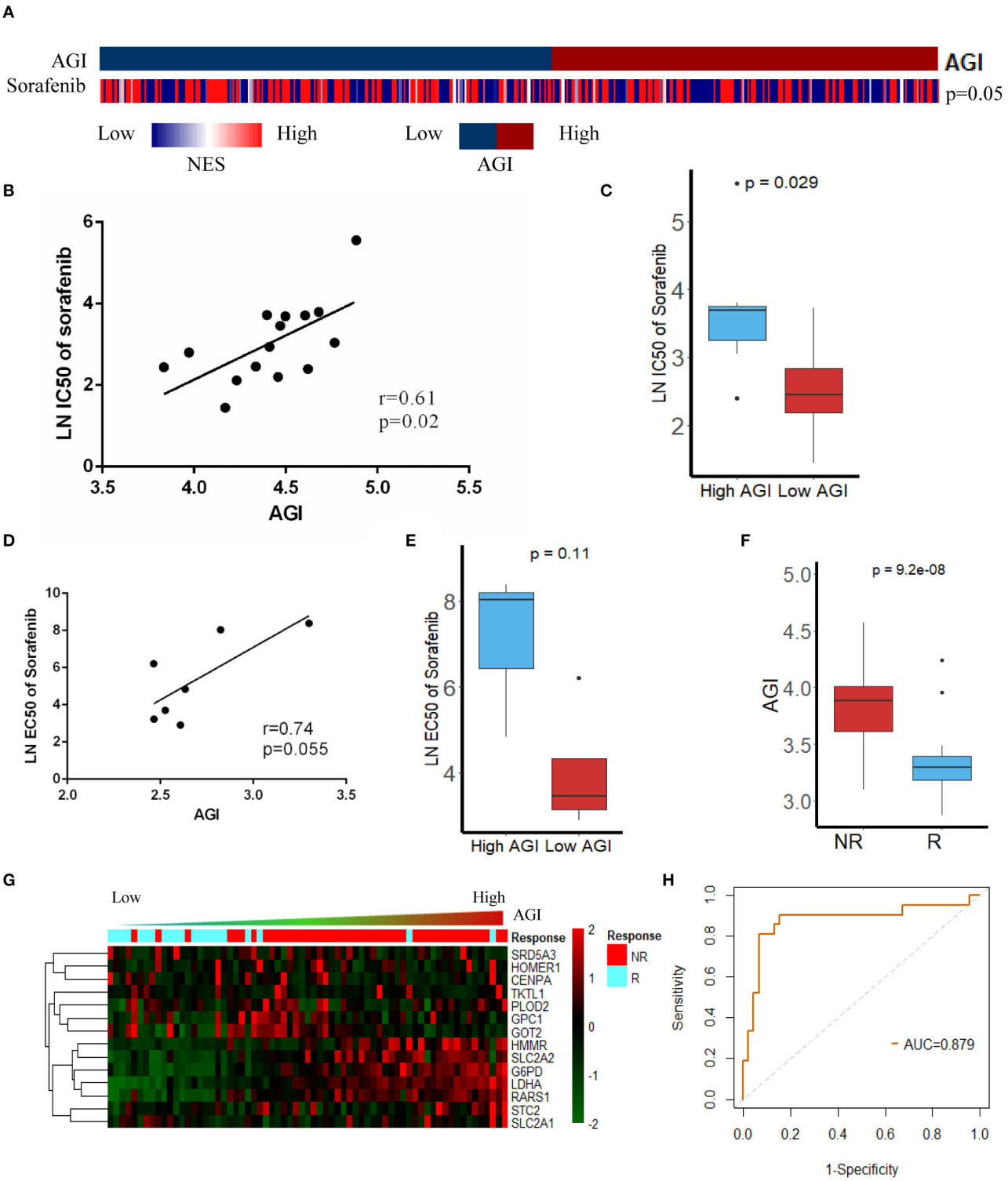

FIGURE 6 | Association between the aerobic glycolysis index (AGI) and Sorafenib resistance. **(A)** The Gene Set Variation Analysis (GSVA) results showed that the Sorafenib sensitivity signature was enriched in patients with a low AGI. **(B)** AGI positively was correlated with the IC_{50} of Sorafenib in hepatocellular carcinoma (HCC) cell line data from the Genomics of Drug Sensitivity in Cancer (GDSC) database. **(C)** The IC_{50} of Sorafenib in HCC cell line data from the GDSC database with high and low AGIs. **(D)** AGI positively correlated with the EC_{50} of Sorafenib in HCC cell line data from the Cancer Cell Line Encyclopedia (CCLE) database. **(E)** EC_{50} of Sorafenib in HCC cell line data from the CCLE database with high and low AGIs. **(F)** Patient sensitive to Sorafenib presented significantly low AGI. **(G)** The heatmap and distribution of the 14 AGI-related gene expression profiles in GSE109211. **(H)** Receiver operating characteristic (ROC) analysis showed an area under the curve (AUC) of 0.879 for the AGI in predicting the response to Sorafenib.

a commonly used inhibitor of aerobic glycolysis *in vitro*, was added to cell cultures, resulting in the inhibition of cell proliferation (**Figure 7D**) and an increased fraction of apoptotic cells (**Figure 7E**).

DISCUSSION

In the present study, we developed and validated an aerobic glycolysis-related gene signature (named the AGI) to predict the prognosis and Sorafenib sensitivity in patients with HCC. This AGI showed high accuracy in detecting HCC tumors and normal tissues. A low AGI score was significantly associated with early tumor stages, good differentiation, and better OS and DFS in a series of cohorts. Interestingly, the AGI score was correlated with the sensitivity of HCC cell lines to Sorafenib. More importantly, we demonstrated that the AGI could predict the response of patients to Sorafenib using data from clinical trials. Additionally, we observed that the AGI was elevated during the acquisition of Sorafenib resistance, which provides useful information for the development of a potential strategy to enhance Sorafenib sensitivity.

Aerobic glycolysis is a common biological process by which cancer cells tend to produce ATP by decomposing glucose or glycogen into lactic acid at a higher pace despite the presence of abundant oxygen. As an indicator of tumors, aerobic glycolysis activity is regulated by transcription factors, glucose transporters, and key enzymes of glucose metabolism. More importantly, aerobic glycolysis is related to multiple key cell signaling pathways, including PI3K/Akt, mTOR, and AMPK, and tightly associated with various cellular activities, including cell proliferation and EMT. In our study, the AGI was derived from a model consisting of genes encoding glucose transporters (SLC2A1, SLC2A2), key enzymes of glucose metabolism (G6PD, LDHA), and several other genes related to glycolysis (GPC1, HMMR, PLOD2, GOT2, STC2) (48–54), thereby supporting the use of the AGI as a marker of aerobic glycolysis activity. Several important genes related to glucose metabolism including HK2, PFK, and PKM2 are missed in the model of AGI, which had been reported to be associated with poor prognosis of HCC (55–57). The AGI was constructed using a bioinformatics method called LASSO regression. All the genes related to glycolysis were included as factors, and the LASSO regression selected factors to construct a model with minimal bias and acceptable reliability. Although HK2, PFK, and PKM2 were not in the model of AGI, we have calculated and found significant correlation between AGI and these genes. Elevated aerobic glycolysis activity was reported to result in a poor prognosis of multiple solid tumors including HCC (45, 58–60). Furthermore, several microRNAs, such as miR-383, miR-142-3p, and miR-100-5p, were reported to target LDHA, which subsequently inhibited cell proliferation, invasion, and glycolysis (61–63). Shang et al. reported that the transcription factor FOXM1 promoted glycolysis by transactivating SLC2A1 expression (64). In a respective cohort of 192 patients, the glucose transporter GLUT1 was significantly upregulated in HCC tumor tissues and was an independent risk factor of poor OS and relapse-free survival (24). Lu et al. reported that elevated G6PD expression contributed to the enhanced migration and invasion of HCC cells by inducing EMT (65), which was consistent with the correlation between the AGI and EMT signaling in the present study.

A positive correlation between aerobic glycolysis activity and Sorafenib resistance in both HCC cell lines and patients was observed in this study. Patients with a high pretreatment AGI tended to develop resistance to Sorafenib. Previously, Ma et al. and Li et al. found that increased aerobic glycolysis enhanced Sorafenib resistance in both HCC cell lines and xenografts (36, 66, 67). Key enzymes and transcription factors involved in aerobic glycolysis contributed to Sorafenib resistance, through reprogramming and redox adaptation (68), interacting with voltage-dependent anion channel (VDAC) and subsequently inhibiting mitochondrial apoptosis (69, 70) and increasing the expression of HIF-1α and c-Myc, thereby activating various cellular signals related to drug resistance (71, 72). In our previous review, we believed that Sorafenib resistance was associated with complex mechanisms, including metabolic remodeling, microenvironmental interplay, cellular signaling changes, genomic instability, and cancer stem cells (20). In our study, the levels of AGI-related genes substantially elevated following the treatment with Sorafenib, suggesting metabolic switch of glucose metabolism. Tesori et al. also reported metabolic shift toward glycolysis in HCC cells treated with Sorafenib in 48 h (31). Another study by Fiume et al. found that Sorafenib could hinder oxidative phosphorylation and stimulate aerobic glycolysis (32). Enhanced aerobic glycolysis activity was observed during the acquisition of Sorafenib resistance and reflected as an increased AGI. Thus, we speculate that the inhibition of aerobic glycolysis may enhance the sensitivity of Sorafenib. By inhibiting aerobic glycolysis activity, 2-DG resensitized HCC cells to Sorafenib therapy. Furthermore, several drugs targeting glycolysis-related factors such as Metformin, Aspirin, Genistein, Simvastatin, and Proanthocyanidin B2 have been shown to be effective in reversing Sorafenib resistance (33, 34, 36, 55, 70), indicating the aerobic glycolysis pathway as a promising target for exploring new therapies.

Notably, the present study highlighted that the AGI is a reliable biomarker in predicting the response to Sorafenib therapy. To date, several clinical and biological biomarkers have been proposed to evaluate responses to Sorafenib. The GIDEON trial revealed that patients with preserved liver function exhibited better OS after treatment with Sorafenib (73). Similarly, clinical characteristics such as Barcelona Clinic Liver Cancer (BCLC) stage, viral status, and Sorafenib-related adverse events were predictive of better survival (74, 75). As for biological biomarkers, Miyahara et al. reported that high levels of serum cytokines at baseline predicted poor outcomes in HCC patients treated with Sorafenib therapy (76). Arao et al. demonstrated that FGF3/FGF4 amplification was observed in 30% of HCC patients responding to Sorafenib (77). Recently, several exploratory studies investigated the roles of microRNAs in Sorafenib resistance and reported that several

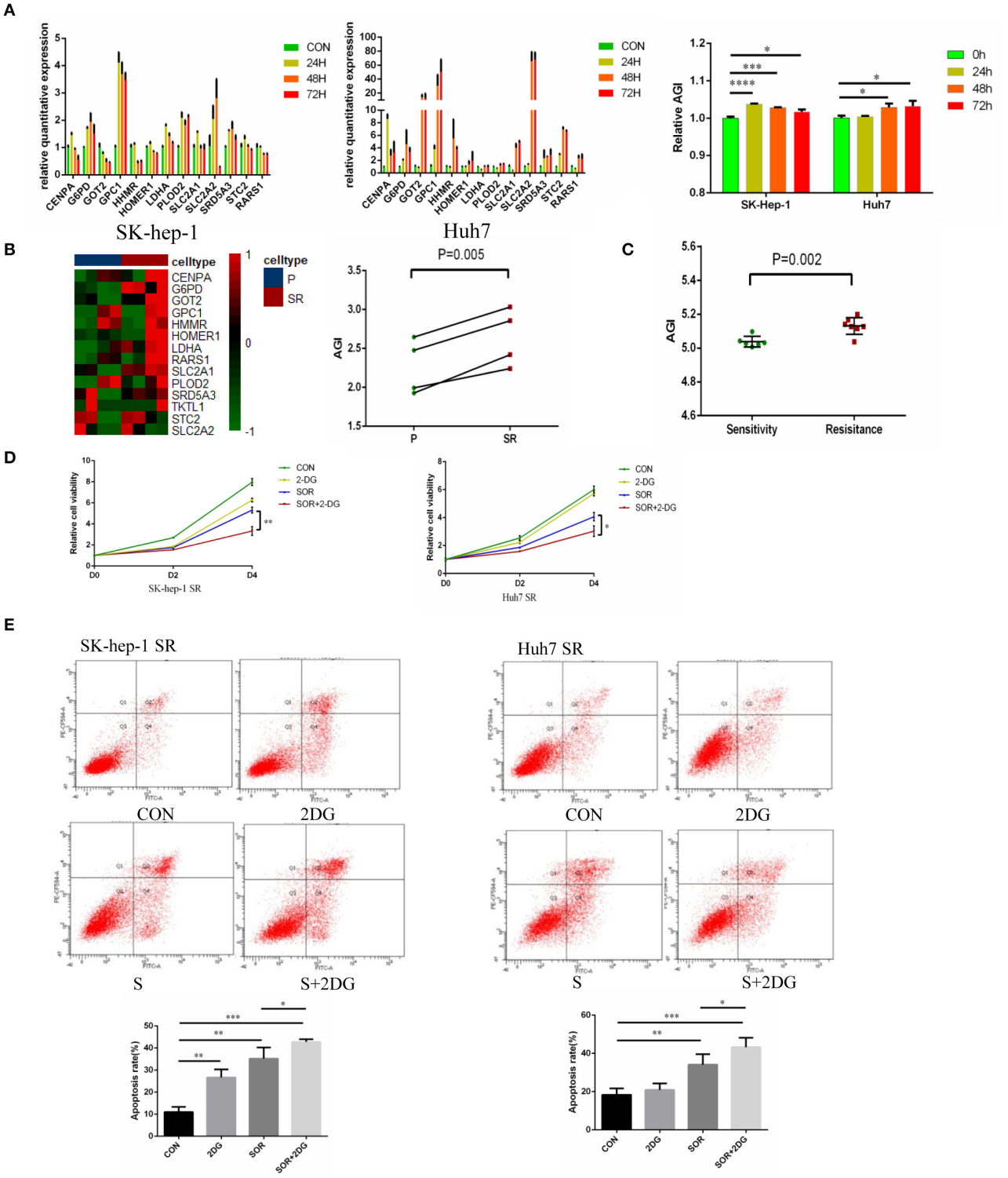

FIGURE 7 | Aerobic glycolysis index (AGI) is increased in Sorafenib-resistant hepatocellular carcinoma (HCC) cells. **(A)** Relative expression of AGI-related genes in HCC cell lines (left, SK-hep-1; right, Huh7) incubated with Sorafenib (5 μM) for 24, 36, and 72 h. **(B)** Distribution of the 14 AGI-related gene expression profiles in parental and Sorafenib-resistant HCC cell lines (SK-hep-1, Huh7). **(C)** AGI of Sorafenib-sensitive and Sorafenib-resistant xenografts from the GSE73571 dataset. **(D)** Combination of 2-DG and Sorafenib resulted in significantly decreased cell viability. **(E)** Combination of 2-DG and Sorafenib enhanced the apoptosis of Sorafenib-resistant cell lines (SK-hep-1 SR and Huh7 SR). $^{*}P < 0.05$, $^{**}P < 0.01$, $^{***}P < 0.001$.

upregulated/downregulated microRNAs, long non-coding RNAs (lncRNAs), and circular RNAs (circRNAs) were predictive biomarkers of survival outcomes following Sorafenib therapy (46, 47, 78–80). Different from previous studies, the present study directly evaluated the performance of the AGI in predicting Sorafenib responses using the ROC curve and observed an optimistic AUC of 0.88, which may be more accurate and suitable in clinical practice.

The present study has several limitations. First, although the available datasets with requisite gene transcript data and clinical and treatment outcome information were all included, the predictive effectiveness of the AGI was evaluated in only a few datasets. A more careful examination is required to further confirm the accuracy of the AGI using larger and multicenter clinical cohorts in the future. Second, the AGI was derived from a model of 14 gene transcripts including several genes with very low weight or minimal detectability. A simplified AGI with fewer key genes is required to improve the robustness and clinical utility of this model. Third, the AGI was demonstrated to be essential in Sorafenib resistance and associated with various tumor hallmarks. However, several genes used to construct the AGI have not yet been reported as prognostic factors of HCC and biomarker of Sorafenib, and their underlying mechanism remains unknown.

In conclusion, we developed a gene signature based on aerobic glycolysis-related genes by integrating several transcriptomic profiles, which showed great promise for predicting prognosis and the response of HCC to Sorafenib. The AGI described in our study can be developed as a predictive biomarker for Sorafenib therapy.

DATA AVAILABILITY STATEMENT

Publicly available datasets were analyzed in this study. This data can be found here: FPKM RNA-Seq data and clinical information of TCGA LIHC was downloaded from the UCSC Cancer Browser (https://xenabrowser.net/datapages). Gene mutation data and GISTIC 2.0 segmentation scores as well as threshold copy number calls for the TCGA LIHC samples were acquired from the cBioPortal (http://www.cbioportal.org). RNA-seq and clinical data of the LIRI-JP cohort was downloaded from the HCCDB (http://lifeome.net/database/hccdb/download.html). The GSE14520, GSE25097, GSE36376, GSE64041, GSE76427, GSE109211, and GSE73571 expression profile was obtained from the GEO database (https://www.ncbi.nlm.nih.gov/geo/). The proteomics data of TCGA LIHC was downloaded from the TCPA database (https://www.tcpaportal.org/tcpa/index.html). Drug sensitivity data of HCC cell lines was obtained from the Genomics of Drug Sensitivity in Cancer (GDSC) database (https://www.cancerrxgene.org) and Cancer Cell Line Encyclopedia (CCLE) database (https://portals.broadinstitute.org/ccle/data).

ETHICS STATEMENT

The studies involving human participants were reviewed and approved by Institutional Review Board of the Sir Run Run Shaw Hospital of Zhejiang University. The patients/participants provided their written informed consent to participate in this study.

AUTHOR CONTRIBUTIONS

YP and G-yH: conceptualization. YP and SJ: data curation. YP, G-yH, SJ, and S-jX: formal analysis. X-jC, J-jX, Y-hX, and L-xC: funding acquisition. Z-jL and Q-jM: investigation. YP, Q-jM, and J-jX: methodology. X-jC and J-jX: project administration. YP, G-yH, and S-jX: software. X-jC, J-jX, and Y-hX: supervision, writing review and editing. YP, JZ, L-xC, and Z-jL: validation. YP: visualization. YP and HM: writing original draft. All authors contributed to the article and approved the submitted version.

FUNDING

This work was supported by the National Natural Science Foundation of China under Grant No. 81827804 (to X-jC), No. 81772546 (to X-jC), and No. 81902367 (to X-jC); Key Research and Development Project of Zhejiang Province under Grand No. 2018C03083 (to X-jC); Zhejiang Provincial Natural Science Foundation of China under Grant No. LQ19H160026 (to J-jX), No. LQ18H160010 (to JZ), and No. Y15H160052 (to L-xC); China Post-doctoral Science Foundation under Grant No. 2020M671755 (to J-jX); Zhejiang Clinical Research Center of Minimally Invasive Diagnosis and Treatment of Abdominal Diseases Grant No. 2018E50003 (to J-jX); and Hepatobiliary and Pancreatic Cancer Research of Hubei Chen Xiaoping Science and Technology Development Foundation under Grant No. CXPJJH11900001-2019308 (to J-jX).

ACKNOWLEDGMENTS

We thank Melissa Crawford, PhD, from Liwen Bianji, Edanz Editing China (www.liwenbianji.cn/ac), for editing the English text of a draft of this manuscript.

SUPPLEMENTARY MATERIAL

The Supplementary Material for this article can be found online at: https://www.frontiersin.org/articles/10.3389/fonc.2021.637971/full#supplementary-material

REFERENCES

1. Bray F, Ferlay J, Soerjomataram I, Siegel RL, Torre LA, Jemal A. Global cancer statistics 2018: GLOBOCAN estimates of incidence and mortality worldwide for 36 cancers in 185 countries. *CA Cancer J Clin*. (2018) 68:394–424. doi: 10.3322/caac.21492
2. Roayaie S, Obeidat K, Sposito C, Mariani L, Bhoori S, Pellegrinelli A, et al. Resection of hepatocellular cancer ≤2 cm: results from

two Western centers. *Hepatology*. (2013) 57:1426–35. doi: 10.1002/hep.25832
3. Sapisochin G, Castells L, Dopazo C, Bilbao I, Minguez B, Lázaro JL, et al. Single HCC in cirrhotic patients: liver resection or liver transplantation? Long-term outcome according to an intention-to-treat basis. *Ann Surg Oncol*. (2013) 20:1194–202. doi: 10.1245/s10434-012-2655-1
4. Vitale A, Peck-Radosavljevic M, Giannini EG, Vibert E, Sieghart W, Van Poucke S, et al. Personalized treatment of patients with very early hepatocellular carcinoma. *J Hepatol*. (2017) 66:412–23. doi: 10.1016/j.jhep.2016.09.012
5. Villanueva A. Hepatocellular carcinoma. *N Engl J Med*. (2019) 380:1450–62. doi: 10.1056/NEJMra1713263
6. Méndez-Blanco C, Fondevila F, García-Palomo A, González-Gallego J, Mauriz JL. Sorafenib resistance in hepatocarcinoma: role of hypoxia-inducible factors. *Exp Mol Med*. (2018) 50:1–9. doi: 10.1038/s12276-018-0159-1
7. Llovet JM, Ricci S, Mazzaferro V, Hilgard P, Gane E, Blanc JF, et al. Sorafenib in advanced hepatocellular carcinoma. *N Engl J Med*. (2008) 359:378–90. doi: 10.1056/NEJMoa0708857
8. Cheng AL, Kang YK, Chen Z, Tsao CJ, Qin S, Kim JS, et al. Efficacy and safety of sorafenib in patients in the Asia-Pacific region with advanced hepatocellular carcinoma: a phase III randomised, double-blind, placebo-controlled trial. *Lancet Oncol*. (2009) 10:25–34. doi: 10.1016/S1470-2045(08)70285-7
9. Kudo M, Finn RS, Qin S, Han KH, Ikeda K, Piscaglia F, et al. Lenvatinib versus sorafenib in first-line treatment of patients with unresectable hepatocellular carcinoma: a randomised phase 3 non-inferiority trial. *Lancet*. (2018) 391:1163–73. doi: 10.1016/S0140-6736(18)30207-1
10. Faivre S, Raymond E, Boucher E, Douillard J, Lim HY, Kim JS, et al. Safety and efficacy of sunitinib in patients with advanced hepatocellular carcinoma: an open-label, multicentre, phase II study. *Lancet Oncol*. (2009) 10:794–800. doi: 10.1016/S1470-2045(09)70171-8
11. Cainap C, Qin S, Huang WT, Chung IJ, Pan H, Cheng Y, et al. Linifanib versus Sorafenib in patients with advanced hepatocellular carcinoma: results of a randomized phase III trial. *J Clin Oncol*. (2015) 33:172–9. doi: 10.1200/JCO.2013.54.3298
12. Xu J, Zheng L, Chen J, Sun Y, Lin H, Jin RA, et al. Increasing AR by HIF-2α inhibitor (PT-2385) overcomes the side-effects of sorafenib by suppressing hepatocellular carcinoma invasion via alteration of pSTAT3, pAKT and pERK signals. *Cell Death Dis*. (2017) 8:e3095. doi: 10.1038/cddis.2017.411
13. Xu J, Lin H, Li G, Sun Y, Shi L, Ma WL, et al. Sorafenib with ASC-J9(®) synergistically suppresses the HCC progression via altering the pSTAT3-CCL2/Bcl2 signals. *Int J Cancer*. (2017) 140:705–17. doi: 10.1002/ijc.30446
14. Xu J, Lin H, Li G, Sun Y, Chen J, Shi L, et al. The miR-367-3p increases sorafenib chemotherapy efficacy to suppress hepatocellular carcinoma metastasis through altering the androgen receptor signals. *EBioMedicine*. (2016) 12:55–67. doi: 10.1016/j.ebiom.2016.07.013
15. Zheng L, Xu M, Xu J, Wu K, Fang Q, Liang Y, et al. ELF3 promotes epithelial-mesenchymal transition by protecting ZEB1 from miR-141-3p-mediated silencing in hepatocellular carcinoma. *Cell Death Dis*. (2018) 9:387. doi: 10.1038/s41419-018-0399-y
16. Warburg O, Wind F, Negelein E. The metabolism of tumors in the body. *J Gen Physiol*. (1927) 8:519–30. doi: 10.1085/jgp.8.6.519
17. DeBerardinis RJ, Mancuso A, Daikhin E, Nissim I, Yudkoff M, Wehrli S, et al. Beyond aerobic glycolysis: transformed cells can engage in glutamine metabolism that exceeds the requirement for protein and nucleotide synthesis. *Proc Natl Acad Sci USA*. (2007) 104:19345–50. doi: 10.1073/pnas.0709747104
18. Gordan JD, Thompson CB, Simon MC. HIF and c-Myc: sibling rivals for control of cancer cell metabolism and proliferation. *Cancer Cell*. (2007) 12:108–13. doi: 10.1016/j.ccr.2007.07.006
19. Kroemer G, Pouyssegur J. Tumor cell metabolism: cancer's achilles' heel. *Cancer Cell*. (2008) 13:472–82. doi: 10.1016/j.ccr.2008.05.005
20. Xia S, Pan Y, Liang Y, Xu J, Cai X. The microenvironmental and metabolic aspects of sorafenib resistance in hepatocellular carcinoma. *EBioMedicine*. (2020) 51:102610. doi: 10.1016/j.ebiom.2019.102610
21. Feng J, Li J, Wu L, Yu Q, Ji J, Wu J, et al. Emerging roles and the regulation of aerobic glycolysis in hepatocellular carcinoma. *J Exp Clin Cancer Res*. (2020) 39:126. doi: 10.1186/s13046-020-01629-4
22. Alves AP, Mamede AC, Alves MG, Oliveira PF, Rocha SM, Botelho MF, et al. Glycolysis inhibition as a strategy for hepatocellular carcinoma treatment? *Curr Cancer Drug Targets*. (2019) 19:26–40. doi: 10.2174/1568009618666180430144441
23. Li X, Zhang Y, Ma W, Fu Q, Liu J, Yin G, et al. Enhanced glucose metabolism mediated by CD147 contributes to immunosuppression in hepatocellular carcinoma. *Cancer Immunol Immunother*. (2020) 69:535–48. doi: 10.1007/s00262-019-02457-y
24. Sun HW, Yu XJ, Wu WC, Chen J, Shi M, Zheng L, et al. GLUT1 and ASCT2 as predictors for prognosis of hepatocellular carcinoma. *PLoS ONE*. (2016) 11:e0168907. doi: 10.1371/journal.pone.0168907
25. Kim YH, Jeong DC, Pak K, Han ME, Kim JY, Liangwen L, et al. SLC2A2 (GLUT2) as a novel prognostic factor for hepatocellular carcinoma. *Oncotarget*. (2017) 8:68381–92. doi: 10.18632/oncotarget.20266
26. Yin X, Tang B, Li JH, Wang Y, Zhang L, Xie XY, et al. ID1 promotes hepatocellular carcinoma proliferation and confers chemoresistance to oxaliplatin by activating pentose phosphate pathway. *J Exp Clin Cancer Res*. (2017) 36:166. doi: 10.1186/s13046-017-0637-7
27. Guo Y, Li X, Sun X, Wang J, Yang X, Zhou X, et al. Combined aberrant expression of NDRG2 and LDHA predicts hepatocellular carcinoma prognosis and mediates the anti-tumor effect of gemcitabine. *Int J Biol Sci*. (2019) 15:1771–86. doi: 10.7150/ijbs.35094
28. Noda T, Yamamoto H, Takemasa I, Yamada D, Uemura M, Wada H, et al. PLOD2 induced under hypoxia is a novel prognostic factor for hepatocellular carcinoma after curative resection. *Liver Int*. (2012) 32:110–8. doi: 10.1111/j.1478-3231.2011.02619.x
29. Chen G, Wu H, Zhang L, Wei S. High glypican-1 expression is a prognostic factor for predicting a poor clinical prognosis in patients with hepatocellular carcinoma. *Oncol Lett*. (2020) 20:197. doi: 10.3892/ol.2020.12058
30. Huang Q, Li J, Xing J, Li W, Li H, Ke X, et al. CD147 promotes reprogramming of glucose metabolism and cell proliferation in HCC cells by inhibiting the p53-dependent signaling pathway. *J Hepatol*. (2014) 61:859–66. doi: 10.1016/j.jhep.2014.04.035
31. Tesori V, Piscaglia AC, Samengo D, Barba M, Bernardini C, Scatena R, et al. The multikinase inhibitor Sorafenib enhances glycolysis and synergizes with glycolysis blockade for cancer cell killing. *Sci Rep*. (2015) 5:9149. doi: 10.1038/srep09149
32. Fiume L, Manerba M, Vettraino M, Di Stefano G. Effect of sorafenib on the energy metabolism of hepatocellular carcinoma cells. *Eur J Pharmacol*. (2011) 670:39–43. doi: 10.1016/j.ejphar.2011.08.038
33. Feng J, Wu L, Ji J, Chen K, Yu Q, Zhang J, et al. PKM2 is the target of proanthocyanidin B2 during the inhibition of hepatocellular carcinoma. *J Exp Clin Cancer Res*. (2019) 38:204. doi: 10.1186/s13046-019-1194-z
34. Feng J, Dai W, Mao Y, Wu L, Li J, Chen K, et al. Simvastatin re-sensitizes hepatocellular carcinoma cells to sorafenib by inhibiting HIF-1α/PPAR-γ/PKM2-mediated glycolysis. *J Exp Clin Cancer Res*. (2020) 39:24. doi: 10.1186/s13046-020-1528-x
35. Yoo JJ, Yu SJ, Na J, Kim K, Cho YY, Lee YB, et al. Hexokinase-II inhibition synergistically augments the anti-tumor efficacy of sorafenib in hepatocellular carcinoma. *Int J Mol Sci*. (2019) 20:1292. doi: 10.3390/ijms20061292
36. Li S, Dai W, Mo W, Li J, Feng J, Wu L, et al. By inhibiting PFKFB3, aspirin overcomes sorafenib resistance in hepatocellular carcinoma. *Int. J Cancer*. (2017) 141:2571–84. doi: 10.1002/ijc.31022
37. Peng X, Chen Z, Farshidfar F, Xu X, Lorenzi PL, Wang Y, et al. Molecular characterization and clinical relevance of metabolic expression subtypes in human cancers. *Cell Rep*. (2018) 23:255–69.e4. doi: 10.1016/j.celrep.2018.03.077
38. Friedman J, Hastie T, Tibshirani R. Regularization paths for generalized linear models via coordinate descent. *J Stat Softw*. (2010) 33:1–22. doi: 10.18637/jss.v033.i01
39. Zheng S, Zou Y, Liang JY, Xiao W, Yang A, Meng T, et al. Identification and validation of a combined hypoxia and immune index for triple-negative breast cancer. *Molecular Oncol*. (2020) 14:2814–33. doi: 10.1002/1878-0261.12747
40. Ji L, Lin Z, Wan Z, Xia S, Jiang S, Cen D, et al. miR-486-3p mediates hepatocellular carcinoma sorafenib resistance by targeting FGFR4 and EGFR. *Cell Death Dis*. (2020) 11:250. doi: 10.1038/s41419-020-2413-4

41. Lin Z, Xia S, Liang Y, Ji L, Pan Y, Jiang S, et al. LXR activation potentiates sorafenib sensitivity in HCC by activating microRNA-378a transcription. *Theranostics*. (2020) 10:8834–50. doi: 10.7150/thno.45158
42. Ren R, Guo J, Shi J, Tian Y, Li M, Kang H. PKM2 regulates angiogenesis of VR-EPCs through modulating glycolysis, mitochondrial fission, and fusion. *J Cell Physiol*. (2020) 235:6204–17. doi: 10.1002/jcp.29549
43. Yetkin-Arik B, Vogels IMC, Nowak-Sliwinska P, Weiss A, Houtkooper RH, Van Noorden CJF, et al. The role of glycolysis and mitochondrial respiration in the formation and functioning of endothelial tip cells during angiogenesis. *Sci Rep*. (2019) 9:12608. doi: 10.1038/s41598-019-48676-2
44. Zhang W, Zhang X, Huang S, Chen J, Ding P, Wang Q, et al. FOXM1D potentiates PKM2-mediated tumor glycolysis and angiogenesis. *Mol Oncol*. (2020). doi: 10.21203/rs.3.rs-40077/v1. [Epub ahead of print].
45. Wang ZH, Zhang YZ, Wang YS, Ma XX. Identification of novel cell glycolysis related gene signature predicting survival in patients with endometrial cancer. *Cancer Cell Int*. (2019) 19:296. doi: 10.1186/s12935-019-1001-0
46. Xu J, Wan Z, Tang M, Lin Z, Jiang S, Ji L, et al. N(6)-methyladenosine-modified CircRNA-SORE sustains sorafenib resistance in hepatocellular carcinoma by regulating β-catenin signaling. *Mol Cancer*. (2020) 19:163. doi: 10.1186/s12943-020-01281-8
47. Xu J, Ji L, Liang Y, Wan Z, Zheng W, Song X, et al. CircRNA-SORE mediates sorafenib resistance in hepatocellular carcinoma by stabilizing YBX1. *Signal Transduct Targeted Ther*. (2020) 5:298. doi: 10.1038/s41392-020-00375-5
48. Yao G, Yin J, Wang Q, Dong R, Lu J. Glypican-3 enhances reprogramming of glucose metabolism in liver cancer cells. *Biomed Res Int*. (2019) 2019:2560650. doi: 10.1155/2019/2560650
49. Zhou H, Wang L, Huang J, Jiang M, Zhang X, Zhang L, et al. High EGFR_1 inside-out activated inflammation-induced motility through SLC2A1-CCNB2-HMMR-KIF11-NUSAP1-PRC1-UBE2C. *J Cancer*. (2015) 6:519–24. doi: 10.7150/jca.11404
50. Du W, Liu N, Zhang Y, Liu X, Yang Y, Chen W, et al. PLOD2 promotes aerobic glycolysis and cell progression in colorectal cancer by upregulating HK2. *Biochem Cell Biol*. (2020) 98:386–95. doi: 10.1139/bcb-2019-0256
51. Yang H, Zhou L, Shi Q, Zhao Y, Lin H, Zhang M, et al. SIRT3-dependent GOT2 acetylation status affects the malate-aspartate NADH shuttle activity and pancreatic tumor growth. *EMBO J*. (2015) 34:1110–25. doi: 10.15252/embj.201591041
52. Wang T, Yao W, Li J, He Q, Shao Y, Huang F. Acetyl-CoA from inflammation-induced fatty acids oxidation promotes hepatic malate-aspartate shuttle activity and glycolysis. *Am J Physiol Endocrinol Metab*. (2018) 315:E496–510. doi: 10.1152/ajpendo.00061.2018
53. Sarapio E, De Souza SK, Model JFA, Trapp M, Da Silva RSM. Stanniocalcin-1 and−2 effects on glucose and lipid metabolism in white adipose tissue from fed and fasted rats. *Can J Physiol Pharmacol*. (2019) 97:916–23. doi: 10.1139/cjpp-2019-0023
54. López JJ, Jardín I, Cantonero Chamorro C, Duran ML, Tarancón Rubio MJ, Reyes Panadero M, et al. Involvement of stanniocalcins in the deregulation of glycaemia in obese mice and type 2 diabetic patients. *J Cell Mol Med*. (2018) 22:684–94. doi: 10.1111/jcmm.13355
55. DeWaal D, Nogueira V, Terry AR, Patra KC, Jeon SM, Guzman G, et al. Hexokinase-2 depletion inhibits glycolysis and induces oxidative phosphorylation in hepatocellular carcinoma and sensitizes to metformin. *Nat Commun*. (2018) 9:446. doi: 10.1038/s41467-018-04182-z
56. Martin SP, Fako V, Dang H, Dominguez DA, Khatib S, Ma L, et al. PKM2 inhibition may reverse therapeutic resistance to transarterial chemoembolization in hepatocellular carcinoma. *J Exp Clin Cancer Res*. (2020) 39:99. doi: 10.1186/s13046-020-01605-y
57. Feng Y, Zhang Y, Cai Y, Liu R, Lu M, Li T, et al. A20 targets PFKL and glycolysis to inhibit the progression of hepatocellular carcinoma. *Cell Death Dis*. (2020) 11:89. doi: 10.1038/s41419-020-2278-6
58. Zhang L, Zhang Z, Yu Z. Identification of a novel glycolysis-related gene signature for predicting metastasis and survival in patients with lung adenocarcinoma. *J Transl Med*. (2019) 17:423. doi: 10.1186/s12967-019-02173-2
59. Zhou Z, Huang R, Chai R, Zhou X, Hu Z, Wang W, et al. Identification of an energy metabolism-related signature associated with clinical prognosis in diffuse glioma. *Aging*. (2018) 10:3185–209. doi: 10.18632/aging.101625
60. Liu J, Li S, Feng G, Meng H, Nie S, Sun R, et al. Nine glycolysis-related gene signature predicting the survival of patients with endometrial adenocarcinoma. *Cancer Cell Int*. (2020) 20:183. doi: 10.1186/s12935-020-01264-1
61. Fang Z, He L, Jia H, Huang Q, Chen D, Zhang Z. The miR-383-LDHA axis regulates cell proliferation, invasion and glycolysis in hepatocellular cancer. *Iran J Basic Med Sci*. (2017) 20:187–92. doi: 10.22038/ijbms.2017.8246
62. Hua S, Liu C, Liu L, Wu D. miR-142-3p inhibits aerobic glycolysis and cell proliferation in hepatocellular carcinoma via targeting LDHA. *Biochem Biophys Res Commun*. (2018) 496:947–54. doi: 10.1016/j.bbrc.2018.01.112
63. Zhou Y, Huang Y, Hu K, Zhang Z, Yang J, Wang Z. HIF1A activates the transcription of lncRNA RAET1K to modulate hypoxia-induced glycolysis in hepatocellular carcinoma cells via miR-100-5p. *Cell Death Dis*. (2020) 11:176. doi: 10.1038/s41419-020-2366-7
64. Shang R, Pu M, Li Y, Wang D. FOXM1 regulates glycolysis in hepatocellular carcinoma by transactivating glucose transporter 1 expression. *Oncol Rep*. (2017) 37:2261–9. doi: 10.3892/or.2017.5472
65. Lu M, Lu L, Dong Q, Yu G, Chen J, Qin L, et al. Elevated G6PD expression contributes to migration and invasion of hepatocellular carcinoma cells by inducing epithelial-mesenchymal transition. *Acta Biochim Biophys Sin*. (2018) 50:370–80. doi: 10.1093/abbs/gmy009
66. Ma L, Liu W, Xu A, Ji Q, Ma Y, Tai Y, et al. Activator of thyroid and retinoid receptor increases sorafenib resistance in hepatocellular carcinoma by facilitating the Warburg effect. *Cancer Sci*. (2020) 111:2028–40. doi: 10.1111/cas.14412
67. Shen YC, Ou DL, Hsu C, Lin KL, Chang CY, Lin CY, et al. Activating oxidative phosphorylation by a pyruvate dehydrogenase kinase inhibitor overcomes sorafenib resistance of hepatocellular carcinoma. *Br J Cancer*. (2013) 108:72–81. doi: 10.1038/bjc.2012.559
68. You X, Jiang W, Lu W, Zhang H, Yu T, Tian J, et al. Metabolic reprogramming and redox adaptation in sorafenib-resistant leukemia cells: detected by untargeted metabolomics and stable isotope tracing analysis. *Cancer Commun*. (2019) 39:17. doi: 10.1186/s40880-019-0362-z
69. Pastorino JG, Shulga N, Hoek JB. Mitochondrial binding of hexokinase II inhibits Bax-induced cytochrome c release and apoptosis. *J Biol Chem*. (2002) 277:7610–8. doi: 10.1074/jbc.M109950200
70. Li S, Li J, Dai W, Zhang Q, Feng J, Wu L, et al. Genistein suppresses aerobic glycolysis and induces hepatocellular carcinoma cell death. *Br J Cancer*. (2017) 117:1518–28. doi: 10.1038/bjc.2017.323
71. Comerford KM, Wallace TJ, Karhausen J, Louis NA, Montalto MC, Colgan SP. Hypoxia-inducible factor-1-dependent regulation of the multidrug resistance (MDR1) gene. *Cancer Res*. (2002) 62:3387–94.
72. Liu R, Li Y, Tian L, Shi H, Wang J, Liang Y, et al. Gankyrin drives metabolic reprogramming to promote tumorigenesis, metastasis and drug resistance through activating β-catenin/c-Myc signaling in human hepatocellular carcinoma. *Cancer Lett*. (2019) 443:34–46. doi: 10.1016/j.canlet.2018.11.030
73. Marrero JA, Kudo M, Venook AP, Ye SL, Bronowicki JP, Chen XP, et al. Observational registry of sorafenib use in clinical practice across child-pugh subgroups: the GIDEON study. *J Hepatol*. (2016) 65:1140–7. doi: 10.1016/j.jhep.2016.07.020
74. Bruix J, Cheng AL, Meinhardt G, Nakajima K, De Sanctis Y, Llovet J. Prognostic factors and predictors of sorafenib benefit in patients with hepatocellular carcinoma: analysis of two phase III studies. *J Hepatol*. (2017) 67:999–1008. doi: 10.1016/j.jhep.2017.06.026
75. Casadei Gardini A, Marisi G, Scarpi E, Scartozzi M, Faloppi L, Silvestris N, et al. Effects of metformin on clinical outcome in diabetic patients with advanced HCC receiving sorafenib. *Expert Opin Pharmacother*. (2015) 16:2719–25. doi: 10.1517/14656566.2015.1102887
76. Miyahara K, Nouso K, Tomoda T, Kobayashi S, Hagihara H, Kuwaki K, et al. Predicting the treatment effect of sorafenib using serum angiogenesis markers in patients with hepatocellular carcinoma. *J Gastroenterol Hepatol*. (2011) 26:1604–11. doi: 10.1111/j.1440-1746.2011.06887.x
77. Arao T, Ueshima K, Matsumoto K, Nagai T, Kimura H, Hagiwara S, et al. FGF3/FGF4 amplification and multiple lung metastases in responders to sorafenib in hepatocellular carcinoma. *Hepatology*. (2013) 57:1407–15. doi: 10.1002/hep.25956

78. Vaira V, Roncalli M, Carnaghi C, Faversani A, Maggioni M, Augello C, et al. MicroRNA-425-3p predicts response to sorafenib therapy in patients with hepatocellular carcinoma. *Liver Int*. (2015) 35:1077–86. doi: 10.1111/liv.12636
79. Gyöngyösi B, Végh É, Járay B, Székely E, Fassan M, Bodoky G, et al. Pretreatment MicroRNA level and outcome in sorafenib-treated hepatocellular carcinoma. *J Histochem Cytochem*. (2014) 62:547–55. doi: 10.1369/0022155414537277
80. Yoon EL, Yeon JE, Ko E, Lee HJ, Je JH, Yoo YJ, et al. An explorative analysis for the role of serum miR-10b-3p levels in predicting response to sorafenib in patients with advanced hepatocellular carcinoma. *J Korean Med Sci*. (2017) 32:212–20. doi: 10.3346/jkms.2017.32.2.212

Conflict of Interest: The authors declare that the research was conducted in the absence of any commercial or financial relationships that could be construed as a potential conflict of interest.

frontiers in Oncology

ORIGINAL RESEARCH
published: 21 May 2021
doi: 10.3389/fonc.2021.645979

HOXA13, Negatively Regulated by miR-139-5p, Decreases the Sensitivity of Gastric Cancer to 5-Fluorouracil Possibly by Targeting ABCC4

Zhengqian Chen[1,2†], *Zhiwei Qin*[2†], *Lei Li*[2], *Qi Wo*[2] *and Xia Chen*[1*]

[1] Department of Breast Surgical Oncology, Fujian Medical University Cancer Hospital & Fujian Cancer Hospital, Fuzhou, China, [2] Department of General Surgery, Shanghai General Hospital, Shanghai Jiao Tong University School of Medicine, Shanghai, China

OPEN ACCESS

Edited by:
Prathibha Ranganathan, Centre for Human Genetics (CHG), India

Reviewed by:
Anil Mukund Limaye, Indian Institute of Technology Guwahati, India
Haruhiko Sugimura, Hamamatsu University School of Medicine, Japan

***Correspondence:**
Xia Chen
chenxia61@sina.com

[†]*These authors have contributed equally to this work*

Specialty section:
This article was submitted to Gastrointestinal Cancers, a section of the journal Frontiers in Oncology

Received: *24 December 2020*
Accepted: *19 April 2021*
Published: *21 May 2021*

Citation:
Chen Z, Qin Z, Li L, Wo Q and Chen X (2021) HOXA13, Negatively Regulated by miR-139-5p, Decreases the Sensitivity of Gastric Cancer to 5-Fluorouracil Possibly by Targeting ABCC4. Front. Oncol. 11:645979. doi: 10.3389/fonc.2021.645979

Purpose: Chemoresistance remains a major challenge in the therapy of gastric cancer (GC). The homeobox (HOX) gene family has gained attention in carcinogenesis and chemoresistance. Here, this study aimed to explore the mechanism of HOXA13 in GC chemoresistance.

Methods: Quantitative real-time PCR (qRT-PCR) and Western blot were used to evaluate the expression of HOXA13 in GC tissues. The Kaplan–Meier plotter database was mined for prognosis analysis of GC patients with different HOXA13 expression receiving 5-Fluorouracil (5-FU) therapy. The effects of HOXA13 on sensitivity of GC cells to 5-FU were investigated by Cell Counting Kit-8 (CCK-8), 5-Ethynyl-2'-deoxyuridine (EdU) incorporation, flow cytometry and experiment *in vivo*. RNA-Sequencing analysis was performed to explore the underlying mechanism of HOXA13-mediated 5-FU resistance in GC. Chromatin immunoprecipitation (ChIP) and rescue experiments were applied to determine the relationship between HOXA13 and ABCC4. Luciferase reporter assay was performed to assess interaction of miR-139-5p and HOXA13.

Results: HOXA13 was upregulated in GC and its high expression was associated with poor prognosis of GC patients with 5-FU treatment. Overexpression of HOXA13 impaired the inhibitory effects of 5-FU on GC cells proliferation *in vitro* and *vivo*, and knockdown of HOXA13 exacerbated 5-FU-induced GC cells apoptosis. Mechanistically, HOXA13, directly targeted by miR-139-5p in GC, might upregulate ABCC4 expression, thereby accentuating 5-FU resistance of GC cells.

Conclusion: Our study suggests that HOXA13 attenuates 5-FU sensitivity of GC possibly by upregulating ABCC4. Thus, targeting HOXA13 would provide a novel prospective into the potential therapeutic strategy for reversing chemoresistance.

Keywords: chemoresistance, gastric cancer, HOXA13, ABCC4, miR-139-5p

INTRODUCTION

Gastric cancer (GC) is one of the most common malignancies and faces high risk of fatality worldwide, especially in East Asia (1). Chemotherapy has been identified as one of the typical treatments for GC for decades. 5-Fluorouracil (5-FU), which is the most commonly administrated anti-cancer agent in GC, has noteworthily improved survival in patients with advanced GC (2, 3). However, the emergence of drug resistance turns out to be a major challenge to treatment efficacy, particularly in patients with recurrence and metastasis (4). Thus, probing into the underlying mechanisms and potential targets of chemoresistance of GC is crucial and could further facilitate ameliorating the prognosis of GC patients.

Homeobox (HOX) genes constitute a set of transcription factors that are essential for embryonic development and their dysregulation is involved in the tumorigenesis and chemosensitivity of multiple cancers (5–9). Recently, the role of HOXA13, a member of HOX family, in carcinogenesis and chemotherapy resistance has attracted increasing attention. For instance, the high HOXA13 expression in hepatocellular carcinoma (HCC) is associated with patients' clinical progression and predicts disease outcome (10). Downregulation of HOXA13 inhibits cell proliferation and chemoresistance in small cell lung cancer (11). Upregulation of HOXA13 promotes resistance to gemcitabine of pancreatic ductal adenocarcinoma (PDAC) cells (12). While the significant role HOXA13 plays in various cancers, the specific mechanism of HOXA13 in GC chemoresistance remains to be further explored.

ATP-binding cassette (ABC) transporters, a group of membrane protein complexes, are divided into seven subfamilies, ABCA through ABCG (13). ABCC-subfamily (the multidrug resistance-associated proteins, MRPs), the main branch of ABC transporters, has been proven to actively pump drugs out of tumor cells, thereby avoiding the cytotoxicity of chemotherapeutics (14). Recently, many studies have illustrated the relationship between ATP-binding cassette subfamily C member 4 (ABCC4) and tumor chemoresistance. Gazzaniga et al. demonstrated that ABCC4 enhances resistance to multiple chemotherapeutic drugs in metastatic breast cancer (15). In addition, inhibiting the expression of ABCC4 sensitizes neuroblastoma to irinotecan (16).

Our previous study indicated that HOXA13 was upregulated in GC tissues and promoted proliferation and metastasis in GC cells (17). In this study, we found that high expression of HOXA13 was in association with poorer 5-FU treatment response in GC. It showed that HOXA13 overexpression increased 5-FU resistance in GC cells, while HOXA13 knockdown led to the opposite results. HOXA13 impaired the anti-proliferative effect of 5-FU and suppressed 5-FU-induced apoptosis. Mechanistically, we demonstrated that HOXA13 upregulated ABCC4 expression *via* binding to its promoter region, which was further testified to reverse HOXA13-induced 5-FU resistance in GC cells. Inquiring the probable regulation mechanism of HOXA13, bioinformatics analysis and experimental verification revealed that HOXA13 was directly targeted by miR-139-5p. Together, these results indicated that HOXA13 played an indispensable part in 5-FU chemoresistance in GC, during which process ABC transporters activation, especially ABCC4 upregulation, might serve as one of the essential downstream signal transduction mechanisms.

MATERIAL AND METHODS

Patients and Tissue Samples

Forty-two pairs of GC tissues and matched normal tissues were collected from patients undergoing GC resection at Shanghai General Hospital (Shanghai, China). The samples were obtained from the patients with informed consent. The study was approved by the Ethics Committee of Shanghai General Hospital.

Cell Lines and Cell Culture

The human gastric cancer cell lines (AGS, MKN28, MKN45, SGC7901) and normal human gastric epithelial cells-1 (GES-1) were preserved by the General Surgery Institute, Shanghai General Hospital. Cells were cultured in RPMI-1640 medium containing 10% fetal bovine serum (Gibco, California, USA) and 1% penicillin–streptomycin. Cells were maintained at 37°C in a humidified atmosphere with 5% CO_2.

Lentiviral Transduction and Transient Transfection

The HOXA13 lentiviral vector and HOXA13 shRNA lentiviral vector were supplied by Genomeditech (Shanghai, China). Lentivirus were transfected into GC cells and then stable transfected cells were selected with puromycin. Also, stable cell lines with luciferase were selected by blasticidin according to manufacturer's instructions. The cell lines were divided into the following categories: Vector, infected with the lentiviral vector containing the control fragment; HOXA13, infected with the lentiviral vector containing the HOXA13 fragment; shNC, infected with the control shRNA lentivirus; shHOXA13, infected with Lenti-shRNA. In rescue experiments, cells were transiently transfected with siRNA targeting ABCC4 (Genomeditech) or ABCC4-overexpressing plasmid (NovaBio, Shanghai, China) using Lipo3000 (Invitrogen, California, USA).

Quantitative Real-Time PCR (qRT-PCR)

Total RNA was extracted from tissues and cells using TRIzol (Takara, Shiga, Japan) according to the manufacturer's instructions. RNA was reverse transcribed to cDNA using the Hifair™ First Strand cDNA Synthesis SuperMix (Yeasen, Shanghai, China). Quantitative real-time PCR was performed using the Hifair™ qPCR SYBR Green Master Mix (Yeasen) in three technical replicates. The expression values of indicated genes were normalized to GAPDH and calculated using the $2^{-\Delta\Delta Ct}$ method. The primers were listed below: GAPDH F: 5'-GGGAAGGTGAAGGTCGGAGT-3', R: 5'-GGGGTCATTGATGGCAACA-3'; HOXA13 F: 5'-GAACGGCCAAATGTACTGCC-3', R: 5'-GTATAAGGCACGCGCTTCTTTC-3'; ABCC4 F: 5'-GCAAAATCATCGTGTTTGTGAC-3', R: 5'-AAAAGGTCTGGATTCTTCGGAT-3'.

Western Blot Analysis

Total proteins from tissues and cells were extracted using RIPA lysis buffer with 1% protease and phosphatase inhibitor cocktail (NCM, Jiangsu, China). Cell lysates were separated by SDS-PAGE and transferred onto PVDF membranes. After blocking with protein free rapid blocking buffer (EpiZyme, Shanghai, China), the membranes were incubated with primary antibodies at 4°C overnight. The next day, the membranes were washed and incubated with HRP-conjugated goat anti-rabbit or anti-mouse secondary antibody (Cell Signaling Technology, MA, USA). Then protein bands were visualized using ECL chemiluminescent reagent (Millipore, MA, USA). The antibodies used in this study included anti-HOXA13 (1:1,000; Abcam, Cambridge, UK), anti-ABCC4 (1:1,000; Santa Cruz, CA, USA), anti-tubulin (1:1,000; Cell Signaling Technology), anti-cleaved caspase-3 (1:1,000; Cell Signaling Technology), anti-cleaved caspase-9 (1:1,000; Cell Signaling Technology), anti-MDM2 (1:1,000; Cell Signaling Technology), and anti-p53 (1:1,000; Abcam, Cambridge, UK).

The Kaplan–Meier Plotter

Survival analyses based on HOXA13 and ABCC4 expression level in GC were analyzed from the Kaplan–Meier plotter (http://kmplot.com/analysis/) (18). The GC cases with their acceptance of 5-FU were divided into two cohorts according to the auto select best cutoff. Overall survival (OS) and post progression survival (PPS) of GC patients in different groups were assessed by the Kaplan–Meier plot with hazard ratio (HR) and log-rank P value.

Drug Sensitivity Assay

To evaluate the toxicity of 5-FU in cells, GC cells were seeded into each well of 96-well plates and cultured at 37°C for 24 h. Cells were treated with graded concentrations of 5-FU for 48 h. Then 10 μl of Cell Counting Kit-8 (CCK-8) solution (Dojindo, Kumamoto, Japan) was added to each well. The absorbance at 450 nm was measured using a Gen5 microplate reader (BioTek, Vermont, USA). The experiment was tested in three technical replicates.

5-Ethynyl-2'-Deoxyuridine (EdU) Staining and Colony Formation Assays

The effect of HOXA13 on cell proliferation upon 5-FU treatment was determined by EdU incorporation assay (RiboBio, Guangdong, China). In brief, cells (1×10^4) were seeded into each well of 96-well plates. After 24 h, cells were cultured in medium supplemented with or without 5-FU for 48 h. Then, medium containing EdU was added for 2 h. The cells were fixed with methanol and stained according to manufacturer's instructions. Cell proliferation was observed using a fluorescence microscope (DMI6000B, Leica, Germany).

For colony formation assay, cells (1×10^3) were plated in each well of 6-well plates and incubated in medium supplemented with or without 5-FU. After two weeks, colonies were fixed with methanol and dyed with 0.1% crystal violet. Then the colonies were counted.

Each experiment was performed in three technical replicates.

Apoptosis Assay

Cell apoptosis was performed by using the Annexin V-PE/7-AAD apoptosis kit (MultiSciences, Zhejiang, China). After treatment with or without 5-FU for 48 h, cells were harvested in PBS, and then approximately 5×10^5 cells were resuspended in 500 μl 1× binding buffer and mixed with 5 μl Annexin V-PE and 10 μl 7-AAD for 5 min. The stained cells were analyzed by flow cytometry (Accuri C6, BD Biosciences, USA). The experiment was performed in three technical replicates.

RNA Sequencing Analysis

AGS-HOXA13 and AGS-Vector cells were treated with 5-FU for the indicated time and total RNA was extracted using TRIzol reagent. The integrity of the purified RNA was analyzed by the 2200 Electrophoresis Bioanalyzer System (Agilent, CA, USA). RNA with RIN (RNA integrity number) >6.0 was considered acceptable for cDNA library construction. Genes were considered significantly differentially expressed under the following criteria using DESeq2: Fold change >1.5, $P < 0.05$. The analysis was performed in three biological replicates.

Chromatin Immunoprecipitation (ChIP) Assay

ChIP assay was performed as described previously (19). Briefly, AGS cells transfected Flag-HOXA13 was fixed with 1% formaldehyde to crosslink DNA and proteins. Chromatin was sonicated to shear DNA to 200–1,000 bp size and incubated with IgG (Sangon, Shanghai, China) or anti-Flag (Cell Signaling Technology). After reversing the protein-DNA cross linking, purified DNA was used to detect the possible binding sites of HOXA13 in promoter region of ABCC4 by agarose gel electrophoresis. The primers were listed below: Primer 1 F: 5'-ACAGAGCCTCACTATGCTGGC-3', R: 5'-CCTTAACA AGGTCAGCAGCTGC-3'; Primer 2 F: 5'-CCAGCCTGGGCA ACAAAGTG-3', R: 5'-CCACCACACCCGGCTCATAT-3'; Primer 3 F: 5'-AGCCTGGAACTCCTGGGCTAA-3', R: 5'-TTGATAATTTCCCATGTATATTT-3'; Primer 4 F: 5'-AAAG AAAACCAAATTCTCAAA-3', R: 5'-AATCCTCCCAACT CAGTTTAAG-3'.

In Vivo Xenograft Model

GC cells (5×10^6) were subcutaneously injected into the back of BALB/c male mice. When the volume of xenografts reached approximately 100 mm^3, mice were randomly divided into two treatment groups (n = 3): the 5-FU-treated group (shNC + 5-FU and shHOXA13 + 5-FU) and the untreated control group (shNC + CON and shHOXA13 + CON). 5-FU (20 mg/kg) was intraperitoneally injected three times a week for 2 weeks in the treated group and the untreated control group receiving PBS according to the same schedule. Then all mice were euthanized. Tumor volume was calculated by the following formula: V = length × $width^2 \times 0.5$. All animal studies were approved by Animal Care and Use Committee of Shanghai General Hospital.

Immunohistochemical Staining (IHC)

IHC assay was conducted as described previously (17). Briefly, the tumor sections were deparaffinized and rehydrated before

boiling in sodium citrate solution (0.01 M, pH 6.0) for antigen retrieval. After blocking endogenous peroxidase activity using 3% hydrogen peroxide, the slices were incubated with anti-HOXA13 (1:100; Abcam), anti-ABCC4 (1:100; Abcam), and anti-cleaved caspase-3 (1:100; Affinity, OH, USA) overnight 4°C. After incubation with the suitable secondary antibody, slides were counterstained with hematoxylin.

Luciferase Reporter Assay

The binding and mutant sequences of HOXA13 3'-UTR were respectively inserted into pGL3 luciferase vector (Genomeditech). Then, the plasmids were co-transfected with miR-139-5p mimics or mimics NC into HEK-293T cells. After a 48-h incubation, the relative luciferase activities were examined using Dual luciferase Assay System (Promega, WI, USA).

Statistical Analysis

Statistical analyses were conducted using SPSS 22.0 or GraphPad Prism software. The data were presented as the mean ± SD. Comparisons between two groups were performed by Student's t-test. The correlation of the mRNA expression levels was analyzed using Pearson's test. $P < 0.05$ was considered statistically significant.

RESULTS

High Expression of HOXA13 Is Associated With Poor 5-FU Treatment Response in GC

Our previous study revealed that HOXA13 was elevated in GC samples. To confirm the results, qRT-PCR was conducted and showed that the expression of HOXA13 was upregulated in 85.71% (36/42) GC tissues (**Figure 1A**). Correspondently, the protein levels of HOXA13 were increased in GC tissues compared with matched normal tissues (**Figure 1B**). To clarify the clinical significance of HOXA13 in human GC, we analyzed the data in the Kaplan–Meier plotter. As shown in **Figure 1C**, high HOXA13 expression was correlated with poorer OS and PPS in the patients with 5-FU based chemotherapy. These findings suggested that HOXA13 might be associated with poor 5-FU chemotherapy response. However, the worse efficacy of chemotherapy usually involves multiple factors,

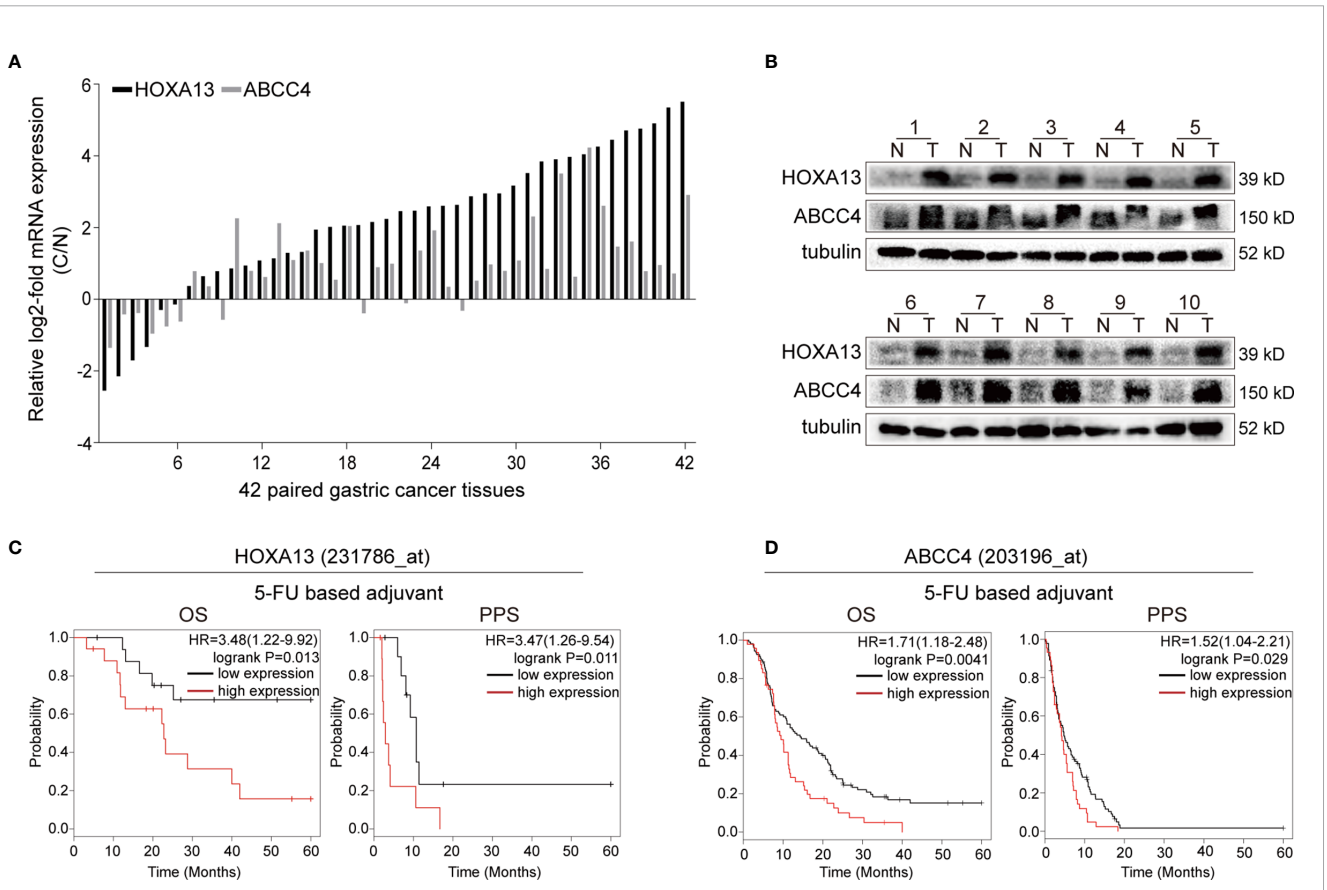

FIGURE 1 | High HOXA13 expression is associated with 5-FU resistance. **(A)** qRT-PCR analysis of HOXA13 and ABCC4 expression in GC tissues compared with paired normal tissues. **(B)** Western blot analysis of HOXA13 and ABCC4 expression in GC tissues compared with paired normal tissues. **(C)** The Kaplan–Meier plotter showed that upregulation of HOXA13 was significantly associated with lower OS and PPS in GC patients with 5-FU treatment. **(D)** In 5-FU based chemotherapy, GC patients with high ABCC4 expression had poorer prognosis (http://kmplot.com/analysis/).

among which chemoresistance is one of the most common causes. Thus, we hypothesized that HOXA13 played a role in GC resistance to 5-FU and identified it for further investigation.

HOXA13 Enhances 5-FU Resistance in GC Cells

To explore the relationship between HOXA13 expression and 5-FU cytotoxic effect on GC cells, we selected AGS and MKN28 to generate stable overexpression cell lines and SGC7901 and MKN45 to generate stable knockdown cell lines, respectively (**Figures 2A–C**, **Supplementary Figures 1A**, **B**). The cytotoxicity of gradient concentrations of 5-FU was detected by CCK-8 assays. As shown in **Figures 2D** and **E**, overexpression of HOXA13 enhanced AGS and MKN28 cells resistance to 5-FU. Conversely, knockdown of HOXA13 decreased 5-FU resistance in SGC7901 and MKN45 cells. In addition, we examined the effects of HOXA13 on cell proliferation in condition of 5-FU. EdU assays indicated that HOXA13-overexpressing cells displayed less significant 5-FU inhibition than the Vector cells did, while HOXA13 knockdown cells showed the opposite (**Figures 2F, G**). Consistently, HOXA13 overexpression cells had relatively higher colony survival rates compared to Vector groups, when treated with 5-FU for colony formation. On the contrary, the colony number of HOXA13-silencing groups was less than that of shNC groups (**Figures 2H, I**). These results indicated that HOXA13 overexpression enhanced 5-FU resistance, reducing the cellular 5-FU sensitivity.

HOXA13 Knockdown Exacerbates 5-FU-Induced Apoptosis in GC Cells

Inducing tumor cell apoptosis is considered a critical mechanism of chemotherapy (20). We used flow cytometry to study the effect of HOXA13 on 5-FU-induced apoptosis ability. Compared with Vector group, overexpression of HOXA13 weakened the capacity of 5-FU inducing apoptosis (**Figure 3A**). On the other hand, the apoptosis rates were significantly increased after knockdown of HOXA13 with 5-FU treatment (**Figure 3B**). Additionally, we analyzed the levels of apoptosis-related proteins by Western blot. As predicted, the results of 5-FU treatment showed lower levels of cleaved caspase-9 and cleaved caspase-3 in HOXA13 overexpressing-cells, as well as higher expression levels in HOXA13 knockdown cells (**Figures 3C, D**). The above results revealed that downregulation of HOXA13 expression exacerbated the apoptosis-inducing effect of 5-FU.

HOXA13 Upregulates ABCC4 Expression *Via* Binding to its Promoter Region

To elucidate the underlying mechanism of HOXA13-mediated 5-FU resistance in GC cells, we performed RNA sequencing to compare the transcriptional alterations of AGS-HOXA13 + 5-FU and AGS-Vector + 5-FU cells. The volcano plot indicated 64 upregulated genes and 121 downregulated genes in the AGS-HOXA13 + 5-FU group (Fold change >1.5, $P < 0.05$, **Figure 4A**). Subsequently, we performed pathway analysis based on the KEGG database and found that the upregulated genes were significantly relevant to ABC transporters (**Figure 4B**). Due to the potential clinical significance of ABC transporters in chemoresistance (21, 22), we postulated that ABC transporters activation might play an important role in HOXA13-mediated 5-FU resistance. Further analyzing the relationship between HOXA13 and ABC transporters, we found upregulation in transcript amounts of four ABC transporter genes, ABCC4, ABCA5, ABCA8 and ABCA12, detected in the AGS-HOXA13 cells treated by 5-FU, among which the differential expression of ABCC4 was prominent (**Figure 4C**). Subsequently, we examined ABCC4 expression in GC cells with different HOXA13 expression. It showed that the significant increase in ABCC4 expression was accompanied by elevated level of HOXA13. Likewise, in SGC7901 and MKN45 cells, ABCC4 downregulation was linked to HOXA13 knockdown (**Figure 4D**). ABCC4 was upregulated in 76.19% (32/42) GC samples indicated by qRT-PCR (**Figure 1A**), and positively correlated with HOXA13 in mRNA levels disclosed by the correlation analysis (**Figure 4E**). The patients with high ABCC4 expression had shorter OS and PPS with treatment of 5-FU shown by the Kaplan–Meier plotter (**Figure 1D**). To explore the relationship between HOXA13 and ABCC4, we predicted the binding sites of HOXA13 in ABCC4 promoter region by JASPAR (http://jaspar.genereg.net/) and designed four primer sequences (**Supplementary Figure 1C**). HOXA13 was demonstrated to enriched in primer 1 within the ABCC4 promoter tested by ChIP assay and agarose gel electrophoresis (**Figures 4F, G**). These results indicated that HOXA13 might upregulate ABCC4 expression *via* binding to its promoter region.

siABCC4 Reverses HOXA13-Induced 5-FU Resistance in GC Cells

To further investigate the role of ABCC4 in HOXA13-mediated chemoresistance, we used siRNA to silence ABCC4 expression in AGS-HOXA13 cells. Also, MKN45-shHOXA13 cells were transiently transfected with ABCC4-overexpressing plasmid (**Figure 5A**). Upregulating ABCC4 expression reversed partly the effects of HOXA13 knockdown on 5-FU anti-proliferation process, while decreasing ABCC4 expression, the cell proliferation inhibitory effects of 5-FU were restored, indicated by CCK-8, EdU and colony formation assays (**Figures 5B–D**). In addition, after downregulating ABCC4, the apoptotic rate of AGS-HOXA13 cells partly increased suggested by flow cytometry. Conversely, in MKN45-shHOXA13 cells, upregulation of ABCC4 produced the same rescue effect (**Figure 5E**). Overall, the results demonstrated that HOXA13 promoted 5-FU resistance of GC cells through upregulating ABCC4 expression.

HOXA13 Knockdown Sensitizes GC Cells to 5-FU *In Vivo*

We generated a subcutaneous tumor model to assess the role of HOXA13 in 5-FU anti-tumor effect *in vivo*. The result showed that the tumor volumes of MKN45-shHOXA13 group were smaller than those of shNC group, indicating knockdown of HOXA13 weakened tumorigenicity of MKN45 cells. Even more

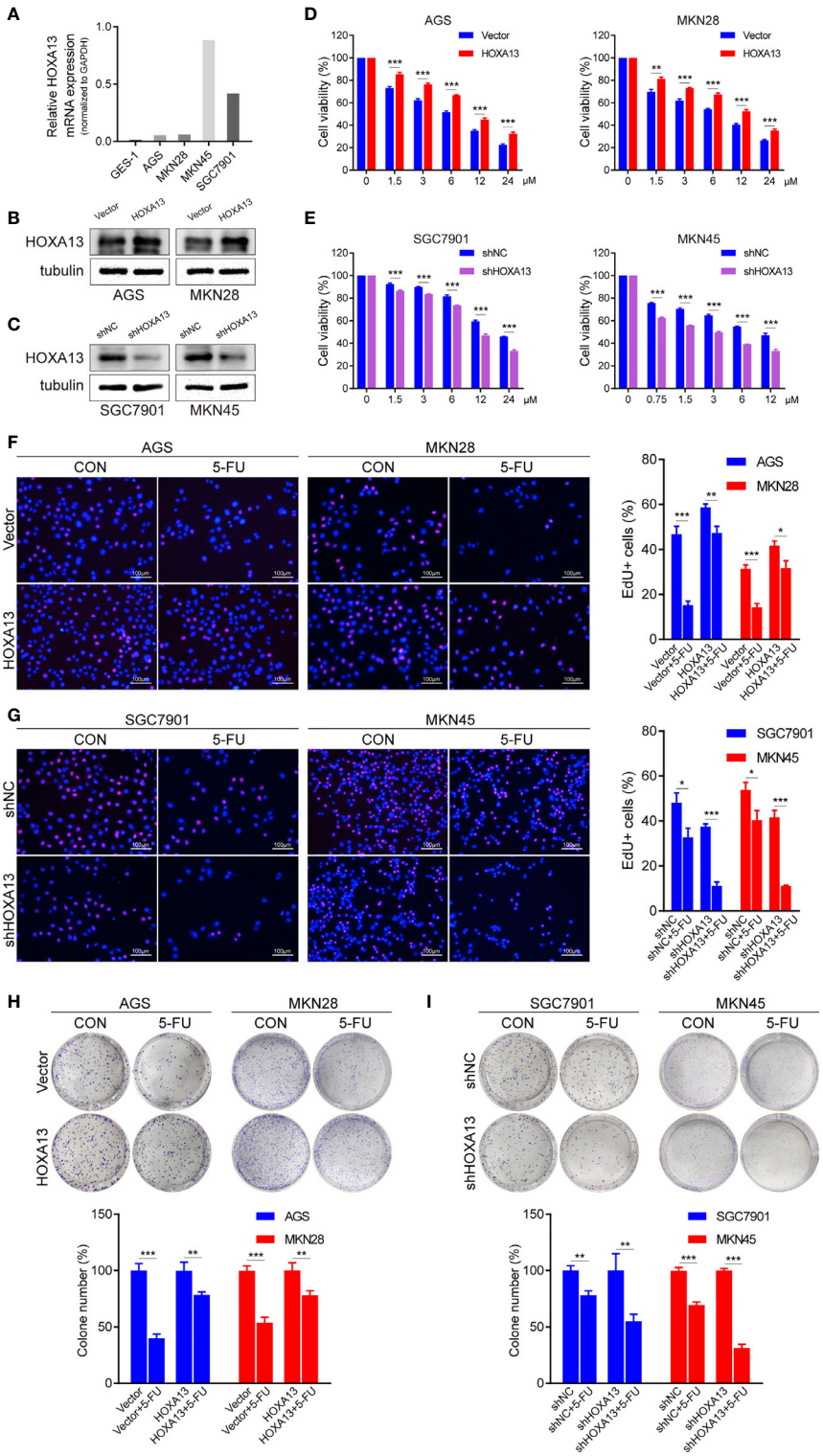

FIGURE 2 | HOXA13 promotes 5-FU resistance in GC cells. **(A)** Relative expression levels of HOXA13 in cell lines were detected by qRT-PCR. **(B, C)** The expression levels of HOXA13 were verified by Western blot in GC cells after transfection. **(D, E)** CCK-8 assays detected relative cell viability of GC cells with various concentrations of 5-FU. **(F G)** The rates of EdU staining in HOXA13+5-FU groups were higher than those of Vector + 5-FU groups, while knockdown of HOXA13 had the opposite effect. Magnification ×200. **(H, I)** After 5-FU treatment, the relative colony formation rates of HOXA13-overexpressing cells were higher than that of Vector groups, while the relative rates of colonies were reduced in HOXA13 knockdown cells. $^{*}P < 0.05$, $^{**}P < 0.01$, $^{***}P < 0.001$.

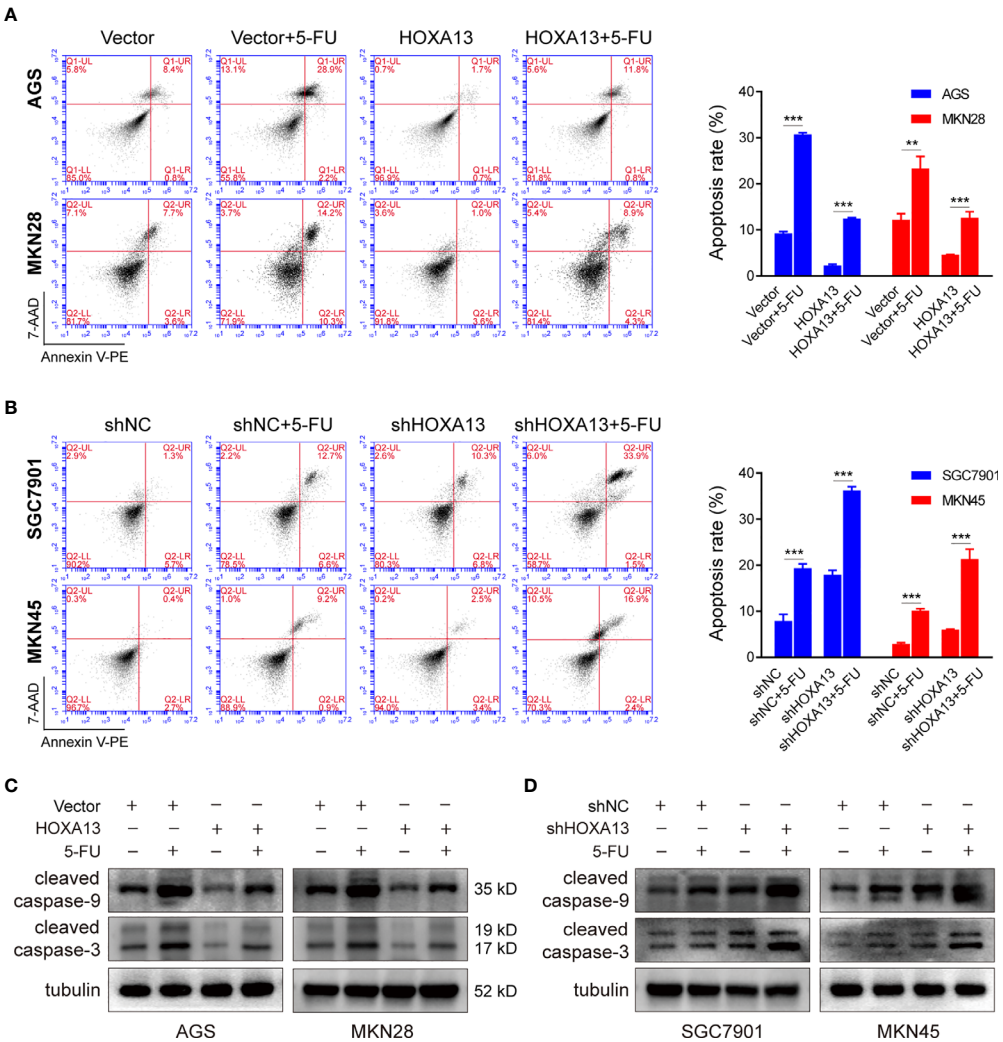

FIGURE 3 | HOXA13 knockdown exacerbates apoptosis induced by 5-FU in GC cells. **(A, B)** Flow cytometry assays detected the effect of altered HOXA13 expression and 5-FU treatment on GC cells apoptosis. **(C, D)** The protein levels of cleaved caspase-9 and cleaved caspase-3 in GC cells were determined by Western blot. $^{**}P < 0.01$, $^{***}P < 0.001$.

remarkably, although the tumor sizes of 5-FU groups were smaller than those of CON groups, 5-FU impeded tumor formation of shHOXA13 group more significantly (402.19 to 128.92 mm^3; −67.95%), compared with shNC group (529.75 to 448.38 mm^3; −15.36%), suggesting that suppression of HOXA13 improved the sensitivity of MKN45 cells to 5-FU (**Figures 6A, B**). The positive staining of HOXA13 and ABCC4, shown by IHC, was detected in shNC group, whereas the expression of ABCC4 was reduced in shHOXA13 group (**Figure 6C**). When comparing four groups of xenograft tumors (shNC + CON, shNC + 5-FU, shHOXA13 + CON and shHOXA13 + 5-FU), it showed that the staining intensity of cleaved caspase-3 was the lowest in shNC + CON group, mild in shNC + 5-FU and shHOXA13 + CON groups, and the most significant in shHOXA13 + 5-FU group (**Figure 6D**).

HOXA13 Is Directly Targeted by miR-139-5p

MicroRNAs (miRNAs), a class of small non-coding RNAs, can regulate the expression of target mRNAs by interacting with the 3'-UTR region (23). To further investigate whether HOXA13 expression can be directly regulated by miRNAs in GC, we analyzed downregulated miRNAs in microarray expression dataset (GSE23739). Combined with bioinformatics analysis (TargetScan, miRDB and miRWalk), we discovered that three candidate miRNAs potentially bound with HOXA13 (**Figure 7A**). Among these miRNAs, only miR-139-5p was involved in the progression of gastric cancer according to previous reports (24–26), which was further verified downregulated in GC cells compared to GES-1 and negatively associated with the expression of HOXA13 in GC tissues in our

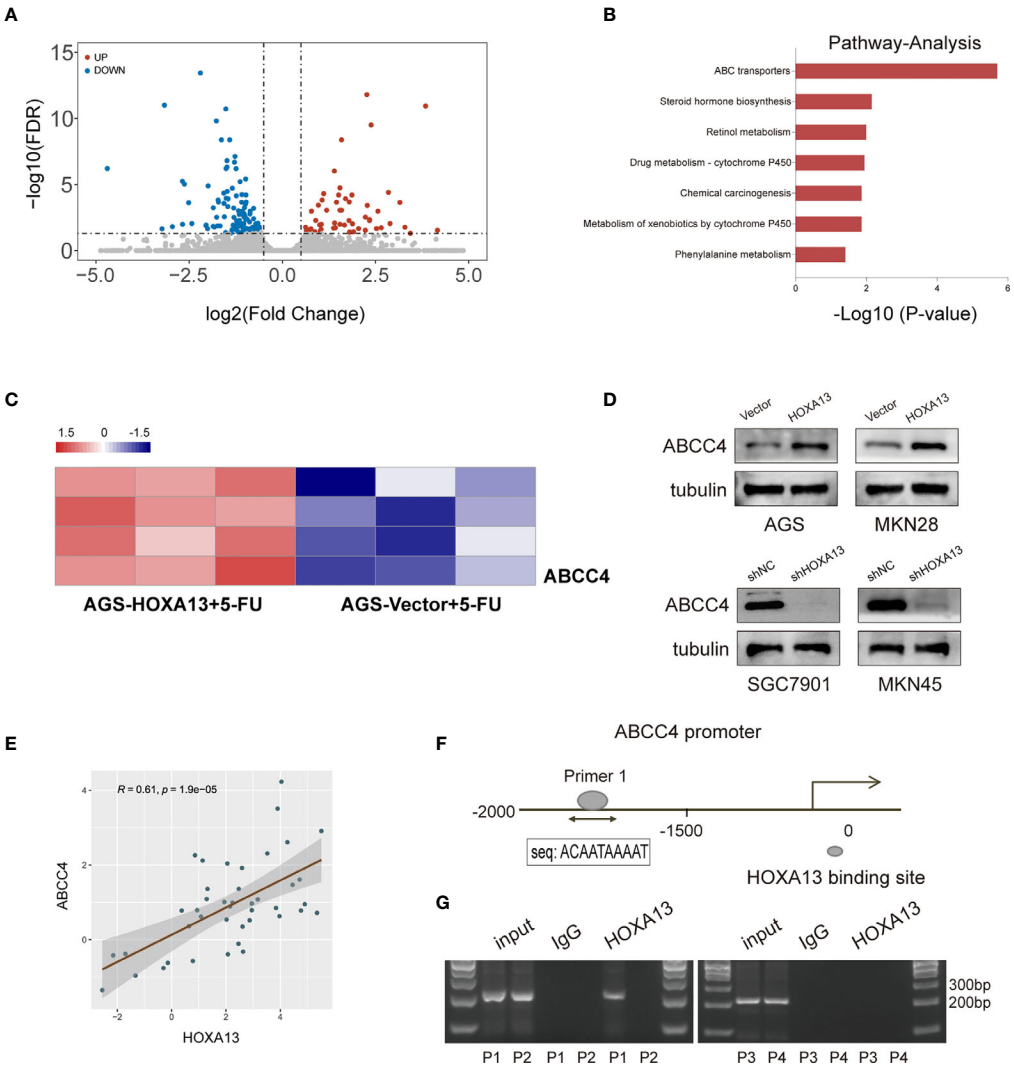

FIGURE 4 | HOXA13 upregulates ABCC4 expression *via* binding to its promoter region. **(A)** Volcano plot showed significantly upregulated genes in AGS-HOXA13 + 5-FU relative to AGS-Vector + 5-FU. **(B)** Pathway analysis revealed that ABC transporter pathway was significantly enriched. **(C)** Heatmap showed that ABCC4 was obviously upregulated in ABC transporter family. **(D)** The protein expression levels of ABCC4 in the indicated cell lines with altered HOXA13 expression. **(E)** Pearson's correlation analysis of the mRNA levels of HOXA13 and ABCC4 in GC samples. **(F)** HOXA13 binding to the ABCC4 promoter region was predicted by JASPAR (http://jaspar.genereg.net/). **(G)** The results of ChIP assay and agarose gel electrophoresis indicated HOXA13 enriched in primer 1 within the ABCC4 promoter.

study (**Figures 7B, C**). Therefore, miR-139-5p was selected as a putative candidate for further validation. The luciferase reporter assay of HEK-293T cells showed that fluorescence activity was significantly reduced after co-transfection of miR-139-5p mimics and wild-type HOXA13, while co-transfection of miR-139-5p mimics and mutant HOXA13 had no effect on luciferase activity (**Figures 7D, E**). Meanwhile, miR-139-5p mimics transfection decreased the protein level of HOXA13 compare to that in mimics NC, whereas transfecting miR-139-5p inhibitor led to a converse response (**Figure 7F**). Previous research revealed that HOXA13 conferred 5-FU resistance *via* MDM2-p53 pathway (27). In this study, we observed that MDM2 expression was decreased with downregulation of HOXA13 transfected with mimics, while p53 expression was increased (**Figure 7F**). Taken together, these findings indicated that miR-139-5p could directly target HOXA13 in GC.

DISCUSSION

HOXA13 has been reported to play a pivotal role in the normal growth and differentiation of mammalian tissues (28). Recently, a booming number of studies have demonstrated that aberrant HOXA13 expression correlates with proliferation, metastasis,

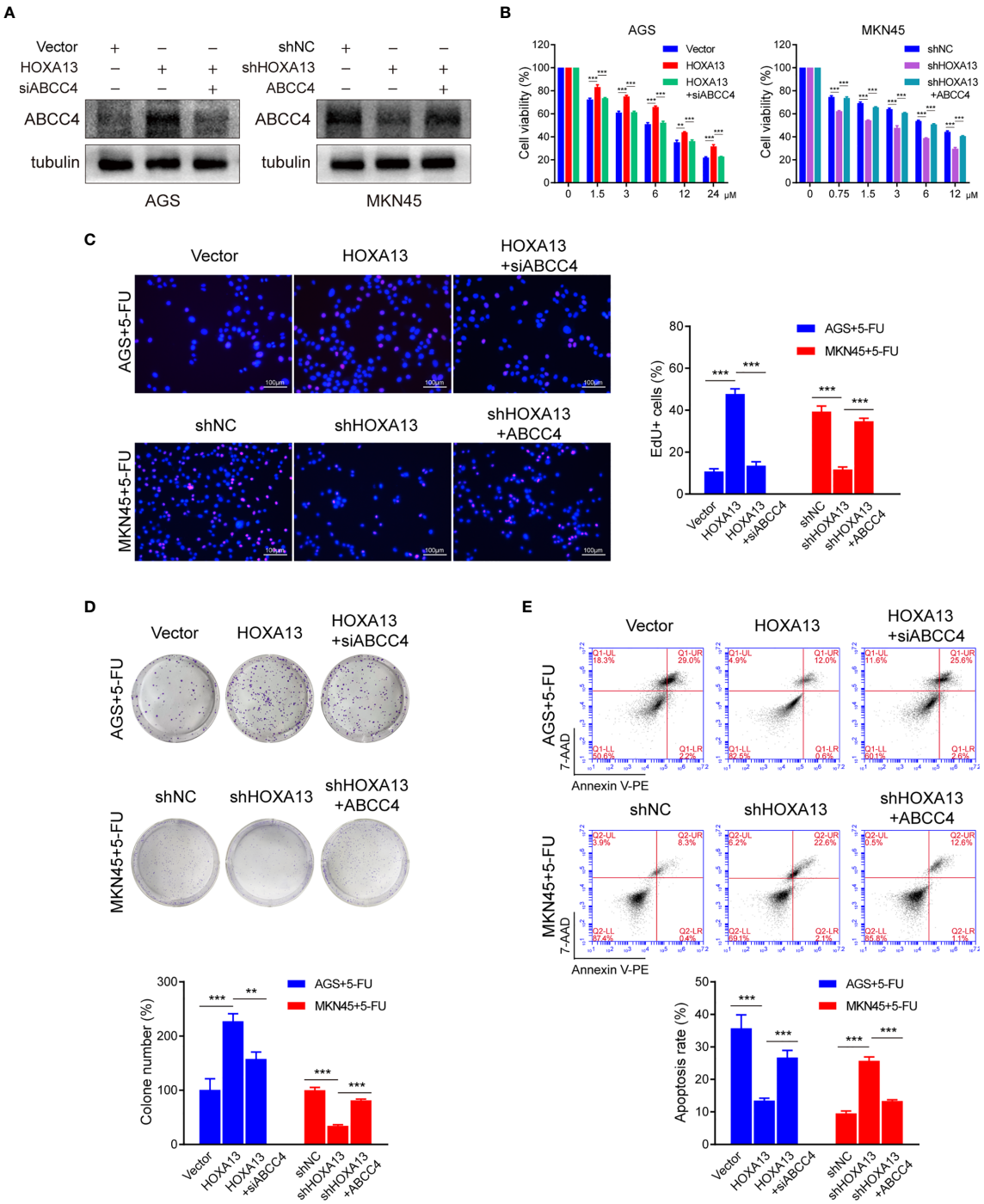

FIGURE 5 | siABCC4 reverses HOXA13-mediated 5-FU resistance in GC cells. **(A)** The protein levels of ABCC4 were detected in AGS cells including Vector, HOXA13 and HOXA13 + siABCC4 groups and MKN45 cells including shNC, shHOXA13 and shHOXA13 + ABCC4 groups. **(B–D)** CCK-8 assays, EdU assays and colony formation assays revealed that depletion of ABCC4 enhanced anti-proliferative effect of 5-FU in HOXA13-overexpressing cells, while overexpression of ABCC4 weakened that of 5-FU in HOXA13 knockdown cells. Magnification ×200. **(E)** After inhibiting of ABCC4 expression, the apoptotic levels of HOXA13-overexpressing cells induced by 5-FU was increased, while ABCC4 overexpression in HOXA13 knockdown cells had the same rescue effect. $^{**}P < 0.01$, $^{***}P < 0.001$.

prognosis and chemoresistance in various types of cancer (29–31). High expression of HOXA13 was an independent prognostic marker of poor outcome in GC elucidated in our previous study (32). HOXA13 overexpression promoted the growth and metastasis of GC cells (17). Herein, we further explore the role and mechanism of HOXA13 in chemosensitivity of GC.

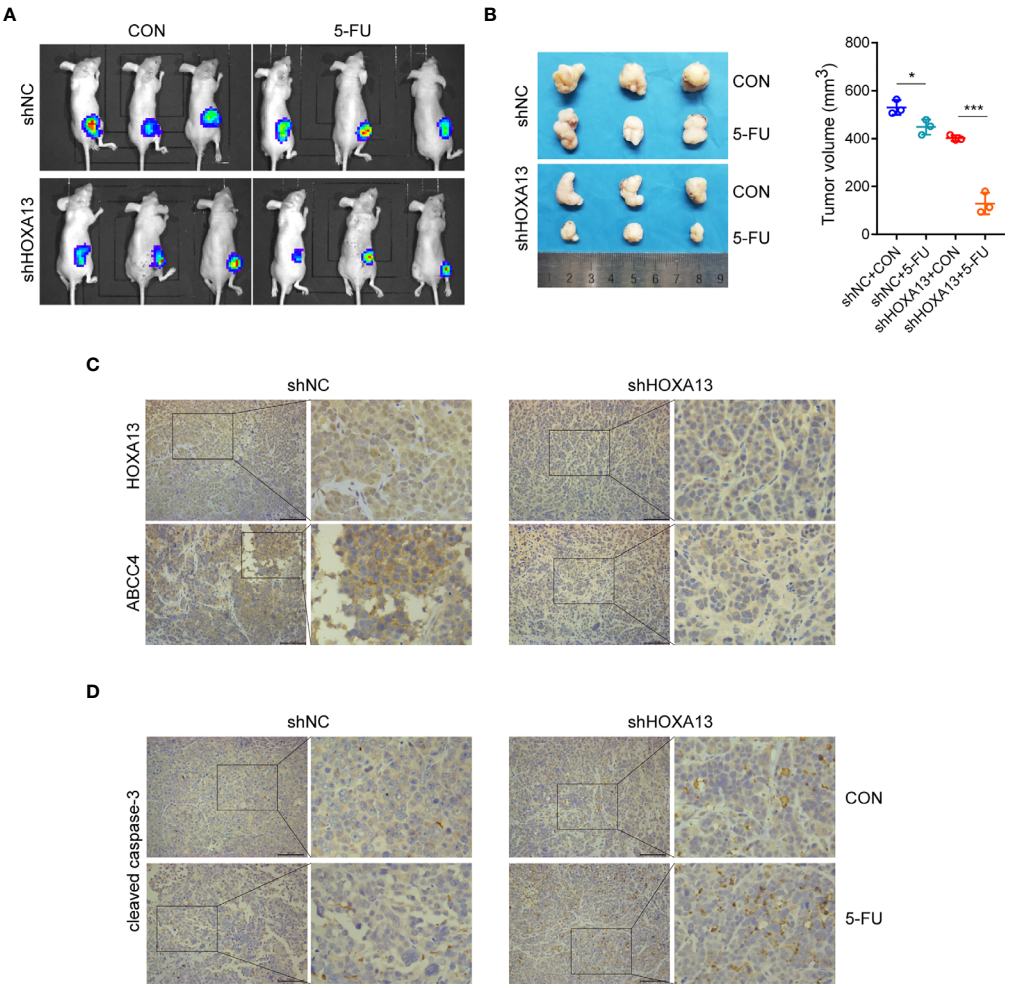

FIGURE 6 | HOXA13 knockdown increases sensitivity of GC cells to 5-FU *in vivo*. **(A)** Bioluminescence images of tumors formed by subcutaneously injecting MKN45 cells, followed by 5-FU or control (CON) treatment. **(B)** The final tumor volumes in each group were measured. **(C)** IHC staining of HOXA13 and ABCC4 were performed in tumor tissues. **(D)** IHC staining of cleaved caspase-3 was obvious in shHOXA13 + 5-FU group. Magnification ×200. $^{*}P < 0.05$, $^{***}P < 0.001$.

In the present study, we reconfirmed that HOXA13 was upregulated in GC samples. Next, we analyzed the prognosis of GC patients receiving 5-FU based chemotherapy. And the Kaplan–Meier plotter suggested that high expression of HOXA13 was associated with poor response of 5-FU treatment in GC. However, whether the unfavorable prognosis of 5-FU treatment in GC was directly attributed to chemoresistance required detailed validation.

In order to confirm the possibility of the hypothesis, we examined that whether altered HOXA13 expression had influence on 5-FU sensitivity of GC cells. The results showed that HOXA13 overexpression promoted GC cells to be resistant to 5-FU, whereas 5-FU resistance of HOXA13 knockdown groups significantly diminished compared with that of shNC groups, indicating that HOXA13 upregulation enhanced 5-FU resistance, namely weakened sensitivity of GC cells to 5-FU.

Subsequently, we observed the effect of HOXA13 expression on GC cell growth with 5-FU treatment. Cells in each group with low expression of HOX13 treated with 5-FU showed the slowest proliferation rate and smallest colony ratio, demonstrated by EdU staining and colony formation assay respectively. Afterward, we used flow apoptosis assay to examine the proportion of apoptotic cells in GC cells upon 5-FU treatment. The results showed that the apoptotic rate of shHOXA13 + 5-FU groups was significantly increased compared with shNC+5-FU groups, suggesting that HOXA13 knockdown enhanced 5-FU-induced apoptosis. The above experiments indicated that HOXA13 knockdown enhanced the inhibition effect of 5-FU on cell proliferation and promoted 5-FU-induced apoptosis, thereby increasing the sensitivity of GC cells to 5-FU.

In vivo experiment also verified the above results. Compared with shNC group, the tumor sizes of shHOXA13 group were more significantly inhibited by 5-FU, indicating that downregulation of HOXA13 expression improved the sensitivity of GC cells to 5-FU *in vivo*. What's more, the expression of cleaved caspase-3 in shHOXA13 + 5-FU group was significantly higher than other three groups, suggesting

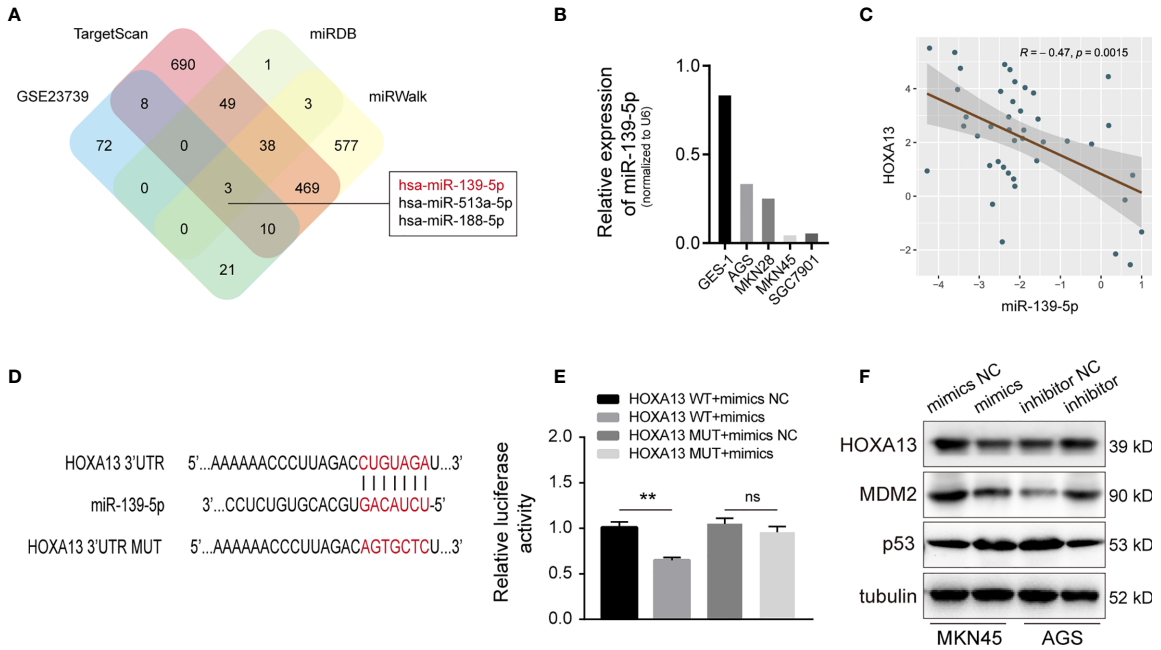

FIGURE 7 | HOXA13 is directly targeted by miR-139-5p in GC. **(A)** Potential miRNAs that target HOXA13 were predicted by GEO dataset and online prediction tools. **(B)** Relative expression levels of miR-139-5p in cell lines were detected by qRT-PCR. **(C)** Pearson's correlation analysis of the mRNA levels of miR-139-5p and HOXA13 in GC samples. **(D)** The predicted miR-139-5p binding site in HOXA13 and sequences of wild-type (WT) and mutant (MUT) 3'-UTR of HOXA13. **(E)** Relative luciferase activity were performed in HEK-293T cells after co-transfection with HOXA13 WT or HOXA13 MUT and miR-139-5p mimics or NC. **(F)** The protein expression levels of HOXA13, MDM2 and p53 were detected in MKN45 cells transfected with miR-139-5p mimics or NC and AGS cells transfected with miR-139-5p inhibitor or NC. $^{**}P < 0.01$. ns, no significant.

that HOXA13 knockdown augmented 5-FU induced apoptosis *in vivo*.

To explore the underlying mechanisms of HOXA13-mediated 5-FU resistance in GC cells, transcriptome sequencing was utilized to profile differentially expressed genes in AGS cells with 5-FU treatment (AGS-HOXA13 + 5-FU *vs.* AGS-Vector + 5-FU). The results showed that in AGS-HOXA13 + 5-FU group, upregulated genes were predominantly enriched in the following pathways: ABC transporters, drug metabolism-cytochrome P450 and chemical carcinogenesis, among which the enrichment of ABC transporters dominated. To date, ample studies have demonstrated that a major mechanism of chemoresistance in cancers is the upregulation of ABC transporters expression (33, 34). ABC transporters, located in cell membrane, are a group of ATP-dependent pumps that transports substrates out of cells (35). Of these, the C subgroup, also called the multidrug resistance-associated proteins (MRPs), has attracted growing attention in tumor chemoresistance (36, 37). Combined with the sequencing results, we speculated that 5-FU resistance induced by HOXA13 might be related to activation of ABC transporters. Further analysis confirmed that ABCC4 was significantly upregulated in AGS-HOXA13+5-FU cells leading to the inference that ABCC4 might be a potential downstream target of HOXA13. As a member of MRPs, ABCC4 is a versatile efflux transporter for many drugs, including chemotherapeutic drugs (38). As shown by research in prostate cancer, inhibition of ABCC4 expression restores the docetaxel sensitivity (39). ABCC4 is transcriptional regulated by FoxM1, promoting carboplatin resistance in retinoblastoma (40). Abbaszadegan et al. found that KCTD12 decreases 5-FU resistance in esophageal squamous carcinoma cell by down-regulating ABCC4 (41). Interestingly, this study revealed that ABCC4 was upregulated in GC tissues, and mRNA expression of HOXA13 was positively correlated with that of ABCC4. The unfavorable prognosis of GC patients with high ABCC4 expression was found in the case of 5-FU based chemotherapy, suggesting that ABCC4 expression was associated with efficacy of 5-FU in GC patients.

To further investigate whether there was a regulatory relationship between HOXA13 and ABCC4, we examined the impact of HOXA13 expression alternation on ABCC4 in GC cells. The results showed that ABCC4 expression was upregulated in HOXA13-overexpressing cells and downregulated in HOXA13 knockdown cells, prompting that HOXA13 might modulate the expression of ABCC4. Noticeably, the JASPAR database indicated the possibility of HOXA13 binding to the ABCC4 promoter. Therefore, we designed four primer sequences for ChIP assay and studied whether HOXA13 could bind to promoter region of ABCC4. The result showed that HOXA13 might enrich in the ABCC4 promoter region. Subsequent rescue experiments confirmed that inhibition of ABCC4 expression attenuated the ability of HOXA13 overexpression enhanced 5-FU resistance of GC cells, while upregulation of ABCC4 partly reversed the process of HOXA13 knockdown promoted GC cells sensitivity to 5-FU. These findings

suggested that HOXA13 upregulated ABCC4 expression possibly by binding to its promoter, and ABCC4 might play a crucial role in HOXA13-mediated insensitivity of GC to 5-FU.

Increasing evidences have demonstrated that miRNAs play an important role in tumor progression through post-transcriptionally regulating functional mRNAs expression (42). In this study, miR-139-5p, identified by GEO dataset and bioinformatics analyses, was downregulated in GC cells and negatively correlated with HOXA13 in GC tissues. Moreover, by mechanism experiments, we confirmed that miR-139-5p directly might bind to HOXA13 3'-UTR to downregulate its expression. However, the role of miR-139-5p in chemoresistance of GC cells remains to further researched.

In conclusion, our study shows that HOXA13 is upregulated in GC samples and associated with poor prognosis of GC patients in the case of 5-FU treatment. High HOXA13 expression enhances 5-FU resistance and reduces 5-FU sensitivity, as well as alleviates the anti-proliferative effect of 5-FU and suppresses 5-FU-induced cell apoptosis. And ABC transporter pathway activation, especially ABCC4 upregulation, may play an important role in HOXA13-mediated 5-FU resistance. HOXA13 expression is directly suppressed by miR-139-5p in GC cells. Targeting the HOXA13/ABCC4 axis is expected to be a potential therapeutic strategy for reducing resistance to chemotherapy.

DATA AVAILABILITY STATEMENT

The RNA sequencing data are available on Figshare (https://figshare.com/articles/dataset/RNA-seq_AGS-HOXA13_5-FU_vs_AGS-Vector_5-FU_All_xlsx/14546811).

ETHICS STATEMENT

The studies involving human participants were reviewed and approved by Shanghai General Hospital. The patients/participants provided their written informed consent to participate in this study. The animal study was reviewed and approved by Shanghai General Hospital.

AUTHOR CONTRIBUTIONS

ZC, ZQ, and XC designed and performed the experiments. LL and QW performed animal experiments. ZC and ZQ analyzed the data and wrote the manuscript. XC supervised the project. All authors contributed to the article and approved the submitted version.

SUPPLEMENTARY MATERIAL

The Supplementary Material for this article can be found online at: https://www.frontiersin.org/articles/10.3389/fonc.2021.645979/full#supplementary-material

Supplementary Figure 1 | (A) Establishment of HOXA13-overexpressing cell lines in AGS and MKN28 cells, confirmed by qRT-PCR. **(B)** Establishment of HOXA13 knockdown cell lines in SGC7901 and MKN45 cells, confirmed by qRT-PCR. **(C)** The binding sites of HOXA13 in ABCC4 promoter region were predicted by JASPAR database and primer sequences were designed. ***$P < 0.001$.

REFERENCES

1. Bray F, Ferlay J, Soerjomataram I, Siegel RL, Torre LA, Jemal A. Global Cancer Statistics 2018: GLOBOCAN Estimates of Incidence and Mortality Worldwide for 36 Cancers in 185 Countries. *CA Cancer J Clin* (2018) 68 (6):394–424. doi: 10.3322/caac.21492
2. Ajani JA, D'Amico TA, Almhanna K, Bentrem DJ, Chao J, Das P, et al. Gastric Cancer, Version 3.2016, NCCN Clinical Practice Guidelines in Oncology. *J Natl Compr Canc Netw* (2016) 14(10):1286–312. doi: 10.6004/jnccn.2016.0137
3. Longley DB, Harkin DP, Johnston PG. 5-Fluorouracil: Mechanisms of Action and Clinical Strategies. *Nat Rev Cancer* (2003) 3(5):330–8. doi: 10.1038/nrc1074
4. Zhang F, Li K, Yao X, Wang H, Li W, Wu J, et al. A miR-567-PIK3AP1-PI3K/AKT-c-Myc Feedback Loop Regulates Tumour Growth and Chemoresistance in Gastric Cancer. *EBioMedicine* (2019) 44:311–21. doi: 10.1016/j.ebiom.2019.05.003
5. Mallo M. Reassessing the Role of Hox Genes During Vertebrate Development and Evolution. *Trends Genet* (2018) 34(3):209–17. doi: 10.1016/j.tig.2017.11.007
6. Shah N, Sukumar S. The Hox Genes and Their Roles in Oncogenesis. *Nat Rev Cancer* (2010) 10(5):361–71. doi: 10.1038/nrc2826
7. Liao WT, Jiang D, Yuan J, Cui YM, Shi XW, Chen CM, et al. HOXB7 as a Prognostic Factor and Mediator of Colorectal Cancer Progression. *Clin Cancer Res* (2011) 17(11):3569–78. doi: 10.1158/1078-0432.ccr-10-2533
8. Liu H, Zhang M, Xu S, Zhang J, Zou J, Yang C, et al. HOXC8 Promotes Proliferation and Migration Through Transcriptional Up-Regulation of TGFbeta1 in non-Small Cell Lung Cancer. *Oncogenesis* (2018) 7(2):1. doi: 10.1038/s41389-017-0016-4
9. Song C, Han Y, Luo H, Qin Z, Chen Z, Liu Y, et al. HOXA10 Induces BCL2 Expression, Inhibits Apoptosis, and Promotes Cell Proliferation in Gastric Cancer. *Cancer Med* (2019) 8(12):5651–61. doi: 10.1002/cam4.2440
10. Quagliata L, Matter MS, Piscuoglio S, Arabi L, Ruiz C, Procino A, et al. Long Noncoding RNA HOTTIP/HOXA13 Expression is Associated With Disease Progression and Predicts Outcome in Hepatocellular Carcinoma Patients. *Hepatology* (2014) 59(3):911–23. doi: 10.1002/hep.26740
11. Sun Y, Hu B, Wang Q, Ye M, Qiu Q, Zhou Y, et al. Long non-Coding RNA HOTTIP Promotes BCL-2 Expression and Induces Chemoresistance in Small Cell Lung Cancer by Sponging Mir-216a. *Cell Death Dis* (2018) 9(2):85. doi: 10.1038/s41419-017-0113-5
12. Li Z, Zhao X, Zhou Y, Liu Y, Zhou Q, Ye H, et al. The Long non-Coding RNA HOTTIP Promotes Progression and Gemcitabine Resistance by Regulating HOXA13 in Pancreatic Cancer. *J Transl Med* (2015) 13:84. doi: 10.1186/s12967-015-0442-z
13. Kathawala RJ, Gupta P, Ashby CR, Jr., Chen ZS. The Modulation of ABC Transporter-Mediated Multidrug Resistance in Cancer: A Review of the Past Decade. *Drug Resist Updat Rev Comment Antimicrob Anticancer Chemother* (2015) 18:1–17. doi: 10.1016/j.drup.2014.11.002
14. Sodani K, Patel A, Kathawala RJ, Chen ZS. Multidrug Resistance Associated Proteins in Multidrug Resistance. *Chin J Cancer* (2012) 31(2):58–72. doi: 10.5732/cjc.011.10329
15. Gazzaniga P, Naso G, Gradilone A, Cortesi E, Gandini O, Gianni W, et al. Chemosensitivity Profile Assay of Circulating Cancer Cells: Prognostic and Predictive Value in Epithelial Tumors. *Int J Cancer* (2010) 126(10):2437–47. doi: 10.1002/ijc.24953
16. Murray J, Valli E, Yu DMT, Truong AM, Gifford AJ, Eden GL, et al. Suppression of the ATP-binding Cassette Transporter ABCC4 Impairs Neuroblastoma Tumour Growth and Sensitises to Irinotecan In Vivo. *Eur J Cancer* (2017) 83:132–41. doi: 10.1016/j.ejca.2017.06.024
17. Qin Z, Chen Z, Weng J, Li S, Rong Z, Zhou C. Elevated HOXA13 Expression Promotes the Proliferation and Metastasis of Gastric Cancer Partly Via Activating Erk1/2. *Onco Targets Ther* (2019) 12:1803–13. doi: 10.2147/ott.s196986

18. Szász AM, Lánczky A, Nagy Á, Förster S, Hark K, Green JE, et al. Cross-Validation of Survival Associated Biomarkers in Gastric Cancer Using Transcriptomic Data of 1,065 patients. *Oncotarget* (2016) 7(31):49322–33. doi: 10.18632/oncotarget.10337
19. Xu S, Ni H, Chen H, Dai Q. The Interaction Between STAT3 and nAChRalpha1 Interferes With Nicotine-Induced Atherosclerosis Via Akt/mTOR Signaling Cascade. *Aging (Albany N Y)* (2019) 11(19):8120–38. doi: 10.18632/aging.102296
20. Wu X, Luo Q, Zhao P, Chang W, Wang Y, Shu T, et al. JOSD1 Inhibits Mitochondrial Apoptotic Signalling to Drive Acquired Chemoresistance in Gynaecological Cancer by Stabilizing MCL1. *Cell Death Differ* (2020) 27 (1):55–70. doi: 10.1038/s41418-019-0339-0
21. Mo D, Fang H, Niu K, Liu J, Wu M, Li S, et al. Human Helicase Recql4 Drives Cisplatin Resistance in Gastric Cancer by Activating an AKT-YB1-MDR1 Signaling Pathway. *Cancer Res* (2016) 76(10):3057–66. doi: 10.1158/0008-5472.can-15-2361
22. Shang Y, Zhang Z, Liu Z, Feng B, Ren G, Li K, et al. miR-508-5p Regulates Multidrug Resistance of Gastric Cancer by Targeting ABCB1 and ZNRD1. *Oncogene* (2014) 33(25):3267–76. doi: 10.1038/onc.2013.297
23. Rupaimoole R, Slack FJ. MicroRNA Therapeutics: Towards a New Era for the Management of Cancer and Other Diseases. *Nat Rev Drug Discovery* (2017) 16 (3):203–22. doi: 10.1038/nrd.2016.246
24. Sun K, Hu P, Xu F. Linc00152/miR-139-5p Regulates Gastric Cancer Cell Aerobic Glycolysis by Targeting PRKAA1. *BioMed Pharmacother* (2018) 97:1296–302. doi: 10.1016/j.biopha.2017.11.015
25. Wenquan L, Hongqing X, Yuhua L, Lili W, Wang Z, Ziwei Z, et al. MiR-139-5p Inhibits the Proliferation of Gastric Cancer Cells by Targeting Regulation of Nuclear Pre-Mrna Domain Containing 1b. *Biochem Biophys Res Commun* (2020) 527(2):393–400. doi: 10.1016/j.bbrc.2020.04.067
26. Hou J, Zhuo H, Chen X, Cheng J, Zheng W, Zhong M, et al. MiR-139-5p Negatively Regulates PMP22 to Repress Cell Proliferation by Targeting the NF-κb Signaling Pathway in Gastric Cancer. *Int J Biol Sci* (2020) 16(7):1218–29. doi: 10.7150/ijbs.40338
27. Han Y, Song C, Wang J, Tang H, Peng Z, Lu S. HOXA13 Contributes to Gastric Carcinogenesis Through DHRS2 Interacting With MDM2 and Confers 5-FU Resistance by a p53-dependent Pathway. *Mol Carcinog* (2018) 57(6):722–34. doi: 10.1002/mc.22793
28. Bhatlekar S, Fields JZ, Boman BM. HOX Genes and Their Role in the Development of Human Cancers. *J Mol Med (Berl)* (2014) 92(8):811–23. doi: 10.1007/s00109-014-1181-y
29. Liu C, Tian X, Zhang J, Jiang L. Long Non-coding Rna DLEU1 Promotes Proliferation and Invasion by Interacting With miR-381 and Enhancing Hoxa13 Expression in Cervical Cancer. *Front Genet* (2018) 9:629. doi: 10.3389/fgene.2018.00629
30. Gu ZD, Shen LY, Wang H, Chen XM, Li Y, Ning T, et al. HOXA13 Promotes Cancer Cell Growth and Predicts Poor Survival of Patients With Esophageal Squamous Cell Carcinoma. *Cancer Res* (2009) 69(12):4969–73. doi: 10.1158/0008-5472.can-08-4546
31. Quagliata L, Quintavalle C, Lanzafame M, Matter MS, Novello C, di Tommaso L, et al. High Expression of HOXA13 Correlates With Poorly Differentiated Hepatocellular Carcinomas and Modulates Sorafenib Response in In Vitro Models. *Lab Invest* (2018) 98(1):95–105. doi: 10.1038/labinvest.2017.107
32. Han Y, Tu WW, Wen YG, Li DP, Qiu GQ, Tang HM, et al. Identification and Validation That Up-Expression of HOXA13 is a Novel Independent Prognostic Marker of a Worse Outcome in Gastric Cancer Based on Immunohistochemistry. *Med Oncol* (2013) 30(2):564. doi: 10.1007/s12032-013-0564-1
33. Robey RW, Pluchino KM, Hall MD, Fojo AT, Bates SE, Gottesman MM. Revisiting the Role of ABC Transporters in Multidrug-Resistant Cancer. *Nat Rev Cancer* (2018) 18(7):452–64. doi: 10.1038/s41568-018-0005-8
34. Borst P, Elferink RO. Mammalian ABC Transporters in Health and Disease. *Annu Rev Biochem* (2002) 71:537–92. doi: 10.1146/annurev.biochem.71.102301.093055
35. Locher KP. Mechanistic Diversity in ATP-binding Cassette (ABC) Transporters. *Nat Struct Mol Biol* (2016) 23(6):487–93. doi: 10.1038/nsmb.3216
36. Borst P, Evers R, Kool M, Wijnholds J. A Family of Drug Transporters: The Multidrug Resistance-Associated Proteins. *J Natl Cancer Inst* (2000) 92 (16):1295–302. doi: 10.1093/jnci/92.16.1295
37. Chen ZS, Tiwari AK. Multidrug Resistance Proteins (Mrps/Abccs) in Cancer Chemotherapy and Genetic Diseases. *FEBS J* (2011) 278(18):3226–45. doi: 10.1111/j.1742-4658.2011.08235.x
38. Wen J, Luo J, Huang W, Tang J, Zhou H, Zhang W. The Pharmacological and Physiological Role of Multidrug-Resistant Protein 4. *J Pharmacol Exp Ther* (2015) 354(3):358–75. doi: 10.1124/jpet.115.225656
39. Orellana-Serradell O, Herrera D, Castellon EA, Contreras HR. The Transcription Factor ZEB1 Promotes Chemoresistance in Prostate Cancer Cell Lines. *Asian J Androl* (2019) 21(5):460–7. doi: 10.4103/aja.aja_1_19
40. Zhu X, Xue L, Yao Y, Wang K, Tan C, Zhuang M, et al. The FoxM1-ABCC4 Axis Mediates Carboplatin Resistance in Human Retinoblastoma Y-79 Cells. *Acta Biochim Biophys Sin* (2018) 50(9):914–20. doi: 10.1093/abbs/gmy080
41. Abbaszadegan MR, Taghehchian N, Li L, Aarabi A, Moghbeli M. Contribution of KCTD12 to Esophageal Squamous Cell Carcinoma. *BMC Cancer* (2018) 18(1):853. doi: 10.1186/s12885-018-4765-z
42. Lin S, Gregory RI. MicroRNA Biogenesis Pathways in Cancer. *Nat Rev Cancer* (2015) 15(6):321–33. doi: 10.1038/nrc3932

Conflict of Interest: The authors declare that the research was conducted in the absence of any commercial or financial relationships that could be construed as a potential conflict of interest.

frontiers in Oncology

MINI REVIEW
published: 24 May 2021
doi: 10.3389/fonc.2021.684309

Combination of Anti-EGFR and Anti-VEGF Drugs for the Treatment of Previously Treated Metastatic Colorectal Cancer: A Case Report and Literature Review

*Yong Li[1], Xian Chen[1], Wenzhu Li[1], Yongsong Ye[2], Xiaohua Du[3], Shaodan Sun[4], Lirong Liu[1] and Haibo Zhang[1,5]**

[1] Department of Oncology, Guangdong Provincial Hospital of Chinese Medicine, Guangzhou, China, [2] Department of Image, Guangdong Provincial Hospital of Chinese Medicine, Guangzhou, China, [3] Department of Pathology, Guangdong Provincial Hospital of Chinese Medicine, Guangzhou, China, [4] Deparment of Pharmacology of Traditional Chinese Medicine, Guangdong Provincial Hospital of Chinese Medicine, Guangzhou, China, [5] State Key Laboratory of Dampness Syndrome of Chinese Medicine, Guangdong Provincial Hospital of Chinese Medicine, Guangzhou, China

OPEN ACCESS

Edited by:
Dong-Hua Yang,
St. John's University, United States

Reviewed by:
Rongbo Lin,
Fujian Provincial Cancer Hospital, China
Min Shi,
Southern Medical University, China

***Correspondence:**
Haibo Zhang
haibozh@gzucm.edu.cn

Specialty section:
This article was submitted to Gastrointestinal Cancers, a section of the journal Frontiers in Oncology

Received: *23 March 2021*
Accepted: *03 May 2021*
Published: *24 May 2021*

Citation:
Li Y, Chen X, Li W, Ye Y, Du X, Sun S, Liu L and Zhang H (2021) Combination of Anti-EGFR and Anti-VEGF Drugs for the Treatment of Previously Treated Metastatic Colorectal Cancer: A Case Report and Literature Review. Front. Oncol. 11:684309. doi: 10.3389/fonc.2021.684309

The standard third-line treatment of metastatic colorectal cancer (mCRC) includes the small-molecule anti-vascular drugs (Regofenib and Fruquintinib) and the chemotherapy drug trifluridine and tipiracil hydrochloride (TAS-102). There is no standard treatment for mCRC if the third-line treatment failed. Therefore, it is a pressing need to develop new therapeutic approaches to improve the survival of patients who developed drug resistance to the third-line treatment. In this study, we report a case of mCRC with RAS/BRAF wild-type, who was successfully treated using cetuximab in combination with fruquintinib after resistance to chemotherapy, bevacizumab, cetuximab and regorafenib. This patient responded to this combination regimen. Then, we discuss the mechanisms of action of this combination. Furthermore, we introduce the clinical trials on the combination regimens of anti-EGFR with anti-vascular monoclonal antibodies. Finally, we discuss the clinical explorations of using combination of anti-EGFR with small-molecule anti-VEGF drugs and their potential benefits. The clinical effects of small-molecule anti-vascular drugs in combination with anti-EGFR in the treatment of CRC warrant further explored.

Keywords: resistance, cetuximab, fruquintinib, chemotherapy, metastatic colorectal cancer

INTRODUCTION

Therapeutic regimens for metastatic colorectal cancer (mCRC) include chemotherapy and targeted therapy. The chemotherapeutic drugs generally include fluorouracil, oxaliplatin, and irinotecan, while targeted drugs include the antiangiogenic drugs (bevacizumab, ziv-aflibercept, and ramucirumab) and anti-EGFR drugs (cetuximab or panitumumab for RAS, BRAF wild-type patients). With the application of these drugs and the development of predictive factors, the median overall survival (OS) of patients with mCRC has exceeded 30 months (1). However, the

prognosis of patients who failed the first- and second-line treatments is still poor. At present, the third-line standard treatment of mCRC include small-molecule anti-vascular drugs, such as regorafenib and fruquintinib, and chemotherapeutic drugs, such as trifluridine and tipiracil hydrochloride tablets (TAS-102). For patients with RAS/BRAF wild-type who have not used the anti-EGFR drug, cetuximab in combination with irinotecan can be selected (2–6). For patients with rare mutations, including HER2 amplification, BRAF mutation, and MSI-H, corresponding targeted drugs (7) can be applied.

Currently, there is no standard treatment available after CRC patients develop drug resistance to the third-line treatment. The treatments for those patients include different combination of drugs and are in the exploratory stage. Anti-VEGF drugs combined with immune checkpoint inhibitors in proficient mismatch repair(pMMR) patients (8) or TAS-102 combined with Anti-VEGF drugs (9) are commonly used. Rechallenge of chemotherapy, cetuximab and the combination of anti-EGFR and anti-VEGF are alternatives.

Hear we report a case of advanced CRC who is RAS/BRAF wild-type and developed drug resistance to the previous therapy. This patient was treated successfully by a small-molecule anti-vascular drug in combination with cetuximab. The aim of this study is to present the mechanisms of action and clinical applications of anti-EGFR combined with anti-VEGF drugs, and discuss the potential benefits of this combination.

CASE PRESENTATION

The patient was a 52-year-old male. In March 2017, the patient presented with hematochezia without obvious causes, and a mass of about 2.7 × 3.5 cm was found 35 cm from the anus through electronic colonoscopy. CT imaging showed a sigmoid colon neoplasm, invading to the serosa, local multiple lymph node metastases, liver, and lung multiple metastases. The biopsy confirmed the patient had moderately differentiated adenocarcinoma of the sigmoid colon. The blood level of carcinoembryonic antigen (CEA) and CA199 in this patient was normal. The tumor stage was diagnosed as T3N1M1b. The hepatobiliary surgeon assessed liver metastasis as unresectable. A genetic testing was performed and revealed wild type KRAS, NRAS, BRAF, and PIK3CA of the cancer. Immunohistochemical (IHC) staining showed positive for mutS homolog 2 (MSH2), mutS homolog 6 (MSH6), and mutl homolog l gene (MLH1), and weakly positive for PMS1 homolog 2 (PMS2). The DNA mismatch repair (MMR) was proficient mismatch repair (pMMR). IHC staining of HER2 was negative. According to the treatment guidelines, the first-line treatment should be chemotherapy combined with cetuximab. Because cetuximab was not included in the national medical insurance at that time, bevacizumab in combination with XELOX chemotherapy was applied as the first-line treatment from May to August 2017. The treatment efficacy was partial response (PR). The patient was followed with maintenance treatment using capecitabine. The efficacy was progressive disease (PD) in June 2018. Bevacizumab in combination with FOLFOX chemotherapy was introduced in August 2019, and the efficacy was PD in January 2019. Cetuximab in combination with irinotecan chemotherapy was started as the third-line treatment in January 2019. CT imaging indicated cancer progression in September 2019. Therefore, he was treated with regorafenib as the fourth-line therapy in October 2019 for two cycles. Reexamination indicated PD in December 2019. CEA level was 48.6 mmol/L and CA199 level was 39.3 mmol/L. Because TAS-102 is not approved in China, from January 30 to August 6, 2020, this patient received 11 cycles of cetuximab, 500 mg/m (2) biweekly, in combination with fruquintinib, 5 mg once daily for the first 3 weeks of each 4 weeks as the fifth-line therapy. During this period, reexamination by abdominal contrast-enhanced CT on April 3, 2020, indicated stable disease (SD) with tumor shrinkage. Reexamination by the chest and abdominal contrast-enhanced CT on June 6, 2020, indicated SD (**Figure 1**). CEA and CA199 levels were decreased to 20.33 mmol/L and 13.89 mmol/L, respectively. The last evaluation was conducted in August 2020, and the progression-free survival (PFS) was 8 months. During the treatment, the patient had elevated grade 1 aspartate aminotransferase and alanine aminotransferase, elevated grade 1 hypercalcemia, and grade 1 acne-like rash. There was no other obvious side effect.

CURRENT STATUS OF THE THIRD-LINE REGIMEN

As an oral small-molecule multi-target kinase inhibitor, regorafenib inhibits multiple targets, including VEGFR1, VEGFR2, VEGFR3, TIE2, Kit, RET, PDGFR, and FGFR1 (2). The CORRECT trial and the CONCUR trial using the third-line therapy in CRC patients have shown that the median OS (mOS) of the regorafenib group is significantly better compared with the placebo group (6.4, 8.8 months vs. 5.0, 6.3 months, HR=0.77) (3, 4). Fruquintinib is a small-molecule antiangiogenic agent independently developed in China. The results of the FRESCO trial have indicated that the mOS of Chinese CRC patients treated with fruquintinib as the third-line therapy is significantly prolonged compared with the patients receiving placebo (mOS: 9.3 months vs. 6.6 months, HR=0.65) (5). TAS-102 is a new type of cytotoxic antineoplastic drug used in the third-line therapy. TAS-102 significantly prolonged the OS compared with the placebo group in advanced CRC patients (6, 10). Cetuximab is an anti-EGFR monoclonal antibody recommended to be used as a third-line therapy for anti-EGFR-therapy naïve, RAS wild-type advanced CRC patients (11). Cetuximab can be rechallenged in CRC patients resistant to cetuximab. It has been found that after the discontinuation of anti-EGFR monoclonal antibodies, *RAS* and *EGFR* relative mutant allele frequency decays exponentially (r^2 = 0.93 for *RAS*; r^2 = 0.94 for *EGFR*) with a cumulative half-life of 4.4 months. This finding supported the re-challenge of anti-EGFR monoclonal antibodies after the initial failure and guided the optimal timing of re-challenge initiation (12). A phase II single-arm study has reported a response rate of

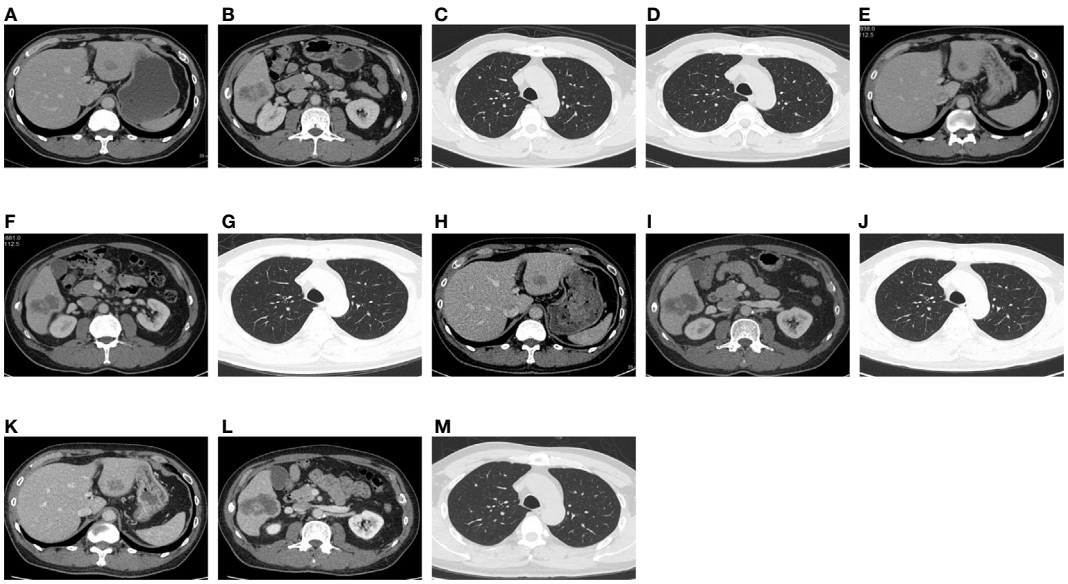

FIGURE 1 | On December 18, 2019, CT showed hepatic S3 metastases with a long diameter of 1.8 cm **(A)**, hepatic S6 metastases with a long diameter of 4.4 cm **(B)**, right upper lung metastases with a long diameter of 0.3 cm **(C)**, and a metastatic tumor of left upper lung, with a long diameter of 0.25 cm **(D)**. On April 3, 2020, CT showed hepatic S3 metastases with a long diameter of 1.4 cm **(E)**, hepatic S6 metastases with a long diameter of 4.5 cm **(F)**, and right upper lung metastases with a long diameter of 0.3 cm **(G)**. The original left upper pulmonary nodule was not shown. On June 6, 2020, CT showed hepatic S3 metastases with a long diameter of 2.1 cm **(H)**, hepatic S6 metastases with a long diameter of 5.2 cm **(I)**, and right upper lung metastases with a long diameter of 0.3 cm **(J)**. The original left upper pulmonary nodule was not shown. On August 6, 2020, CT showed hepatic S3 metastases with a long diameter of 2.1 cm **(K)**, hepatic S6 metastases with a long diameter of 5.5 cm **(L)**, and right upper lung metastases with a long diameter of 0.3 cm **(M)**. The original left upper pulmonary nodule was not shown.

21% for the rechallenged use of cetuximab. Patients with RAS wild-type ctDNA have significantly longer PFS than RAS-mutated patients (median PFS, 4.0 vs. 1.9 months) (13). The re-challenging regimen usually uses cetuximab plus irinotecan. However, only few studies have focused on the combined use of cetuximab and antiangiogenic agents.

THE MECHANISMS OF COMBINATION OF ANTI-EGFR AND ANTI-VEGF DRUGS

The VEGF and EGFR share the same downstream signal transduction components. Therefore, therapies targeting these two pathways may have additive or even synergistic therapeutic effects. Compared with the inhibition of a single pathway, the combination of VEGF antisense oligonucleotides and cetuximab to block VEGF and EGFR enhanced the antitumor activity and improve the survival rate in mice carrying CRC xenografts of human GEO colon cancer cells (14). Similarly, the combination treatment of cetuximab and antiVEGF-2 monoclonal antibodies improved the antitumor activity of mice with metastasis induced by the intraperitoneal injection of KM12L4 human colon cancer cells (15). Treatment with anti-EGFR monoclonal antibodies can inhibit VEGF production, while treatment with vandetanib (a tyrosine kinase inhibitor of VEGF receptors) can prevent epidermal growth factor-induced EGFR phosphorylation (16). Anti-VEGF and EGFR antibodies could not only reduce CRC cells proliferation and invasion *in vitro*, but also inhibit the tumor growth and angiogenesis *in vivo* through inhibiting the activation of AKT and ERK signaling pathways. This study partly explains the underlying mechanisms of the combinational use of anti-VEGF and anti-EGFR drugs (17). These preclinical studies with improved tumor inhibition may be attributed to elucidate the interaction between VEGF and EGFR signaling pathways.

Furthermore, anti-VEGF and anti-EGFR can also affect tumor microenvironment (TME). Cetuximab can stimulate antibody-dependent cell-mediated cytotoxicity (ADCC) and induce innate and adaptive immunity (18). Anti-VEGF can increase the infiltration of immune effector cells into tumors and convert the intrinsically immunosuppressive tumor microenvironment to an immune-supportive one (19). Regorafenib has the important effect of enhancing anti-tumor immunity *via* macrophage modulation and anti-immunosuppression by inhibiting CSF1R (20, 21). But their combinational effect on TME remains unknown. Therefore, the effect of this combination regimen on TME warrants further investigation.

CLINICAL TRIALS ON COMBINATIONAL USE OF ANTI-EGFR AND ANTI-VASCULAR MONOCLONAL ANTIBODIES

The BOND-2 study is a phase II clinical trial of cetuximab, bevacizumab, and irinotecan compared with cetuximab and

bevacizumab alone in irinotecan-refractory colorectal cancer. It showed that the time to tumor progression (TTP) is 7.3 months in patients receiving the combination treatment of cetuximab, bevacizumab, and irinotecan. The response rate is 37%, and the OS is 14.5 months. These response rates are superior to that of other studies involving patients with refractory mCRC (22). However, the subsequent phase III trial does not show the same results. PACCE is a phase III randomized open-label clinical trial to evaluate the efficacy of oxaliplatin or irinotecan plus bevacizumab with or without panitumumab as the first-line therapy in mCRC (23).

The results in the combination group do not indicate benefit in PFS and OS (PFS: 10.0 months vs.11.4 months; HR 1.27; OS: 19.4 *vs.* 24.5 months; HR, 1.43). CAIRO2 is a phase III randomized open-label clinical trial, which evaluates the efficacy and safety of bevacizumab and capecitabine/oxaliplatin with or without cetuximab as the first-line therapy in 755 mCRC patients (24). The efficacy endpoint showed a shortened PFS in the patients receiving the combination treatment of bevacizumab and cetuximab (9.4 months vs. 10.7 months; HR, 1.22). The overall incidence of grade 3/4 toxicity in the combination treatment group is significantly increased. Therefore, the current anti-EGFR drug in combination with macromolecule bevacizumab for the treatment of advanced CRC has not been approved (**Table 1**).

CLINICAL TRIALS ON COMBINATION TREATMENT OF ANTI-EGFR AND SMALL-MOLECULE ANTI-VEGF DRUGS

Fruquintinib and regorafenib are all small-molecule anti-VEGF agents. Fruquintinib and regorafenib are VEGFR1/2/3 inhibitors with high selectivity (25), that inhibit tumor cell proliferation and angiogenesis (26). Clinical studies have indicated that bevacizumab-resistant CRC patients can be benefited from fruquintinib and regorafenib treatment (3–5), most likely associated with the fact that bevacizumab only targets VEGF1, and the bypass is activated. The resistance to bevacizumab is mostly attributed to the activation of other VEGFs. Therefore, switching to fruquintinib and regorafenib has some efficacy and been clinically validated. The macromolecular anti-vascular drug bevacizumab in combination with anti-EGFR drugs has no clinical effect in the treatment of CRC, which may be related to the single inhibitory target of bevacizumab and macromolecular monoclonal antibody. According to preclinical studies (12–14), anti-VEGF and anti-EGFR may have a synergistic effect. An exploratory study of regorafenib in combination with cetuximab in the treatment of advanced tumors has been performed. Early clinical studies and subsequent phase IB studies have shown a certain effective rate in the treatment of advanced tumors (27, 28). In the early clinical trial, one CRC patient achieves PR, and the subsequent phase IB study has reported that one CRC patient among five patients achieves PR. These two clinical studies have demonstrated a certain efficacy of regorafenib in combination with cetuximab in cancers. The patients can generally tolerate the toxic and side effects after dose adjustment. However, the patients enrolled in these two studies have diverse cancers. Therefore, the trials do not clearly reflect the efficacy of CRC patients.

Currently, there is no report on fruquintinib in combination with cetuximab in the treatment of mCRC. In this case, the patient with mCRC underwent the fourth-line treatment with cetuximab and regorafenib. The efficacy was SD and the PFS exceeded 8 months. No serious side effects were observed in this patient, and the tolerability was acceptable. Compared with the single-agent fruquintinib with a PFS of 3.71 months, the combinational treatment was more effective than treatment with fruquitinib alone, and it may help to reverse the resistance to chemotherapy, cetuximab and regorafenib. The reason might be partly attributed to the mutual synergy of anti-EGFR drug cetuximab in combination with the anti-vascular drug fruquintinib. The mechanism underlying the reversed resistance should be further explored. The major limitation of this study is that, this combinational use is in only one case study. The clinical effects of small-molecule anti-vascular drugs in combination with cetuximab in the treatment of CRC should be further investigated.

CONCLUSION

Patients with advanced RAS/BRAF wild-type CRC after resistance to third-line therapy should consider using the

TABLE 1 | Combination treatment of anti-EGFR and anti-VEGF drugs in patients with metastatic colorectal Cancer.

Trails	Phase	Arm	Number	(RR%)	P Value	Time (m)	P Value	OS (m)	P Value
Saltz LB (22)	II	CBI	43	37	NA	7.3 (TTP)	NA	14.5	NA
		CB	40	22		4.9		11.4	
Hecht JR (23)	IIIB	PBC	823	46	NS	10 (PFS)	NA	18.4	0.16
		BC	230	48		11.4		not reached	
Tol J (24)	III	CB*	378	50	0.49	10.7 (PFS)	P=0.01	20.3	NS
		CBC*	377	52.7		9.4		19.4	

RR, response rate; TTP, time to tumor progression; OS, overall survival; CBI, cetuximab bevacizumab and irinotecan; CB, cetuximab and bevacizumab alone; PBC, bevacizumab and chemotherapy with panitumumab; BC, bevacizumab and chemotherapy; CB, capecitabine oxaliplatin, and bevacizumab; CBC*, capecitabine oxaliplatin, and bevacizumab plus cetuximab; NA, not applicable; NS, not statistically significant.*

combination of small-molecule antiangiogenic agents and anti-EGFR drugs.

AUTHOR CONTRIBUTIONS

HZ conceived and designed the study. YL drafted the manuscript. All authors contributed to the article and approved the submitted version.

FUNDING

This work was supported by the Foundation of Guangdong Provincial Hospital of Chinese Medicine (2017KT1820).

ACKNOWLEDGMENTS

Authors would like to thank UNIWINSCI. INC for editing the article.

REFERENCES

1. Venook AP, Niedzwiecki D, Lenz HJ, Innocenti F, Fruth B, Meyerhardt JA, et al. Effect of First-Line Chemotherapy Combined With Cetuximab or Bevacizumab on Overall Survival in Patients With KRAS Wild-Type Advanced or Metastatic Colorectal Cancer: A Randomized Clinical Trial. *JAMA* (2017) 317:2392–401. doi: 10.1001/jama.2017.7105
2. Wilhelm SM, Dumas J, Adnane L, Lynch M, Carter CA, Schütz G, et al. Regorafenib (BAY 73-4506): A New Oral Multikinase Inhibitor of Angiogenic, Stromal and Oncogenic Receptor Tyrosine Kinases With Potent Preclinical Antitumor Activity. *Int J Cancer* (2011) 129(1):245–55. doi: 10.1002/ijc.25864
3. Grothey A, Van Cutsem E, Sobrero A, Siena S, Falcone A, Ychou M, et al. Regorafenib Monotherapy for Previously Treated Metastatic Colorectal Cancer (CORRECT): An International, Multicentre, Randomised, Placebo-Controlled, Phase 3 Trial. *Lancet* (2013) 381(9863):303–12. doi: 10.1016/S0140-6736(12)61900-X
4. Li J, Qin S, Xu R, Yau TC, Ma B, Pan H, et al. Regorafenib Plus Best Supportive Care Versus Placebo Plus Best Supportive Care in Asian Patients With Previously Treated Metastatic Colorectal Cancer (CONCUR): A Randomised, Double-Blind, Placebo-Controlled, Phase 3 Trial. *Lancet Oncol* (2015) 16(6):619–29. doi: 10.1016/S1470-2045(15)70156-7
5. Li J, Qin S, Xu RH, Shen L, Xu J, Bai Y, et al. Effect of Fruquintinib vs Placebo on Overall Survival in Patients With Previously Treated Metastatic Colorectal Cancer: The FRESCO Randomized Clinical Trial. *JAMA* (2018) 319(24):2486. doi: 10.1001/jama.2018.7855
6. Mayer RJ, Van Cutsem E, Falcone A, Yoshino T, Garcia-Carbonero R, Mizunuma N, et al. Randomized Trial of TAS-102 for Refractory Metastatic Colorectal Cancer. *N Engl J Med* (2015) 372(20):1909–19. doi: 10.1056/NEJMoa1414325
7. Huynh JC, Schwab E, Ji J, Kim E, Joseph A, Hendifar A, et al. Recent Advances in Targeted Therapies for Advanced Gastrointestinal Malignancies. *Cancers (Basel)* (2020) 12(5):1168. doi: 10.3390/cancers12051168
8. Fukuoka S, Hara H, Takahashi N, Kojima T, Kawazoe A, Asayama M, et al. Regorafenib Plus Nivolumab in Patients With Advanced Gastric or Colorectal Cancer: An Open-Label, Dose-Escalation, and Dose-Expansion Phase Ib Trial (Regonivo, Epoc1603). *J Clin Oncol* (2020) 38(18):2053–61. doi: 10.1200/JCO.19.03296
9. Nakajima H, Fukuoka S, Moriwaki T, Masuishi T, Takashima A, Kumekawa Y, et al. Clinical impact of primary tumor location in patients with metastatic colorectal cancer (mCRC) treated with regorafenib or trifluridine/tipiracil as later-line. *J Clin Oncol* (2020) 38(suppl 4; abstr 105):25.
10. Xu J, Kim TW, Shen L, Sriuranpong V, Pan H, Xu R, et al. Results of a Randomized, Doubleblind, Placebo-Controlled, Phase III Trial of Trifluridine/Tipiracil (Tas-102) Monotherapy in Asian Patients With Previously Treated Metastatic Colorectal Cancer: The Terra Study. *J Clin Oncol* (2018) 36(4):350–8. doi: 10.1200/JCO.2017.74.3245
11. Cunningham D, Humblet Y, Siena S, Khayat D, Bleiberg H, Santoro A, et al. Cetuximab Monotherapy and Cetuximab Plus Irinotecan in Irinotecan Refractory Metastatic Colorectal Cancer. Cetuximab Monotherapy and Cetuximab Plus Irinotecan in Irinotecan Refractory Metastatic Colorectal Cancer. *N Engl J Med* (2004) 351:337–45. doi: 10.1056/NEJMoa033025
12. Parseghian CM, Loree JM, Morris VK, Liu X, Clifton KK, Napolitano S, et al. Anti-EGFR-resistant Clones Decay Exponentially After Progression: Implications for anti-EGFR Re-Challenge. *Ann Oncol* (2019) 30(2):243–9. doi: 10.1093/annonc/mdy509
13. Cremolini C, Rossini D, Dell'Aquila E, Lonardi S, Conca E, Del Re M, et al. Rechallenge for Patients With RAS and BRAF Wild-Type Metastatic Colorectal Cancer With Acquired Resistance to First-line Cetuximab and Irinotecan: A Phase 2 Single-Arm Clinical Trial. *JAMA Oncol* (2019) 5 (3):343–50. doi: 10.1001/jamaoncol.2018.5080
14. Ciardiello F, Bianco R, Damiano V, Fontanini G, Caputo R, Pomatico G, et al. Antiangiogenic and Antitumor Activity of Anti-Epidermal Growth Factor Receptor C225 Monoclonal Antibody in Combination With Vascular Endothelial Growth Factor Antisense Oligonucleotide in Human GEO Colon Cancer Cells. *Clin Cancer Res* (2000) 6:3739–47.
15. Shaheen RM, Ahmad SA, Liu W, Reinmuth N, Jung YD, Tseng WW, et al. Inhibited Growth of Colon Cancer Carcinomatosis by Antibodies to Vascular Endothelial and Epidermal Growth Factor Receptors. *Brit J Cancer* (2001) 85:584–9. doi: 10.1054/bjoc.2001.1936
16. Ciardiello F, Caputo R, Damiano V, Caputo R, Troiani T, Vitagliano D, et al. Antitumor Effffects of ZD6474, a Small Molecule Vascular Endothelial Growth Factor Receptor Tyrosine Kinase Inhibitor, With Additional Activity Against Epidermal Growth Factor Receptor Tyrosine Kinase. *Clin Cancer Res* (2003) 9:1546–56.
17. Ding C, Li L, Yang T, Fan X, Wu G. Combined Application of anti-VEGF and anti-EGFR Attenuates the Growth and Angiogenesis of Colorectal Cancer Mainly Through Suppressing AKT and ERK Signaling in Mice Model. *BMC Cancer* (2016) 16(1):791. doi: 10.1186/s12885-016-2834-8
18. Ferris RL, Lenz HJ, Trotta AM, García-Foncillas J, Schulten J, Audhuy F, et al. Rationale for Combination of Therapeutic Antibodies Targeting Tumor Cells and Immune Checkpoint Receptors: Harnessing Innate and Adaptive Immunity Through IgG1 Isotype Immune Effector Stimulation. *Cancer Treat Rev* (2018) 63:48–60. doi: 10.1016/j.ctrv.2017.11.008
19. Fukumura D, Kloepper J, Amoozgar Z, Duda DG, Jain RK. Enhancing Cancer Immunotherapy Using Antiangiogenics: Opportunities and Challenges. *Nat Rev Clin Oncol* (2018) 15(5):325–40. doi: 10.1038/nrclinonc.2018.29
20. Arai H, Battaglin F, Wang J, Lo JH, Soni S, Zhang W, et al. Molecular Insight of Regorafenib Treatment for Colorectal Cancer. *Cancer Treat Rev* (2019) 81:101912. doi: 10.1016/j.ctrv.2019.101912
21. Hoff S, Grünewald S, Röse L, Zopf D. Immunomodulation by Regorafenibalone and in Combination With Anti PD1 Antibody on Murine Models of Colorectal Cancer. *Ann Oncol* (2017) 28(suppl_5):1198. doi: 10.1093/annonc/mdx376.060
22. Saltz LB, Lenz HJ, Kindler HL, Hochster HS, Wadler S, Hoff PM, et al. Randomized Phase II Trial of Cetuximab, Bevacizumab, and Irinotecan Compared With Cetuximab and Bevacizumab Alone in Irinotecan Refractory Colorectal Cancer: The BOND-2 Study. *J Clin Oncol* (2007) 25:4557–61. doi: 10.1200/JCO.2007.12.0949
23. Hecht JR, Mitchell E, Chidiac T, Scroggin C, Hagenstad C, Spigel D, et al. A Randomized Phase IIIB Trial of Chemotherapy, Bevacizumab, and Panitumumab Compared With Chemotherapy and Bevacizumab Alone for Metastatic Colorectal Cancer. *J Clin Oncol* (2009) 27:672–80. doi: 10.1200/JCO.2008.19.8135
24. Tol J, Koopman M, Cats A, Rodenburg CJ, Creemers GJ, Schrama JG, et al. Chemotherapy, Bevacizumab, and Cetuximab in Metastatic Colorectal Cancer. *N Eng J Med* (2009) 360:563–72. doi: 10.1056/NEJMoa0808268
25. Cao J, Zhang J, Peng W, Chen Z, Fan S, Su W, et al. A Phase I Study of Safety and Pharmacokinetics of Fruquintinib, a Novel Selective Inhibitor of Vascular

Endothelial Growth Factor receptor-1, –2, and –3 Tyrosine Kinases in Chinese Patients With Advanced Solid Tumors. *Cancer Chemother Pharmacol* (2016) 78:259–69. doi: 10.1007/s00280-016-3069-8

26. Hicklin DJ, Ellis LM. Role of the Vascular Endothelial Growth Factor Pathway in Tumor Growth and Angiogenesis. *J Clin Oncol* (2005) 23:1011–27. doi: 10.1200/JCO.2005.06.081
27. Weekes C, Lockhart AC, Lee JJ, Sturm I, Cleton A, Huang F, et al. A Phase 1b Study Evaluating the Safety and Pharmacokinetics of Regorafenib in Combination With Cetuximab in Patients With Advanced Solid Tumors. *Int J Cancer* (2019) 145:2450–8. doi: 10.1002/ijc.32317
28. Subbiah V, Khawaja MR, Hong DS, Amini B, Yungfang J, Liu H, et al. First-in-Human Trial of Multikinase VEGF Inhibitor Regorafenib and anti-EGFR Antibody Cetuximab in Advanced Cancer Patients. *JCI Insight* (2017) 2(8): e90380. doi: 10.1172/jci.insight.90380

Conflict of Interest: The authors declare that the research was conducted in the absence of any commercial or financial relationships that could be construed as a potential conflict of interest.

frontiers in Oncology

ORIGINAL RESEARCH
published: 03 June 2021
doi: 10.3389/fonc.2021.672222

EMT and Cancer Cell Stemness Associated With Chemotherapeutic Resistance in Esophageal Cancer

Xiaojie Liu[1,2,3], *Mingjing He*[1,2,3], *Linlin Li*[1,2,3], *Xiya Wang*[1,2,3], *Shuhua Han*[1,2,3], *Jinzhu Zhao*[1,2,3], *Yalong Dong*[1,2,3], *Mushtaq Ahmad*[1,2,3], *Leilei Li*[1,2,3], *Xueyan Zhang*[1,2,3], *Junfeng Huo*[1,2,3], *Yunfan Liu*[1], *Chengxue Pan*[1,3*] *and Cong Wang*[1,2,3*]

[1] School of Pharmaceutical Sciences, Zhengzhou University, Zhengzhou, China, [2] State Key Laboratory of Esophageal Cancer Prevention and Treatment, Zhengzhou, China, [3] Key Laboratory of Advanced Drug Preparation Technologies, Ministry of Education of China, Zhengzhou, China

OPEN ACCESS

Edited by:
Dong-Hua Yang,
St. John's University,
United States

Reviewed by:
Zheng Qiu,
China Pharmaceutical University,
China
Lingzhi Li,
University of Texas MD Anderson
Cancer Center,
United States

***Correspondence:**
Cong Wang
wangcong@zzu.edu.cn
Chengxue Pan
pancx@zzu.edu.cn

Specialty section:
This article was submitted to
Gastrointestinal Cancers,
a section of the journal
Frontiers in Oncology

Received: 25 February 2021
Accepted: 05 May 2021
Published: 03 June 2021

Citation:
Liu X, He M, Li L, Wang X, Han S, Zhao J, Dong Y, Ahmad M, Li L, Zhang X, Huo J, Liu Y, Pan C and Wang C (2021) EMT and Cancer Cell Stemness Associated With Chemotherapeutic Resistance in Esophageal Cancer. Front. Oncol. 11:672222. doi: 10.3389/fonc.2021.672222

Drug resistance often occurs after chemotherapy in esophageal cancer patients, leading to cancer metastasis and recurrence. However, the relationship among cancer cell migration, recurrence and drug resistance in esophageal cancer drug-resistant cells has not been clearly explained. In this study, we constructed paclitaxel (PTX)-resistant esophageal cancer cells to explore the causes of drug resistance and poor prognosis after chemotherapy in esophageal cancer. Colony formation assay was used to evaluate the difference of colony formation between parental cells and drug resistance cells. Microsphere formation assay was used to examine the phenotype of stem cells. Wound healing and Transwell assays were used to detect the migration ability of drug-resistant cells. Western blotting and immunofluorescence assays were used to explore the mechanisms. Finally, we used nude mouse xenograft model to explore the tumor characteristics and the expression of relative proteins to verify our findings *in vivo*. Our study demonstrated that the cancer cell stemness characteristics exist in drug-resistant esophageal cancer cells, that expressed the biomarkers of stem cells and were prone to epithelial-mesenchymal transition (EMT). Our results suggested that the expression of EMT biomarkers and stemness-related proteins increased in esophageal cancer cells after continuously using chemotherapeutic drugs for a period of time. This study indicated that simultaneously targeting EMT and stemness could be a better strategy for the treatment of esophageal cancer drug resistance.

Keywords: esophageal cancer, drug resistance, paclitaxel, epithelial-mesenchymal transition, stemness

INTRODUCTION

Esophageal cancer is one of the most common human digestive tract cancers and ranked as the sixth leading cause of cancer-related death worldwide (1). The 5-year overall survival rate of patients with advanced esophageal cancer is less than 10% (2). Esophageal squamous cell carcinoma (ESCC), as the predominant histologic type in China, seriously endangering people's health (3). Surgical treatment, radiation therapy, chemotherapy, targeted therapy, and immunotherapy are accepted treatment options

for patients. Among them, chemotherapy plays a dominant role. Chemotherapeutic agents, such as paclitaxel (PTX), are used widely for the treatment of advanced human cancers. However, long-term application of chemotherapeutic agents often leads to drug resistance even they are effective initially (4). In particular, tumor cells are more prone to invasion, metastasis, and recurrence after cancers develop chemotherapeutic resistance, leading to poor prognosis.

Cancer stem cells (CSCs) refer to a group of tumor cells with self-renewal capacity and differentiation potential, which can re-initiate tumor formation (5, 6). Studies have shown that the increase of recognizable stemness-related biomarkers in tumor cells is associated with driving the proliferation of tumor cells, the resistance of treatment and the recurrence of cancers (7–10). Previous studies have shown that CSCs exist in esophageal cancer (11). Although there is less consensus on biomarkers of CSCs in esophageal cancer so far, it has been determined that the poor prognosis of esophageal cancer patients is closely related to CSCs (12, 13).

CSCs also showed the tendency to invade and metastasize (14, 15). Epithelial-mesenchymal transition (EMT) plays a significant role in cancer metastasis and invasion (16). EMT, which transforms polarized epithelial cells to a motile mesenchymal phenotype, plays a primary role in morphologic changes in various physiological processes (17). A number of studies have shown that EMT contributes to the early spread of cancer cells, which is often activated during tumor invasion and metastasis (18). EMT is closely associated with poor prognosis in multiple types of cancers, including prostate cancer (19), breast cancer (20), lung cancer (21), hepatocellular carcinoma (22), and other cancers.

In this study, we investigate the association of cancer cell stemness along with EMT characteristics in drug-resistant esophageal cancer cells.

MATERIALS AND METHODS

Materials

Paclitaxel was purchased from Hainan Quanxing Pharmaceutical Co., Ltd. (Hainan, China). MTT (3-(4,5-dimethyl-2-thiazolyl)-2,5-diphenyl-2-H-tetrazolium bromide) was purchased from Solarbio (Beijing, China). DMSO (Dimethyl sulfoxide) was acquired from Solarbio (Shanghai, China). Hoechst 33258 was purchased from Beyotime Biotechnology (Shanghai, China). Primary antibodies against ZO-1, Claudin-1, E-cadherin, β-catenin, Vimentin, N-cadherin, NANOG, SOX2, and OCT4 were purchased from Cell Signaling Technology, Inc. (Danvers, MA, USA).

Cell Culture

Human esophageal cancer cell lines TE-1 was purchased from the Chinese Academy of Sciences (Shanghai, China), EC109 was purchased from the Institute of Basic Medical Sciences Chinese Academy of Medical Sciences & School of Basic Medicine Peking Union Medical College (Beijing, China). Esophageal cancer cell lines resistant to paclitaxel (TE-1/PTX and EC109/PTX) were established in our team according to the method of LIU-BIN GUO (23). All the cell lines were cultured in Roswell Park Memorial Institute (RPMI) 1640 (Biological Industries, Kibbutz Beit HaEmek, Israe) with 10% fetal bovine serum (FBS, purchased from Biological Industries, Kibbutz Beit HaEmek, Israel). Cells were incubated at 37°C in a humidified atmosphere containing 5% CO_2.

Cell Sensitivity Assay

Cell sensitivity to PTX was examined by MTT assay. Briefly, cells were seeded in the 96-well plate at a density of 4.5×10^3 cells per well and incubated overnight. After that, the medium was changed to fresh medium containing various concentrations of PTX. After 72 h, 20 μl MTT was added to each well and cells were incubated for 4 h with MTT at the concentration of 500 mg/ml. Then, the precipitate was dissolved completely by 150 μl DMSO and the light absorbance was measured at 570 nm using the Multiskan Spectrum spectrophotometer (BioTek Instruments, Inc. Vermont, USA).

Wound Healing Assay and Transwell Assay

Cells were seeded in six-well plate overnight and a sterile 100 μl pipette tip was used to scraped off a part of cells in each well. After that, plates were washed twice with PBS buffer solution to remove the detached cells. Subsequently, cells were incubated in culture medium with 2% FBS. The wound gaps were acquired by a microscope connected to a digital camera. After 24 and 48 h incubation, the wound gaps were acquired again, and the migration rates were evaluated.

Transwell assays were performed by Transwell chamber (Corning Life Sciences, NY, USA) in a 24-well plate. About 1×10^4 EC109 and EC109/PTX cells and 1×10^3 TE-1 and TE-1/PTX cells were added in the upper chamber in 300 μl culture medium with 0% FBS and 600 μl culture medium with 20% FBS was placed in the lower chamber. The cells were incubated at 37°C with 5% CO_2 for 24 h. At the end, the cells were stained by 1% crystal violet solution and imaged under a Nikon microscope.

Colony Formation Assay

1×10^3 cells were seeded per well in 6-wells plate with culture medium with 10% FBS. The cells were incubated for 10 days. After that, the cells were washed three times with PBS and fixed in methanol for 30 min. Cells were stained with 1% crystal violet for 30 min. Then, the cells were washed with PBS at least five times.

Sphere Formation Assay

200 cells of EC109, EC109/PTX, and TE-1, TE-1/PTX were cultured in serum-free medium DMEM/F12 containing supplement 2% B27 (Gibco, USA) and 0.1% growth factor EGF (Gibco, USA) in the ultra-low adsorption 96-well plate. Take photos every 24 h for a week under the microscope. The sphere numbers (diameter ≥50 μm) were calculated.

Limit Dilution Assay -Sphere Formation Assay

Limit dilution assay (LDA) was used to select the tight cloning of cells. 30 to 50 cells were seeded in the 6-well plates. After 2 to 3 weeks, the cells of tight cloning were selected under microscope. Cells were suspended, counted, and cultured in the medium of cancer stem cells (98 ml DMEM/F12 + 2 μg EGF + 2 μg bFGF + 275 2 μl insulin + 2 ml B27) in the ultra-low adsorption 24-well plate. 10 days later, take photos under the microscope.

Western Blotting

Cells were lysed on ice by RIPA lysis buffer containing phosphatase inhibitor cocktail and 1% protease for 30 min. Then, the lysates of the cells were centrifuged at 12,000 rpm for 10 min at 4°C and supernatant liquid were collected. The lysates were measured for protein concentration with a BCA protein assay kit. Total protein was resolved in 10% polyacrylamide gel by SDS-PAGE and transferred to polyvinylidene difluoride membranes. The nonspecific binding was blocked by 5% non-fat milk. The membranes were incubated with primary antibodies overnight at 4°C and then incubated with the secondary antibodies for 2 h at room temperature. The resolved protein bands were visualized by enhanced chemiluminescence (ECL) detection system. The densitometric analysis were performed using Image J software.

Immunofluorescence Analysis

The cells were seeded in 24-well plates. After incubating overnight, the cells were fixed with methanol, permeabilized 10 min with 0.1% Triton X-100, blocked 1 h with 5% BSA and incubated with the primary antibodies (SOX2 1: 200, NANOG 1: 200, OCT4 1: 200) at 4°C overnight. After that, the cells were washed with PBS and incubated 1 h with Alexa Fluor 561 goat anti-rabbit IgG and Alexa Fluor 488 goat anti- rabbit IgG at room temperature. The nuclei of the cells were counterstained 20 min with 10 μg/ml of Hoechst 33258 in the dark. Images were acquired by laser scanning confocal microscopy (Nikon, A1, Tokyo, Japan). Target protein staining was presented in red (TE-1 and TE-1/PTX) and green (EC109 and EC109/PTX), and the nuclei were stained with Hoechst 33258 (blue).

Tumor Growth *In Vivo*

Animal experiments were approved by the Institutional Animal Care and Use Committee of the Zhengzhou University. Approximately 5-week-old female nude mice were purchased from Hunan SJA Animal Laboratory Co. Ltd. The xenograft tumor model of nude mice was established. Briefly, 3×10^6 EC109 cells and EC109/PTX cells were subcutaneously implanted into the right scapula of the mice. The volume of the tumors and the weight of the mice were measured every 2 days. Tumor size were calculated using the formula (A×B×B)/2 (A was the longest diameter and B was the shortest diameter of the tumor). The mice were sacrificed after 20 days. Then, tumors were dissected and weighed. Besides, the whole blood and the serum were obtained before the mice were sacrificed.

Hematoxylin-Eosin Staining

Tumor tissues were embedded in paraffin, and the paraffin-embedded tissue was cut into 4- to 5-μm slices with a microtome. The slices were pasted on clean slides with ultrapure water, heated slightly with an alcohol lamp to make them flat. After that the paraffin slices were soaked in xylene for 20 min, they were soaked in gradient alcohol, soaked in ultrapure water for 5 min, then, soaked in PBS 20 min twice to carry out dewaxing and hydration. The slices were stained in hematoxylin staining solution for 2 min, rinsed with tap water and put into 1% alcoholic hydrochloric acid to decolorize and 1% ammonia solution to turn blue, and the nuclear staining was observed under a microscope, followed by putting into eosin staining solution for 1 min, tap water rinse and the staining was observed under the microscope. Before covering the slices, slides were dehydrated in gradient alcohol and cleared in xylene. They were sealed with neutral resin. The slices were dried and photographed using the Leica DM 3000 microscope at 200× magnification.

Statistical Analysis

All the experiments were independently repeated three times. Data were shown as mean ± SD. Statistical analysis was performed using one-way ANOVA, using the GraphPad Prism 8.0. All comparisons were made relative to controls and significance of difference was indicated as * $P < 0.05$ and ** $P < 0.01$.

RESULTS

Characterization of the Parental Cells and the Drug-Resistant Cells

EC109 and TE-1 were treated with different concentrations of PTX for 72 h, and MTT assay was applied to evaluate the sensitivity of cells to PTX. The results showed that the IC_{50} value is about 8.69 nmol and 93.88 nmol in the EC109 and its drug-resistant cells (EC109/PTX), respectively. The PTX-resistant index is 10.80. The IC_{50} value is about 5.47 nmol and 56.84 nmol in the TE-1 and its drug-resistant cells (TE-1/PTX), respectively. The PTX-resistant index is 10.38 (**Figure 1A** and **Table 1**). This result indicated that EC109/PTX and TE-1/PTX exhibited moderate drug resistance. Besides, we applied Cis-platinum and 5-Fluorouracil as the other drug sensitivity results upon PTX-resistant esophageal cancer cells. As a result, the Cis-platinum-resistant index is 2.36 (TE-1/PTX) and 1.54 (EC109/PTX), showed as mild drug resistance. The 5-Fluorouracil-resistant index is 3.10 (TE-1/PTX) and 9.93 (EC109/PTX), showed as mild drug resistance (TE-1/PTX) and moderate drug resistance (EC109/PTX). In other words, the resistant cells we stimulated were not only more resistant to the inducible drug PTX than the other therapeutic drugs but also showed different degrees of resistance to other therapeutic drugs (**Figure 1B** and **Table 2**). Morphologically, EC109 and TE-1 had regular form and uniform size, in contrast, EC109/PTX and TE-1/PTX lost their original shape and became elongated (**Figure 1C**), indicating that the cells changed after they gained drug resistance. The colony formation ability of the parental cells was significantly higher than that of the drug-resistant cancer cells in the colony formation assay. While when the parental cells and resistant cells were treated with PTX solvent as control, the colony formation ability of the parental cells was significantly lower than that of the drug-resistant cancer cells. This result further suggested that the drug-resistant cells were more resistant to paclitaxel than the parental cells (**Figures 1D, E**).

PTX-Treated Cancer Cell Lines Showed Properties of Cancer Cell Stemness

The microsphere formation assay was used to test the property of cancer cell stemness, and the results showed that the

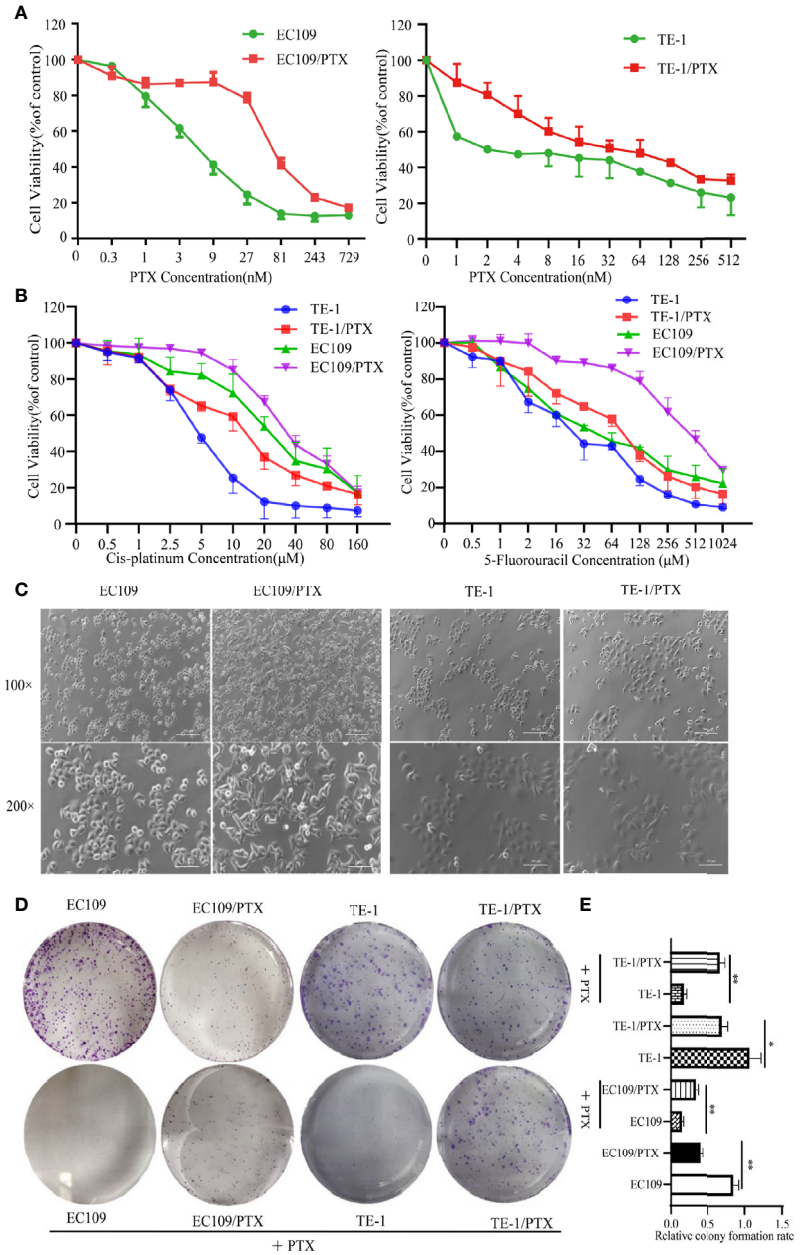

FIGURE 1 | PTX-resistant EC109 and TE-1cells. **(A, B)** MTT assay on the survival of parental cells and PTX-resistant cells under the treatment with PTX, Cis-platinum and 5-Fluorouracil. **(C)** Cell morphology photographed under an inverted microscope. Scale bar: 500 μm (100×), 250 μm (200×). **(D)** Colony formation assay on the two groups of cells and the corresponding PTX solvent as control. **(E)** The corresponding statistical results of colony formation. *$P < 0.05$ indicates statistically significance *vs*. parental cells. **$P < 0.01$ indicates highly statistically significant *vs*. parental cells.

TABLE 1 | Drug sensitivity tests (PTX).

Cell lines	IC_{50} ± SD (nM)	Resistant Index
EC109	8.69 ± 2.06	–
EC109/PTX	93.88 ± 7.36	10.80 ± 2.32
TE-1	5.47 ± 0.18	–
TE-1/PTX	56.84 ± 2.31	10.38 ± 0.08

The results are shown as mean ± SD.

TABLE 2 | Drug sensitivity tests (Cis-platinum and 5-Fluorouracil).

Cell lines	IC_{50} ± SD (Cis-platinum, μM)	Resistant Index	IC_{50} ± SD (5-Fluorouracil, μM)	Resistant Index
EC109	5.52 ± 0.73	–	21.53 ± 4.04	–
EC109/PTX	13.01 ± 0.14	2.36 ± 0.03	66.81 ± 2.18	3.10 ± 1.29
TE-1	25.84 ± 1.45	–	47.29 ± 3.67	–
TE-1/PTX	39.72 ± 3.09	1.54 ± 0.29	469.64 ± 24.31	9.93 ± 0.49

The results are shown as mean ± SD.

microsphere formation rate in EC109/PTX and TE-1/PTX is 1.63-fold and 3.35-fold greater than their parental cells respectively (**Figures 2A, B**). Besides, we used LDA to repeat sphere formation. The results showed that the microsphere formation rate in EC109/PTX and TE-1/PTX was greater than their parental cells respectively. Also, in general, the microsphere in EC109/PTX and TE-1/PTX was bigger than that in their parental cells, respectively (**Figures 2C, D**). These results indicated that the self-renewal ability of drug-resistant cells is stronger than the parental cells. Western blotting assay was used to examine the expression of related proteins, and the result showed that the expression of embryonic stem cell transcription factors NANOG, OCT4, and SOX2 enhanced in the drug-resistant cell lines (TE-1/PTX and EC109/PTX) (**Figures 2E, F**). The immunofluorescence analysis showed similar results as the Western blotting (**Figures 2G, H**).

The Migratory Ability Enhanced and the Expression of EMT-Related Protein Changed in the drug-Resistant Cells

Wound healing and Transwell assays were used to investigate the difference of cell migration ability in the drug sensitive and -resistant cells. The results of the wound healing assay indicated that after culturing the cells for 24 and 48 h, the size of the healed space in EC109 and TE-1 cells is 1.875-fold and 1.64-fold greater than that of EC109/PTX and TE-1/PTX cells (**Figures 3A, B**). The results of the Transwell assay indicated that the number of the migrated EC109/PTX and TE-1/PTX cells was 4.2-fold and 2.3-fold of that of EC109 and TE-1 cells (**Figures 3C, D**). These results suggested that once the cells gained the drug-resistant property, they have stronger ability of migration and invasion than their parental cells. Western blotting assay was used to explore the expression of EMT-related proteins. The results showed that the expression of the epithelial protein biomarkers Claudin-1, ZO-1, and E-cadherin were decreased in the drug-resistant cells, while the expression of the mesenchymal protein biomarkers Vimentin, N-cadherin, and the transcription factor β-catenin were increased (**Figures 3E–G**).

EMT-Related and Stemness-Related Proteins in the Drug-Resistant Cells Increased *In Vivo*

To further explore the EMT and stemness in the drug-resistant esophageal cancer, we applied the xenograft tumor model in nude mice. It was found that, there is hardly any difference in the Blood Biochemical Index and Serum Biochemical Indices(ALT, AST and creatinine), except the uric acid and white blood cells. The level of Uric acid in the drug-resistant cells group is lower than that in the parental cells group, but both of them are in the normal range. It was also found that there was no significant difference in liver and kidney function between the mice in the parental cells group and the drug-resistant cells group. The difference in the white blood cells exist in the PTX -resistant cells group, and might due to the bone marrow inhibition, causing decrease of white blood cells (**Tables 3**, **4**). The mice were sacrificed when we finished collecting blood from the eyeball. The average volume and the tumor weight of the in the mice of implanting EC109/PTX were smaller than the parental cells-group while the body weight was minimally affected (**Figures 4A–D**). The expression of EMT- and stemness-related proteins was analyzed. It was found that except E-cadherin, the expression of epithelial protein biomarkers ZO-1 and Claudin-1 were decreased in the group of EC109/PTX cells, while the expression of mesenchymal protein biomarkers Vimentin, N-cadherin, and the transcription factor TCF-8 and β-catenin were increased. The expression stemness-related proteins SOX2 and NANOG enhanced (**Figures 4E, F**). Besides, E-cadherin is related to proliferation closely and the volume of tumor tissue in the parent group increased significantly compared with the drug-resistant group *in vivo*. The expression of E-cadherin enhanced *in vivo*, which may be caused by the xenograft tumor model. In addition, hematoxylin-eosin staining was performed in tumor tissues (**Figure 4G**). These *in vivo* results showed that once the tumor cells became drug resistant, the expression of the CSCs biomarkers and the EMT biomarkers enhanced. All the results were in consistent with the results *in vitro*.

DISCUSSION

Chemotherapy using PTX as a first-line chemotherapeutic agent is the main treatment for patients with esophageal cancer (24, 25). However, drug resistance occurs in a large proportion of patients after treatment, which affects the efficacy of PTX treatment (26). In this study, we showed that esophageal cancer cells became less sensitive to PTX and exhibited moderate-drug-resistance after treatment with PTX. Moreover, the PTX-resistant cells develop stemness characteristics. We found that the expression of stem cell biomarkers NANOG, OCT4, SOX2 increased in the PTX-resistant esophageal cancer cells. Simultaneously, we found that the expression of epithelial biomarkers decreased and the mesenchymal biomarkers increased in drug-resistant esophageal cancer cells. Also, we verified these findings *in vivo* (**Figure 5**). OCT4, SOX2 and NANOG, as the embryonic stem cell transcription factors,

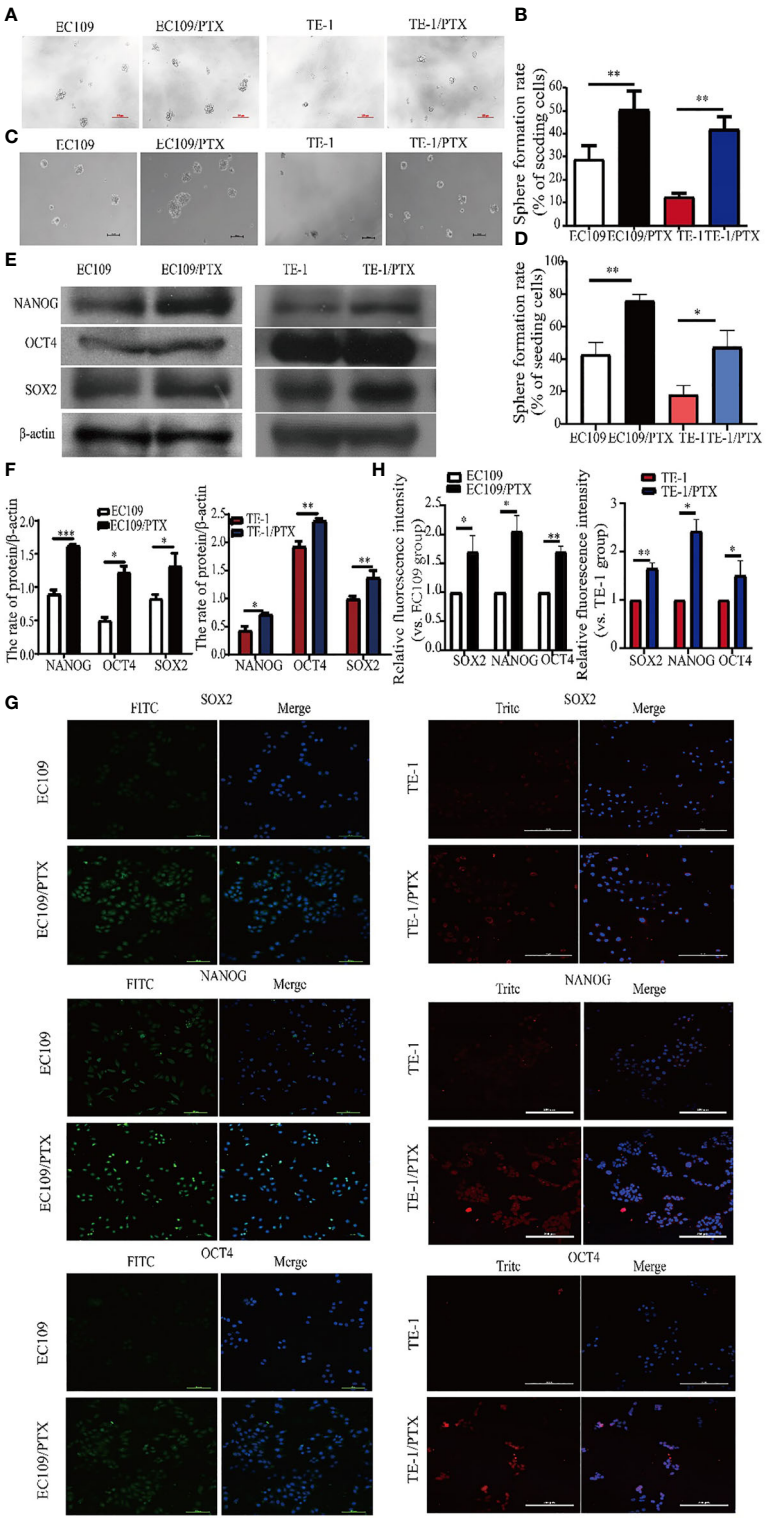

FIGURE 2 | Enhanced cancer cell stemness in the drug-resistant cells. **(A, B)** Sphere formation assay on the two groups of cells and the corresponding statistical results. Scale bar: 100 μm. **(C, D)** LDA-Sphere formation assay on the two groups of cells and the corresponding statistical results. Scale bar: 100 μm. **(E, F)** Western blotting on the stem cell protein biomarkers and the corresponding statistical results. **(G, H)** Immunofluorescence analysis detected the expression of stem cell protein biomarkers NANOG, OCT4 and SOX2 in the two groups of cells. Scale bar: 100 μm (TE-1, TE-1/PTX), 200 μm (EC109, EC109/PTX). *$P < 0.05$ indicates statistically significance *vs*. parental cells. **$P < 0.01$ indicates highly statistically significant *vs*. parental cells.

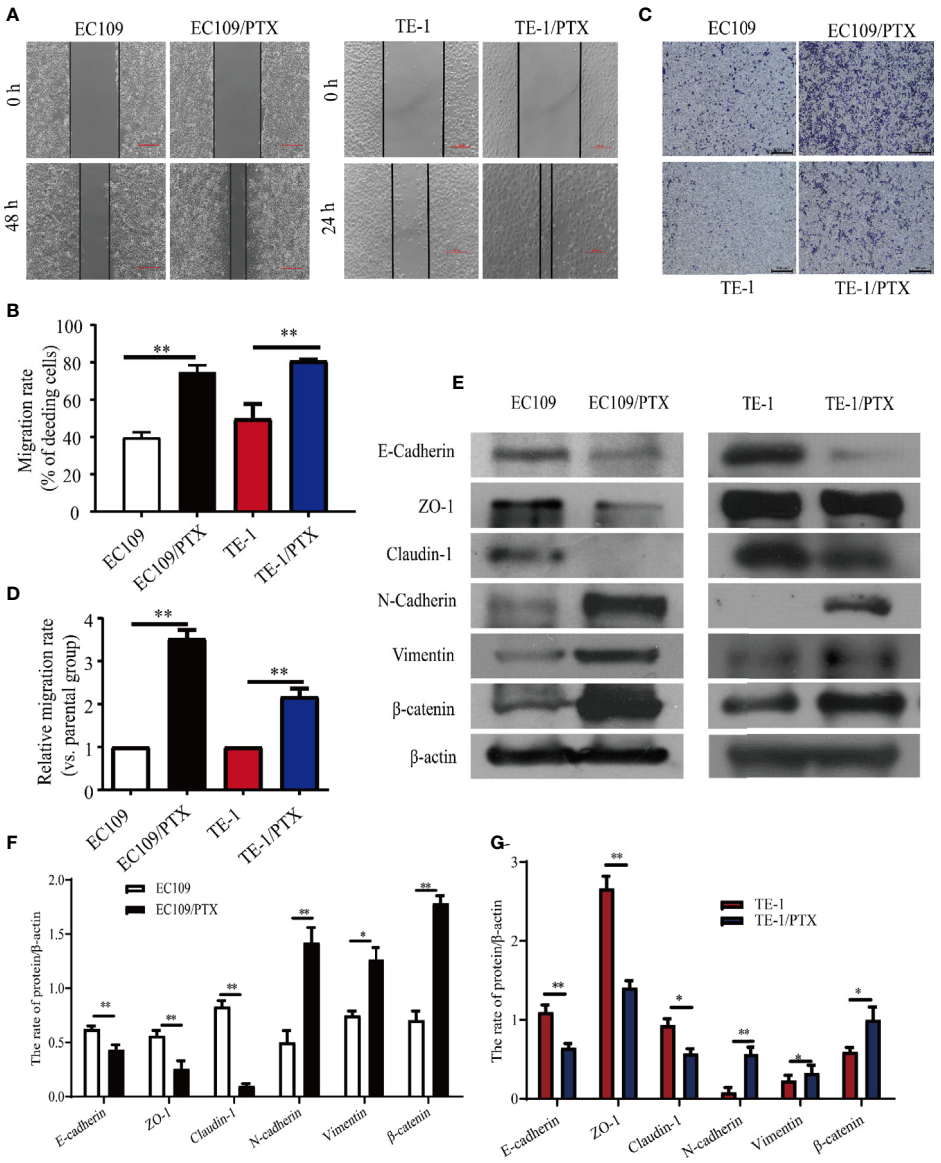

FIGURE 3 | The migratory ability enhanced and the expression of EMT biomarkers changed in the PTX-treated cells. **(A, B)** Wound healing assay was used for the migration ability of the two groups of the cells and the corresponding statistical results. Scale bar: 500 μm. **(C, D)** Transwell assay on the two groups of the cells and the corresponding statistical results. Scale bar: 500 μm. **(E–G)** Western blotting evaluated the representative proteins of EMT and the corresponding statistical results. *$P < 0.05$ indicates statistically significance *vs*. parental cells. **$P < 0.01$ indicates highly statistically significant *vs*. parental cells.

TABLE 3 | Biochemical Indexes of Serum.

Biochemical Indexes	EC109	EC109/PTX
ALT	13.41 ± 1.89 IU/L	15.01 ± 1.18 IU/L
AST	28.04 ± 6.39 IU/L	29.75 ± 1.93 IU/L
Creatinine	15.63 ± 2.82 mol/L	20.40 ± 3.21 mol/L
Uric acid	107.50 ± 12.24 mol/L	74.28 ± 16.14 mol/L **

**$P < 0.01$ indicates highly statistically significant vs. EC109 cells.*

TABLE 4 | Blood Biochemical Index.

Blood Biochemical Index	EC109	EC109/PTX
WBC	7.49 ± 1.80 10^9/L	3.81 ± 2.20 10^9/L **
RBC	9.81 ± 0.39 10^{12}/L	8.95 ± 0.71 10^{12}/L
HGB	155.83 ± 5.46 g/L	146.60 ± 5.31 g/L
HCT	49.7 ± 2.19%	45.23 ± 2.98%
MCV	50.62 ± 0.57 fL	50.38 ± 0.80 fL
MCH	15.85 ± 0.28 pg	16.50 ± 1.52 pg
MCHC	313.5 ± 3.86 g/L	327.40 ± 25.41 g/L
RDW-S	14.13 ± 0.26%	14.33 ± 0.59%
RDW-SD	29.67 ± 0.75 Fl	30.00 ± 1.55 Fl
PLT	826.67 ± 80.77 10^9/L	727.60 ± 115.32 10^9/L
PCT	0.59 ± 0.04%	0.52 ± 0.10%
MPV	7.13 ± 0.35 fL	7.06 ± 0.32 fL
PDW	16.63 ± 0.11%	15.94 ± 0.28%

***P < 0.01 indicates highly statistically significant vs. EC109 cells.*

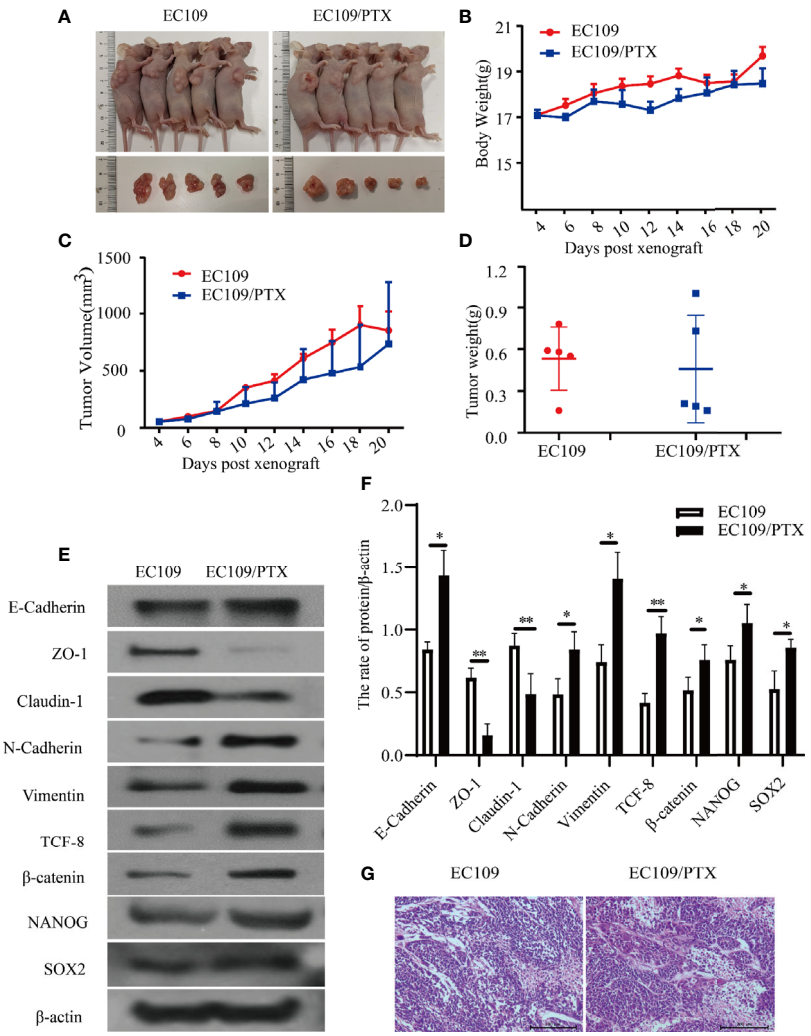

FIGURE 4 | EC109 and EC109/PTX cell growth *in vivo* and the expression of EMT-related and stemness-related proteins. **(A)** The mice and tumor tissues of the two groups after implanting tumor cells for 20 days. **(B–D)** The body weight, tumor volume and tumor weight of the mice and tumor. **(E, F)** Western blotting for the expression of the EMT-related and stemness-related proteins and the corresponding statistical results. **(G)** Tumor tissue was stained with HE, the nucleus was stained blue-violet, and the cytoplasm was stained red. Scale bar: 200 μm. **P* < 0.05 indicates statistically significance *vs*. EC109 cells. ***P* < 0.01 indicates highly statistically significant *vs*. EC109 cells.

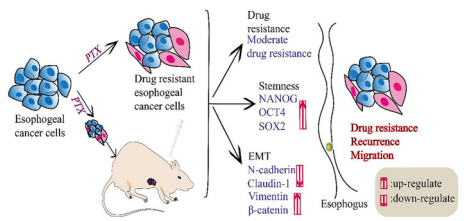

FIGURE 5 | A schema summarized this study.

transform cancer cells to stem-like cell phenotype in different tumor types (27). Among them, NANOG is an important transcription factor involved in the regulation of cell stemness (28). NANOG plays an important role in self-renewal, undifferentiated state and differentiation ability, high tumorigenicity, and resistance to current standard chemotherapy and radiotherapy (29–31). It can be activated by different transcription factors, such as OCT4 and SOX2 (32, 33). Previous studies have shown that NANOG is closely related to the poor prognosis of cancers (34).

In addition, we also found that after the cells were induced into drug-resistant esophageal cancer cells by PTX, the expression of EMT-related transcription factor β-catenin was up-regulated, the expression of epithelial biomarkers Claudin-1, ZO-1 and E-cadherin was reduced and the mesenchymal biomarkers N-cadherin, Vimentin expression increased. EMT plays an important role in the infiltration and metastasis of tumor cells, the formation of tumor drug resistance and tumor stem cells (35). The results indicated that once esophageal cancer cells become drug resistant, the expression of both cancer stem cell biomarkers and EMT-related biomarkers changed, which indicated clinical recurrence and migration ability (36, 37). Some studies have demonstrated that mesenchymal cells share similar molecular characteristics with CSCs, to some extent (38). Previous studies also revealed that the activation of EMT program led to the acquisition of the characteristics of CSCs in tumor cells (39).

In conclusion, our study suggested that drug resistance and cancer cell stemness develop at the same time during chemotherapy in esophageal cancer. The emergence of stemness explained why recurrence and metastasis occurred after drug resistance and caused poor prognosis. Our results indicated that targeting EMT and stemness at the same time in drug-resistant esophageal cancer could provide a better therapeutic effect.

DATA AVAILABILITY STATEMENT

The original contributions presented in the study are included in the article/supplementary material. Further inquiries can be directed to the corresponding authors.

ETHICS STATEMENT

The animal study was reviewed and approved by the Institutional Animal Care and Use Committee of the Zhengzhou University.

AUTHOR CONTRIBUTIONS

CW, CP, and XL designed and performed the experiments. XL drafted the manuscript. MH, LinL, XW, SH, JZ, YD, MA, LeiL, XZ, JH, and YL participated in the experiments and revised the manuscript. CW supervised this study. All authors contributed to the article and approved the submitted version.

FUNDING

This work was supported by grants from the National Natural Science Foundation of China (no. U1904156) and Zhengzhou University Student Innovation Experiment Project (UIEP).

REFERENCES

1. Bray F, Ferlay J, Soerjomataram I, Siegel RL, Torre LA, Jemal A. Global Cancer Statistics 2018: GLOBOCAN Estimates of Incidence and Mortality Worldwide for 36 Cancers in 185 Countries. *CA Cancer J Clin* (2018) 68:394–424. doi: 10.3322/caac.21492
2. Chen W, Zheng R, Baade PD, Zhang S, Zeng H, Bray F, et al. Cancer Statistics in China, 2015. *CA Cancer J Clin* (2016) 66:115–32. doi: 10.3322/caac.21338
3. Liu Y, Xiong Z, Beasley A, D'Amico T, Chen XL. Personalized and Targeted Therapy of Esophageal Squamous Cell Carcinoma: An Update. *Ann N Y Acad Sci* (2016) 1381:66–73. doi: 10.1111/nyas.13144
4. Yang CS, Chen X, Tu S. Etiology and Prevention of Esophageal Cancer. *Gastrointest Tumors* (2016) 3:3–16. doi: 10.1159/000443155
5. Lathia JD, Liu H. Overview of Cancer Stem Cells and Stemness for Community Oncologists. *Target Oncol* (2017) 12:387–99. doi: 10.1007/s11523-017-0508-3
6. Wicha MS, Liu S, Dontu G. Cancer Stem Cells: An Old Idea–a Paradigm Shift. *Cancer Res* (2006) 66:1883–90. doi: 10.1158/0008-5472. discussion 1895-1886CAN-05-3153.
7. Brown Y, Hua S, Tanwar PS. Extracellular Matrix-Mediated Regulation of Cancer Stem Cells and Chemoresistance. *Int J Biochem Cell Biol* (2019) 109:90–104. doi: 10.1016/j.biocel.2019.02.002
8. Kolev VN, Tam WF, Wright QG, McDermott SP, Vidal CM, Shapiro IM, et al. Inhibition of FAK Kinase Activity Preferentially Targets Cancer Stem Cells. *Oncotarget* (2017) 8:51733–47. doi: 10.18632/oncotarget.18517
9. Reya T, Morrison SJ, Clarke MF, Weissman IL. Stem Cells, Cancer, and Cancer Stem Cells. *Nature* (2001) 414:105–11. doi: 10.1038/35102167
10. Liu K, Zhao T, Wang J, Chen Y, Zhang R, Lan X, et al. Etiology, Cancer Stem Cells and Potential Diagnostic Biomarkers for Esophageal Cancer. *Cancer Lett* (2019) 458:21–8. doi: 10.1016/j.canlet.2019.05.018
11. Wise JGV, Pia DL, Alexander RN, Amila KA, Maha A. Inhibitors of Multidrug Resistance Transporter P-glycoprotein. United States Patent US. 20190216811 (2019).
12. Taniguchi D, Saeki H, Nakashima Y, Kudou K, Nakanishi R, Kubo N, et al. CD44v9 is Associated With Epithelial-Mesenchymal Transition and Poor Outcomes in Esophageal Squamous Cell Carcinoma. *Cancer Med* (2018) 7:6258–68. doi: 10.1002/cam4.1874

13. Huang D, Gao Q, Guo L, Zhang C, Jiang W, Li H, et al. Isolation and Identification of Cancer Stem-Like Cells in Esophageal Carcinoma Cell Lines. *Stem Cells Dev* (2009) 18:465–73. doi: 10.1089/scd.2008.0033
14. Zhang F, Wang J, Wang X, Wei N, Liu H, Zhang X. CD146-Mediated Acquisition of Stemness Phenotype Enhances Tumour Invasion and Metastasis After EGFR-TKI Resistance in Lung Cancer. *Clin Respir J* (2019) 13:23–33. doi: 10.1111/crj.12976
15. Steinbichler TB, Savic D, Dudás J, Kvitsaridze I, Skvortsov S, Riechelmann H. Cancer Stem Cells and Their Unique Role in Metastatic Spread. *Semin Cancer Biol* (2020) 60:148–56. doi: 10.1016/j.semcancer.2019.09.007
16. Du B, Shim JS. Targeting Epithelial-Mesenchymal Transition (EMT) to Overcome Drug Resistance in Cancer. *Molecules* (2016) 21:965. doi: 10.3390/molecules21070965
17. Polyak K, Weinberg RA. Transitions Between Epithelial and Mesenchymal States: Acquisition of Malignant and Stem Cell Traits. *Nat Rev Cancer* (2009) 9:265–73. doi: 10.1038/nrc2620
18. Yeung KT, Yang J. Epithelial-Mesenchymal Transition in Tumor Metastasis. *Mol Oncol* (2017) 11:28–39. doi: 10.1002/1878-0261.12017
19. Montanari M, Rossetti S, Cavaliere C, D'Aniello C, Malzone MG, Vanacore D. Epithelial-Mesenchymal Transition in Prostate Cancer: An Overview. *Oncotarget* (2017) 8:35376–89. doi: 10.18632/oncotarget.15686
20. Zeng K, He B, Yang BB, Xu T, Chen X, Xu M. The Pro-Metastasis Effect of circANKS1B in Breast Cancer. *Mol Cancer* (2018) 17:160. doi: 10.1186/s12943-018-0914-x
21. Che D, Zhang S, Jing Z, Shang L, Jin S, Liu F. Macrophages Induce EMT to Promote Invasion of Lung Cancer Cells Through the IL-6-mediated Cox-2/PGE2/beta-catenin Signalling Pathway. *Mol Immunol* (2017) 90:197–210. doi: 10.1016/j.molimm.2017.06.018
22. Li X, Zeng X. Shikonin Suppresses Progression and Epithelial Mesenchymal Transition in Hepatocellular Carcinoma (HCC) Cells Via Modulating miR-106b/SMAD7/TGF-beta Signaling Pathway. *Cell Biol Int* (2020) 44:467–76. doi: 10.1002/cbin.11247
23. Wang C, Guo LB, Ma JY, Li YM, Liu HM. Establishment and Characterization of a Paclitaxelresistant Human Esophageal Carcinoma Cell Line. *Int J Oncol* (2013) 43:1607–17. doi: 10.3892/ijo.2013.2083
24. Ajani JA, D'Amico TA, Bentrem DJ, Chao J, Corvera C, Das P. Esophageal and Esophagogastric Junction Cancers, Version 2.2019, NCCN Clinical Practice Guidelines in Oncology. *J Natl Compr Cancer Net: JNCCN* (2019) 17:855–83. doi: 10.6004/jnccn.2019.0033
25. Feng W, Xiaoyan X, Xuan Y, Xiangke L, Zichang Y, Ran Z. Silencing Stathmin-Modulating Efficiency of Chemotherapy for Esophageal Squamous Cell Cancer With Paclitaxel. *Cancer Gene Ther* (2015) 22:115–21. doi: 10.1038/cgt.2014.74
26. Zhao WS, Yan WP, Chen DB, Dai L, Yang YB, Kang XZ. Genome-Scale CRISPR Activation Screening Identifies a Role of ELAVL2-CDKN1A Axis in Paclitaxel Resistance in Esophageal Squamous Cell Carcinoma. *Am J Cancer Res* (2019) 9:1183–200.
27. Ben-Porath I, Thomson MW, Carey VJ, Ge R, Bell GW, Regev A, et al. An Embryonic Stem Cell-Like Gene Expression Signature in Poorly Differentiated Aggressive Human Tumors. *Nat Genet* (2008) 40:499–507. doi: 10.1038/ng.127
28. de Vicente JC, Rodríguez-Santamarta T, Rodrigo JP, Allonca E, Vallina A, Singhania A, et al. The Emerging Role of NANOG as an Early Cancer Risk Biomarker in Patients With Oral Potentially Malignant Disorders. *J Clin Med* (2019) 8:1376. doi: 10.3390/jcm8091376
29. Siddiqui Z, Srivastava AN, Sankhwar SN, Dalela D, Singh V, Zaidi N, et al. Synergic Effects of Cancer Stem Cells Markers, CD44 and Embryonic Stem Cell Transcription Factor Nanog, on Bladder Cancer Prognosis. *Br J BioMed Sci* (2020) 77:69–75. doi: 10.1080/09674845.2019.1692761
30. Lin T, Ding YQ, Li JM. Overexpression of Nanog Protein is Associated With Poor Prognosis in Gastric Adenocarcinoma. *Med Oncol* (2012) 29:878–85. doi: 10.1007/s12032-011-9860-9
31. Meng HM, Zheng P, Wang XY, Liu C, Sui HM, Wu SJ, et al. Over-Expression of Nanog Predicts Tumor Progression and Poor Prognosis in Colorectal Cancer. *Cancer Biol Ther* (2010) 9:295–302. doi: 10.4161/cbt.9.4.10666
32. Lu Y, Zhu H, Shan H Lu Y, Zhu H, Shan H, Lu J, et al. Knockdown of Oct4 and Nanog Expression Inhibits the Stemness of Pancreatic Cancer Cells. *Cancer Lett* (2013) 340:113–23. doi: 10.1016/j.canlet.2013.07.009
33. Wang X, Jin J, Wan F, Zhao L, Chu H, Chen C, et al. Ampk Promotes Spop-Mediated NANOG Degradation to Regulate Prostate Cancer Cell Stemness. *Dev Cell* (2019) 48:345–60.e347. doi: 10.1016/j.devcel.2018.11.033
34. Yang L, Zhang X, Zhang M, Zhang J, Sheng Y, Sun X, et al. Increased Nanog Expression Promotes Tumor Development and Cisplatin Resistance in Human Esophageal Cancer Cells. *Cell Physiol Biochem* (2012) 30:943–52. doi: 10.1159/000341471
35. Culig Z. Epithelial Mesenchymal Transition and Resistance in Endocrine-Related Cancers. *Biochim Biophys Acta Mol Cell Res* (2019) 1866:1368–75. doi: 10.1016/j.bbamcr.2019.05.003
36. Martins-Neves SR, Cleton-Jansen AM, Gomes CMF. Therapy-Induced Enrichment of Cancer Stem-Like Cells in Solid Human Tumors: Where do We Stand? *Pharmacol Res* (2018) 137:193–204. doi: 10.1016/j.phrs.2018.10.011
37. Li J, Qi D, Hsieh TC, Huang JH, Wu JM, Wu E. Trailblazing Perspectives on Targeting Breast Cancer Stem Cells. *J Pharmacol Ther* (2021) 223:107800. doi: 10.1016/j.pharmthera.2021.107800
38. Li Y, Kong D, Ahmad A, Bao B, Sarkar FH. Pancreatic Cancer Stem Cells: Emerging Target for Designing Novel Therapy. *Cancer Lett* (2013) 338:94–100. doi: 10.1016/j.canlet.2012.03.018
39. Zhou JM, Hu SQ, Jiang H, Chen YL, Feng JH, Chen ZQ, et al. Oct4b1 Promoted EMT and Regulated the Self-Renewal of CSCs in CRC: Effects Associated With the Balance of Mir-8064/PLK1. *Mol Ther Oncol* (2019) 15:7–20. doi: 10.1016/j.omto.2019.08.004

Conflict of Interest: The authors declare that the research was conducted in the absence of any commercial or financial relationships that could be construed as a potential conflict of interest.

frontiers in Oncology

ORIGINAL RESEARCH
published: 13 July 2021
doi: 10.3389/fonc.2021.663944

Suppressing ERK Pathway Impairs Glycochenodeoxycholate-Mediated Survival and Drug-Resistance in Hepatocellular Carcinoma Cells

Bingxin Li[1†], *Maojun Zhou*[2†], *Jue Wang*[1], *Hongjuan Xu*[1] *and Manyi Yang*[1*]

[1] Department of Hepatobiliary and Pancreatic Surgery, National Health Commission (NHC) Key Laboratory of Nanobiological Technology, Xiangya Hospital, Central South University, Changsha, China, [2] Department of Oncology, NHC Key Laboratory of Cancer Proteomics, National Center for Geriatrics Clinical Research, State Local Joint Engineering Laboratory for Anticancer Drugs, Xiangya Hospital, Central South University, Changsha, China

OPEN ACCESS

Edited by:
Xia Li,
Shenzhen Institutes of Advanced Technology (CAS), China

Reviewed by:
Mingwei Chen,
The First Affiliated Hospital of Soochow University, China
Edmund Ui-Hang Sim,
Universiti Malaysia Sarawak, Malaysia
Kevin Tak-Pan Ng,
The University of Hong Kong, Hong Kong

***Correspondence:**
Manyi Yang
yangmanyi@csu.edu.cn

[†]These authors have contributed equally to this work

Specialty section:
This article was submitted to Gastrointestinal Cancers, a section of the journal Frontiers in Oncology

Received: 04 February 2021
Accepted: 22 June 2021
Published: 13 July 2021

Citation:
Li B, Zhou M, Wang J, Xu H and Yang M (2021) Suppressing ERK Pathway Impairs Glycochenodeoxycholate-Mediated Survival and Drug-Resistance in Hepatocellular Carcinoma Cells. Front. Oncol. 11:663944. doi: 10.3389/fonc.2021.663944

Glycochenodeoxycholate (GCDA), a toxic component in bile salts, is involved in carcinogenesis of gastrointestinal tumors. The objective of this research was to study the function of ERK1/2 in the GCDA-mediated survival and drug-resistance in hepatocellular carcinoma cells (HCCs). Firstly, extracellular signal-regulated kinase 1/2 (ERK1/2) was detected extensively expressed in liver cancer cells, and silencing ERK1/2 by RNA interference could suppress GCDA-stimulated survival and promote apoptosis. Furthermore, phosphorylation of endogenous ERK1/2 could be potently stimulated by GCDA in combination with enhanced chemoresistance in QGY-7703 hepatocellular carcinoma cells. The GCDA-mediated proliferation and chemoresistance could be impaired by PD98059, which acted as an inhibitor to block the phosphorylation of ERK1/2. Mechanistically, PD98059 was able to potently suppress GCDA-stimulated nuclear aggregation of ERK1/2 and p-ERK1/2, upregulate pro-survival protein Mcl-1 and downregulate pro-apoptotic protein Bim. The results of this study indicated that disruption of ERK1/2 by blocking phosphorylation or nuclear translocation may put forward new methods for solving the problem of GCDA-related proliferation and drug-resistance in liver cancer treatment.

Keywords: hepatocellular carcinoma cells, glycochenodeoxycholate, extracellular signal-regulated kinase 1/2, anti-apoptosis proteins, pro-apoptotic proteins

INTRODUCTION

Hepatocellular carcinoma (HCC) is the most common liver cancer nowadays, and more than 700,000 cases are diagnosed every year (1). The pathogenesis of HCC is extremely complex, but evolving information suggests that the major risk factors for HCC in contemporary clinical practice include alcoholism, non-alcoholic fatty liver disease (NFLD), hepatitis B virus (HBV), and hepatitis C virus (HCV) (2, 3). Most patients with advanced liver cancer will choose chemotherapy. However, patients with HCC usually develop resistance to 5-fluorouracil, doxorubicin or cisplatin, which are the traditional chemotherapeutics. Unfortunately, sorafenib, the new generation of drugs, did not

achieve the desired results (4). Thus, it is very important to explore the resistance mechanism of HCC.

Bile salts are the major ingredients in bile, which are secreted by liver cells and involved in fat digestion and absorption. Glycochenodeoxycholate (glycine conjugate of chenodeoxycholate, GCDA), a toxic component in bile salts, is involved in carcinogenesis of gastrointestinal tumors (5). Previous researches have indicated that GCDA could stimulate the growth of Barrett's adenocarcinoma cells and non-neoplastic Barrett cell lines through PI3 kinase/Akt pathway and p38/ERK/MAPK pathway respectively (6, 7). Satoshi et al. (8) found that glycochenodeoxycholate acid could promote the proliferation of intestinal epithelia *via* decreasing cyclic AMP and increasing histone H2AX phosphorylation after exposure to γ-rays. Another study demonstrated that the biliary tract cancer could be induced by GCDA *via* aggregation of 8-OHdG and oxidative DNA damage (9). The metabolic disorder of bile salts could lead to abnormal bile salt accumulation; it could be a direct factor in the development of HCC. A study by Wang et al. (10) found that GCDA might upregulate pro-survival proteins (Mcl-1, Survivin, and Bcl-2) and eventually results in chemoresistance of HCC cells. However, the specific intracellular mechanism of GCDA-mediated hepatocellular carcinoma development remains to be further studied.

As a member of the mitogen activated protein kinase family, the extracellular signal-regulated kinase (ERK) takes a key part in transmitting signals from receptors on the cell surface into the nucleus (11). Signals transmitted from MEK1/2 can phosphorylate ERK1/2 at Thr and Tyr residues (12). Then the activated ERK1/2 phosphorylates downstream substrates and eventually causes cell proliferation, differentiation, and canceration (13). Usually, ERK1/2 is mainly distributed in the cytoplasm of normal cells. Upon stimulation, many ERK1/2 molecules shift to the nucleus, Golgi, mitochondria, endosomes/lysosomes and endoplasmic reticulum (14). The main translocation seems to be the entry into the nucleus, which is an important place for signal transmission downstream of ERK (13). Because the nuclear translocation of ERK is mainly important for cell proliferation, prevention of such translocation can be used as a novel strategy to combat cancer (15). Furthermore, ERK1/2 signaling is an important regulator of cell-intrinsic Bcl-2-regulated apoptotic signaling (16). In most situations, ERK1/2 signaling accelerates cell growth *via* stimulating anti-apoptosis proteins (Bcl-2, Mcl-1, and Bcl-xL) and inhibiting pro-apoptotic proteins (Bim, Bad, Bmf, and Puma) (14). Thus, suppression of ERK1/2 pathway in tumor cells might serve as an effective way to prevent cancer development.

The chemoresistance of ERK1/2 has been extensively studied in other cancers. In radioresistant glioblastoma multiforme cells, cell survival could be promoted through ERK1/2 signaling when pSTAT3(Y705) was inhibited (17). ERK1/2 and p38 MAPK signaling pathways were significantly involved in neoplastic transformation and cisplatin-resistance in nasopharyngeal carcinoma cell lines (18). However, there was little in-depth research for the chemoresistance of ERK1/2 in HCC. A published study has shown that the activation of ERK1/2 could decrease the sensitivity to sorafenib in the HCC cells (Bel-7402 and SMMC-7721) (19). Our previous studies have confirmed the association of GCDA with drug resistance in HCC cells (10, 20). But the exact function of ERK1/2 in such process has not been clarified. In this research, we proved that GCDA mediates activation and nuclear accumulation of ERK1/2, which finally results in promoting anti-apoptotic function in human liver cancer cells.

MATERIALS AND METHODS

Cell Culture

LO2, HepG2, Bel-7402, Bel-7404, SMMC-7721, Huh7, MHC97-H, and QGY-7703 HCC cell lines were originally from the Institute of Biochemistry and Cell Biology (CAS, Shanghai, China). LO2 and Bel-7402 cell line were maintained in RPMI-1640 medium (Thermo Fisher Scientific, Waltham, USA) with 10% fetal bovine serum (ExCell Bio, Shanghai, China). HepG2, Bel-7404, SMMC-7721, Huh7, MHC97-H, and SMMC-7721 QGY-7703 cell lines were cultivated in Dulbecco's modified Eagle's medium (Hyclone, Logan, USA) supplemented 10% FBS. Cell lines were incubated at 37°C with 5% CO_2.

Reagents and Antibodies

The antibodies of ERK1 + ERK2 and ERK1 (pT202/pY204) + ERK2 (pT185/pT187) were obtained from Abcam (Cambridge, UK). Goat-anti rabbit HRP antibody and anti-GAPDH antibody were from Cell Signaling Technology (Danvers, MA, USA). PD98059, a specific inhibitor of ERK kinase, was from Calbiochem (San Diego, CA, USA). Glycochenodeoxycholate (GCDA) and cisplatin were obtained from Sigma-Aldrich (St. Louis, USA). 5-Fluorouracil (5-FU) was purchased from Xudong Haipu Pharmaceutical (Shanghai, China). The Annexin V-FITC apoptosis detection kit was purchased from Becton, Dickinson and Company (BD, Franklin Lake, NJ).

siRNA and Transfections

For RNA interference, siRNA 225 (ACACGCAGUU GCAGUACAU), 888 (GACCGGAUGUUAACCUUUA), and 933 (GAAACUACCUACAGUCUCU) targeting human ERK1, siRNA 355 (GUGCUCUGCUUAUGAUAAU), 513 (CACCAACCAUCGAGCAAAU) and 714 (CCACC UGUGAUCUCAAGAU) targeting human ERK2 and negative control siRNA (UUCUCCGAACGUGUCACGU) were from Shanghai Gene Pharma, Co., Ltd (Shanghai, China). QGY-7703 cells were transfected with siRNAs for 24 h using Lipofectamine RNAi max (Invitrogen, NY, USA).

CCK8 Assay

QGY-7703 cells were seeded in 96 well plates. Then GCDA, drugs, or inhibitors were used to treat cells. After various treatments, each well was supplemented with 10 μl of CCK8 solution and incubated for 1.5 h. After that, the absorbance was determined by microplate microscopy at 450 nm (BioTek, Winooski, VT).

Western Blot Analysis

The samples of QGY-7703 cells were lysed with detergent buffer for 30 min on ice. Then cell products were scraped from the wells and centrifuged for 15 min at 12,000 rpm. Protein, 30 μg, was loaded onto 10% SDS-PAGE and transferred to a polyvinylidene difluoride (PVDF) membrane. After blocking with blocking solution for 2 h at room temperature, cells were then incubated at 4°C overnight with primary antibodies, followed by washing with 1× TBST and incubating with horseradish peroxidase-conjugated anti-mouse or anti-rabbit secondary antibodies (1:5,000) with shaking for 1 h. Results were detected using WesternBright™ ECL (Advansta, USA), and the bands were scanned and quantified using the FluorChem FC3 system.

Flow Cytometry

QGY-7703 cells were transfected with siRNA888 and siRNA513 together for 24 h. Following treatment with 100 μM GCDA, cells were collected and washed with cold PBS. After resuspending with 1× binding buffer, 3 μl Annexin V-FITC and propidium iodide (PI) (Becton, Dickinson and Company, NJ) were used to treat the cells for 15 min. The apoptotic rate was detected by flow cytometry.

Immunofluorescence

In 24-well plates, QGY-7703 cells were cultured with a glass coverslip overnight. After cells were exposed to GCDA or GCDA + PD98059 for 8 h, 4% paraformaldehyde was used to fix cells for 15 min. The cells were washed with TBST and performed using ERK1/2 or p-ERK1/2 antibody at 4°C overnight after incubating with Alexa Fluor®594 goat antibody at 37°C for 1 h. Cell nuclei were stained with DAPI for 2 min. At last, the results were photographed with a fluorescence microscope.

Statistical Analysis

SPSS software V17.0 was used to perform the statistical analysis. All data were displayed as the means ± SD. Inter-group differences were assessed by Student's t-test. P <0.05 was the considered level of statistical significance.

RESULTS

ERK1/2 Acts a Part in GCDA-Induced Survival of Human Liver Carcinoma Cells

The ERK1/2 cascade is best known for its role in proliferation, differentiation, and tumorigenesis (13). Firstly, we measured the endogenous protein levels of ERK1/2 in normal liver cells (LO2) and seven HCC cell lines (HepG2, Bel-7402, Bel-7404, SMMC7721, Huh7, MHC97-H, and QGY-7703. The result of Western blot showed that ERK1/2 was extensively expressed in all the liver cancer cells we detected (**Figure 1A**). Next, to test whether GCDA promoted HCC cell proliferation, we treated

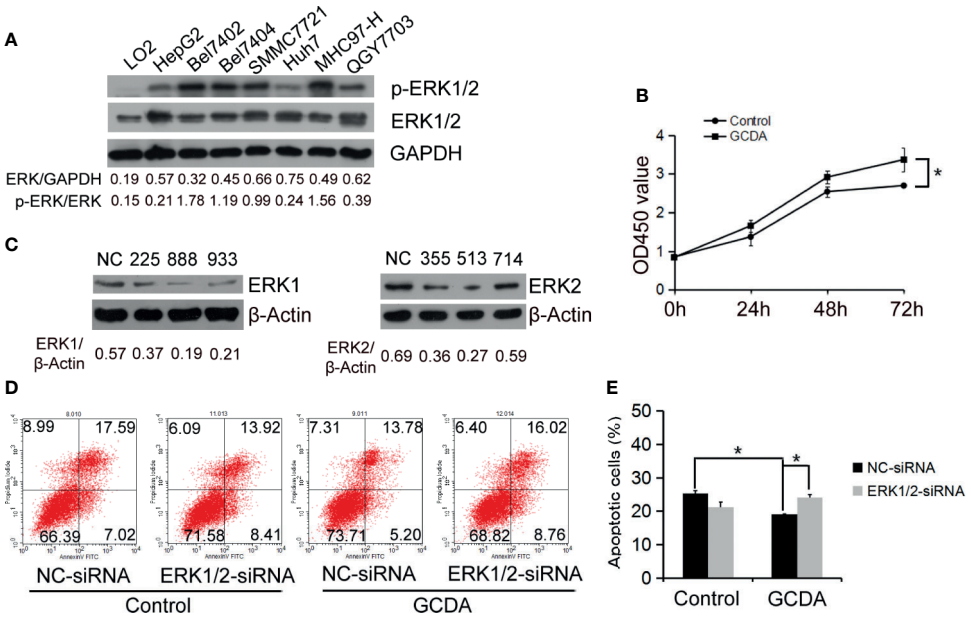

FIGURE 1 | ERK1/2 act a part in GCDA-mediated survival of human liver carcinoma cells. **(A)** Expression of ERK1/2 in normal liver cells (LO2) and seven liver carcinomas cell lines (HepG2, Bel7402, Bel7404, SMMC7721, Huh7, MHC97-H and QGY7703) was detected by western blot and quantified by Alphaview software. **(B)** GCDA (100μM) was used to treat QGY7703 cells for 0h, 24h, 48h and 72h. CCK8 was performed to determine the viable cells. **(C)** QGY7703 cells were transfected with siRNA targeting ERK1 (225, 888 and 933) and ERK2 (355, 513 and 714). After 24h, whole cell extracts were analyzed by western blot using ERK1 and ERK2 antibodies. NC, negative; control siRNA. **(D, E)** siRNA888 targeting ERK1 and siRNA513 targeting ERK2 were transfected into QGY7703 cells together. 24 hours later, 100μM GCDA was used to treat cells for 24h. Apoptosis were determined using flow cytometry. All data represent the mean±SD and were obtained from at least three independent experiments. *P < 0.05, (Student's t-test).

QGY-7703 cell line with 100 μM GCDA for 0, 24, 48, and 72 h, and then checked the viable cells by CCK8. Results indicated that viable cells significantly increased after treatment with GCDA for72 h (**Figure 1B**).

To determine whether ERK1/2 affected the GCDA-induced survival of HCC cells, we designed siRNAs targeting ERK1 (225, 888, and 933) and ERK2 (355, 513, and 714). All the siRNAs were transfected into QGY-7703 cells. Then immunoblotting was done to determine the interference efficiency. As shown in **Figure 1C**, ERK1 and ERK2 protein expressions were inhibited by siRNA888 and siRNA513, respectively. After siRNA888 targeting, ERK1 and siRNA513 targeting, ERK2 was transfected into QGY-7703 cell line together; GCDA was used to treat the cells for 24 h. Apoptotic cells were analyzed using annexin V binding on FASC. Flow cytometry results demonstrated that GCDA could repress apoptosis. But after ERK1/2 was silenced, the apoptotic cells were increased (**Figures 1D, E**). In other words, specific depletion of ERK1/2 blocked GCDA-stimulated cell survival. These results indicated that ERK1 and ERK2 molecules have played a role in the survival of hepatoma cells mediated by GCDA.

GCDA Induces ERK1/2 Phosphorylation, Which May Be Involved in Prolonged Survival of Human Liver Cancer Cells

Furthermore, we investigated potential mechanisms involved in the GCDA-induced HCC cell survival. QGY-7703 and Huh7 cells were treated with 100 μM GCDA for 0, 0.5, 1, 2, 4, 8, 12, and 24 h. Results demonstrated that the activated ERK1/2 increased obviously after GCDA treatment in QGY-7703 and Huh7 cells, while the expression of endogenous ERK1/2 changed little (**Figures 2A, B**).

Cisplatin has been known as one of the most potential and widely used drugs, which is effective in a variety of solid cancers such as testicular, ovarian, head and neck, bladder, lung, cervical, melanoma, and lymphomas (21–25). The antimetabolite 5-fluorouracil (5-FU), which can inhibit thymidylate synthase, is a widely used antitumor agent (26). In order to check the effect of GCDA-induced ERK1/2 activation on cell survival, QGY-7703 and Huh7 cells were treated with antitumor drug (cisplatin or 5-FU) or GCDA (100 μM) + antitumor drug (cisplatin or 5-FU) for 72 h. The IC50 of cisplatin for QGY-7703 is 8.8 μM (**Figure 2C**). The IC50 value of 5-FU is 0.9 μg/ml for QGY-7703 and 2.7 μg/ml for Huh7, respectively (**Figures 2D, E**). However, following GCDA treatment, the IC50 concentrations were increased obviously. Such results indicate that GCDA can significantly enhance resistance to drugs. Therefore, we speculated the involvement of activated ERK1/2 in chemoresistance induced by GCDA.

The MAPK/ERK1/2 Inhibitor PD98059 Decreases GCDA-Stimulated Cell Proliferation

To further verify the role of activated ERK1/2 in HCC cells, the MAPK/ERK1/2 inhibitor PD98059, which could inhibit phosphorylation of ERK1/2, was used (27). We treated QGY-

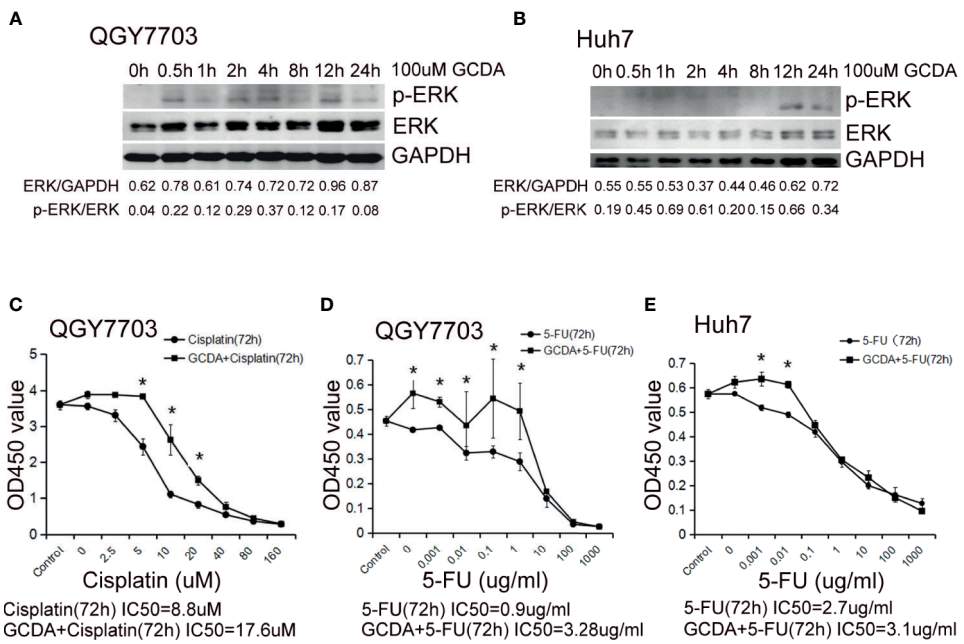

FIGURE 2 | GCDA induces ERK1/2 phosphorylation, which may be involved in prolonged survival of human liver cancer cells. **(A, B)** 100μM GCDA was used to treat QGY7703 and Huh7 cells for 0h, 0.5h, 1h, 2h, 4h, 8h, 12h and 24h. The expression level of ERK1/2 and p-ERK1/2 were tested by western blot and quantified by Alphaview software. **(C–E)** Antitumor drug (Cisplatin or 5-FU) or GCDA (100μM)+antitumor drug(Cisplatin or 5-FU) were used to treat QGY-7703 and Huh7 cells for 72h. CCK8 was performed to determine the viable cells. IC50 is calculated as the concentration of Cisplatin or 5-FU inducing a 50% reduction in cell viability. All data represent the mean±SD and were obtained from at least three independent experiments. *P < 0.05 (Student's t-test).

7703 cells with GCDA (100 μM) or GCDA (100 μM) + PD98059 (10 μM) for 24, 48, and 72 h. Then, CCK8 was done to test the viability of QGY-7703 cells. CCK8 experiments showed that suppression of ERK1/2 activation by PD98059 would decrease proliferation of liver cancer cells (**Figure 3A**). Next, QGY-7703 cells were treated with or without PD98059 (10 μM) for 0.5 h, followed by treatment with GCDA (100 μM) or GCDA (100 μM) + antitumor drug (1 μg/ml 5-FU) for 72 h. Results of CCK8 showed that PD98059 significantly attenuated the chemoresistance induced by GCDA, which could prolong cell survival following treatment with 5-FU (**Figure 3B**). In conclusion, these findings implied that phosphorylation (or activation) of ERK1/2, which is attenuated by PD98059, is important for the survival and chemoresistance of GCDA-mediated HCC cells.

PD98059 Suppresses GCDA-Induced Nuclear Aggregation of ERK1/2 and p-ERK1/2

In unstimulated cells, ERK1/2 molecules are usually located in the cytoplasm (15). Under stimulation, numerous ERK1/2 molecules are translocated to the nucleus (15). ERK1/2 localization plays a significant role in determining the strength of this pathway. Therefore, we examined the localization of ERK1/2 and p-ERK1/2 following GCDA (100 μM) or GCDA (100 μM) + PD98059 (10 μM) treatment. The results of immunofluorescence staining showed that ERK1/2 proteins were distributed in both cytoplasm and nucleus and more p-ERK1/2 proteins accumulated in the nucleus as small spots in resting HCC cells (**Figures 4A, B**). Following GCDA treatment,

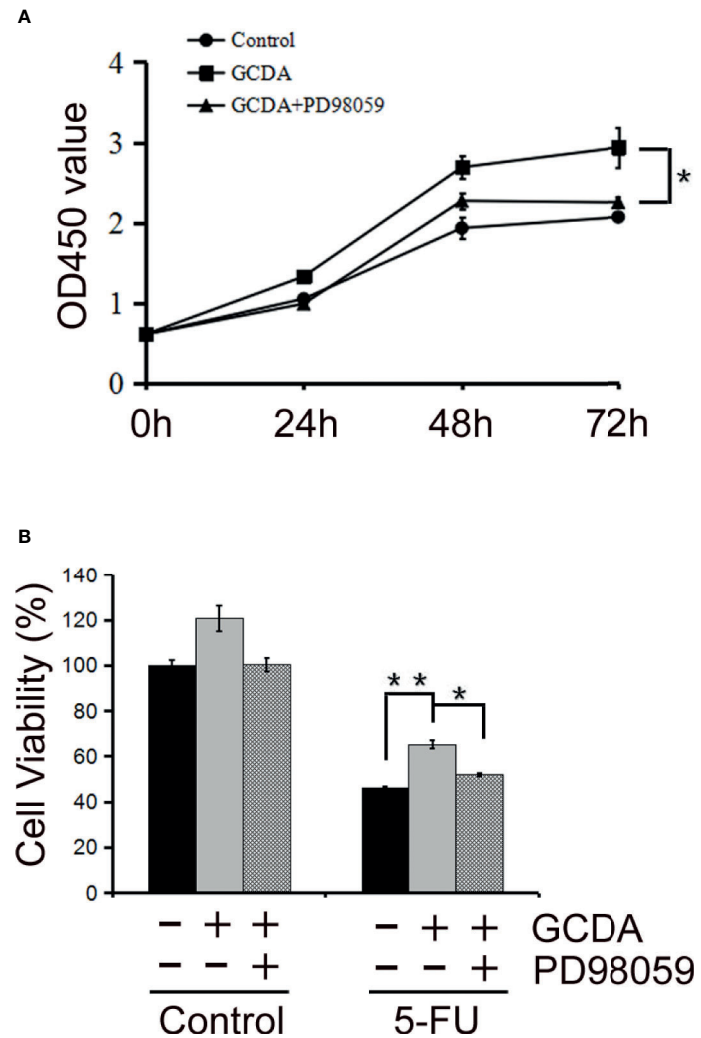

FIGURE 3 | PD98059, the ERK1/2 inhibitor, attenuates GCDA-mediated survival and drug-resistance in HCC cells. **(A)** PD98059 could inhibit phosphorylation of ERK1/2. QGY-7703 cells were preincubated with PD98059 (10μM) for 0.5 h, followed by treatment with 100μM GCDA for 24h, 48h and 72h. CCK8 was performed to determine the viable cells.**(B)** QGY7703 cells were treated with or without PD98059 (10μM) for 0.5 h, followed by treatment with GCDA (100μM) or GCDA(100μM) +antitumor drug (1μg/ml 5-FU) for 72h. Then CCK8 was performed to determine the viable cells. Data in graphs are as mean±SD. All experiments data were repeated at least three independent experiments. *P < 0.05, **P < 0.01 (Student's t-test).

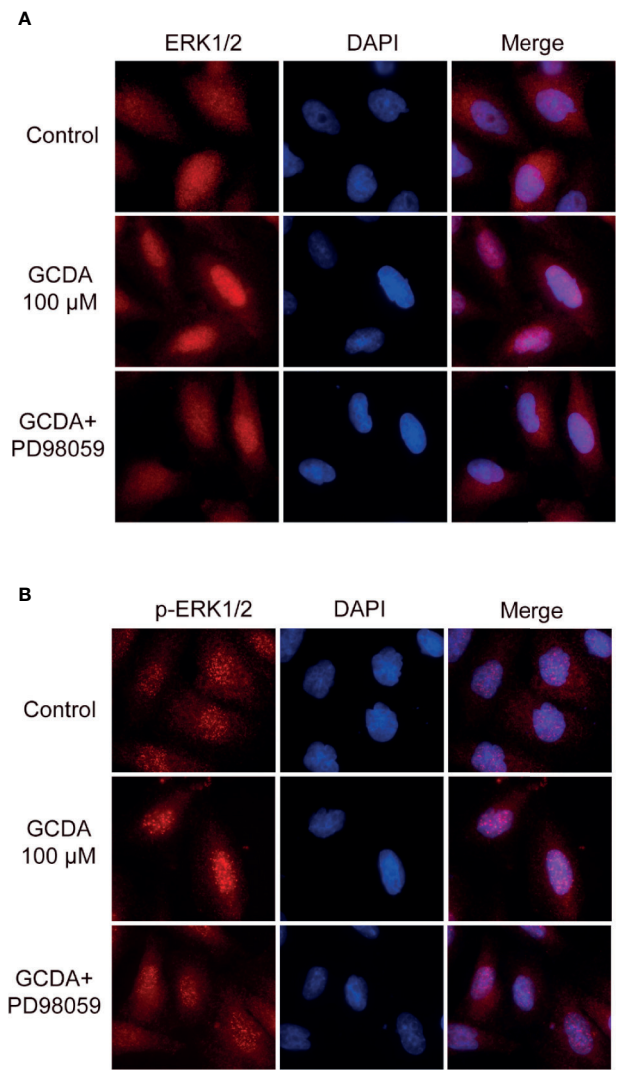

FIGURE 4 | PD98059 suppresses GCDA-induced nuclear aggregation of ERK1/2 and p-ERK1/2. **(A, B)** QGY-7703 cells were preincubated with PD98059 (10μM) for 0.5 h, followed by treatment with 100μM GCDA for 8h. Immunofluorescence staining was done using ERK1/2 or p-ERK1/2 antibody. Cell nuclei were stained with DAPI for 2 min. The experiments were repeated three times.

most ERK1/2 proteins gathered in the nucleus, while more p-ERK1/2 proteins accumulated in the nucleus as bigger speckles. However, after PD98059 treatment, the aggregation of ERK1/2 and p-ERK1/2 proteins in the nucleus significantly decreased (**Figures 4A, B**). Collectively, the above data suggested that nuclear accumulation of ERK1/2 and p-ERK1/2 induced by GCDA could be impaired by PD98059.

PD98059 Restrains GCDA-Induced Increase of Mcl-1 and Decrease of Bim

ERK1/2 signaling has been verified to have the ability to regulate some members of the Bcl-2 family, which can contribute to tumor cell survival *via* increasing anti-apoptotic factors and decreasing pro-apoptotic members of Bcl-2 family (16). Hence, we inspected the level of some Bcl-2 family members following GCDA (which can activate ERK1/2 pathway) or PD98059 (which can repress ERK1/2 pathway) treatment. Firstly, 100 μM GCDA was used to treat QGY-7703 cells for 0, 0.5, 1, 2, 4, and 8 h. Immunoblot had been done to check the levels of Bcl-2, Mcl-1, Bim, and Bak. We observed that GCDA could promote expression of Bcl-2 and Mcl-1, both of which are anti-apoptotic Bcl-2 family members and decrease expression of Bim and Bak, both of which are pro-apoptotic Bcl-2 family members (**Figure 5A**). Next, in order to determine whether the suppression of ERK1/2 signaling regulated expression of Bcl-2 family members, GCDA (100 μM) or GCDA (100 μM) + PD98059 (10 μM) was used to treat QGY-7703 cells for 8 h. Results showed that inhibition of ERK1/2 by PD98059 could block GCDA-induced increase of Mcl-1 and decrease of Bim. However, Bcl-2 and Bak did not change significantly (**Figure 5B**). Our data supported the notion that GCDA might facilitate cell survival *via* regulation proteins of Bcl-2 family, some of which could be inhibited by PD98059. Such results indicated that activation of ERK1/2 pathway induced by GCDA could mediate certain members of the Bcl-2 family.

DISCUSSION

Glycochenodeoxycholate is one of the toxic bile salts and may promote HCC invasion *via* activation of autophagy (28, 29). In the current study, survival and chemoresistance to cisplatin and 5-FU induced by GCDA have been verified in QGY-7703 cell line (**Figures 1B** and **2C–E**).

The ERK1/2 signaling pathway is considered to have great effects on proliferation, invasion, and migration in cancer cells. Numerous studies have confirmed that ERK1/2 signaling is the main regulator that promotes the progression of human hepatocellular carcinoma (30–34). ERK1/2 participates in liver injury in human liver stem cells (35, 36). Also, the aggressive behavior of HCC cells has a positive relationship with the level of phosphorylated ERK and activated level of hepatic stellate cells (aHSCs) (37). Thus, we speculated GCDA mediated survival and chemoresistance *via* the ERK1/2 pathway in liver cancer cells. Our results showed that activation levels of ERK1/2 increased significantly following GCDA treatment in hepatocellular carcinoma cells (**Figures 2A, B**). After ERK1/2 was silenced by siRNA or phosphorylation of ERK1/2 was blocked by PD98059, cell proliferation was significantly decreased (**Figures 1D, E** and **3A**). In the light of those results, it is reasonable to suggest that the ERK1/2 pathway is involved with GCDA-induced survival in HCC cells.

Because of binding to many scaffold proteins or cytoplasmic anchors in resting cells, ERK1/2 is usually localized in the cytoplasm (15). Upon stimulation, numerous ERK1/2 molecules are translocated to the nucleus (14). In QGY-7703 cells, ERK1/2 and p-ERK1/2 could aggregate in the nucleus after treatment with GCDA (**Figures 4A, B**). Therefore, nuclear aggregation of ERK1/2 molecules must be relevant to HCC cell

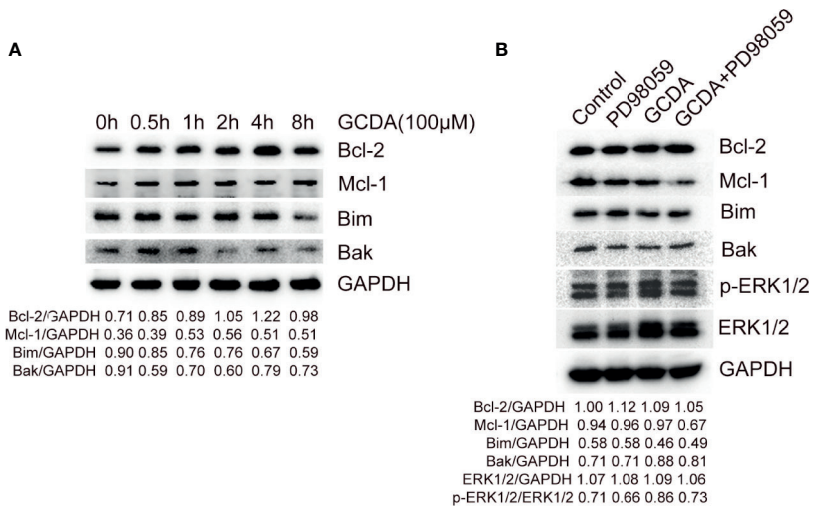

FIGURE 5 | PD98059 suppresses GCDA-stimulated increase of Mcl-1 and decrease of Bim. **(A)** 100μM GCDA was used to treat QGY-7703 cells for 0h, 0.5h, 1h, 2h, 4h and 8h. Expression of Bcl-2, Mcl-1, Bim and Bak was tested by western blot and quantified by Alphaview software. **(B)** QGY-7703 cells were preincubated with 10μM PD98059 for 0.5 h, followed by treatment with 100μM GCDA for 8h. All cell extracts were analyzed using Bcl-2, Mcl-1, Bim, Bak, p-ERK1/2 and ERK1/2 antibodies by Western blotting and quantified by Alphaview.

proliferation signal transduction following GCDA treatment. However, such nuclear accumulation could be decreased by inhibitor PD98059 (**Figures 4A, B**), which meant that the GCDA-induced survival signal is impaired by PD98059. Based on the evidence in this study, preventing ERK1/2 from entering the nucleus may be considered as a novel strategy to arrest liver cancer growth.

Activated ERK1/2 is also translocated to mitochondria, Golgi, the endoplasmic reticulum, or endosomes/lysosomes, thereby influencing cell physiology (38). Among them, the mitochondrial anchored ERK1/2 molecules are involved with the mitochondrial apoptosis pathway *via* affecting Bcl-2 family members (16). Usually, ERK1/2 signaling facilitates cell survival *via* activating pro-survival proteins (Bcl-2, Mcl-1, and Bcl-xL) and inhibiting pro-apoptotic proteins (Bim, Bad, Bmf, and Puma) (16). Among them, the transcription of pro-survival protein Bcl-2 can be promoted by ERK1/2 signaling through cAMP-responsive element-binding protein (CREB) (39). Besides, Bcl-2 itself can also be phosphorylated at Ser87 by ERK1/2, which is proposed to inhibit its pro-survival function (14). The mRNA level of Mcl-1 is verified to be promoted in response to ERK1/2 pathway *via* CREB or transcription factor ELK1 (40). Also, the short half-life of Mcl-1 protein can be prolonged *via* direct phosphorylation by ERK1/2 (41). Bim, is a prominent target of ERK1/2 signaling (42). ERK1/2-induced activation of Bim leads to ubiquitylation and degradation (43). Bak is the apoptotic effector protein of Bcl-2 family. Bak can be directly activated by Bim and cause the release of cytochrome c (44). In the present research, we observed that inhibiting ERK1/2 phosphorylation by PD98059 blocked GCDA-induced increase of Mcl-1 and decrease of Bim. However, Bcl-2 and Bak did not change significantly (**Figures 5A, B**). These results showed that the GCDA-induced change of Mcl-1 and Bim might be regulated by ERK1/2 pathway, while the variation of Bcl-2 and Bak may be induced by GCDA in an ERK-independent manner.

In conclusion, the present results found that GCDA-stimulated cell proliferation and chemoresistance could be attenuated *via* targeting the ERK pathway. GCDA was able to potently promote phosphorylation and nuclear aggregation of ERK1/2 molecules, which eventually led to the increased level of anti-apoptotic Bcl-2 family member proteins (Bcl-2 and Mcl-1) and the decreased expression of pro-apoptotic Bcl-2 family members (Bim and Bak). The inhibitor PD98059 not only suppressed the phosphorylation of ERK1/2, but also blocked ERK1/2 nuclear accumulation of the nucleus and attenuated GCDA-stimulated increase of Mcl-1 and decrease of Bim. Therefore, disruption of the pro-survival function of GCDA by blocking phosphorylation and nuclear accumulation of ERK1/2 molecules represents tactics for treating GCDA-related liver cancer and chemoresistance.

DATA AVAILABILITY STATEMENT

The original contributions presented in the study are included in the article/**Supplementary Material**. Further inquiries can be directed to the corresponding author.

AUTHOR CONTRIBUTIONS

MY contributed to conceive and designed the experiments. BL performed the data analyses and wrote the manuscript. MZ contributed significantly to analysis and manuscript preparation. JW and HX helped perform the analysis with constructive

discussions. All authors contributed to the article and approved the submitted version.

FUNDING

This work was supported by the National Natural Science Foundation of China (grant numbers 81703412, 81402001) and the Natural Science Foundation of Hunan Province (grant numbers 2020JJ4889, 2018JJ3830, and 2016JJ3177).

SUPPLEMENTARY MATERIAL

The Supplementary Material for this article can be found online at: https://www.frontiersin.org/articles/10.3389/fonc.2021.663944/full#supplementary-material

REFERENCES

1. Bruix J, Gores GJ, Mazzaferro V. Hepatocellular Carcinoma: Clinical Frontiers and Perspectives. *Gut* (2014) 63(5):844–55. doi: 10.1136/gutjnl-2013-306627
2. Ioannou GN, Feld JJ. What Are the Benefits of a Sustained Virologic Response to Direct-Acting Antiviral Therapy for Hepatitis C Virus Infection? *Gastroenterology* (2019) 156(2):446–60.e2. doi: 10.1053/j.gastro.2018.10.033
3. Kulik L, El-Serag HB. Epidemiology and Management of Hepatocellular Carcinoma. *Gastroenterology* (2019) 156(2):477–91.e1. doi: 10.1053/j.gastro.2018.08.065
4. Dhanasekaran R, Nault JC, Roberts LR, Zucman-Rossi J. Genomic Medicine and Implications for Hepatocellular Carcinoma Prevention and Therapy. *Gastroenterology* (2019) 156(2):492–509. doi: 10.1053/j.gastro.2018.11.001
5. Zhou M, Zhang Q, Zhao J, Liao M, Wen S, Yang M. Phosphorylation of Bcl-2 Plays an Important Role in Glycochenodeoxycholate-Induced Survival and Chemoresistance in HCC. *Oncol Rep* (2017) 38(3):1742–50. doi: 10.3892/or.2017.5830
6. Jaiswal K, Lopez-Guzman C, Souza RF, Spechler SJ, Sarosi GAJr. Bile Salt Exposure Increases Proliferation Through P38 and ERK MAPK Pathways in a Non-Neoplastic Barrett's Cell Line. *Am J Physiol Gastrointest Liver Physiol* (2006) 290(2):G335–42. doi: 10.1152/ajpgi.00167.2005
7. Jaiswal K, Tello V, Lopez-Guzman C, Nwariaku F, Anthony T, Sarosi GAJr. Bile Salt Exposure Causes Phosphatidyl-Inositol-3-Kinase-Mediated Proliferation in a Barrett's Adenocarcinoma Cell Line. *Surgery* (2004) 136(2):160–8. doi: 10.1016/j.surg.2004.04.008
8. Ishizuka S, Shiwaku M, Hagio M, Suzuki T, Hira T, Hara H. Glycochenodeoxycholic Acid Promotes Proliferation of Intestinal Epithelia via Reduction of Cyclic AMP and Increase in H2AX Phosphorylation After Exposure to γ-Rays. *Biomed Res* (2012) 33(3)159–65. doi: 10.2220/biomedres.33.159
9. Komichi D, Tazuma S, Nishioka T, Hyogo H, Chayama K. Glycochenodeoxycholate Plays a Carcinogenic Role in Immortalized Mouse Cholangiocytes via Oxidative DNA Damage. *Free Radic Biol Med* (2005) 39(11):1418–27. doi: 10.1016/j.freeradbiomed.2005.07.005
10. Wang C, Yang M, Zhao J, Li X, Xiao X, Zhang Y, et al. Bile Salt (Glycochenodeoxycholate Acid) Induces Cell Survival and Chemoresistance in Hepatocellular Carcinoma. *J Cell Physiol* (2019) 234(7):10899–906. doi: 10.1002/jcp.27905
11. Sun MH, Chen XC, Han M, Yang YN, Gao XM, Ma X, et al. Cardioprotective Effects of Constitutively Active MEK1 Against H2O2-Induced Apoptosis and Autophagy in Cardiomyocytes via the ERK1/2 Signaling Pathway. *Biochem Biophys Res Commun* (2019) 512(1):125–30. doi: 10.1016/j.bbrc.2019.03.008
12. Caragarajah BJ, Khokhlatchev A, Cobb MH, Goldsmith EJ. Activation Mechanism of the MAP Kinase ERK2 by Dual Phosphorylation. *Cell* (1997) 90(5):859–69. doi: 10.1016/S0092-8674(00)80351-7
13. Yao Z, Seger R. The ERK Signaling Cascade–Views From Different Subcellular Compartments. *BioFactors (Oxford England)* (2009) 35(5):407–16. doi: 10.1002/biof.52
14. Cook SJ, Stuart K, Gilley R, Sale MJ. Control of Cell Death and Mitochondrial Fission by ERK1/2 MAP Kinase Signalling. *FEBS J* (2017) 284(24):4177–95. doi: 10.1111/febs.14122
15. Wainstein E, Seger R. The Dynamic Subcellular Localization of ERK: Mechanisms of Translocation and Role. *Curr Opin Cell Biol* (2016) 39:15–20. doi: 10.1016/j.ceb.2016.01.007
16. .Sale MJ, Cook SJ. That Which Does Not Kill Me Makes Me Stronger; Combining ERK1/2 Pathway. *Br J Pharmacol* (2013) 169(8):1708–22.
17. Xie B, Zhang L, Hu W, Fan M, Jiang N, Duan Y, et al. Dual Blockage of STAT3 and ERK1/2 Eliminates Radioresistant GBM Cells. *Redox Biol* (2019) 24:101189. doi: 10.1016/j.redox.2019.101189
18. Hsieh MJ, Wang CW, Lin JT, Chuang YC, Hsi YT, Lo YS, et al. Celastrol, a Plant-Derived Triterpene, Induces Cisplatin-Resistance Nasopharyngeal Carcinoma Cancer Cell Apoptosis Though ERK1/2 and P38 MAPK Signaling Pathway. *Phytomed Int J Phytotherapy Phytopharmacol* (2019) 58:152805. doi: 10.1016/j.phymed.2018.12.028
19. Zhong J, Yu X, Dong X, Lu H, Zhou W, Li L, et al. Downregulation of Secreted Clusterin Potentiates the Lethality of Sorafenib in Hepatocellular Carcinoma in Association With the Inhibition of ERK1/2 Signals. *Int J Mol Med* (2018) 41(5):2893–900. doi: 10.3892/ijmm.2018.3463
20. Liao M, Zhao J, Wang T, Duan J, Zhang Y, Deng X. Role of Bile Salt in Regulating Mcl-1 Phosphorylation and Chemoresistance in Hepatocellular Carcinoma Cells. *Mol Cancer* (2011) 10:44. doi: 10.1186/1476-4598-10-44
21. Chen M, Zhuang C, Liu Y, Li J, Dai F, Xia M, et al. Tetracycline-Inducible shRNA Targeting Antisense Long Non-Coding RNA HIF1A-AS2 Represses the Malignant Phenotypes of Bladder Cancer. *Cancer Lett* (2016) 376(1):155–64. doi: 10.1016/j.canlet.2016.03.037
22. Chen M, Li J, Zhuang C, Cai Z. Increased lncRNA ABHD11-AS1 Represses the Malignant Phenotypes of Bladder Cancer. *Oncotarget* (2017) 8(17):28176–86. doi: 10.18632/oncotarget14945
23. Chen M, Zhang R, Lu L, Du J, Chen C, Ding K, et al. LncRNA PVT1 Accelerates Malignant Phenotypes of Bladder Cancer Cells by Modulating. *Aging (Albany NY)* (2020) 12(21):22291–312. doi: 10.18632/aging.202203
24. Ghosh S. Cisplatin: The First Metal Based Anticancer Drug. *Bioorg Chem* (2019) 88:102925. doi: 10.1016/j.bioorg.2019.102925
25. Sun Z, Niu S, Xu F, Zhao W, Ma R, Chen M. CircAMOTL1 Promotes Tumorigenesis Through miR-526b/SIK2 Axis in Cervical Cancer. *Front Cell Dev Biol* (2020) 8:568190. doi: 10.3389/fcell.2020.568190
26. Marin JJG, Cives-Losada C, Asensio M, Lozano E, Briz O, Macias RIR. Mechanisms of Anticancer Drug Resistance in Hepatoblastoma. *Cancers* (2019) 11(3). doi: 10.3390/cancers11030407
27. Chen LC, Shibu MA, Liu CJ, Han CK, Ju DT, Chen PY, et al. ERK1/2 Mediates the Lipopolysaccharide-Induced Upregulation of FGF-2, uPA, MMP-2, MMP-9 and Cellular Migration in Cardiac Fibroblasts. *Chemico-biol Interact* (2019) 306:62–9. doi: 10.1016/j.cbi.2019.04.010
28. Wang K, Brems JJ, Gamelli RL, Ding J. Reversibility of Caspase Activation and its Role During Glycochenodeoxycholate-Induced Hepatocyte Apoptosis. *J Biol Chem* (2005) 280(25):23490–5. doi: 10.1074/jbc.M411607200
29. Gao L, Lv G, Li R, Liu WT, Zong C, Ye F, et al. Glycochenodeoxycholate Promotes Hepatocellular Carcinoma Invasion and Migration by AMPK/mTOR Dependent Autophagy Activation. *Cancer Lett* (2019) 454:215–23. doi: 10.1016/j.canlet.2019.04.009
30. Odagiri N, Matsubara T, Higuchi M, Takada S, Urushima H, Sato-Matsubara M, et al. Involvement of ERK1/2 Activation in the Gene Expression of Senescence-Associated Secretory Factors in Human Hepatic Stellate Cells. *Mol Cell Biochem* (2019) 455(1-2):7–19. doi: 10.1007/s11010-018-3466-x
31. Li H, Zhang M, Linghu E, Zhou F, Herman JG, Hu L, et al. Epigenetic Silencing of TMEM176A Activates ERK Signaling in Human Hepatocellular Carcinoma. *Clin Epigenet* (2018) 10(1):137. doi: 10.1186/s13148-018-0570-4
32. Hou H, Ge C, Sun H, Li H, Li J, Tian H. Tunicamycin Inhibits Cell Proliferation and Migration in Hepatocellular Carcinoma Through Suppression of CD44s and the ERK1/2 Pathway. *Cancer Sci* (2018) 109(4):1088–100. doi: 10.1111/cas.13518

33. Chen P, Lei L, Wang J, Zou X, Zhang D, Deng L, et al. Downregulation of Talin1 Promotes Hepatocellular Carcinoma Progression Through Activation of the ERK1/2 Pathway. *Cancer Sci* (2017) 108(6):1157–68. doi: 10.1111/cas.13247
34. Cong N, Li Z, Shao W, Li J, Yu S. Activation of ETA Receptor by Endothelin-1 Induces Hepatocellular Carcinoma Cell Migration and Invasion via ERK1/2 and AKT Signaling Pathway. *J Membrane Biol* (2016) 249(1-2):119–28. doi: 10.1007/s00232-015-9854-1
35. Wei Y, Zhang X, Wen S, Huang S, Huang Q, Lu S, et al. Methyl Helicterate Inhibits Hepatic Stellate Cell Activation Through Downregulating the ERK1/2 Signaling Pathway. *J Cell Biochem* (2019). doi: 10.1002/jcb.28756
36. Raška J, Čtveráčková L, Dydowiczová A, Sovadinová I, Bláha L, Babica P. Cylindrospermopsin Induces Cellular Stress and Activation of ERK1/2 and P38 MAPK Pathways in Adult Human Liver Stem Cells. *Chemosphere* (2019) 227:43–52. doi: 10.1016/j.chemosphere.2019.03.131
37. Xie YX, Liao R, Pan L, Du CY. ERK Pathway Activation Contributes to the Tumor-Promoting Effects of Hepatic Stellate Cells in Hepatocellular Carcinoma. *Immunol Lett* (2017) 188:116–23. doi: 10.1016/j.imlet.2017.06.009
38. Wortzel I, Seger R. The ERK Cascade: Distinct Functions Within Various Subcellular Organelle. *Genes Cancer* (2011) 2(3):195–209. doi: 10.1177/1947601911407328
39. Liu YL, Lai F, Wilmott JS, Yan XG, Liu XY, Luan Q, et al. Noxa Upregulation by Oncogenic Activation of MEK/ERK Through CREB Promotes. *Oncotarget* (2014) 5(22):11237–51. doi: 10.18632/oncotarget.2616
40. Domina AM, Vrana JA, Gregory MA, Hann SR, Craig RW. MCL1 is Phosphorylated in the PEST Region and Stabilized Upon ERK Activation in Viable Cells, and at Additional sites With Cytotoxic Okadaic Acid or Taxol. *Oncogene* (2004) 23(31):5301–15.
41. Maurer U, Charvet C, Wagman AS, Dejardin E, Green DR. Glycogen Synthase Kinase-3 Regulates Mitochondrial Outer Membrane. *Mol Cell* (2006) 21 (6):749–60.
42. Yang JY, Zong CS, Xia W, Yamaguchi H, Ding Q, Xie X, et al. ERK Promotes Tumorigenesis by Inhibiting FOXO3a via MDM2-Mediated Degradation. *Nat Cell Biol* (2008) 10(2):138–48.doi: 10.1038/ncb1676
43. Ley R, Balmanno K, Hadfield K, Weston C, Cook SJ. Activation of the ERK1/2 Signaling Pathway Promotes Phosphorylation and Proteasome-Dependent Degradation of the BH3-Only Protein, Bim. *J Biol Chem* (2003) 278 (21):18811–6.
44. Kuwana T, Hayes LB, Chipuk JE, Bonzon C, Sullivan BA, Green DR, et al. BH3 Domains of BH3-Only Proteins Differentially Regulate Bax-Mediated. *Mol Cell* (2005) 17(4):525–35. doi: 10.1016/jmolcel200502003

Conflict of Interest: The authors declare that the research was conducted in the absence of any commercial or financial relationships that could be construed as a potential conflict of interest.

frontiers in Oncology

ORIGINAL RESEARCH
published: 02 September 2021
doi: 10.3389/fonc.2021.715541

Long Noncoding RNA AC007639.1 Promotes the Pathogenesis and Progression of Hepatocellular Carcinoma Through Inhibiting Apoptosis and Stimulating Chemotherapeutic Resistance

Yun Bai[1†], Meijuan Ding[2†], Dan Lu[1], Yiwen Li[1], Shuai Yao[3], Lei Wang[4], Hui Li[1], Guanghua Cui[1], Xue Li[1], Xiaoke Sun[1] and Yu Yang[1]*

[1] Department of Oncology, Second Affiliated Hospital of Harbin Medical University, Harbin, China, [2] Department of Oncology, Harbin Medical University Cancer Hospital, Harbin, China, [3] Department of Technology, Harbin Nachuan Bio-Science Technology Co., Ltd., Harbin, China, [4] Department of Internal Medicine, Second Hospital of Heilongjiang Province, Harbin, China

OPEN ACCESS

Edited by:
Dong-Hua Yang,
St. John's University, United States

Reviewed by:
Samer Daher,
Rutgers University, Newark, United States
Sirisha Kondle,
Wayne State University, United States

***Correspondence:**
Yu Yang
yangyu13836125585@163.com

[†]These authors have contributed equally to this work

Specialty section:
This article was submitted to Gastrointestinal Cancers, a section of the journal Frontiers in Oncology

Received: 27 May 2021
Accepted: 12 August 2021
Published: 02 September 2021

Citation:
Bai Y, Ding M, Lu D, Li Y, Yao S, Wang L, Li H, Cui G, Li X, Sun X and Yang Y (2021) Long Noncoding RNA AC007639.1 Promotes the Pathogenesis and Progression of Hepatocellular Carcinoma Through Inhibiting Apoptosis and Stimulating Chemotherapeutic Resistance. Front. Oncol. 11:715541. doi: 10.3389/fonc.2021.715541

Background: Hepatocellular carcinoma (HCC) is known for its poor prognosis. Long noncoding RNAs (lncRNAs) are critical in the pathogenesis of various types of cancers. We tried to explore the role of lncRNA in the development of HCC.

Methods: We identified the role of lncRNA AC007639.1 in the pathogenesis of HCC through bioinformatics and biological experiments in HepG2, Hep3B, and SMMC-7721 cells as well as the nude mice xenograft model.

Results: We found that lncRNA AC007639.1 was overexpressed in hepatocellular carcinoma. Knocking down of lncRNA AC007639.1 by specific siRNAs or shRNAs promoted cancer cell death. The growth of mouse xenograft tumor created using lncRNA AC007639.1 deficient HepG2 cells was significantly slowed down. Furthermore, the knockdown of lncRNA AC007639.1 in HCC cells led to the increased expression of p53 and decreased expression of angiopoietin-like 4.

Conclusion: LncRNA AC007639.1 was involved in the pathogenesis and progression of hepatocellular carcinoma by inhibition of apoptosis and increasing HCC resistance to chemotherapy.

Keywords: long noncoding RNA, hepatocellular carcinoma, bioinformatics, p53, chemotherapy

INTRODUCTION

The American Cancer Society estimates that there will be about 42,230 new cases of liver cancer, with 30,230 deaths due to liver cancer in the United States in 2021, representing a more than tripled incidence and more than doubled mortality since 1980. Worldwide, people diagnosed with liver cancer exceed 800,000 and more than 700,000 deaths are due to liver cancer each year, making liver

cancer a leading cause of cancer-related deaths (1). One of the main causes of liver cancer, hepatitis B virus infection, is even more deleterious in leading to fulminant hepatitis (2–5), and the virus can be passed to the newborns without proper control of HBV level and HBV vaccination (6). Therefore, the mechanisms of tumorigenesis and factors affecting the prognosis of hepatocellular carcinoma (HCC) deserve more attention.

Long noncoding RNAs (lncRNAs), by definition, are not translated into proteins (7). Increasing evidence has shown that lncRNAs are involved in the pathogenesis and progression of different types of cancers (8, 9). Many of the lncRNAs are promising markers for the diagnosis and prognosis of liver cancer (10).

In this study, the role of lncRNA AC007639.1 in the pathogenesis and prognosis of HCC was explored by bioinformatics analysis and biological experiments using three different liver cancer cell lines. We found that lncRNA AC007639.1 knockdown led to increased cancer cell death. Importantly, lncRNA AC007639.1 could inhibit the p53 signaling pathway and increase the expression of Angiopoietin-like 4 (ANGPTL4) leading to inhibition of apoptosis and increasing of HCC resistance to chemotherapy.

MATERIALS AND METHODS

Bioinformatic Analysis

Transcriptome sequencing data including mRNA and lncRNA were generated by R package in Liver Hepatocellular Carcinoma Project of The Cancer Genome Atlas (TCGA-LIHC) dataset (n=420) using TCGA biolinks (https://bioconductor.org/packages/release/data/experiment/vignettes/TCGAbiolinksGUI.data/inst/doc/vignettes.html), and SRP069212 (n=355) using Gene Expression Profiling Interactive Analysis (GEPIA; http://gepia.cancer-pku.cn/). Differential mRNA abundance was analyzed using DESeq2 (11). Genes with reads > 5 were included in the final quantitative and statistical analysis. Heatmaps and volcano plots were prepared using the R package. Normalized gene expression levels were analyzed by Gene Set Variation Analysis (GSVA). Survival analysis was done by R package survival. Cox proportional hazard (PH) model was constructed by R package (survminer). The best-scanned cutoff points had the most significant split (log-rank test).

Cell Culture

Human HCC cell lines HepG2 (RRID : CVCL_ 0027), SMMC-7721 (RRID : CVCL_ 0534), and Hep3B (RRID : CVCL_ 0326), were obtained from the Shanghai Zhong Qiao Xin Zhou Biothechnology Co., Ltd., (Shanghai, China). The cells were confirmed to have no mycoplasma contamination using Mycoplasma Detection Kit (R&D Systems China Co., Ltd., Shanghai, China). Dulbecco's modified Eagle's medium (DMEM, Gibco, Thermo Fisher Scientific, Inc.) was used for cell culture, with 10% fetal bovine serum (FBS, Gibco), 2 mM L-glutamine (Gibco), 10 mM HEPES (Gibco), 1 mM pyruvate sodium (Gibco), and 100 U/ml penicillin with 100 μg/ml streptomycin (Gibco). Cells were grown at 37°C with 5% CO_2.

Construction of Stable Knockdown of Lnc RNA AC007639.1 in HepG2 and Hep3B Cells

Cells with stable lnc RNA AC007639.1-knockdown, ANGPTL4-knockdown, or control HepG2-LNC-NC cells were created using shRNA 5'- GGUGAGUGCAUGUAGUCAUTT -3', 5'- AGAA CAGCAGGAUCCAGCAACUCUU -3', or scramble control sequence 5'- UUCUCCGAACGUGUCACGUTT -3'. shRNA oligos were cloned into a LV3(H1/GFP&Puro) vector (map shown in **Figure S1**), respectively. The corresponding plasmids were packaged using lentivirus (Shanghai GenePharma, China). Puromycin (5 μg/ml final concentration, Sigma, St. Louis, MO) was used to select HCC cells carrying the transfected shRNA.

siRNAs Transfection Into HCC Cells

Specific short interfering RNAs (siRNAs) or control siRNA to knock down lnc RNA AC007639.1 were purchased from the Shanghai GenePharma (Shanghai, China). 30nM of siRNAs (**Table S1**) were used for transfection in the HCC cells using X-tremeGENE reagent (Roche Applied Science, Shanghai, China).

RNA Extraction and Quantitative RT-PCR

For RNA extraction, cells or tissues were homogenized with TRIzol reagent (Thermo Fisher Scientific, Inc.). RNAs were purified and quantified using the NanoDrop 2000 Spectrophotometer (Thermo Fisher Scientific, Inc.). RNAs were reversely transcribed by the RT reagent Kit (Nachuan Bio-Tech Co., Binzhou, China). qRT-PCR experiments were done in 10 μL total volume, which contained 1x SYBR Green Master mix (Nachuan Bio-Tech Co., China), cDNA (10 ng), and primers (75 nM of forward and 75 nM reverse primers, **Table S1**) in an Exicycle 96 Real-Time Quantitative Thermal Block (Bioneer, China), with initial incubation at 95°C (10 min), 40 cycles at 95°C (15 s) and 60°C (1 min). qRT-PCR experiments were triplicated, the averages of which were normalized (by β-actin), and the relative expression of AC007639.1 was calculated using the $2^{-\Delta\Delta Ct}$ method.

Cell Count Kit-8 Assay

Cell proliferation was determined using the CCK-8 assay kit (DOJINDO, Japan). Briefly, cells (1 x 10^4/well) were grown in 96-well plates. At the same time of each day (10 am), CCK-8 reagent (10 μl) was diluted with 100 μl medium and added to each well. After incubation for 2 hours, the light absorbance at 450 nm was recorded with a microplate spectrophotometer (K8001, Shanghai Yoke Instrument Co., Ltd., China) (12).

EdU Assay

The EdU assay was performed using a KFluor488 Click It 5-ethynyl-2'-deoxyuridine Imaging Test Kit (KGA331-500; keyGen, Nanjing, China). At 24 hours after transfection, 10^5 cells were seeded in each well of a 24-well plate. After incubation for 24 hours, EdU was added (final concentration of 50 μM). After 2 hours incubation with EdU, cells were fixed with 150 μl of 4% formaldehyde in PBS for 20 min. A 495-nm laser was used to excite kFluor488-azide and images were captured under a fluorescence microscope (IX81, Olympus Corporation, Beijing, China). Nuclei were counterstained with DAPI.

Western Blotting

Forty-eight hours post transfection, cells were lysed in RIPA lysis buffer (Merck Group, Germany) for 30 min on ice. Protein concentrations were determined using a BCA assay kit (Solarbio, China). Lysates with equal amounts were loaded and separated by 12% SDS-polyacrylamide gel electrophoresis. Proteins were transferred onto polyvinylidene difluoride membranes, followed by probing with target antibodies. Primary antibodies included: Beta-actin (Affinity T0022, 1:1000), and p53 (Affinity AF0879, 1:1000), and the secondary antibody (Affinity S0001, 1:5000) were obtained from Xiangtai Biological Technology Co., Ltd. (China); and ANGPTL4 (Boster A01147, 1:1000) was purchased from Boster Biological Technology (Pleasanton, CA).

Establishment of Mouse Xenograft Tumor Model

The animal protocol was approved by the Ethical Committee of the Second Affiliated Hospital of Harbin Medical University (a tertiary hospital in northeast China). Male BALB/c nude mice were purchased from Beijing Vital River Laboratory Animal Technology Co., Ltd., and housed in a temperature-controlled, specific-pathogen-free animal facility, with a 12h light/12h dark cycle and free access to food and water. Animals were properly treated in accordance with the national and institutional ethical requirements of experimental animals. 1.5×10^6 of HepG2-LNC-KD or HepG2-LNC-NC cells were resuspended in 0.1 ml sterile PBS, and subcutaneously injected in the left flank of mice at the age of 8 weeks. The size of tumor was monitored every morning (length x width x depth in mm^3). Mice were sacrificed 2 weeks after cell injection (n = 7 per group).

Immunohistochemistry

Sections (10 μm) of paraffin-embedded xenograft tissue samples were used for immunohistochemistry staining. Slides were incubated with PCNA antibody (1:100 dilution in PBS; AF0239, Affinity Biosciences LTD.) or p53 (1:100 in PBS; Affinity AF0879) at overnight 4°C. After gentle rinsing off primary antibody solutions, slides were incubated with the secondary antibody (1:200 dilution in PBS; S0001, Affinity Biosciences LTD.) at 37°C for 1 hour. Finally, nuclei were counterstained with hematoxylin.

Statistics

Except for bioinformatics, statistical analyses were done with SPSS version 24.0 (Armonk, NY: IBM Corp.). Continuous data were shown as mean ± SD. Differences between the two groups were analyzed by independent Student's t-test. $p < 0.05$ was considered significant in 2-tailed statistical tests.

RESULTS

LncRNA AC007639.1 Expression in HCC

According to the bioinformatic analysis of TCGA-LIHC dataset using the DESeq2 software package, lncRNA AC007639.1 expression in HCC tissues was found to be significantly higher than that of adjacent non-tumor liver tissue (**Figures 1A, B**). The median level of lncRNA AC007639.1 was used as a cut-off to differentiate the high- and low- AC007639.1 expression groups. Using the GEPIA online tool (13) and R language survival analysis, the patients in the high AC007639.1 expression group were found to have a shorter survival period (**Figures 1C, D**). These results indicated that AC007639.1 was overexpressed in HCC tissues and the high level of AC007639.1 was indicative of poor prognoses.

Prediction of the Functions of LncRNA AC007639.1 in HCC

Differentially expressed genes in the high- and low- AC007639.1 expression groups in the TCGA-LIHC dataset were analyzed by DEseq2 (**Figure 2A**). The enrichment of genes was analyzed using GSVA. The AC007639.1 high expression group was found to have highly enriched HCC up-regulating gene sets (**Figure 2B**). GO enrichment analysis (14) showed that AC007639.1 was involved in diverse cell functions such as immune functions (**Figures 2C, D**). LncRNA AC007639.1 was found to regulate the cell cycle (**Figure 3A**), increase HCC resistance to Doxorubicin (**Figure 3B**), and decrease the protein expression of p53 (**Figure 3C**).

LncRNA AC007639.1 in the Proliferation of HCC Cells

In order to investigate the function of AC007639.1 in HCC, three specific siRNAs were designed to knock down its expression in HCC cell lines, among which both siRNA1 and siRNA3 significantly downregulated AC007639.1 in HepG2, Hep3B, and SMMC-7721 cells ($p<0.001$ for both siRNAs, **Figure 4A**). The lncRNA AC007639.1 knockdown cells showed higher inhibition of proliferation after treated with different concentrations of Doxorubicin than that of the control groups (**Figure 4B**), which was also confirmed by EdU analysis (**Figure 4C**). Expression of p53 protein in HepG2, Hep3B, and SMMC-7721 cells were increased when treated with DOX after siRNA1 and siRNA3 transfection (**Figure 4D**). The above findings suggested that knocking down of AC007639.1 inhibited HCC cell growth, and promoted HCC apoptosis.

LncRNA AC007639.1 in Nude Mice Xenografts

To explore the role of AC007639.1 *in vivo*, we developed the HepG2-LNC-KD cells that carried a stable knockdown level of AC007639.1 (confirmed by qRT-PCR, data not shown), and used the cells to create a xenograft tumor mouse model in nude mice. The size of xenograft tumor was significantly smaller in the stable knockdown group at 2 weeks compared with the knockdown group (**Figures 5A, B**), with a slower time-course growth rate (**Figure 5C**). The expression of AC007639.1 in the xenograft were significantly lower in the knockdown group, with a significant higher P53 expression (**Figure 5D**). P53 and PCNA immunohistochemistry showed increased p53-positive cells,

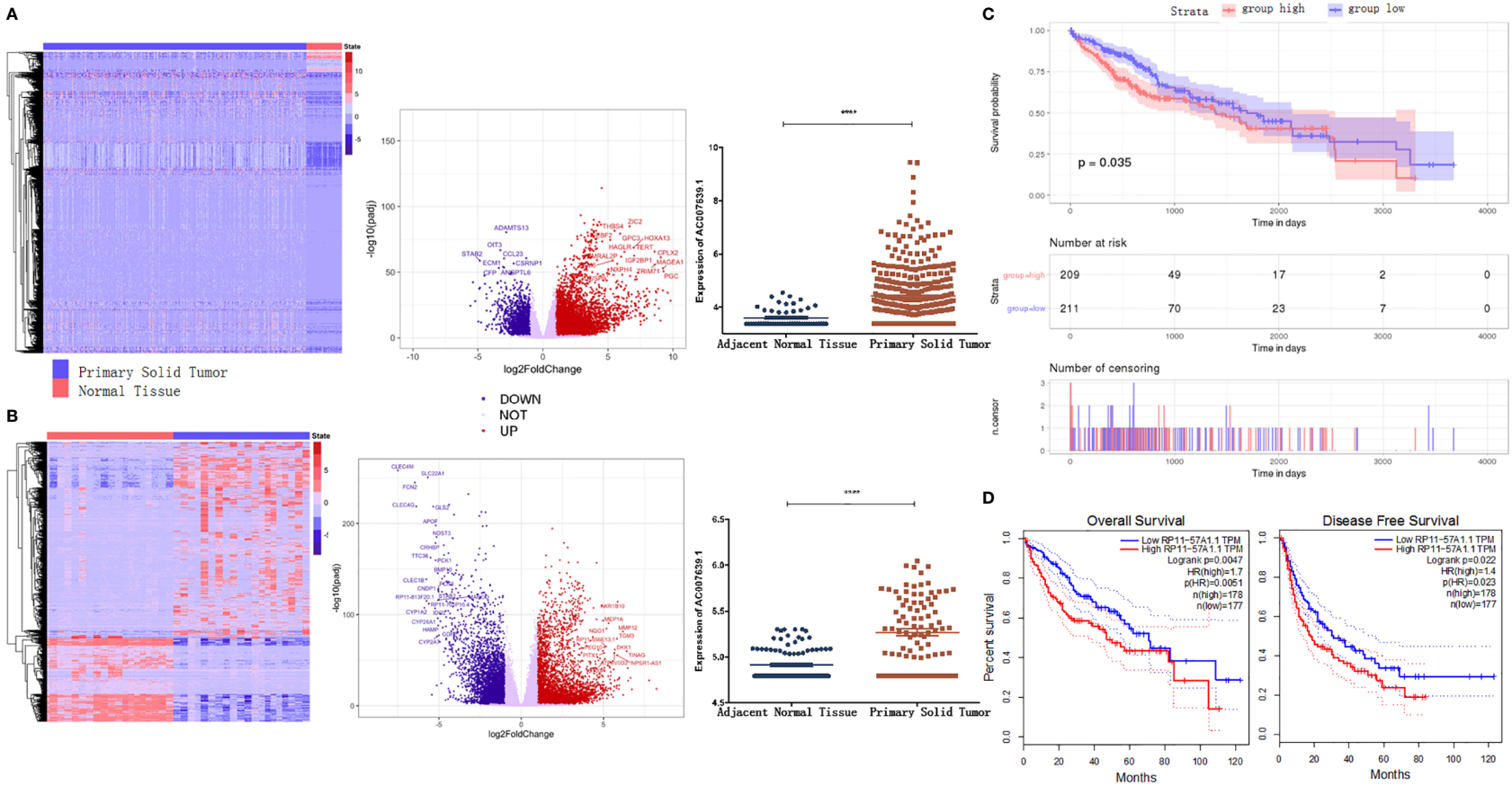

FIGURE 1 | LncRNA AC007639.1 is highly expressed in hepatocellular carcinoma tissues and implies a poor prognosis. **(A)** Heatmap of transcriptome (left) and volcano plot (middle) of different genes, and lncRNA AC007639.1 expressions in TCGA-LIHC cases (right, n=420, https://gdc.cancer.gov/resources-tcga-users/tcga-code-tables/data-levels); **(B)** Heatmap of transcriptome (left) and volcano plot (middle) of different genes, and lncRNA AC007639.1 expressions in SRP069212 cases (right, n=355); **(C, D)** Kaplan-Meier survival curves of TCGA-LIHC dataset analyzed by TCGAbiolinks or SRP069212 dataset analyzed by GEPIA, respectively. ****p < 0.001 (Mann-Whitney test).

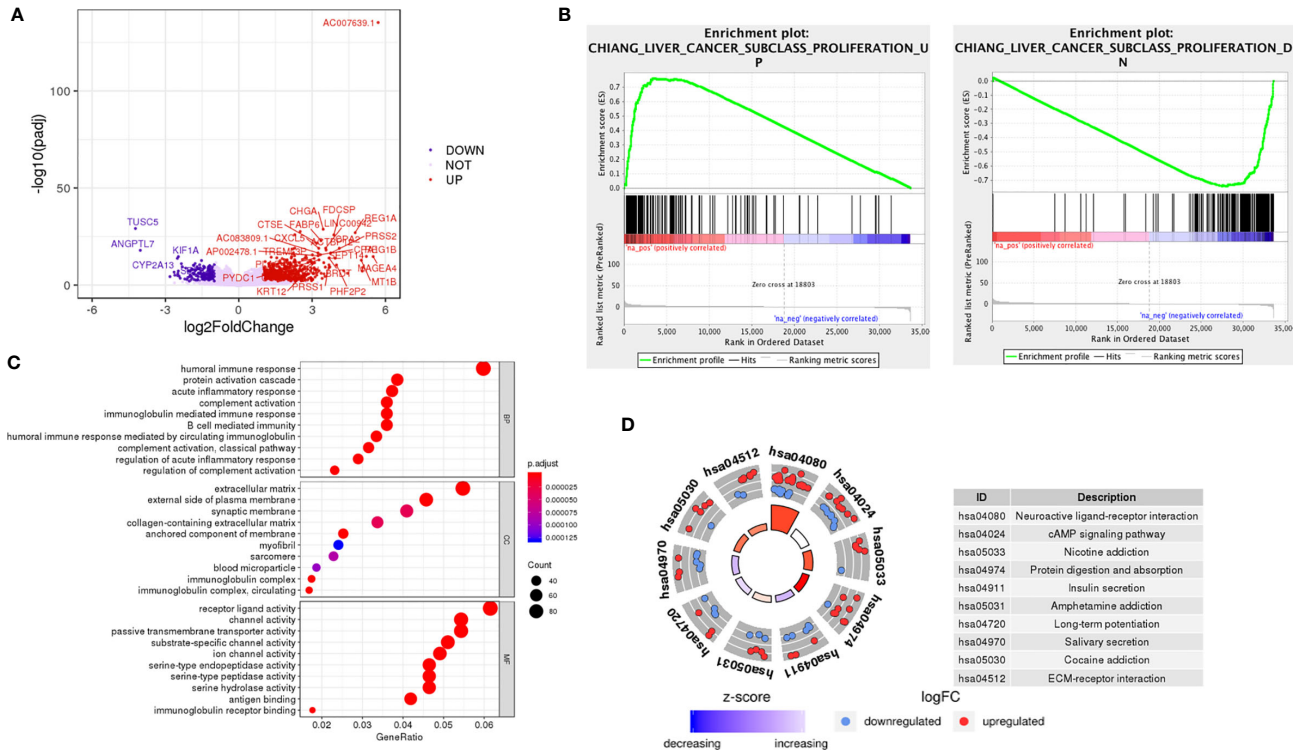

FIGURE 2 | The role of LncRNA AC007639.1 in liver cancer. **(A)** Differential gene expressions between the high- and low- expression of lncRNA AC007639.1 groups (TCGA-LIHC). **(B)** LncRNA AC007639.1 functions analyzed by GSVA. The up-regulated genes in proliferative liver cancer were highly enriched in the AC007639.1 high expression group (p<0.001), while the down-regulated genes in proliferative liver cancer is highly enriched in the AC007639.1 low expression group (p<0.001). **(C)** GO analysis and **(D)** KEGG and cluster network analysis using Clusterprofiler Package of R language, screening criteria p < 0.05, correction p < 0.05.

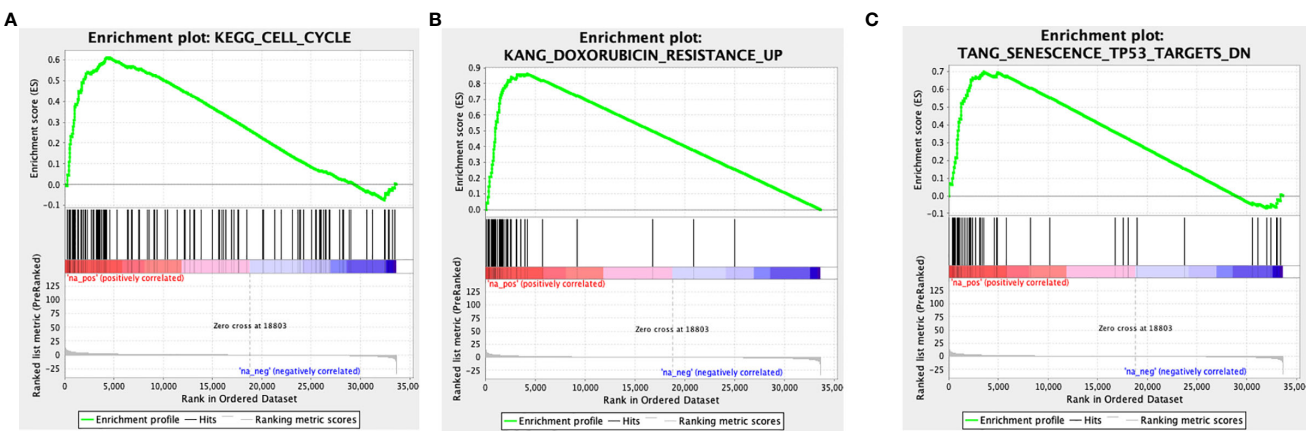

FIGURE 3 | LncRNA AC007639.1 regulates the susceptibility of liver cancer to doxorubicin by inhibiting the p53 pathway, analyzed by GSVA. **(A)** The effect of lncRNA AC007639.1 on cell cycle (p < 0.001); **(B)** The effects of lncRNA AC007639.1 on doxorubicin resistance (p < 0.001); **(C)** The effects of lncRNA AC007639.1 on p53 target genes (p < 0.001).

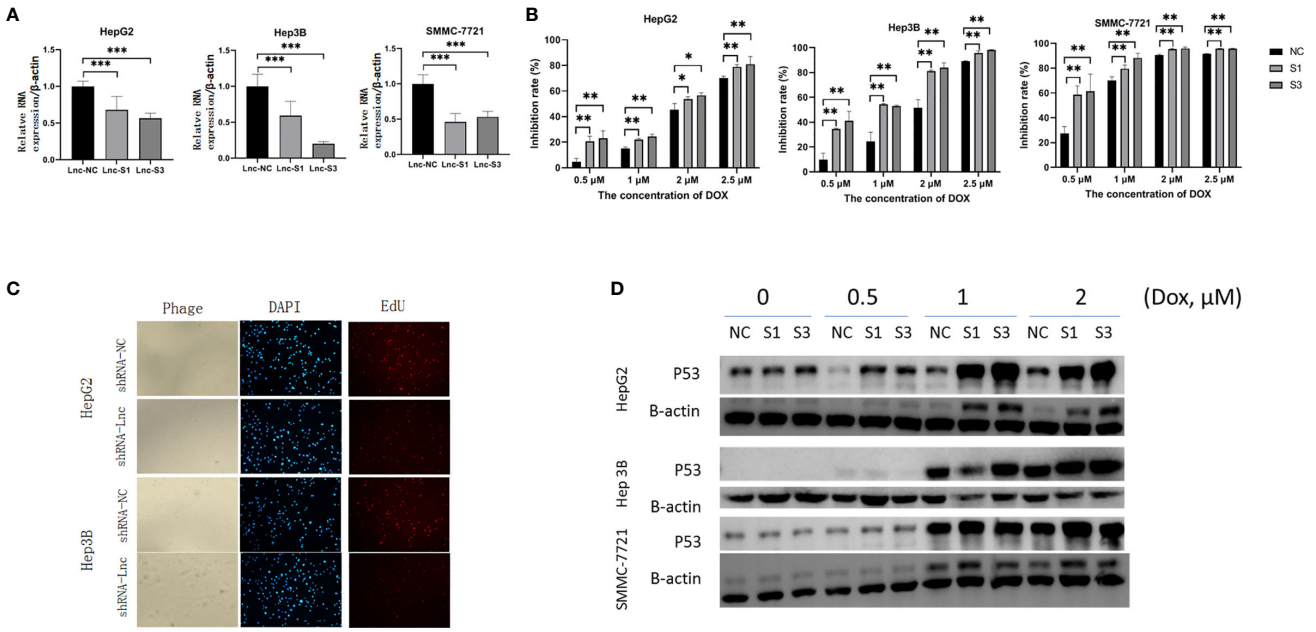

FIGURE 4 | Knockdown of lncRNA AC007639.1 inhibits the growth of hepatocellular carcinoma cells and promotes apoptosis. **(A)** qRT-PCR on the relative AC007639.1 expression in HepG2, Hep3B, and SMMC-7721 cells transfected with two lncRNA AC007639.1 or control siRNAs (Lnc-S1, Lnc-S3, or Lnc-NC, respectively); **(B)** CCK-8 assay showing inhibition of HepG2, Hep3B, and SMMC-7721 cells at different concentrations of doxorubicin after siRNAs transfection; **(C)** EdU analysis showing cell proliferation after transfection of scrambled shRNA (NC) or shRNA for lncRNA (shRNA-Lnc) (field of view: 200x) in HepG2 or Hep3B cells treated with 2.5 μM doxorubicin for 48 hours; **(D)** Western blots of p53 in the three cells lines after exposure to different concentrations of doxorubicin. NC: scrambled control siRNA or shRNA. S1, siRNA1; S3, siRNA3. *p < 0.05, **p < 0.01, ***p < 0.001.

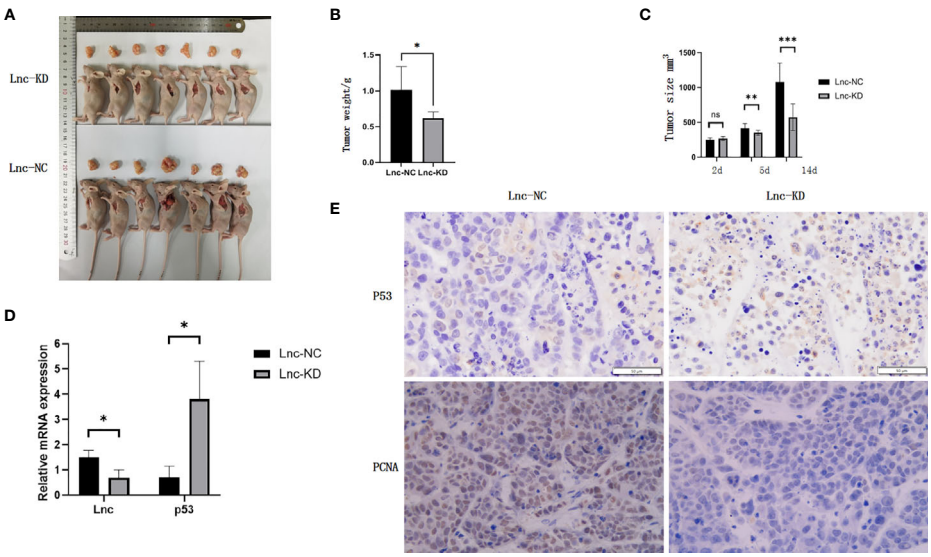

FIGURE 5 | Knockdown of lncRNA AC007639.1 inhibits the growth of tumor xenografts in nude mice. **(A)** The size of HepG2 xenografts using HepG2-LNC-KD or HepG2-LNC-NC cells at 14 days; **(B)** Weight of xenografts at collection; **(C)** Xenografts growth monitored in mm^3; **(D)** Relative AC007639.1 and p53 expressions (normalized to β-actin) in xenografts with HepG2-LNC-KD or HepG2-LNC-NC cells; **(E)** p53 and PCNA immunohistochemistry in xenograft tissues (field of view: 200x). Brown colored cells were positive for P53 or PCNA, respectively. *p < 0.05, **p < 0.01, ***p < 0.001; ns, not statistically significant.

reduced cell atypia, and reduced PCNA-positive cells after AC007639.1 was knocked down (**Figure 5E**). These results showed that lncRNA AC007639.1 is important in xenograft tumor growth.

The Mechanism of AC007639.1 in Regulating Cell Functions

The above bioinformatics analysis indicated that AC007639.1 regulated HCC cell proliferation. We further analyzed the role of lncRNA AC007639.1 by sequencing gene expressions in HepG2 (**Figures 6A–C**) cells after the transfection of siRNA3. Among the genes with significant changes, ANGPTL4 was selected for further analysis. ANGPTL4 protein was significantly lower in HepG2 cells after AC007639.1 was knocked down (**Figure 7A**), and ANGPTL4 protein level also decreased in xenografts injected with HepG2-LNC-KD (**Figures 7B, C**). Knocking down of ANGPTL4 increased the inhibitory effect of Doxorubicin in HepG2, Hep3B, and SMMC-7721 cells (**Figures 7D, E**).

DISCUSSION

LncRNAs and endonuclease (15) are involved in the pathogenesis of liver cancer. Most lncRNAs promote the proliferation of HCC through microRNAs (16).

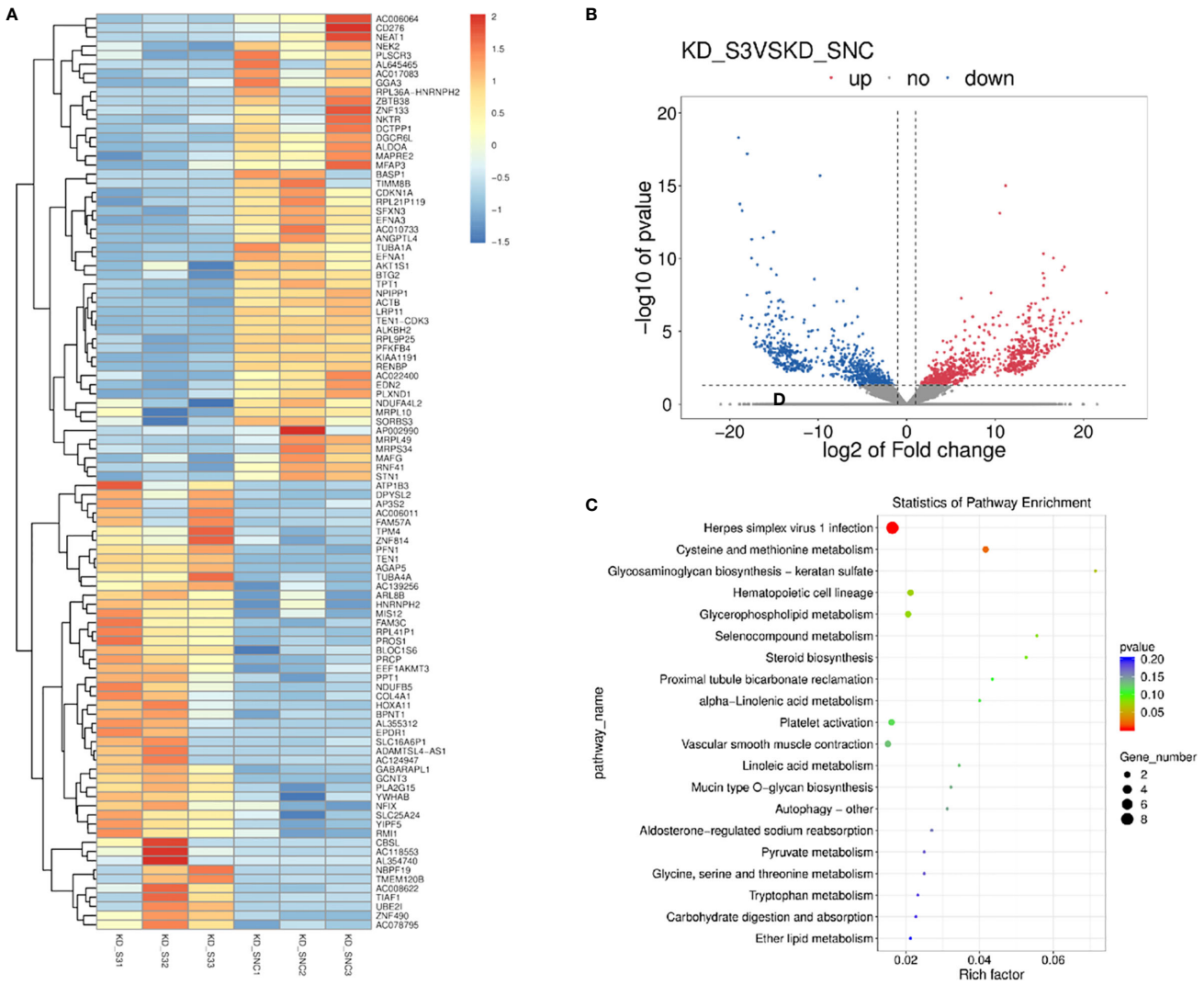

FIGURE 6 | The involvement of lncRNA AC007639.1 in different pathways. **(A)** Heatmap showing different gene expressions after the knock down of lncRNA AC007639.1 in HepG2 cells using siRNA3; **(B)** Volcano plot of different gene expressions after the knock down of lncRNA AC007639.1 in HepG2 cell line; **(C)** Pathways enrichment after the knock down of lncRNA AC007639.1 in HepG2 cell line.

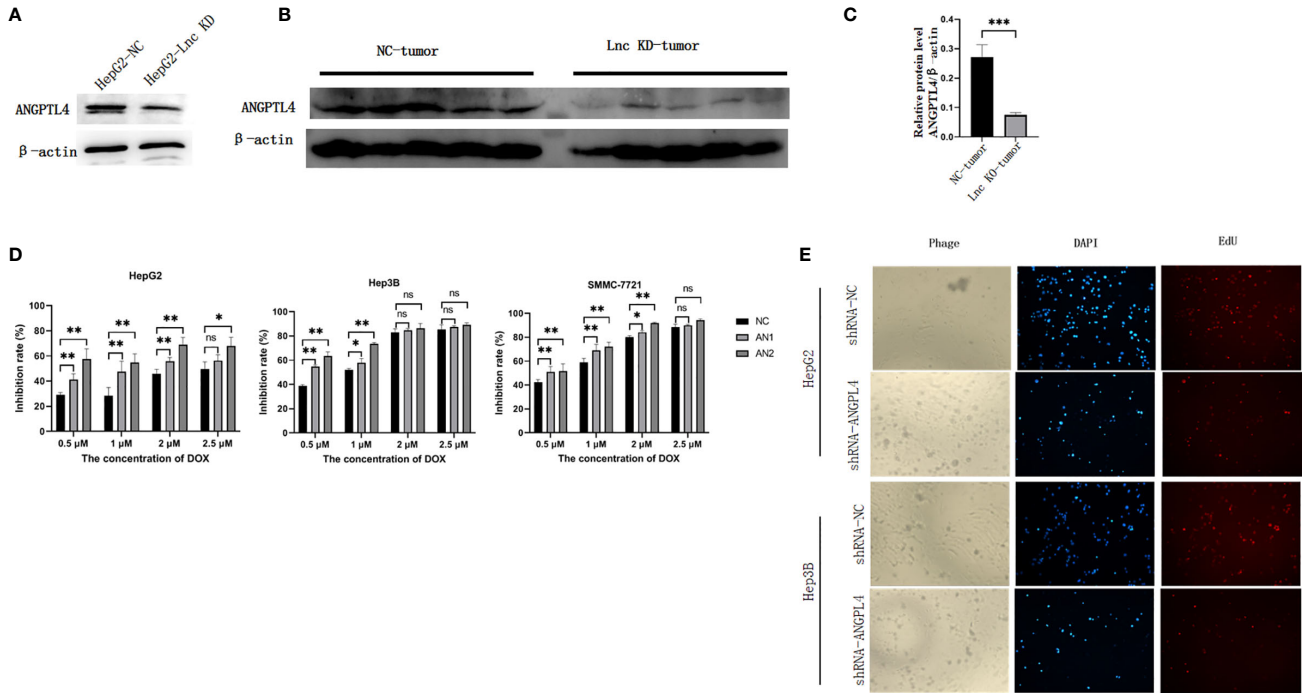

FIGURE 7 | The role of ANGPTL4 in hepatocellular carcinoma cells. **(A)** The protein expression of ANGPTL4 in HepG2 cells after transfection of NC siRNA or siRNA3 (n=5). Protein **(B)** or RNA **(C)** expression of ANGPTL4 in HepG2 xenografts. **(D)** Knocking down of ANGPTL4 using ANGPTL4-siRNA 1 (AN1) or ANGPTL4-siRNA 2 (AN2) increased the inhibition of Doxorubicin in HepG2, Hep3B, and SMMC-7721 cells. **(E)** EdU analysis showing cell proliferation after transfection of scrambled shRNA (shRNA-NC) or shRNA-ANGPTL4 (field of view: 200x) in HepG2 or Hep3B cells treated with 2.5 μM doxorubicin for 48 hours. *p < 0.05, **p < 0.01, ***p < 0.001; ns, not statistically significant.

The application of bioinformatic analyses facilitated the identification of candidate lncRNAs and related signaling pathways for indispensable mechanistic studies. According to the findings from the TCGA-LIHC dataset, lncRNA AC007639.1 was knocked down in three HCC cell lines using specific siRNAs or shRNA, with the finding of significantly more cell death and inhibition of cell proliferation, which showed lncRNA AC007639.1 is involved in HCC pathogenesis.

We tested the role of lncRNA AC007639.1 in three cell lines of hepatic origin, HepG2, Hep3B, and SMMC-7721. HepG2 is characterized by hepatitis B virus negative and non-tumorigenic, while Hep3B is characterized by hepatitis B virus positive and tumorigenic (17), and SMMC-7721 has been suspected of its liver origin due to contamination concerns (18). Therefore, to avoid controversies, SMMC-7721 cells were just used to test the efficacy of siRNA knock down (19), but not selected for further mechanistic experiments. Doxorubicin is among the most used chemotherapeutics against human cancers (20), the resistance of which is related with lncRNA AC007639.1 as shown in this study.

ANGPTL4 protein belongs to the angiopoietin (ANG)-related family. It is highly expressed in numerous organs including liver, and is be stimulated by inflammatory or hypoxic conditions (21, 22). However, the roles of ANGPTL4 in human cancers are controversial in different experimental models and proposed pathways. Overexpression of ANGPTL4 promotes tumorigenesis and metastasis (23), whereas it presents anti-metastatic activity through inhibition of vascular permeability and invasiveness (24). In the clinical settings, a high serum ANGPTL4 protein level in HCC patients is predictive of liver cirrhosis and intrahepatic metastasis (25). But levels of ANGPTL4 protein in tumor tissues are significantly lower than that in non-tumor tissues of the same HCC patients (26). Knockdown of ANGPTL4 inhibits the development of human gastric cancer (27). Our findings showed that the expression of ANGPTL4 is controlled by lncRNA AC007639.1, and ANGPTL4 contributed to the resistance of HCC cells to doxorubicin.

Taken together, we showed by bioinformatics and mechanistic studies that lncRNA AC007639.1 was involved in the pathogenesis of HCC by decreasing apoptosis and increasing resistance to chemotherapy. LncRNA AC007639.1 could be a valuable prognostic predictor as well as treatment target in HCC patients.

DATA AVAILABILITY STATEMENT

The datasets presented in this study can be found in online repositories. The names of the repository/repositories and

accession number(s) can be found below: (https://www.ncbi.nlm.nih.gov/genbank/), PRJNA716423.

ETHICS STATEMENT

The animal study was reviewed and approved by Ethical Committee of Second Affiliated Hospital of Harbin Medical University.

AUTHOR CONTRIBUTIONS

YY and YB conceived the study, analyzed and interpreted patient data, and were major contributors in writing the manuscript. YB, MD, DL, YL, SY, LW, HL, GC, XL, and XS obtained experiment data. All authors contributed to the article and approved the submitted version.

SUPPLEMENTARY MATERIAL

The Supplementary Material for this article can be found online at: https://www.frontiersin.org/articles/10.3389/fonc.2021.715541/full#supplementary-material

Supplementary Figure 1 | The map of shRNA vector.

Supplementary Table 1 | Primers for qRT-PCR and siRNAs.

REFERENCES

1. The American Cancer Society medical and editorial content team. *Key Statistics About Liver Cancer* (2021). Available at: https://www.cancer.org/cancer/liver-cancer/about/what-is-key-statistics.html (Accessed March 2, 2020).
2. Li XM, Ma L, Yang YB, Shi ZJ, Zhou SS. Analyses of Prognostic Indices of Chronic Liver Failure Caused by Hepatitis Virus. *World J Gastroenterol* (2005) 11(18):2841–3. doi: 10.3748/wjg.v11.i18.2841
3. Yang Y, Deng L, Li X, Shi Z, Chen D, Chen X, et al. Evaluation of the Prognosis of Fulminant Viral Hepatitis in Late Pregnancy by the MELD Scoring System. *Eur J Clin Microbiol Infect Dis* (2012) 31(10):2673–8. doi: 10.1007/s10096-012-1613-y
4. Yang Y, Deng L, Li X, Shi Z, Jiang P, Chen D, et al. Analysis of Prognosis-Associated Factors in Fulminant Viral Hepatitis During Pregnancy in China. *Int J Gynaecol Obstet* (2011) 114(3):242–5. doi: 10.1016/j.ijgo.2011.03.017
5. Deng L, Li X, Shi Z, Jiang P, Chen D, Ma L. Maternal and Perinatal Outcome in Cases of Fulminant Viral Hepatitis in Late Pregnancy. *Int J Gynecol Obstet* (2012) 119(2):145–8. doi: 10.1016/j.ijgo.2012.05.041
6. Ma L, Alla N, Li X, Mynbaev O, Shi Z. Mother to Child Transmission of HBV: Review of Current Clinical Management and Prevention Strategies. *Rev Med Virol* (2014) 24(6):396–406. doi: 10.1002/rmv.1801
7. Engreitz JM, Haines JE, Perez EM, Munson G, Chen J, Kane M, et al. Local Regulation of Gene Expression by Lncrna Promoters, Transcription and Splicing. *Nature* (2016) 539(7629):452–5. doi: 10.1038/nature20149
8. Lin X, Xiang X, Feng B, Zhou H, Wang T, Chu X, et al. Targeting Long non-Coding Rnas in Hepatocellular Carcinoma: Progress and Prospects. *Front Oncol* (2021) 11:670838. doi: 10.3389/fonc.2021.670838
9. Naipauer J, García Solá ME, Salyakina D, Rosario S, Williams S, Coso O, et al. A non-Coding RNA Network Involved in KSHV Tumorigenesis. *Front Oncol* (2021) 11:687629. doi: 10.3389/fonc.2021.687629
10. Huang J, Zheng Y, Xiao X, Liu C, Lin J, Zheng S, et al. A Circulating Long Noncoding RNA Panel Serves as a Diagnostic Marker for Hepatocellular Carcinoma. *Dis Markers* (2020) 2020:5417598. doi: 10.1155/2020/5417598
11. Love MI, Huber W, Anders S. Moderated Estimation of Fold Change and Dispersion for RNA-Seq Data With Deseq2. *Genome Biol* (2014) 15(12):550. doi: 10.1186/s13059-014-0550-8
12. Yuan Q, Gao C, Lai XD, Chen LY, Lai TB. Analysis of Long Noncoding RNA ZNF667-AS1 as a Potential Biomarker for Diagnosis and Prognosis of Glioma Patients. *Dis Markers* (2020) 2020:8895968. doi: 10.1155/2020/8895968
13. Tang Z, Li C, Kang B, Gao G, Li C, Zhang Z. GEPIA: A Web Server for Cancer and Normal Gene Expression Profiling and Interactive Analyses. *Nucleic Acids Res* (2017) 45(W1):W98–102. doi: 10.1093/nar/gkx247
14. The Gene Ontology Consortium. The Gene Ontology Resource: 20 Years and Still Going Strong. *Nucleic Acids Res* (2019) 47(D1):D330–8. doi: 10.1093/nar/gky1055
15. Zhang Y, Liu X, Liu L, Chen J, Hu Q, Shen S, et al. Upregulation of FEN1 Is Associated With the Tumor Progression and Prognosis of Hepatocellular Carcinoma. *Dis Markers* (2020) 2020:2514090. doi: 10.1155/2020/2514090
16. Xiong D, He R, Dang Y, Wu H, Feng Z, Chen G. The Latest Overview of Circrna in the Progression, Diagnosis, Prognosis, Treatment, and Drug Resistance of Hepatocellular Carcinoma. *Front Oncol* (2020) 10:608257. doi: 10.3389/fonc.2020.608257
17. Qiu GH, Xie X, Xu F, Shi X, Wang Y, Deng L. Distinctive Pharmacological Differences Between Liver Cancer Cell Lines Hepg2 and Hep3B. *Cytotechnology* (2015) 67(1):1–12. doi: 10.1007/s10616-014-9761-9
18. Rebouissou S, Zucman-Rossi J, Moreau R, Qiu Z, Hui L. Note of Caution: Contaminations of Hepatocellular Cell Lines. *J Hepatol* (2017) 67(5):896–7. doi: 10.1016/j.jhep.2017.08.002
19. Shi Z, Nicholson RH, Jaggi R, Nicholson AW. Characterization of Aquifex Aeolicus Ribonuclease III and the Reactivity Epitopes of its Pre-Ribosomal RNA Substrates. *Nucleic Acids Res* (2011) 39(7):2756–68. doi: 10.1093/nar/gkq1030
20. Xu B, Yuan L, Hu Y, Xu Z, Qin JJ, Cheng XD. Synthesis, Characterization, Cellular Uptake, and *In Vitro* Anticancer Activity of Fullerenol-Doxorubicin Conjugates. *Front Pharmacol* (2020) 11:598155. doi: 10.3389/fphar.2020.598155
21. Ng KT, Xu A, Cheng Q, Guo DY, Lim ZX, Sun CK, et al. Clinical Relevance and Therapeutic Potential of Angiopoietin-Like Protein 4 in Hepatocellular Carcinoma. *Mol Cancer* (2014) 13:196. doi: 10.1186/1476-4598-13-196
22. Zhu P, Goh YY, Chin HF, Kersten S, Tan NS. Angiopoietin-Like 4: A Decade of Research. *Biosci Rep* (2012) 32(3):211–9. doi: 10.1042/BSR20110102
23. Kim SH, Park YY, Kim SW, Lee JS, Wang D, DuBois RN. ANGPTL4 Induction by Prostaglandin E2 Under Hypoxic Conditions Promotes Colorectal Cancer Progression. *Cancer Res* (2011) 71(22):7010–20. doi: 10.1158/0008-5472.CAN-11-1262
24. Galaup A, Cazes A, Le Jan S, Philippe J, Connault E, Le Coz E, et al. Angiopoietin-Like 4 Prevents Metastasis Through Inhibition of Vascular Permeability and Tumor Cell Motility and Invasiveness. *Proc Natl Acad Sci USA* (2006) 103(49):18721–6. doi: 10.1073/pnas.0609025103
25. Li H, Ge C, Zhao F, Yan M, Hu C, Jia D, et al. Hypoxia-Inducible Factor 1 Alpha-Activated Angiopoietin-Like Protein 4 Contributes to Tumor Metastasis *via* Vascular Cell Adhesion Molecule-1/Integrin Beta1 Signaling in Human Hepatocellular Carcinoma. *Hepatology* (2011) 54(3):910–9. doi: 10.1002/hep.24479
26. Zhang H, Wei S, Ning S, Jie Y, Ru Y, Gu Y. Evaluation of Tgfbeta, XPO4, Elf5a2 and ANGPTL4 as Biomarkers in HCC. *Exp Ther Med* (2013) 5(1):119–27. doi: 10.3892/etm.2012.750
27. Chen JW, Luo YJ, Yang ZF, Wen LQ, Huang L. Knockdown of Angiopoietin-Like 4 Inhibits the Development of Human Gastric Cancer. *Oncol Rep* (2018) 39(4):1739–46. doi: 10.3892/or.2018.6253

Conflict of Interest: Author SY was employed by the company "Harbin Nachuan Bio-Science Technology Co., LTD.".

The remaining authors declare that the research was conducted in the absence of any commercial or financial relationships that could be construed as a potential conflict of interest.

Publisher's Note: All claims expressed in this article are solely those of the authors and do not necessarily represent those of their affiliated organizations, or those of the publisher, the editors and the reviewers. Any product that may be evaluated in

this article, or claim that may be made by its manufacturer, is not guaranteed or endorsed by the publisher.

Advantages of publishing in Frontiers

OPEN ACCESS
Articles are free to read for greatest visibility and readership

FAST PUBLICATION
Around 90 days from submission to decision

HIGH QUALITY PEER-REVIEW
Rigorous, collaborative, and constructive peer-review

TRANSPARENT PEER-REVIEW
Editors and reviewers acknowledged by name on published articles

Frontiers
Avenue du Tribunal-Fédéral 34
1005 Lausanne | Switzerland

Visit us: www.frontiersin.org
Contact us: frontiersin.org/about/contact

REPRODUCIBILITY OF RESEARCH
Support open data and methods to enhance research reproducibility

DIGITAL PUBLISHING
Articles designed for optimal readership across devices

FOLLOW US
@frontiersin

IMPACT METRICS
Advanced article metrics track visibility across digital media

EXTENSIVE PROMOTION
Marketing and promotion of impactful research

LOOP RESEARCH NETWORK
Our network increases your article's readership